Nanoparticle-based Sample Preparation and High-Resolution Mass Spectrometry for Bioprocess and Quality Control in Biopharmaceutical Production

Dissertation

der Mathematisch-Naturwissenschaftlichen Fakultät

der Eberhard Karls Universität Tübingen

zur Erlangung des Grades eines

Doktors der Naturwissenschaften

(Dr. rer. nat.)

vorgelegt von

Markus Höldrich

aus Albstadt

Tübingen

2019

Gedruckt mit Genehmigung der Mathematisch-Naturwissenschaftlichen Fakultät der Eberhard Karls Universität Tübingen.

Tag der mündlichen Qualifikation:	18.11.2019
Dekan:	Prof. Dr. Wolfgang Rosenstiel
1. Berichterstatter:	Prof. Dr. Michael Lämmerhofer
2. Berichterstatter:	Prof. Dr. Frank M. Böckler

„…every experiment destroys some of the knowledge of the system which was obtained by previous experiments.“

Werner Heisenberg

Danksagung

Dieses Kapitel ist all jenen gewidmet, die mich auf meiner wissenschaftlichen Reise begleitet haben, mich in meinem Weg mit viel Geduld und Ausdauer bestärkt haben und stehts ein offenes Ohr für mich hatten.

Zuallererst möchte ich meinem Mentor und Doktorvater Prof. Dr. Michael Lämmerhofer danken. Er gab mir die Möglichkeit und schenkte mir das Vertrauen, dieses außerordentlich interessante Thema zu bearbeiten und fortzuführen. Stets hatte er ein offenes Ohr und stand mir mit Rat und Tat zur Seite. Er ermöglichte es mir meine Arbeit auf internationalen Konferenzen vorzustellen. Dies bestärkte und inspirierte mich immer wieder aufs Neue.

Ein weiterer Dank geht an Prof. Dr. Frank Böckler für die Zweitbetreuung meiner Doktorarbeit.

Danke auch an Prof. Dr. Rolf Daniels für den Zugang zum Malvern Zetasizer Nano. Ohne diese Möglichkeit wäre die grundlegende Charakterisierung der Nanobiokatalysatoren nicht möglich gewesen.

Ein besonderer Dank geht an Dr. Jeannie Horak für ihre wertvollen Ratschläge.

Eveline Wachendorfer, Ingrid Straub und Mike Kaupert. Ohne sie wäre ein geregelter Uni-Alltag kaum zu bewältigen.

Natürlich möchte ich mich auch noch bei allen weiteren Kolleginnen und Kollegen bedanken. Mein Platznachbar und Massenspektrometrie-Ass Adrian Sievers-Engler, Corinna Sanwald, Stefanie Bäurer, Malgorzata Cebo, Jörg Schlotterbeck, Bernhard Drotleff, Ulrich Woiwode, Carlos Calderón Castro, Stefan Polnick und Stefan Neubauer. Mal war es der Sport, mal das Feierabendbier, welches einen die Wirren des Alltags für einen kurzen Augenblick vergessen

ließen. Vielen Dank auch an „Sunny“ Siyao Liu für die erfolgreiche Weiterführung und Fortsetzung des Projektes.

Auch meinen Eltern, meinen Geschwistern und dem ganzen Rest meiner Familie möchte ich herzlichst danken. Meine Wege waren teils sehr verschlungen, doch sie haben alle an mich geglaubt und mich über allen Maßen unterstützt.

Der letzte Dank gilt meiner geliebten Frau. Sie ist der Fels in meiner Brandung.

Content

Abbreviations (in alphabetical order)

(m)Ab(s)	(monoclonal) Antibody (Antibodies)
ACTIP	Animal Cell Technology Industrial Platform
API	Active Pharmaceutical Ingredient
BCA	Bicinchoninic Acid Assay
CYC	Cytochrome C
Da	Dalton (atomic mass unit)
DLS	Dynamic Light Scattering
DLVO	Derjaguin-Landau-Verwey-Overbeek theory
ELISA	Enzyme-Linked Immunosorbent Assay
ELS	Electrophoretic Light Scattering
EMA	European Medicines Agency
ESI	Electrospray Ionization
FDA	U. S. Food and Drug Administration
FT-MS	Fourier Transform Ion Cyclotron Mass Spectrometry
GH	Growth Hormone
GNP	Gold Nanoparticles
HPLC	High Performance Liquid Chromatography
IUPAC	International Union of Pure and Applied Chemistry
LC and HC	Light Chain and Heavy Chain (antibody structure)
LC-MS	Liquid Chromatography coupled with Mass Spectrometry
LFIA	Lateral Flow Immunoassay
LSPR	Localized Surface Plasmon Resonance
MALDI	Matrix-Assisted Laser Desorption/Ionization
MS	Mass Spectrometry
MW	Molecular Weight
NTA	Nanoparticle Tracking Analysis
PDI	Polydispersity Index

pI	Isoelectric Point
PSD	Particle Size Distribution
RMM	Resonant Mass Measurement
SAM	Self-Assembled Monolayer
SDS-PAGE	Sodium Dodecyl Sulfate–Polyacrylamide Gel Electrophoresis
SEM	Scanning Electron Microscopy
TDA	Taylor Dispersion Analysis
TEM	Transmission Electron Microscopy
TIC	Total Ion Current
TLC	Thin-Layer Chromatography
TOF	Time Of Flight (mass spectrometry)

Summary

Biopharmaceuticals, such as monoclonal antibodies (mAb), have recently become increasingly important in the treatment of many different diseases. Usually these molecules have complex molecular structures which poses great challenges for their characterization. However, full characterization is essential for FDA and EMA drug approval. Nowadays, antibodies are usually analyzed by high-resolution mass spectrometry (HR-MS). One approach is the middle-down analysis, where enzymes such as pepsin are used to digest the antibodies into specific fragments which are in a more suitable size-range and can be more easily analyzed. However, mAb characterization usually starts with top-down analysis of intact antibodies using HR-MS or liquid chromatography (LC) hyphenated to HR-MS (LC-MS) for determining the molecular mass to charge (m/z) of the protein.

In this work new methods for sample preparation in protein analytics of biopharmaceuticals have been developed. In particular, the main approach discussed herein describes the sample preparation of therapeutic proteins with heterogeneous nanobiocatalysts based on gold nanoparticles (GNPs) with coated or immobilized enzymes such as pepsin. The different synthesis steps of the nanoparticulate carriers were investigated and compared in size and function using classical methods, such as Vis-spectroscopy, dynamic light scattering (DLS), Lowry assay and Michaelis-Menten kinetic analysis. Newer methods such as Resonant Mass Measurement and Taylor Dispersion Analysis were also used for this purpose. In order to extend the toolbox of methods in this regard, the results of these modern characterization methods were compared with those of the classical ones. For functional studies of the gold nanoparticle-conjugated enzyme, the comparison of enzyme activities with free, unbound enzymes (e.g. pepsin) is an important aspect for the performance evaluation of the new nanobiocatalysts. The immobilization of enzymes to nanoparticulate carriers has some advantageous. Since the gold nanoparticles have a high density, separation of the nano biocatalysts from the sample is easily possible with simple benchtop centrifuges, as they are present in almost every modern laboratory. Thus, the enzyme can be easily removed after reaction and does not contaminate the sample with another protein (enzyme) which might

give interferences in subsequent MS analysis. However, it has to be ascertained that immobilization does not reduce the enzyme activity. In this work it is documented that pepsin immobilized on gold nanoparticles has even higher enzymatic efficiencies than pepsin in free solution.

The aim of the present work is to provide an overview of the synthesis and characterization of GNPs as a nano framework for enzymes used for protein and antibody analysis. Also, the current state of technology in methods for the use of GNPs should be pointed out here.

Zusammenfassung der Dissertation

Biopharmazeutika, wie zum Beispiel monoklonale Antikörper (mAb), haben unlängst bei der Behandlung vieler verschiedener Krankheiten an Bedeutung gewonnen. In der Regel haben diese Moleküle komplexe molekulare Strukturen, die ihre Charakterisierung vor große Herausforderungen stellt. Eine vollständige Charakterisierung ist jedoch für die Zulassung von FDA und EMA-Arzneimitteln unerlässlich. Heutzutage werden Antikörper gewöhnlich durch hochauflösende Massenspektrometrie (HR-MS) analysiert. Ein Ansatz ist die Middle-Down Analyse, bei der Enzyme wie Pepsin verwendet werden, um die Antikörper in spezifische Fragmente zu verdauen, die sich in einem geeigneteren Größenbereich befinden und so leichter analysiert werden können. Die mAb-Charakterisierung beginnt jedoch in der Regel mit der Top-Down Analyse von intakten Antikörpern mittels HR-MS oder Flüssigkeitschromatographie (LC) gekoppelt mit HR-MS (LC-MS), welche auch die übliche Methode darstellt, um das Verhältnis Masse zu Ladung (m/z) der Proteine zu bestimmen.

In dieser Arbeit wurden neue Methoden zur Probenvorbereitung in der Proteinanalytik von Biopharmazeutika entwickelt. Der hier diskutierte Hauptansatz beschreibt insbesondere die Probenaufarbeitung von therapeutischen Proteinen mit heterogenen Nanobiokatalysatoren auf der Basis von Goldnanopartikeln, die mit Enzymen wie Pepsin beschichtet oder diese auf ihnen immobilisiert sind. Die verschiedenen Syntheseschritte der nanopartikulären Träger wurden unter Verwendung klassischer Methoden, wie Vis-Spektroskopie, Dynamische Lichtstreuung (DLS), Lowry-Assay und Michaelis-Menten-Kinetik, in Größe und Funktion untersucht und verglichen. Neuere Methoden, wie die Resonanzmassenmessung und die Taylor-Dispersion, wurden ebenfalls für die Studie verwendet. Um den Werkzeugkasten an Methoden in dieser Hinsicht zu erweitern, wurden die Ergebnisse dieser modernen Charakterisierungsmethoden, mit denen der klassischen Modelle verglichen. Für funktionelle Untersuchungen der Enzymaktivität von auf Goldnanopartikel konjugierten Proteinen, ist der Vergleich der Enzymaktivitäten von freien und ungebundenen Enzymen (z. B. Pepsin) ein wichtiger Gesichtspunkt für die Bewertung der Leistung der neuen Nanobiokatalysatoren. Die Immobilisierung von Enzymen an nanopartikuläre Träger hat einige Vorteile. Da die

Goldnanopartikel eine hohe Dichte aufweisen, ist die Trennung der Nanobiokatalysatoren von der Probe mit einfachen Tischzentrifugen, wie sie in fast jedem modernen Labor vorhanden sind, möglich. Somit kann das Enzym nach der Reaktion leicht entfernt werden und kontaminiert die Probe nicht mit einem anderen Protein (Enzym), das Interferenzen bei der nachfolgenden MS-Analyse verursachen kann. Es muss jedoch sichergestellt werden, dass die Immobilisierung die Enzymaktivität nicht verringert. In dieser Arbeit wird dokumentiert, dass auf Goldnanopartikeln immobilisiertes Pepsin, sogar eine höhere enzymatische Effizienz aufweist, als Pepsin in freier Lösung.

Ziel der vorliegenden Arbeit ist es, einen Überblick über die Synthese und Charakterisierung von GNPs zu geben, welche als Nano-Grundgerüst für Enzyme dienen, die für die Protein- und Antikörperanalyse verwendet werden. An dieser Stelle soll auch der aktuelle Stand der Technik an Methoden, welche GNPs verwenden, erörtert werden.

List of Publications

Publication I:

Gold nanoparticle-conjugated pepsin for efficient solution-like heterogeneous biocatalysis in analytical sample preparation protocols

Markus Höldrich, Adrian Sievers-Engler, Michael Lämmerhofer

Analytical and Bioanalytical Chemistry 408 (June 2016), Pages 5415-5427

(doi: 10.1007/s00216-016-9657-y)

Publication II:

Taylor dispersion analysis, resonant mass measurement and bioactivity of pepsin-coated gold nanoparticles

Markus Höldrich, Siyao Liu, Markus Epe, Michael Lämmerhofer

Talanta 167 (February 2017), Pages 67-74

(doi: https://doi.org/10.1016/j.talanta.2017.02.010)

Publication III:

Papain-functionalized gold nanoparticles as heterogeneous biocatalyst for bioanalysis and biopharmaceuticals analysis

Siyao Liu, Markus Höldrich, Adrian Sievers-Engler, Jeannie Horak, Michael Lämmerhofer

Analytica Chimica Acta 963 (April 2017), Pages 33-43

(doi: https://doi.org/10.1016/j.aca.2017.02.009)

Publication IV:

Accurate and reliable quantification of the protein surface coverage on protein-functionalized nanoparticles

Siyao Liu, Jeannie Horak, Markus Höldrich, Michael Lämmerhofer

Analytica Chimica Acta 989 (October 2017), Pages 29-37

(doi: https://doi.org/10.1016/j.aca.2017.08.004)

Publication V (non-peer-reviewed):

Gold nanoparticle-based immobilized enzyme reactors

Straightforward and accelerated sample preparation in protein and biopharmaceuticals analysis

Siyao Liu, Markus Höldrich, Helmut Hinterwirth, Michael Lämmerhofer

Chrom+Food FORUM 04 (2017), Pages 34-37

Author Contributions

Publication I:

Gold nanoparticle-conjugated pepsin for efficient solution-like heterogeneous biocatalysis in analytical sample preparation protocols

Markus Höldrich:

- General concept and work plan
- Synthesis and characterization of GNPs
- Chromatographic characterization of pepsin activity and method development
- Protein/Antibody determination and digestion protocols
- LC-MS analysis of protein digests and antibody fragments
- Interpretation of the analytical data
- Manuscript writing

Adrian Sievers-Engler:

- Developed the LC–HR-MS method for intact protein analysis development
- Proofreading

Michael Lämmerhofer:

- Scientific concept
- Coordination
- Discussions
- Proofreading and final approval of the manuscript
- Corresponding author

Publication II:

Taylor dispersion analysis, resonant mass measurement and bioactivity of pepsin-coated gold nanoparticles

Markus Höldrich:

- General concept and work plan
- Synthesis and characterization of GNPs
- Chromatographic characterization of pepsin activity
- Resonant mass measurement and Taylor dispersion analysis of pepsin-GNP conjugates
- Protein determination and digestion protocols
- Interpretation of the analytical data
- Manuscript writing

Siyao Liu:

- Resonant mass measurement and Taylor dispersion analysis of corresponding papain-GNP conjugates
- Interpretation of the analytical data
- Manuscript writing
- Proofreading

Markus Epe:

- Basic assistance in using the Archimedes and Viscosizer TD from Malvern Instruments

- Proofreading

Michael Lämmerhofer:

- Scientific concept

- Coordination

- Discussions

- Proofreading and final approval of the manuscript

- Corresponding author

Publication III:

Papain-functionalized gold nanoparticles as heterogeneous biocatalyst for bioanalysis and biopharmaceuticals analysis

Siyao Liu:

- General concept and work plan
- Synthesis and characterization of GNPs
- Quantitative determination of papain functionalized GNPs
- Assays of papain activity
- HPLC-µESI-QTOF-MS analysis of IgG and fragments
- Interpretation of the analytical data
- Manuscript writing

Markus Höldrich:

- Basic feasibility studies and proof of concept of the immobilization of papain on GNPs
- Training and assistance in basic work with GNPs
- Assistance with the execution of SDS-PAGE
- Proofreading

Adrian Sievers-Engler:

- Developed the HPLC-µESI-QTOF-MS method for determination of IgG masses
- Proofreading

Jeannie Horak:

- Assistance with the execution of SDS-PAGE
- Proofreading

Michael Lämmerhofer:

- Scientific concept

- Coordination

- Discussions

- Proofreading and final approval of the manuscript

- Corresponding author

Publication IV:

Accurate and reliable quantification of the protein surface coverage on protein-functionalized nanoparticles

Siyao Liu:

- General concept and work plan
- Synthesis and characterization of GNPs
- Digestion of samples and calibrants and AQC derivatization
- Interpretation of the analytical data
- Manuscript writing

Jeannie Horak:

- Assistance with AQC derivatization
- HPLC-FLD analysis method development
- Proofreading

Markus Höldrich:

- Basic feasibility studies and proof of concept of the quantification studies (digestion and AQC derivatization with protein functionalized GNPs)
- Proofreading

Michael Lämmerhofer:

- Scientific concept
- Coordination
- Discussions
- Proofreading and final approval of the manuscript
- Corresponding author

Publication V:

Gold nanoparticle-based immobilized enzyme reactors

Straightforward and accelerated sample preparation in protein and biopharmaceuticals

Siyao Liu:

- General studies with papain functionalized GNPs in previous publications
- Manuscript writing

Markus Höldrich:

- General studies with pepsin functionalized GNPs in previous publications
- Proofreading

Helmut Hinterwirth:

- General studies with trypsin functionalized GNPs in previous publications
- Proofreading

Michael Lämmerhofer:

- Scientific concept
- Coordination
- Discussions
- Proofreading and final approval of the manuscript
- Corresponding author

List of Poster Presentations

HPLC 2013, Amsterdam, Netherlands, June 16th – 20th

Bioconjugation of trypsin onto GNPs: a new heterogeneous nano-structured biocatalyst for LC-MS/MS based proteomics

Hinterwirth H., Höldrich M., Lindner W., Lämmerhofer M.

ISC 2014, Salzburg, Austria, September 14th – 18th

Immobilization of pepsin onto gold nanoparticles

Markus Höldrich, Michael Lämmerhofer

HPLC 2015, Geneva, Switzerland, June 21st – 25th

Heterogeneous nanobiocatalysts for sample preparation in protein analytics

Markus Höldrich, Michael Lämmerhofer

List of Oral Presentations

HPLC 2015, Geneva, Switzerland, June 21st – 25th

Heterogeneous nanobiocatalysts for sample preparation in protein analytics

(Agilent Best Poster Award, incl. 5 min Short Oral Presentation)

Doktorandenseminar 2016 des AK Separation Science (GDCh), Hohenroda, Germany, January 10th – 12th

Immobilized pepsin on gold nanoparticles as heterogeneous nanobiocatalysts

1. General Introduction

1.1. Biopharmaceuticals

Biopharmaceuticals are medicinal products, i.e. drugs that are produced under the aid of biotechnological processes. Active pharmaceutical ingredients (APIs) gained from these kinds of biological sources are usually complex in molecule structure. The analytical claim of such complex molecules, such as proteins and antibodies (Abs), in terms of production and quality is different from those of conventionally synthesized pharmaceutical molecules [1] as the commercial importance of these molecules has increased in recent years. Since the first commercially available therapeutic monoclonal antibody (mAb) Muromonab-CD3 (https://www.drugbank.ca/drugs/DB00075, 01.06.2018) with the trade name Orthoclone OKT3 (1986, Janssen-Cilag) [2], FDA (Food and Drug Administration) approved for the prevention of renal transplant rejection, there are already over 40 monoclonal antibodies (mAbs) available for cancer treatment, orphan drugs and blockbusters for treatment of asthma and rheumatism [3]. Noteworthy here are monoclonal antibodies, such as CD-20 antibody Rituximab [4], which is considered a pioneer of targeted cancer therapy (FDA approval 1997, EMA (European Medicines Agency) approval 1998) and approved for the treatment of rheumatoid arthritis [5]. Also, worth mentioning, are the mAbs for the treatment of asthma like the immunoglobulin E/ IgE Omalizumab (Xolair® market by Novartis and Roche) [6] and interleukin-5/ IL5 antibodies such as Reslizumab (FDA and EMA approval in 2016) [7] and Mepolizumab (FDA and EMA approval in 2015) [8].

All information regarding FDA and EMA approvals, trade names and companies were taken from the URL of Animal Cell Technology Industrial Platform (ACTIP) “Monoclonal Antibodies Approved by the EMA and FDA for Therapeutic Use (status 2017)” (http://www.actip.org/products/monoclonal-antibodies-approved-by-the-ema-and-fda-for-therapeutic-use/).

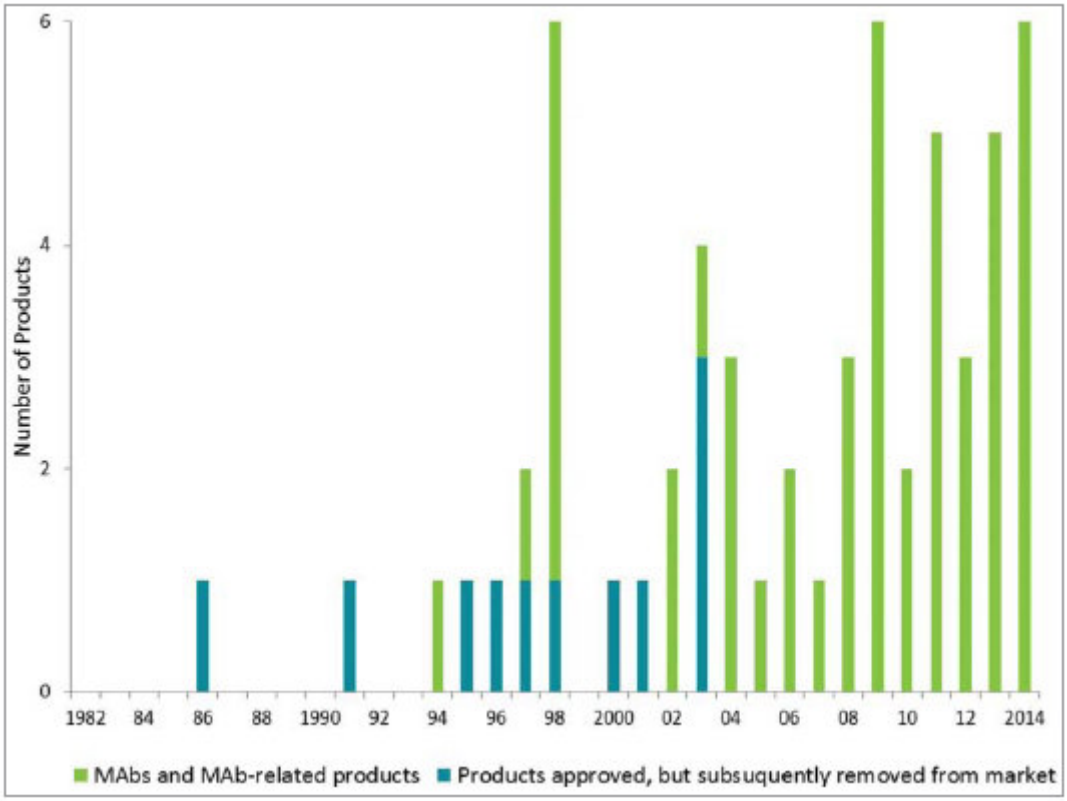

Figure 1: The therapeutic monoclonal antibody market from Dawn M Ecker et al. 2015 [3]. Annual approvals of mAbs products from 1982 to 2014 (Reprinted with permission).

Figure 1 gives an overview of the development of the markets for therapeutic antibodies from 1982 to 2014. A clear increase from the beginning of the 2000s can be clearly seen. In 2016, the global market for mAbs was $ 85.4 billion. A forecast for 2024 published at Grand View Research in 2016 assumes an annual growth rate of approximately 5.7% and around $ 140 billion for 2024 [9].

This growth also poses challenges to the quality and speed of analytical quality control.

1.1.1. Methods for Quality Control of mAbs

To monitor the development and production of therapeutic antibodies, a variety of different analysis tools have been developed in recent years. For this purpose, various electrophoresis methods, but also liquid chromatography, mass spectrometry and their hyphenations are used, to obtain information e.g. about the complete

structural characterization and the glycoprofile [10]. Figure 2 gives a brief overview about possible characterization tools.

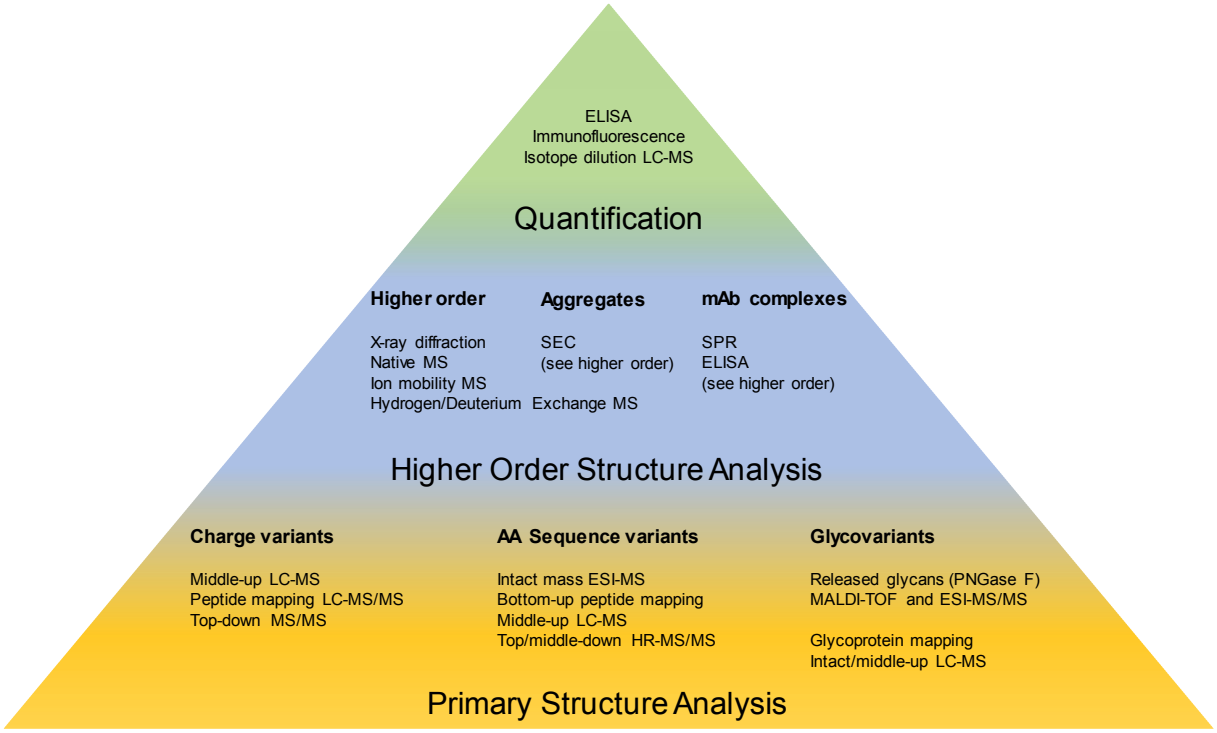

Figure 2: Overview of characterization tools for mAbs (adapted from Beck et al. 2013 [10])

All these methods are mandatory for quality control during research and development, for formulation and scale-up, pre-clinical phases and for the identification of possible optimization parameters, to obtain new therapeutical mAbs [10].

1.1.2. Sample Preparation Protocols

In the case of sample processing for convenient analysis of biopharmaceuticals the typical workflow involves enzymatic digestion or chemical fragmentation prior to LC-MS/MS analysis [10,11]. For classical bottom-up protein analysis at peptide level trypsin is mostly used for proteolytic cleavage [12]. In cases of therapeutic proteins, such as antibodies [11], pepsin, papain, IdeS and/ or a combination of these three biocatalysts along with reducing agents (to cleave disulfide bonds) is usually used to

cut the large intact antibody molecule (about 150 kDa) by specific cleavage into smaller defined fragments [10].

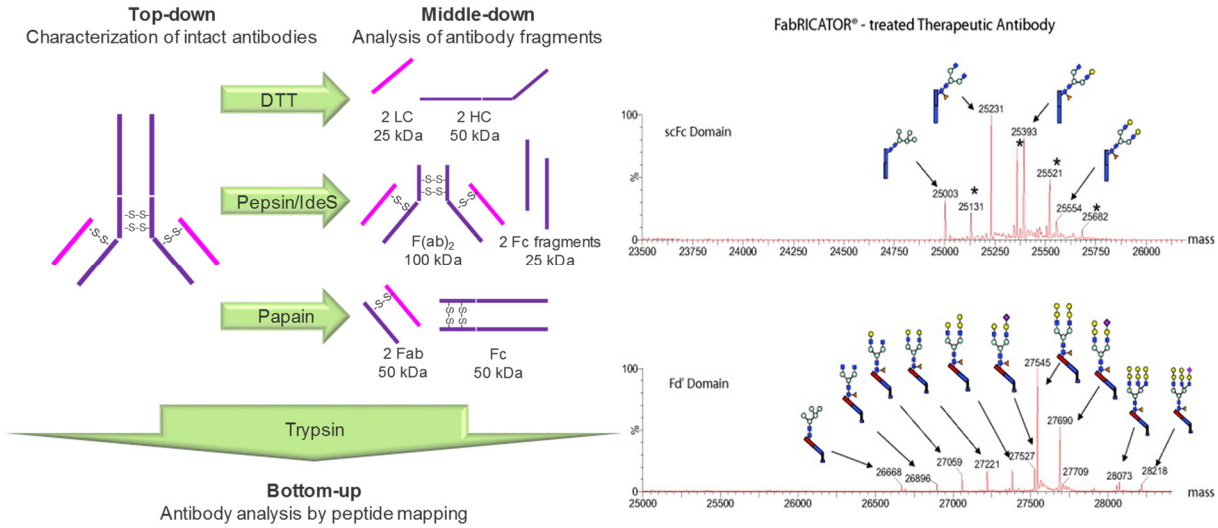

Figure 3: Top-down, middle-down and bottom-up characterization of antibodies. Redrawn in modified form according to "Result part "FabRICATOR® - treated Therapeutic Antibody" was taken from Biofiles Volume 8 No 02, Sigma-Aldrich, 2013" [13].

Pepsin, with a molecular weight (MW) of around 36 kDa and an isoelectric point (pI) of about 3.2 [14,15], cleaves antibodies near the hinge region as a digestive protease. This cleavage leads in particular to $F(ab')_2$ (MW of around 100 kDa) and two 25 kDa Fc fragments (see Figure 3) [10]. In the cleavage of peptide bonds in proteins, pepsin preferentially attaches to the C-terminal side of phenylalanine and leucine [16,17].

Comparable results to pepsin can be also provided by "Immunoglobulin G-degrading enzyme of Streptococcus pyogenes or IdeS. This highly specific enzyme can only use immunoglobulin G (IgG) as a substrate and a full digestion can be done in rapid 30 to 120 minutes [18]. The cleavage near the hinge region results in on 100 kDa $F(ab')_2$ fragment and two 25 kDa Fc fragments. [19-21]. IdeS, recombinantly modified from Streptococcus pyogenes, is being marketed by Genovis under the brand name FabRICATOR®.

(https://www.genovis.com/products/igg-proteases/fabricator/, 10.06.2018)

The cysteine protease papain cleaves antibodies specifically above the hinge region. This middle-down approach results in two Fab fragments and one Fc fragment with around 50 kDa each (see Figure 3) [10]. Papain naturally occurs in Carica papaya. The protein structure analysis was carried out in 1968 by Derenth et al [22]. Papain consists of 212 amino acids, has a MW of about 24 kDa and a pI of approximately 8.8 [23,24].

Dithiothreitol (DTT) is a reducing agent which is used in SDS-PAGE for cleaving disulfide bonds (R1-S-S-R2) to sulfhydryl groups (-SH). Due to this fact is also used to improve the long-term stability of proteins. Here, the oxidation of sulfhydryl groups to disulfide bonds by atmospheric oxygen is prevented [25,26]. The chemical fragmentation of antibodies with DTT leads to two heavy chains (HC) each with about 50 kDa molecular mass, and two light chains (LC) with 25 kDa each (see Figure 3) [10]. Besides DTT, TCEP (tris-(carboxyethyl)phosphine), is nowadays frequently used for the same purpose, the cleavage of disulfide bonds of antibodies.

The most popular protocol now established makes use of IdeS and subsequently reduces the disulfides of the resultant Fc and $F(ab')_2$ to end up with 25 kDa fragments which are advantageous from viewpoint of MS detection than the larger 50kDa or 100 kDa fragments [10,11].

In addition to the middle- and top-down analysis, there is also the possibility of the bottom-up approach. This technique is also referred as peptide level analysis [10,11], since as sample preparation a complete enzymatic digestion is carried out with trypsin or endoproteinase Lys-C, Asp-N, Glu-C. Trypsin as the gold standard cleaves the protein on the carboxyl side of arginine (Arg) and lysine (Lys), protocols are well established and it is easily available. To result in a purified sample, pre-cleaning of

the proteins before digestion by gel electrophoresis or in-gel digestion can be performed [11].

The protein digest mixtures are separated by liquid chromatography and subsequently sequenced by tandem mass spectrometry (e.g. MALDI-MS or ESI-MS). The determined peptide masses are used for protein identification by means of peptide mapping/ peptide mass fingerprint using peptide databases such as Mascot. This requires a well-established protocol to avoid miscleavages and to achieve high sequence coverage in order to obtain a valid result [10,11].

All these are possibilities for the sample preparation of antibodies to make them more amenable for subsequent structure characterization by MS. Techniques of immobilization of such enzymes on nanoparticles, full characterization of all nanoparticle synthesis steps and applications were in the focus of this work and are discussed on the following pages.

1.2. Nanoscience

Nanotechnology and Nanoscience deal with the phenomena of materials according to the IUPAC (International Union of Pure and Applied Chemistry) definition for nano dimension (*vide infra*) [27]. This concerns materials in the atomic, molecular and macromolecular range, where the physical properties are different to them of the corresponding bulk materials [28]. The study of this, for example, optical, electrical or mechanical properties gained more and more scientific interest for comparing different techniques and to complete the impression with new measuring techniques [29].

1.2.1. Definition

In general, according to IUPAC, nanomaterials have minimum one dimension in the range of approximately 1 nm to 100 nm in at least one dimension [27]. This definition

was established at the ICSU-CODATA workshop (23–24 February 2012, Paris) and published in Chemistry International Vol. 34 No. 6, November – December 2012. These materials can only be visualized by microscopic techniques, except nano foils, because here the thickness and not the area is scaled in nanometer range.

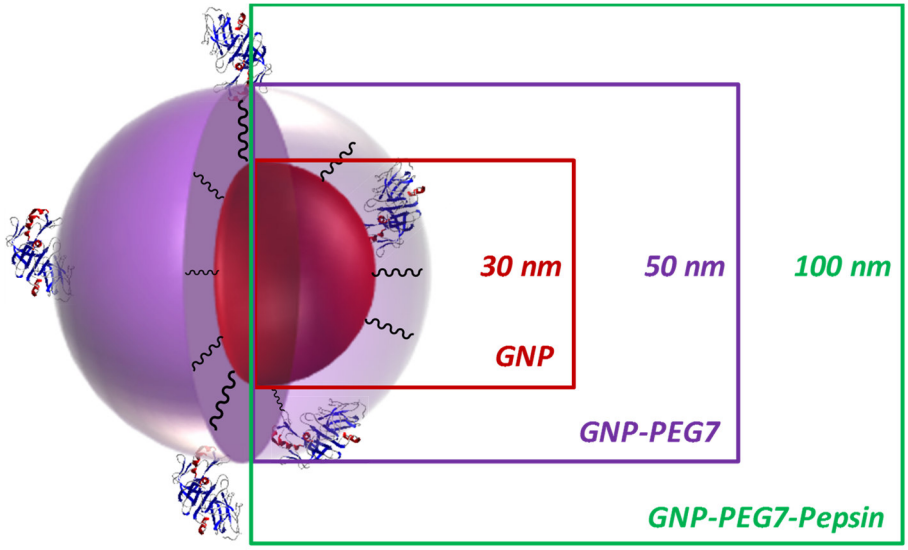

Figure 4: Illustration of the size dimensions on a typical functionalized nanoparticle Explanation of used abbreviations: gold nanoparticle (GNP), pegylated gold nanoparticle with bifunctional crosslinker SH-PEG$_7$-COOH (GNP-PEG$_7$), attached pepsin onto pegylated gold nanoparticle (GNP-PEG$_7$-Pepsin).

1.3. Gold -Bulk Material and Nanoparticles

Gold is a rare precious metal with the elemental symbol Au, the atomic number of 79 and an atomic mass of 196.9666 u. It has a bright and shiny yellowish to reddish appearance, a relative low melting point of 1064.18 °C and it is highly ductile. Due to its density of 19.320 g mL^{-1} gold has a high specific weight [30]. These facts and the relatively simple handling make gold the most precious material for jewelry and valuables for centuries. Also, gold will not lose its shiny appearance by wearing it, like silver jewelry for example does. The reason for this resistance of corrosion is one of the least reactive behaviors of all chemical elements. Gold is only soluble with strongly oxidizing acids. With aqua regia (king`s water or royal water) chloroauric acid will be formed.

Today, gold is not only being important for jewelries and investments, also electronical devises and medicinal products contain gold. Currently, the best estimates suggest a

total mined amount of 190,040 t of gold was mined all over history (end-2017). Around 50 % of the new mined gold will be used for jewelry, 40 % for investments and around 10 % will be used for technology (http://www.gold.org, 21.05.2018).

Gold nanoparticles (GNPs) differ in appearance strongly from the bulk products. Based on the size of the particles, the color spectrum ranges from blood-red for smaller particles to pale violet for larger particles (see Figure 5 below) [31]. This phenomenon is based on the so-called localized surface plasmon resonance (LSPR) which is the light induced resonant oscillation of the electron collective of delocalized electrons which is caused by an external electric field [32,33].

Figure 5: Colloidal gold suspensions of various particle sizes. Photograph courtesy of Dr. Irawati Kandela, University of Wisconsin, BBPIC laboratory [31] (Reprinted with permission).

Size, shape, concentration, aggregation of the nanoparticles, environment and surface-adsorbed species influence the corresponding absorption spectrum when using this technique for the characterization of nanoparticles (SPR spectroscopy) [34,35]. Due to the different density of colloidal gold suspensions compared to solid gold, induced dipole interactions occur, which make the colloids appear more colorful. Here the relative absorption size is influenced by the shape/ geometry of the nanoparticles. Quantification is achieved by optical cross sections whose relative contributions are calculated

according to the Mie theory. The Mie theory offers as a model a correct solution of the Maxwell equations for compact spheres [36,37]. As the size of the particles increases, the plasmon band shifts toward a higher wavelength. This correlates with the Mie theory [38]. If the wavelength of the light becomes much larger in comparison to the size of the nanoparticles, standing resonance conditions are to be expected. The free electrons in the metal structures oscillate excited by the light, which is in resonance with surface plasmon oscillation. Absorption and scattering phenomena determine the resonance condition. This also depends on the shape, size and dielectric constant of the metal nanostructures, as well as on the surrounding material [33].

1.3.1. Historical Background

Metallic nanoparticles have been used since ancient times, especially as a dye in the glass and ceramic industries. A well-known example is the *Lycurgus Cup*, a Roman glass cup manufactured in the 4th century AD, which appears green in reflected light and ruby red when illuminated from the inside. This effect is caused by the presence of traces of gold and silver colloids in the range of about 40 ppm for gold and about 300 ppm for silver [39,40].

The *Lycurgus Cup* illuminated from outside (left) and from inside (middle) © of the British Museum. At the right side the *Mille Fleurs* vase, as an example of the *Family Rose* porcelain © The Guimet Museum in Paris - Réunion des Musées Nationaux [39].

Figure 6: Examples for the use of metallic nanoparticles in ancient times [39] (Reprinted with permission).

The use of gold nanoparticles as a red colorant has also been used for the manufacturing of porcelain goods. During the early seventeen century the secret of the Purple of Cassius described by Andreas Cassius of Leyden in 1685 reached China and was used, e.g. for the manufacturing of the beautiful Family Rose porcelain [41].

1.3.2. Theranostic Properties and Risks

The unique optical properties, such as localized surface plasmon resonance [32] and Mie scattering [42], make gold nanoparticles also interesting for theranostic (theranostic = therapy + diagnostic) approaches in the field of nanobiotechnology. As discussed by Khlebtsov *et. al.* [43] here, the therapeutic and diagnostic properties are combined with sensing properties of gold nanoparticles.

GNPs can be used as contrast imaging agents in cancer therapy for real-time monitoring as well as for controlled drug release. Therefore, GNPs can be used as a

carrier attached with drugs, peptides, proteins, such as antibodies, DNA and RNA to transport them to their place of use and for maximizing the individual and personalized aspects. However, studies are also known where GNPs are described as toxic when interacting with biological systems. Shape, size, surface and charge of the nanoparticles can have a decisive influence here [44].

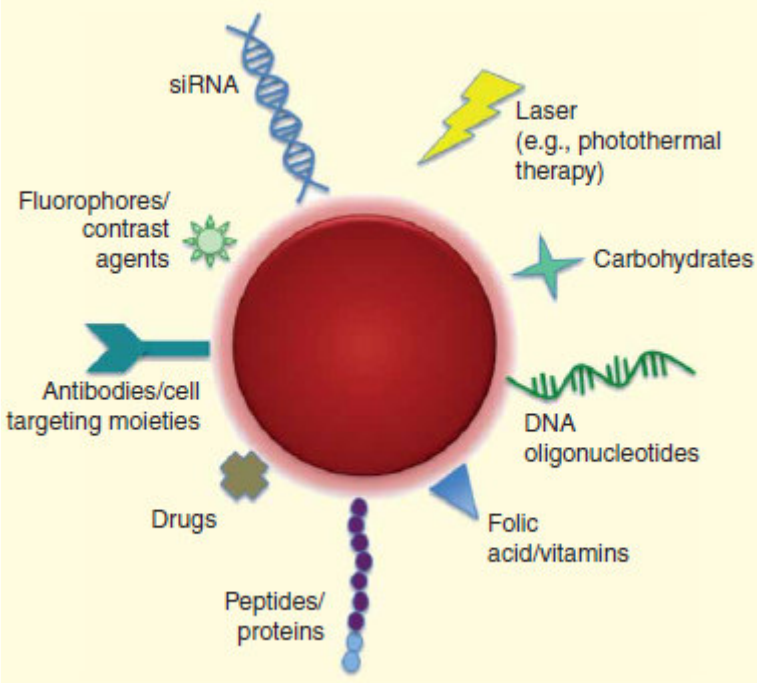

Gold nanoparticles as theranostic platform, e.g. as targeted vehicles for controlled drug release, laser-mediated photothermal therapy and gene therapy, as well as contrast imaging agents to allow for real-time monitoring of both disease and therapeutic progression [44].

Figure 7: GNPs as theranostic platform for several approaches [44] (Reprinted with permission).

Due to their small size, the nanoparticles can penetrate organic membranes such as cell walls. In experiments 2 nm GNPs with cationic ligands were able to penetrate and destabilize lipid membranes and, if the concentration was increased, destroy them. GNPs with anionic ligands did not show these effects. They even had a stabilizing effect on the lipid membrane when the pH was increased [45].

The positive theranostic properties of modified GNPs make them unique tools, but long-term studies should thoroughly test the effects of nanoparticles on living systems to exclude any toxicological side effects.

1.4. Current Technologies

While nanoparticles have been used as dyes in the past, the breakthrough in nanotechnology was initiated by Turkevich and Frens et al. [46-49] and Schmid and Brust et al. [50-52] by developing and describing methods for size-controlled syntheses of gold nanoparticles. Until today there are various methods for synthesis and characterization described, but also various practical applications of gold nanoparticles. A brief review of these utilizations is given in this chapter. Gold nanoparticle synthesis methods, surface modification and characterization are described in the following chapters.

1.4.1. Enzyme-Linked Immunosorbent Assay

The Enzyme-Linked Immunosorbent Assay (ELISA) was developed in parallel by 2 different working groups and published in 1971. The group around Eva Engvall and Peter Perlmann from the University of Stockholm had submitted their work in December 1970, Bauke van Weemen and Anton Schuurs from the Research Laboratories of NV Organon, Oss, The Netherlands, submitted their work in April 1971 [53,54]. This antibody-based assay is based on an enzymatic color reaction, wherein the antigen of interest is attached adsorptively onto a surface (today commonly a microtiter plate is used). An antibody bound to an enzyme is coupled to the antigen, and in the last step, an enzyme reaction with the corresponding substrate-color-complex results in a detectable color change.

These tests can also be modified with gold nanoparticles to achieve an amplification of the optical signal [55] or to modify the color reaction itself [56].

1.4.2. Pregnancy Test by Lateral Flow Immunoassay

Pregnancy tests can be based on a so-called lateral flow immunoassay (LFIA) which is an easy to handle and cheap test that generates results in minutes [57]. This qualitative immunochromatographic technique is based on a combination of thin-layer chromatography (TLC) and immunostaining with proper labeled antibodies. The antibodies are immobilized, bind and enrich human chorionic gonadotropin (hCG) from the urine sample and the result is displayed as a colored area [58,59]. The immobilized antibodies can be labeled with gold nanoparticles which can give a red to pink band at the detection line [59] and in addition amplify the signal [58]. GNPs also allow a different colored negative control (gray to blue) based on an aggregation of nanoparticles [59,60].

1.4.3. Lateral Flow Assay for the Monitoring of Digoxigenin

Apart from the pregnancy test, the lateral flow (immuno)assay (LFA) can also be used for other applications, as shown in a recent publication. The cardiac glycoside digoxigenin, which is used for the treatment of tachycardia, has a small therapeutic window. Minor increases in concentration can already lead to toxic effects. Easy-to-use techniques for examining the blood concentration level, especially for so-called home monitoring, can be essential. For the detection of digoxin and its derivative for the antibody coupling digoxigenin, a common gold nanoparticle lateral flow assay is used, which can be evaluated by means of a smartphone. For this purpose, a so-called dark box made of black cardboard was developed for home monitoring of the blood concentration level. For the visual evaluation of the LFA an app is used. The results of the app were compared with those of a high resolution bioimager and thus the function of the new system for quantitative determination could be confirmed [60].

1.4.4. Drug Test MAVAND Solutions GmbH Rapid STAT®

Drug tests can also be based on the lateral flow test using colloidal gold [61]. These on-site tests are easy to use, robust and deliver fast results for multiple drugs at the same time by analysis of oral fluid [62]. Worth mentioning here is the kit Rapid STAT® from Mavand Solution GmbH, Mössingen, Germany, with which up to 7 analytes can be detected simultaneously. These include amphetamine, benzodiazepine, cocaine, methadone, methamphetamine, ecstasy, opiate and THC (http://www.mavand.de/de/produkte/drogenschnelltests/rapid-statr.html, 06.08.2018). The kit has already been compared for several times with other on-site tests and chromatographic methods for checking the test kit results, and is used, for example, by the German police [62-64].

1.5. Materials and Shapes

In the synthesis of colloidal gold processed by a reduction of tetra chloroauric acid and stabilization of the particles by citrate (see Chapter 1.7 Synthesis of GNPs), typical spherical nanoparticles are formed [65]. Further variants of GNP preparation by changing the synthesis have been already discussed in literature. Thus, by switching from an aqueous system to *N*,*N*-dimethylformamide (DMF), which contains polyvinylpyrrolidone (PVP, commonly called povidone) and by a slight addition of salt (NaCl), forms such as cubes, tetrahedrons and octahedrons be synthesized. By increasing the concentration of tetra chloroauric acid in aqueous solution hexagonal nano sheets with a thickness of about 60 nm and a size of approximately 900 nm can be synthesized [66].

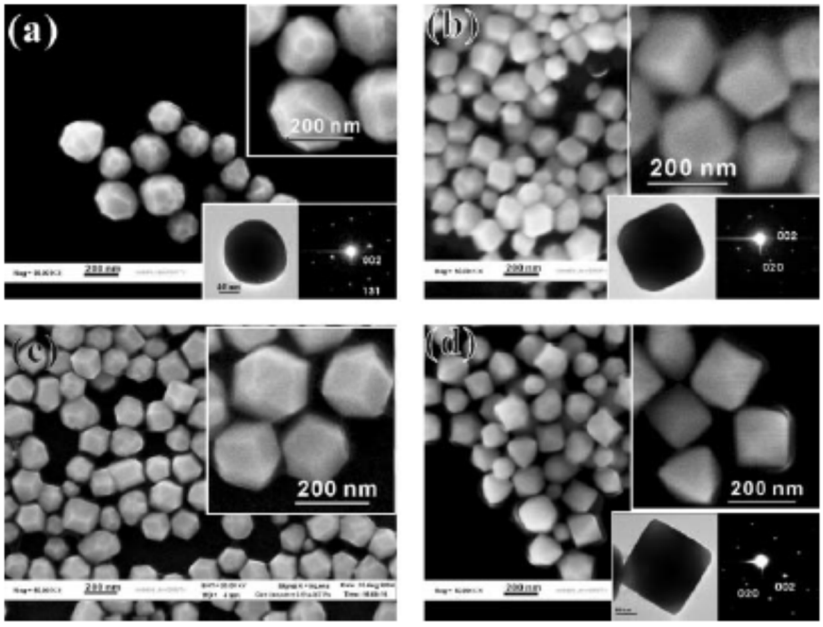

SEM images of the as-prepared truncated tetrahedral (a), cube (b), cubic (c), octahedral (d) gold nanoparticles. Insets in the figures show the enlarged SEM image (top-right), the TEM image of an individual typical nanoparticle (left) and its corresponding SAED (selected area electron diffraction) pattern (right) [66].

Figure 8: SEM images of differently shaped gold nanoparticles [66] (Reprinted with permission).

In addition to the spheres, various other forms of gold nanoparticles, such as Au rods [67], Au stars, Au-Ag cages [43] and silica-gold nanoparticle-clusters [68] are described in literature.

1.6. Why Gold as Starting Material for the Synthesis of Heterogeneous Nanobiocatalysts?

It was decided to start with GNPs as a core for further preparation of the heterogeneous nanobiocatalysts. This decision is based on several interesting properties of these kind of nanoparticles. The handling of colloidal gold suspension is comparable to a liquid. So, it is possible to use classical pipettes for transferring the suspension. This easily enables to accurately and precisely handle miniaturized sample volumes of 1 mL and less down to 1 µL scale or so with appropriate pipettes. A big advantage therefore is to reduce the

volume of valuable samples, such as monoclonal antibodies. These small sample volumes are quite sufficient for analysis by liquid chromatography coupled with mass spectrometry. Due to the materials' specific density of the gold core it is easily possible to remove the nano biocatalysts from the sample by simple centrifugation steps with a bench-top centrifuge/mini spin. Therefore, 12,000 until 13,500 rounds per minute (rpm) have been proven sufficient. These materials' specific advantages make them a useful tool for the analysis of different kind of samples like therapeutic peptides and proteins, including monoclonal antibodies [69]. Additionally, faster reaction kinetics for similar approaches are described in literature due to the immobilization of the enzymes [70]. The reason for this effect is not fully understood yet, however, it seems that locally higher concentrations of substrates can be achieved.

1.7. Synthesis of GNPs

Figure 9 displays the synthesis of spherical GNPs according to the method of Turkevich-Frens [46,49,71]. This classical and straightforward approach is suitable for the synthesis of around 10 to 30 nm particles. It is also possible to prepare larger particles, but this will influence the monodispersity and particle shape negatively.

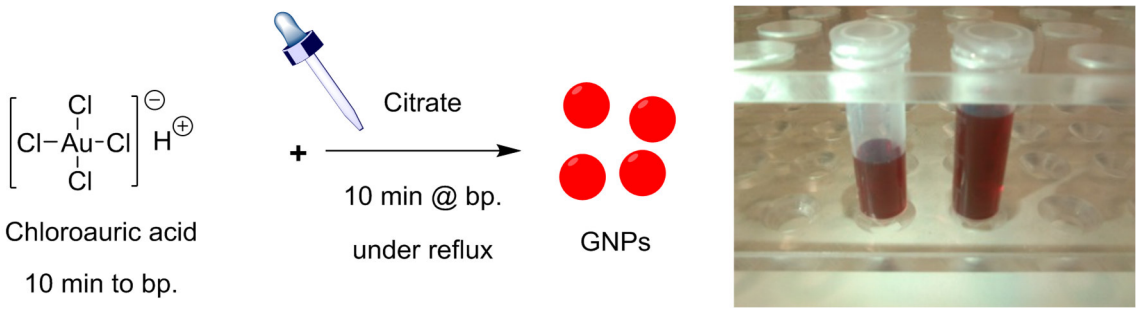

Figure 9: Synthesis method for GNPs described by Turkevich-Frens

The preparation is based on the reduction of gold (III) chloride trihydrate with trisodium citrate and simultaneous stabilization of GNPs by citrate due to attachment on the GNP surface providing them a negative surface charge. Therefore, citrate is a reducing and

stabilization agent for the size-controlled synthesis of gold nanoparticles. With an increasing amount of citrate, the particle size will decrease. This phenomenon was described by the nucleation-growth process (Figure 10) by Polte et al.[72].

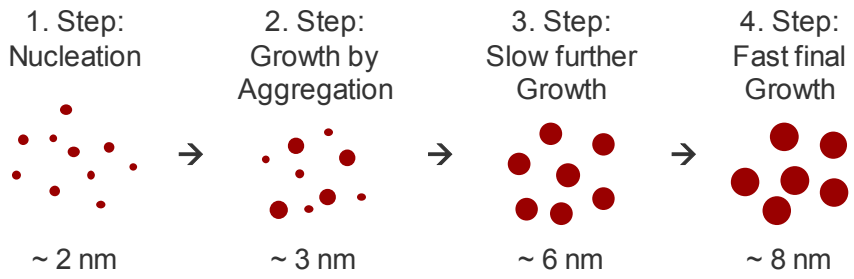

Figure 10: Nucleation-growth process (adapted from Polte et al. [72])

In the first nucleation step, initial cores will be formed. They will grow by fast and slow aggregation steps and will at last reach their final size.

A smaller particle size from 1-3 nm with a surface coating of thiols can be achieved with the Brust method from 1994 [73]. This approach is based on a reduction of $AuCl_4^-$ by sodium borohydride in the presence of an alkanethiol in a two-phasic water–toluene mixture.

A more actual approach is the biological synthesis of gold nanocubes by bacillus licheniformis after a 48 hours' incubation at room temperature in aqueous solution [74]. The gained polydisperse nanocubes are ranged in the size from 10 to 100 nm.

1.8. Surface Modification of GNPs

The synthesized GNPs are an interesting starting material for various functionalization's. Functionalization by coating of polymers or polyelectrolytes, via bifunctional crosslinkers based on polyethylene glycol (PEG), as well as adsorptive binding of proteins should be

mentioned at this point. The gold particles are here used as a solid core which can be modified with a hydrophilic biocompatible shell.

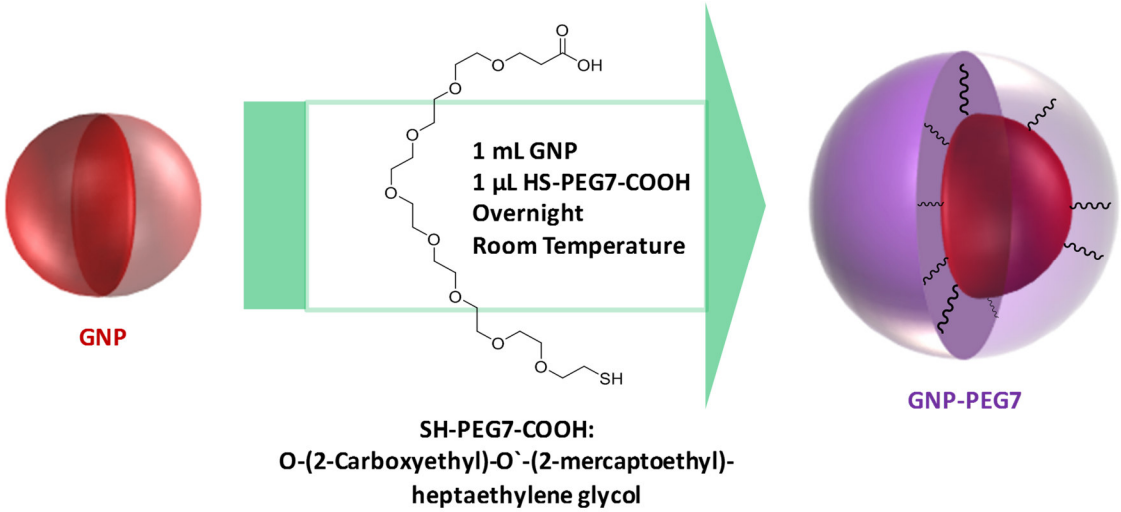

Figure 11: Immobilization of bifunctional crosslinker with SH-PEG$_7$-COOH

For example, by using O-(2-carboxyethyl)-O`-(2-mercaptoethyl)-heptaethylene glycol (SH-PEG$_7$-COOH) a self-assembled monolayer (SAM) obtained by dative Au-S covalent bonding can be formed as a first layer of the gold core.

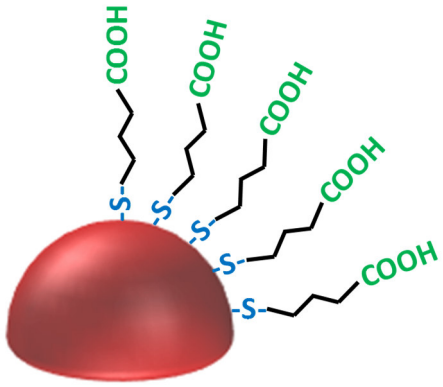

Figure 12: Self-assembled monolayer (SAM)

For building a second layer a crosslinking reaction can be performed with the functional molecule of interest, e.g. an enzyme, affinity ligand, or antibody. Crosslinking can be

described as the building of covalent bonding between two or more molecules. Between the carboxylic acid groups of the attached bifunctional HS-PEG$_7$-COOH linker and the amino groups of the enzyme NHS-EDC coupling is obvious. Here, NHS (*N*-Hydroxysuccinimide) can convert carboxylic acids to NHS esters under neutral to slightly basic conditions if activation reagents like EDC (1-ethyl-3- (3-dimethylaminopropyl) carbodiimide) or EDAC (*N*-(3-dimethylaminopropyl)-*N'*-ethylcarbodiimide) are present. EDC is forming active ester intermediates with carboxylic acids. These intermediates react readily with primary amino functions, such as of peptides or proteins, which are significantly more nucleophilic than alcohols, to form amide crosslinks. NHS is not mandatory for carbodiimide reactions, but the use greatly increases the coupling efficiency by forming NHS ester intermediates [75].

If pepsin is to be crosslinked to the carboxylic acid groups of the attached bifunctional HS-PEG$_7$-COOH linker, a "one-pot reaction" with EDC under weakly acidic conditions can be performed. Since pepsin is irreversibly inactivated from a pH of about 6 [76], the coupling reaction in slightly acidic conditions is preferable to NHS-EDC coupling at neutral to slightly basic conditions. Remaining EDC-activated carboxylic groups can be end-capped with Tris moieties (tris(hydroxymethyl)-aminomethane). In this final synthesis step, pepsin-functionalized GNPs with residual carboxylic acid groups are obtained, which improve the colloidal stability and storage stability of the nanobiocatalysts [69,77].

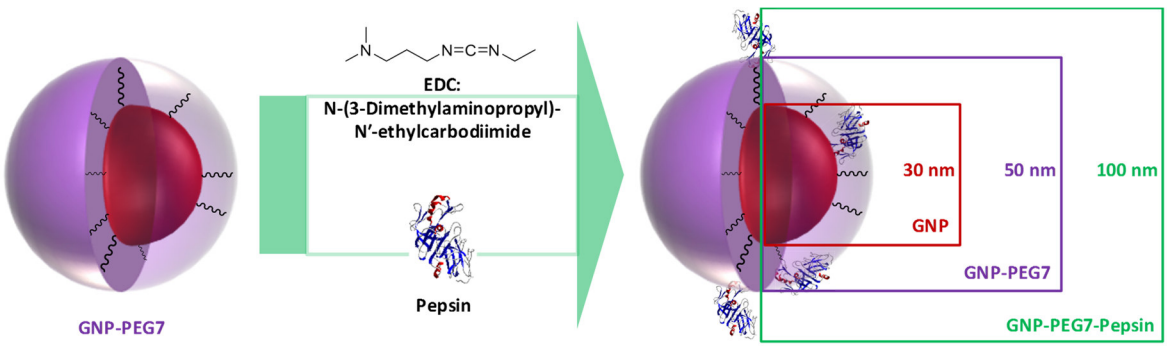

Figure 13: Activation of HS-PEG$_7$-COOH by EDC and immobilization of Pepsin

A direct adsorptive binding of enzymes by ionic and hydrophobic interactions on gold nanoparticles should also be mentioned here as an easy and suitable possibility [69].

1.9. GNP Characterization

An important topic in the synthesis and functionalization of gold nanoparticles is their characterization. Here, techniques are interesting that can give an idea of particle shape and size, but also information about the molecular structure and surface properties are important parameters. Such methods include various techniques, including spectroscopic and microscopic methods. For the characterization of nanobiocatalysts, useful microbiological and biophysical techniques can also be used. Due to the large number of characterization techniques, however, only a brief introduction of some popular techniques is given below, which were also used in the present work.

1.9.1. Electron Microscopy Technique

The crystal structures and surface of the nanoparticles influence their chemical and physical properties. Transmission electron microscopy (TEM) is for the visualization and characterization of nanoparticles a well described technique. Here, an electron beam is focused and transmitted through a sample to form an image. The electron beam is interacting with the sample atoms by elastic and inelastic scattering. A TEM image can be generated since the electron intensity distribution behind the sample can be recorded onto a fluorescent screen. To generate differences in electron densities between sample and matrix, the nanoparticles are placed on a copper grid, dried and coated with a thin carbon layer [78,79]

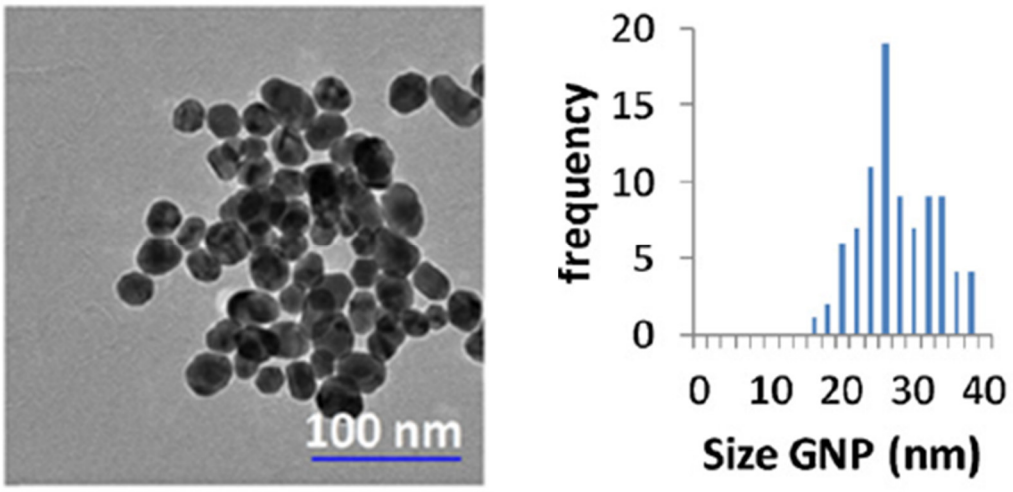

Figure 14: TEM analysis of colloidal gold suspension and histogram of statistical size analysis [70], redrawn in modified form (Reprinted with permission).

A statistical evaluation of the particle size distribution is also possible with TEM analysis. Therefore, the particle size of a defined number of particles can be analyzed and compared [70,80].

1.9.2. Vis-Spectroscopy

UV-Vis spectroscopy is a cost-effective and an easy-to-use characterization technique that can be performed with standard laboratory equipment in almost every laboratory. Colloidal gold has a characteristic UV-Vis absorbance spectrum which can be attributed to the presence of localized surface plasmon resonance in the visible part of the spectra [81]. The size of the gold nanoparticles can be evaluated by a shift in the absorbance maximum of the spectra. Also the peak width of smaller particles is more narrow than that of bigger, e.g. functionalized, particles (see Figure 15) [82].

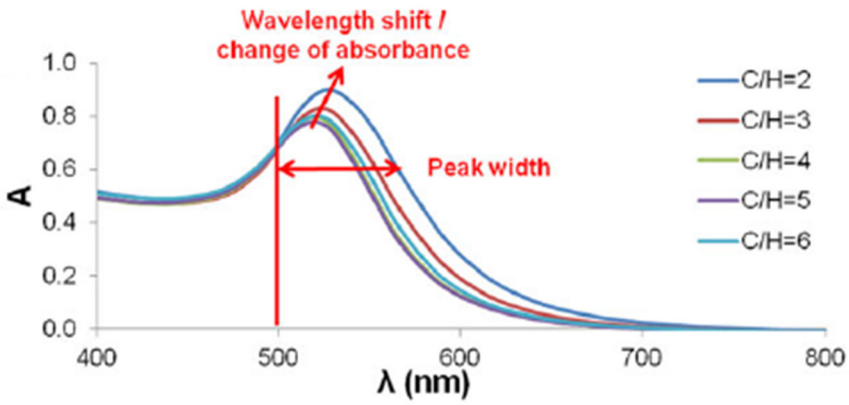

UV-Vis study with different citrate/HAuCl4 (C/H) ratio. With a higher citrate ratio particles and peak width get smaller [82].

Figure 15: Vis-Spectroscopy study of citrate stabilized gold nanoparticles with different particle sizes [82] (Reprinted with permission).

In addition to size, UV-Vis spectroscopy can also be used to determine the concentration of colloidal gold. If the molar concentration and volume of $HAuCl_4$ used is known, and also the number of gold atoms per nanoparticle depends on the particle diameter, the gold atoms in solution can be calculated. With the number of gold atoms in solution, the concentration of GNPs can then be calculated using the known volume of the solution and the Avogadro number [82]. Other approaches for the determination of the GNP concentration by using UV-Vis spectroscopy have already been described in the literature [80].

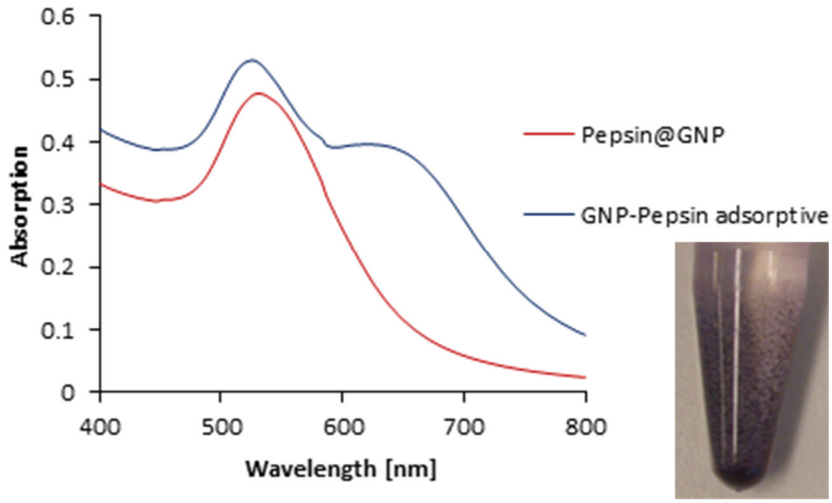

Vis-spectra of Pepsin@GNP (pepsin-modified GNPs with PEG_7 spacer) and adsorptively bound pepsin on GNPs. Because of a high colloidal stability, the peak of Pepsin@GNP shows a good shape. The undefined peak shape of adsorptively bound pepsin is due to particle aggregation [69]. As an addition this figure shows a picture of aggregated functionalized GNPs (own data).

Figure 16: Vis-Spectroscopy study of Pepsin@GNP and GNP-Pepsin adsorptive [69] (Supplementary Material, Reprinted with permission).

The colloidal stability can also be determined by the shape of the Vis spectra. An undefined peak shape, e.g. shoulders or similar, is due to particle aggregation. Good colloidal stability of the nanoparticles can be deduced from nice and narrow peaks in the UV-Vis spectra.

1.9.3. Shelf Life and Stability Studies

For the determination of the shelf life stability of nanoparticles the UV-Vis spectroscopy could be an interesting tool. Based on one batch, measurements can be carried out at defined time points to study the long-term colloidal stability. Different synthesis stages can be checked to complete the results.

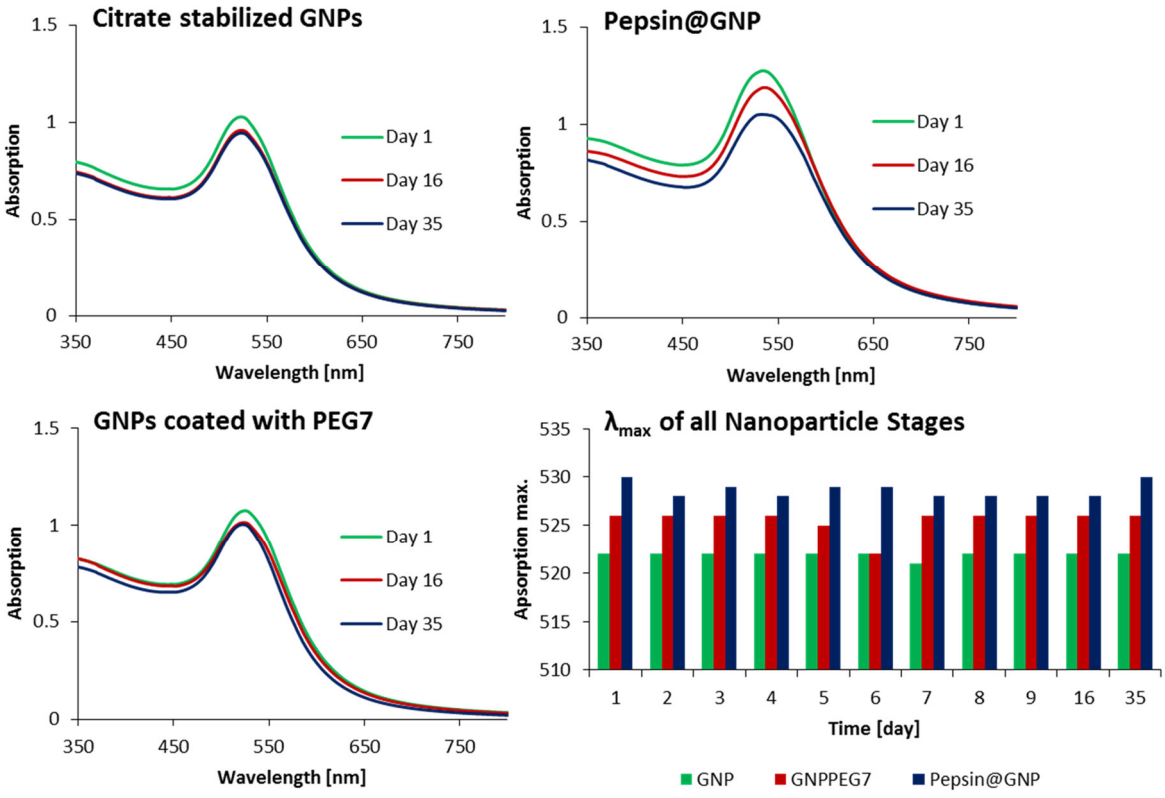

Colloidal stability and shelf life of functionalized nanoparticles. (a) Citrate-stabilized GNPs, (b) GNPs coated with bifunctional PEG spacer having carboxy-terminated surface and (c) immobilized pepsin-GNP conjugate. (d) Absorption maxima of the SPR band of all nanoparticle stages measured over 35 days. All samples were diluted 1:5 in ddH2O. Samples were stored at 4 °C [69].

Figure 17: Shelf Life and Stability Studies of all nanoparticle stages [69] (Supplementary Material, Reprinted with permission).

Based on the quality of the UV-Vis spectra, the colloidal stability of the gold nanoparticles can be deduced and the stability within a defined period can be determined.

1.9.4. Dynamic Light Scattering (DLS)

The determination of the dynamic light scattering (DLS) is a very important tool for the characterization of particle sizes for dissolved analytes, such as dispersions and colloids, in the range from nanometers to micrometers. In polydisperse systems, the particle size of a sample varies. Here, not the particle size but the particle size distribution (PSD) of a sample is determined. Due to the strong light-scattering

properties of colloidal gold, the DLS is particularly well suited for their characterization [83,84].

For the determination of the hydrodynamic radius monochromatic and coherent laser light is used for illumination of the particles. The Rayleigh scattering is analyzed by a photon detector. The scattering intensity fluctuates due to the Brownian motion of the particles and can be analyzed over the time on a microsecond timescale. The measured fluctuations, which reflect the diffusion rate of the particles, are determined via autocorrelation which allows a calculation of the diffusion rate. The diffusion coefficient D can also be seen as a measure of the movement of the particles [85].

$$D = \frac{k_B T}{6\pi\eta r}$$

Stokes-Einstein equation (1)

D	diffusion coefficient (in liquids)
k_B	Boltzmann constant
T	absolute temperature
η	dynamic viscosity
r	hydrodynamic radius for spherical particles

With the Stokes-Einstein equation the hydrodynamic radius R_h can be related to the diffusion coefficient D (replace D by R_h in Stokes-Einstein equation). The rate of diffusion is represented by the term R_r, the diameter of a rigid sphere, their diffusion is comparable to that of the analyte [85].

A sample of synthesized nanoparticles differs normally in particle sizes. They are not homogeneous and therefore not monodisperse but varies in size and shape. This polydispersity is also referred to as size distribution and denotes the degree of particle to particle size variability. This measure of the heterogeneity of molecule and

particle sizes is called dispersity and the polydispersity index (PDI) indicates the variance of the distribution [86,87].

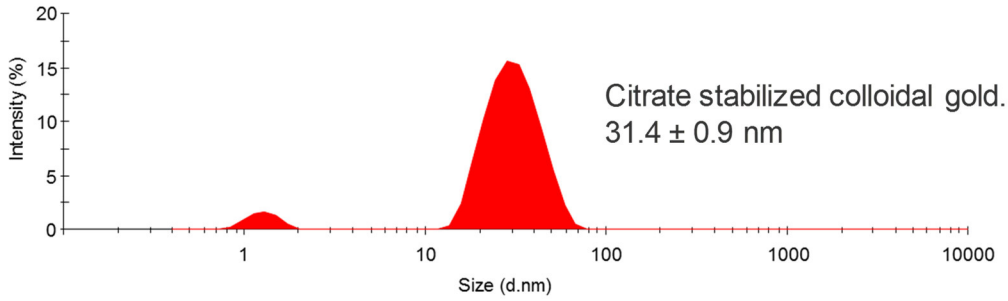

Figure 18: DLS study of citrate stabilized colloidal gold with an average particle size distribution of 31.4 ± 0.9 nm (own data)

For nanoparticles with the diameter d, the intensity of the scattered light is proportional to the square of the molecular mass or to the sixth power of d (d^6). DLS is therefore more sensitive to larger particles than smaller particles, and consequently the relative quantities of multimodal particle distributions are distorted. The average particle size in this situation is usually overestimated. Larger particles generally show much greater scattering than smaller particles. In addition, some aggregates can interfere the analysis of smaller particles, resulting in a less accurate result. A quantification of size distribution is not possible by DLS [85,84].

1.9.5. Nanoparticle Tracking Analysis (NTA)

Nanoparticle tracking analysis (NTA) is a direct real-time analysis. The method is similar in principle to DLS. The Brownian motion of particles is detected and is related to the size. Since the light scattered by the nanoparticles, unlike to DLS, is detected here with a high-resolution CCD camera and thus every particle size can be detected independently of one another, so NTA overcomes the disadvantages of DLS. The result of the size distribution is therefore more accurate and independent of the polydispersity of the analytes. A disadvantage of the NTA, in comparison to DLS, is

the lower working dynamic range and that particles smaller than 20 nm cannot be sufficiently detected [84,88].

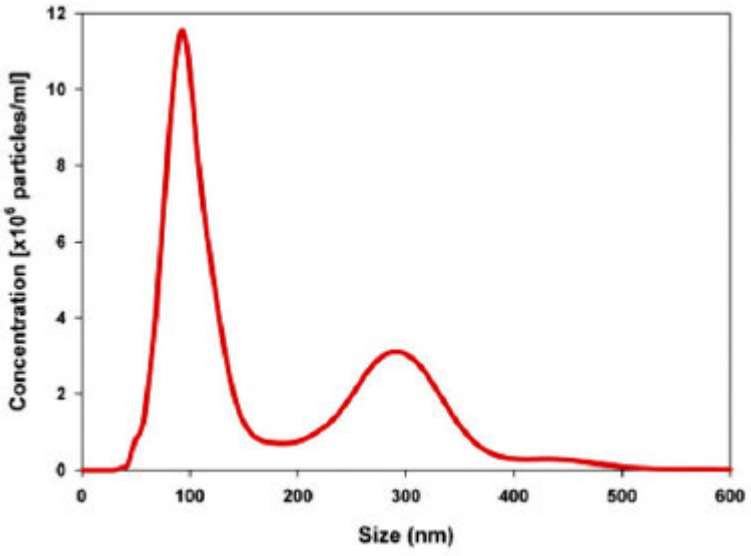

Figure 19: NTA measurement of particle size and concentration. Result of 100 nm and 300 nm polystyrene beads mixture (ratio 5:1) [88] (Reprinted with permission).

1.9.6. Zeta (ζ) Potential by Electrophoretic Light Scattering (ELS)

Colloidal stability, electrophoretic mobility, and the influence of electrolyte solutions can be described using the Derjaguin-Landau-Verwey-Overbeek (DLVO) theory. Traditional forces of particle-particle interactions, such as Van der Waals attraction and electrostatic repulsion, are crucial for the theoretical description. Thereafter, the total potential energy of action is the sum of attractive Van der Waals interactions and electrostatic repulsion or in general, the sum of adsorptive and dissociative processes at the interface. Other structural contributions to the interaction potential can be considered (hydration and osmotic power) if the particles are suspended in a suitable medium (liquid or gaseous) [89,90]. Charge carriers of both phases interact with each other. If charged particles are in suspension, the charge state at the particle surface can be affected by dissociation of adsorbed charged molecules. According to the principle of the electrical double layer of counter ions, which is formed near the surface of a charged particle, the surface charge of the suspended particles is

generally compensated by diffuse distributed counterions for charge neutrality of the overall system (potential tends towards zero and at infinite distance to the particle). This involves the repulsion of co-ions from the solvent, but also the attraction of counterions (see Figure 20).

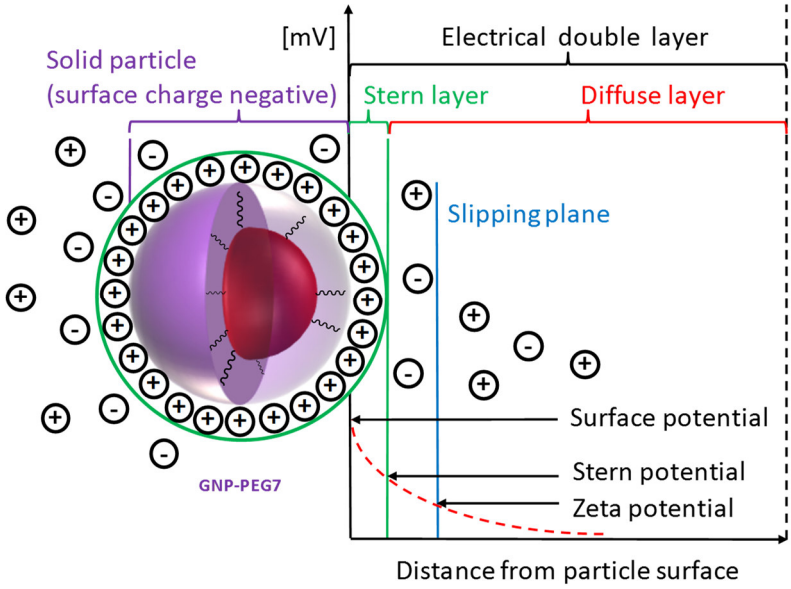

Figure 20: The electrical double layer (adapted from Malvern Instruments Ltd. [90])

The electrical double layer can be divided into a compact layer around the particle and a more diffuse distributed layer beyond. This compact layer is also called Stern layer and is provided by DLS measurement as the hydrodynamic size (particle plus fixed layer of solvent ions, see chapter 1.9.4). Ions within the stern layer are strongly bond on the particle surface, means the counterions in this layer are immobile due to the strong electrostatic attraction. This achieves a linear decrease in the electrostatic potential. The Stern layer followed by the diffuse layer in which the electrostatic potential decreases exponentially with the distance from the particle surface. This layer consists of loosely connected counterions. Solid particles and liquid phase are constantly in motion. In this case ions are sheared off in the diffuse layer. As a result, a measurable potential difference is formed at this shear plane or slipping plane, which is characterized as zeta (ζ) potential, or the electrical potential between the

double layer at the slipping plane and the surrounding solvent [91,90,92].The ζ-potential provides information on colloidal stability by means of the potential difference between the dispersion media and the fixed layer of fluid ions around the particle. The electrophoretic mobility μ_E is the analytically determined value and the ζ-potential will be calculated with the Smoluchowski equation [91].

$$\mu_E = \frac{\varepsilon \cdot \zeta}{\pi\eta}$$

Smoluchowski equation (2)

μ_E electrophoretic mobility

ε dielectric coefficient

ζ zeta potential

η dynamic viscosity

For the experimental determination of the zeta potential, various methods based on the electrokinetic effects, such as electrophoresis, electroosmosis and flow potential, can be used [91]. Electrophoresis refers to the movement of particles in an applied electric field. This principle is also used in electrophoretic light scattering (ELS) for sample testing. In an applied electric field, a laser beam is divided into a respective reference and scattering beams. The scattering beam is passed through the sample, while the reference beam is passed around the measuring cell. The electrophoretic drift velocity can be indicated by the recombination of the scattering and reference beam, since this generates a difference frequency. Finally, the electrophoretic mobility μ_E is mathematically accessible via the electrophoretic drift velocity [93].

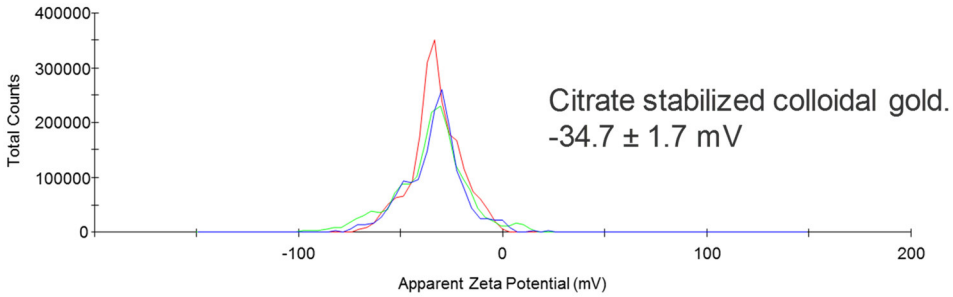

Figure 21: ζ-potential study of citrate stabilized colloidal gold with an average ζ-potential of -31.7 ± 1.7 mV (own data)

By measuring the electrophoretic drift velocity with ELS in disperse systems, the ζ-potential can be determined by electrophoretic mobility. In accordance to the DLVO theory the ζ-potential can be used for the qualitative prediction of colloidal stability. Sufficient colloidal stability is also confirmed by ζ-potentials higher than values of ± 25 to 30 mV, depending on the literature while values of ± 10 mV are considered approximately neutral [94,69]. If the disperse nanoparticle systems are not sufficiently balanced by electrostatic repulsion, these high electrostatic potentials are required to overcome the electrostatic attraction of the Van der Waals interactions, which are considered to be the main cause of aggregation of nanoparticles [69,94].

1.9.7. Resonant Mass Measurement

While the surface coverage of the nanoparticles by proteins can be determined indirectly with microbiological methods such as the Lowry assay (see chapter 6.8), the mass of the nanoparticles in the femtogram to attogram region can be determined directly with the Resonant Mass Measurement (RMM) [95]. With this technique, the particles are detected and counted by micro-electromechanical systems (MEMS). As the resonant frequency of the suspended microchannel resonator (SMR) is very sensitive, particles with a different density compared to the surrounding solvent can be detected. Due to the buoyant mass (M_B) of the particle a frequency shift at the suspended microchannel resonator embedded in a microfluidic channel can be analyzed when a particle passes through. If the resonator is passed by a particle with

a higher density than that of the solvent, this leads to a decrease in the resonance frequency of the microchannel. The decrease of the frequency is proportional to the buoyant mass of the particle [95,29]. When the density of the solvent (e.g. water) and the gold nanoparticles is known the dry mass of the particle can be calculated with the buoyant mass.

$$M = \frac{M_B}{\left(1 - \frac{\rho_{fluid}}{\rho_{particle}}\right)}$$

(Dry) mass calculation (3)

M dry mass

M_B buoyant mass

ρ density of the fluid and the particle

If also the corresponding data for the coating molecules is available ($\rho_{coating}$), the mass of them can be calculated by comparing the RMM data of uncoated and coated particles (mass balance ΔMB) according to equation (3) [29].

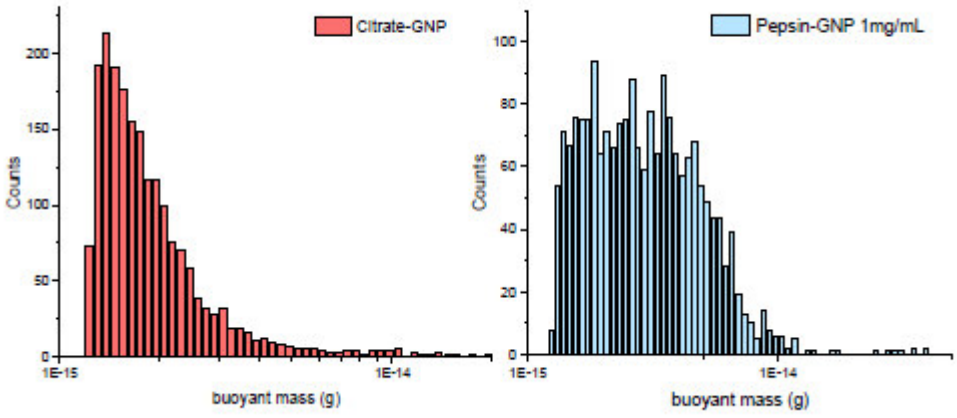

Histograms of buoyant mass measurement by RMM of citrate-capped GNPs and pepsin-coated GNPs (obtained from 1.04 mg mL^{-1} pepsin in reaction mixture). Samples were diluted 1:5 (v/v) with ultrapure water before measurement [29].

Figure 22: Resonant Mass Measurement of coated and uncoated gold nanoparticles [29] (Reprinted with permission).

1.9.8. Taylor Dispersion Analysis

Taylor dispersion analysis (TDA) is a suitable method for the determination of the diffusion coefficient and thus the hydrodynamic radius of biopharmaceuticals [96] [29]. It was described by G. I. Taylor in 1953 [97] and it was enhanced in 1956 by Aris with respect to the longitudinal diffusion of molecules [98]. The Taylor dispersion is an effect in fluid mechanics where shear flow increases the effective diffusivity of a species and thus facilitates the balancing of a concentration gradient. In the case of pressure-driven fluids in cylindrical capillaries, the flow velocity to the channel edge decreases due to the viscosity of the fluid and friction at the tube wall (known as convection). Here the fluid flows under laminar conditions according to Poiseuille and a parabolic flow profile is formed as displayed in Figure 23. This implies that the velocity of the liquid decreases radially from a maximum in the center of the tube to a minimum at the tube walls. The combination of radial diffusion and convection causes a symmetric concentration distribution of the injected sample molecules (see Figure 23) [99].

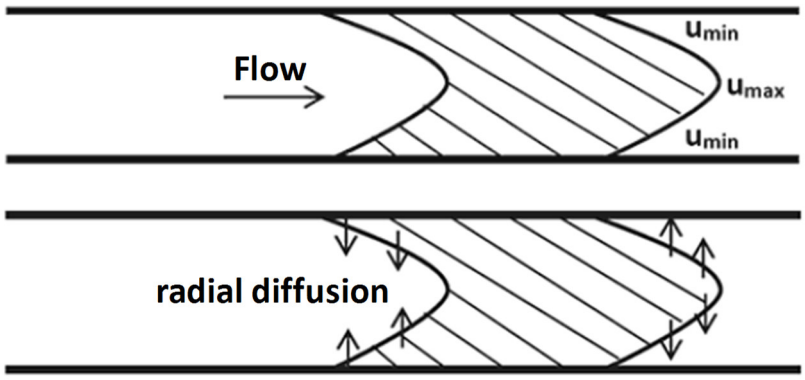

The axial spreading of the solute along the direction of flow whereat the flow velocity decreases radially from the maximum u_{max} in the center of the tube to a minimum u_{min} at the tube walls according to fluid viscosity and friction. Due to the combination of radial diffusion and convection a symmetrical concentration distribution of the injected sample molecules occurs [99].

Figure 23: Axial spreading by convection and radial diffusion (adapted from Malvern Instruments Ltd. [99])

Here, the peak broadening of the sample injected into an existing solvent flow of known viscosity is analyzed. The sample is moved through the capillary due to the hydrodynamic pressure. The peak broadening of the sample zone is monitored by absorbance measurement of a detector at two consecutive measuring windows in the capillary. From this and by using the time data of the two peak centers detected at the two capillary windows the hydrodynamic radius R_h can be deduced [96] [29]. As additional sample information the viscosity can be determined.

$$R_h = \frac{4 \cdot k_B \cdot T \cdot (\tau_2^2 \cdot \tau_1^2)}{\pi \cdot \eta \cdot r^2 \cdot (t_2 - t_1)}$$

R_h calculation (4)

R_h hydrodynamic radius

k_B Boltzmann constant

T temperature

τ standard deviation (peak broadening)

η viscosity

r radius for the capillary

t peak center time

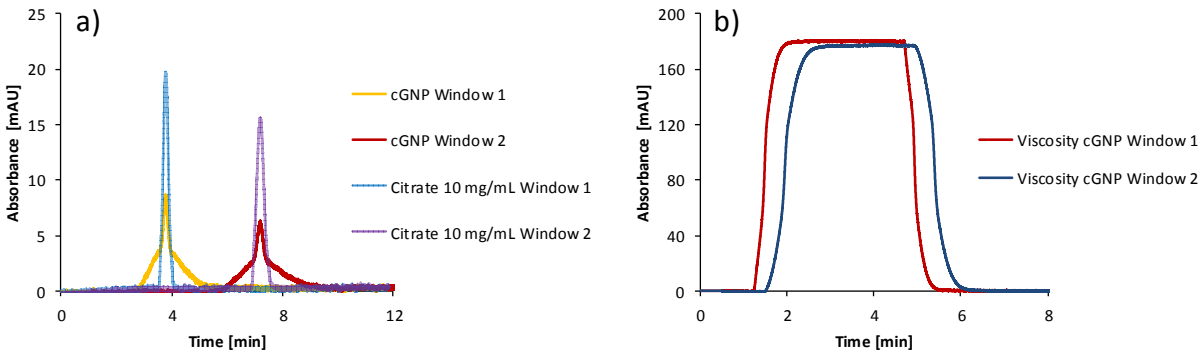

Taylorgram for citrate and citrate stabilized GNPs a) and straylight corrected viscosity measurement of citrate stabilized GNPs b). Both results show the signal shifts of window 1 and 2 [29].

Figure 24: Taylor dispersion analysis of citrate and citrate stabilized GNP [29] (adapted from paper and Supplementary Material, Reprinted with permission).

1.9.9. Protein Determination by Lowry Assay

Another important question in the characterization of protein-functionalized nanoparticles is the amount of protein that could be immobilized on the particles. Since in the present experiments free pepsin is bound onto the nanoparticles, it must be investigated whether such an immobilization has taken place and if yes, what is the amount of immobilized protein? With enzyme assays such as the Lowry assay [100,101], this parameter can be investigated but there are other determination techniques like the Bradford [102] and the bicinchoninic acid or Smith assay (BCA) [103] as displayed in Table 1 [104,105]. Details for the protein assays are described in the Protein assay technical handbook from Thermo Scientific published in 2017 [105]

This chapter gives a brief overview of different methods, but it mainly describes the Lowry assay.

Table 1: Protein determination techniques

Overview of colorimetric protein assay techniques, such as Lowry, BCA and Bradford assay [104,105]

Assay	**Lowry**	**BCA (Smith)**	**Bradford**
Method	Biuret + Folin & Ciocalteu's phenol reagent		Coomassie (Brilliant Blue G-250)
Detection [nm]	650	562	595
Range [µg/mL] (Thermo Scientific Assay Kit)	1 - 1500	0.5 – 20 (Micro BCA)	1 - 1500
Peptides	tyrosine, tryptophan	cysteine, cystine, tryptophan, tyrosine and peptide bond	lysine, arginine

Lowry assay is based on two separate reactions. In the biuret reaction, a blue-violet complex is formed in alkaline solution between the peptide bonds and Cu(II) ions. In the second step, Cu(II) is reduced to Cu(I) due to the peptide bond. Furthermore, Cu(I) reduces the yellow Folin & Ciocalteu's phenol reagent (a solution of molybdophosphoric acid and phosphotungstic acid) to molybdenum blue. Detection is performed with a spectrophotometer at 650 but related to the protein of interest a wavelength modification of 600 or 750 nm is suitable [104,106]. The results can be quantified by using a calibration function. Protein levels in the lowest range of 0.01 to 1 mg/mL can be determined [101]. With assay kits provided by Thermo Scientific a range from 1 to 1500 µg/mL is possible [105].

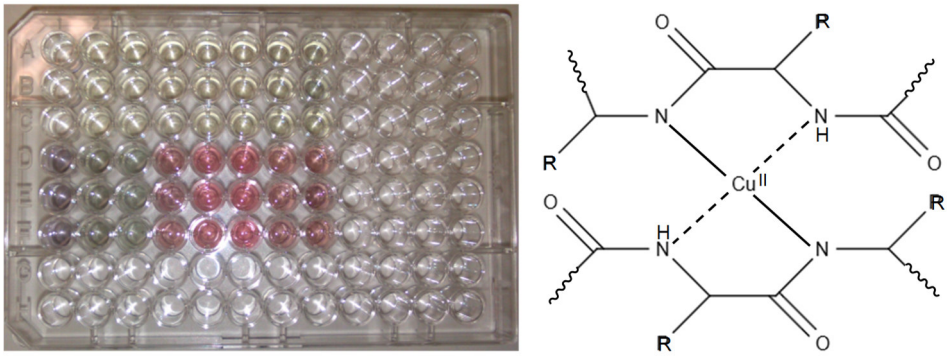

Figure 25: Lowry assay in 96 well plate (own data) and Cu(II)-protein-Biuret complex (adapted from Matissek et al. [107])

To investigate the enzyme immobilization a stock solution of known concentration of pepsin was produced. This solution was added to the gold nanoparticles and separated again from the nanoparticles by centrifugation after defined reaction conditions. The initial concentration of the stock solution and the separated pepsin solution was analyzed by Lowry assay. The amount of immobilized pepsin could then be calculated back by using mass balance equation.

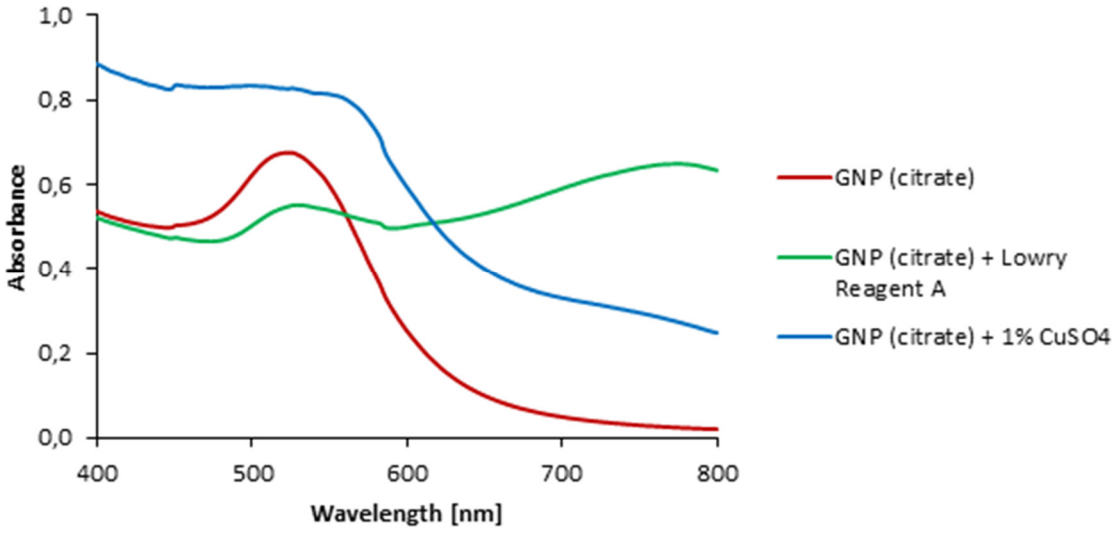

The behavior of citrate stabilized GNPs in the presence of Lowry reagent A and 1 % CuSO4 [69].

Figure 26: Trouble-shooting Lowry assay by vis-spectroscopy [69] (Supplementary Material, Reprinted with permission).

Investigation of the amount of immobilized protein directly on the gold nanoparticles could also be very interesting. Studies show this is not possible because the nanoparticles aggregate in the presence of Lowry reagent A and 1% CuSO4, among other things which could not be clarified. This behavior could be confirmed by UV-Vis spectroscopy [69].

1.9.10. Bioactivity Test by Michaelis-Menten Kinetic Studies

While the amount of immobilized protein could be determined by using Lowry assay, further studies are needed for the determination of the bioactivity of the bound enzymes. This can be done by means of Michaelis-Menten kinetic [108,109], but a suitable method to determine the conversion of a test protein (e.g. CYC) with the functionalized nanoparticles at defined times is required [69]. HPLC analysis can help here. The test protein must be detectable with the appropriate method. The protein peak must be baseline separated from the signals of the degradation products. Thus, a precise quantification of the test protein amount is guaranteed, and the Michaelis-Menten parameters can be calculated according to the Lineweaver-Burk model [110].

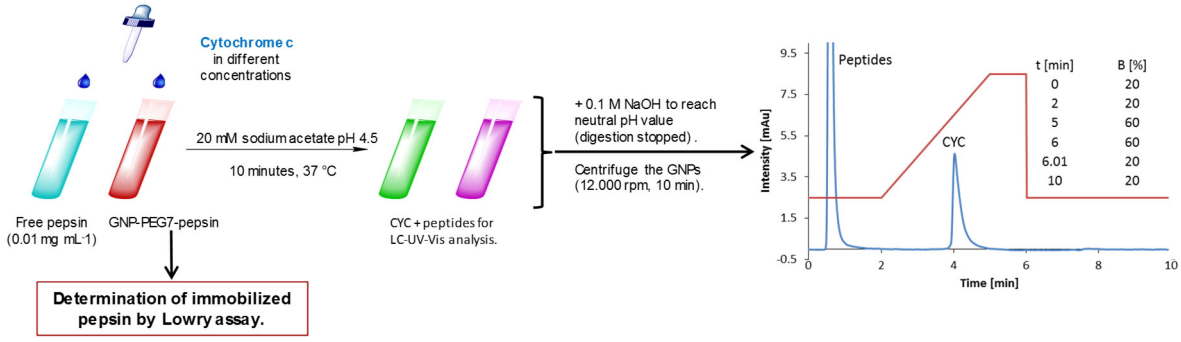

Figure 27: Bioactivity test by Michaelis-Menten Kinetic studies. Chromatogram taken from [69] (Supplementary Material, Reprinted with permission).

The enzyme-substrate reaction can be described by the equation below (see Figure 27). As biocatalysts enzymes E form a reversible complex [ES] with their substrate S.

Both result the enzyme-substrate complex [ES], where the substrate is converted to the product P by the intermediate step of the substrate-product complex [EP].

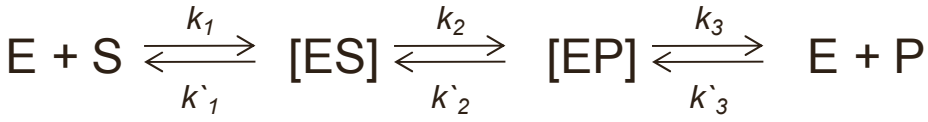

Figure 28: Reaction equation for enzymatic digestion

The velocity constants k_1 to k_3 describe the forward rate and the constant $k`_1$ to $k`_3$ the reverse rate of the enzymatic reaction. The reverse reaction to the substrate is negligible under the conditions of enzyme kinetics with low product concentration. Also, $k´_2$ is usually much smaller than k_3, so the simplification of the formation of E + P without the intermediate step [EP] is justified.

In general, enzymes are able to balance fluctuating substrate concentrations very quickly by adjusting their activity to the substrate amount. This means that the concentration of the enzyme-substrate complex remains constant on the slower time scale which is valid for the process of product formation [111]. For the description according to Michaelis-Menten also the assumption of a steady state applies.

The Michaelis-Menten kinetics derived from the reaction equation can generally be represented as follows:

$$v_0 = \frac{v_{max} \cdot [S]}{K_m + [S]}$$

Michaelis-Menten Equation (4)

Here, v_0 indicates the initial reaction rate at a specific substrate concentration [S]. v_{max} describes the saturation of the reaction. This is attained when all enzyme is bound to

substrate. K_m measures the substrate-enzyme-affinity (a small K_m indicates high affinity).

Another important variable is the turnover number k_{cat}, also described as molecular activity. This constant describes the maximal number of substrate molecules converted by one enzyme molecule into the product. It is also referred to as a constant of the rate-determining step of the reaction, namely the dissociation of the enzyme-product complex into product and enzyme.

The Michaelis-Menten parameters can provide information about the activity of enzymes. Given the requirement, namely the activity determination of pepsin immobilized on gold nanoparticles, a comparison with free pepsin is indispensable in order to be able to compare and classify the results.

1.10. Mass Spectrometry in Protein Analysis

Mass spectrometry is a technique that determines the mass-to-charge ratio (m/z) of ionized analyte molecules. In general, the analytes are ionized in the ion source, transferred into the gas phase and subsequently separated in a mass analyzer in accordance to their mass-to-charge ratio. Finally, the number of ionized analyte molecules at each m/z value is determined with a detector [112].

In protein analysis (proteomics) typical used ion sources are electrospray ionization (ESI) and matrix-assisted laser desorption/ionization (MALDI). Typical instrument configurations are displayed in Figure 29. A much higher diversity is given in mass spectrometry but to convey a good overview, only the most common instruments are described below.

For liquid chromatography coupled with mass spectrometry ESI is widespread and suitable for protein samples. Here, a spray needle with applied voltage is used to ionize the analyte molecules [113]. For protein analysis, ESI is usually coupled with time-of-flight (TOF and TOF-TOF, orbitrap and quadrupole instruments.

In general, TOF instruments use a flight tube in which the ions get accelerated and separated due to their different velocities related to their different masses. A reflector can be used here (reflector time-of-flight instruments, see Figure 29 a) for turning the ions around. This process compensates for slight differences in kinetic energy of the ions before they hit a detector which counts their number of arriving.

TOF instruments can also be coupled via a collision cell (TOF-TOF, see Figure 29 b). In the collision cell after the first TOF section, ions of a particular mass-to-charge ratio can be selected and fragmented. Subsequently the different masses of the individual fragments can be separated in the second TOF section.

Quadrupole instruments are not commonly used for intact protein analysis but widespread for the analysis of proteins at the peptide level in targeted proteomics. An electric quadrupole consists of two oppositely alternating positively and negatively charged rods arranged at the corners of a square. As a component of a mass spectrometer a quadrupole is made up of four metal rods, which generate a time-varying electric field. Only ions with a certain m/z can pass on a stable trajectory. All other ions get distracted. Quadrupoles can also be combined to a triple quadrupole (Q_1-Q_3). In Q_1 ions with specific m/z are selected, fragmented in Q_2 and the fragments get separated in Q_3 (see Figure 29 c).

The linear ion trap does also use quadrupole sets for capturing ions (see dot in Q_3, Figure 29 c). The ions in the trap are in a calm and orderly state. When applying a resonant electric field, ions get excited and fragmented. These fragments leave the trap and can be detected (tandem mass spectrum). The applied electric field determines the ions or fragments that are excited, which are characterized by a defined mass. A multiple repetition of excitation and mass selection is possible.

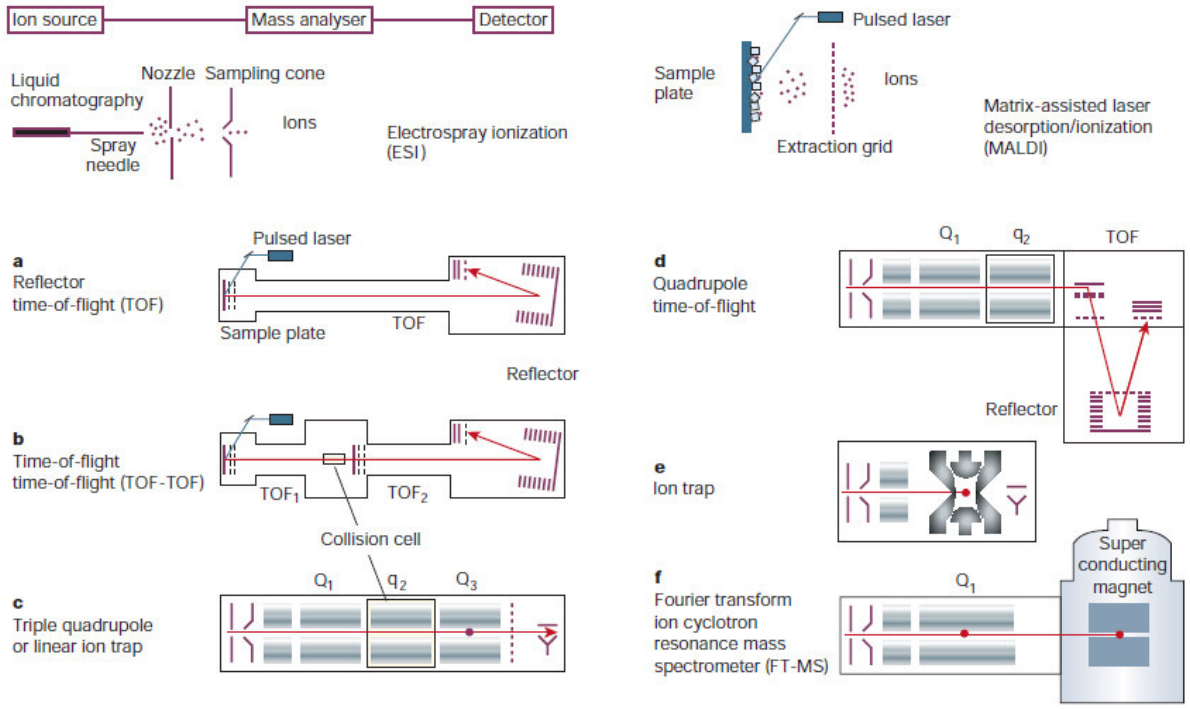

The left and right upper panels depict the ionization and sample introduction process in electrospray ionization (ESI) and matrix-assisted laser desorption/ionization (MALDI). The different instrumental configurations (a–f) are shown with their typical ion source [112].

Figure 29: Mass spectrometers used in protein analysis [112] (Reprinted with permission).

The MALDI method relies on co-crystallized analyte and matrix with a high excess of matrix ionized by pulsed laser beam. It uses small matrix molecules, such as α-cyano-4-hydroxycinnamic acid (HCCA) and 2,5-dihydroxybenzoic acid (DHB), which absorb a lot of energy at the wavelength of the nitrogen laser used [114]. MALDI is usually coupled with a combination of triple quadrupole and reflector TOF instrument (see Figure 29 d), ion trap and FT-MS.

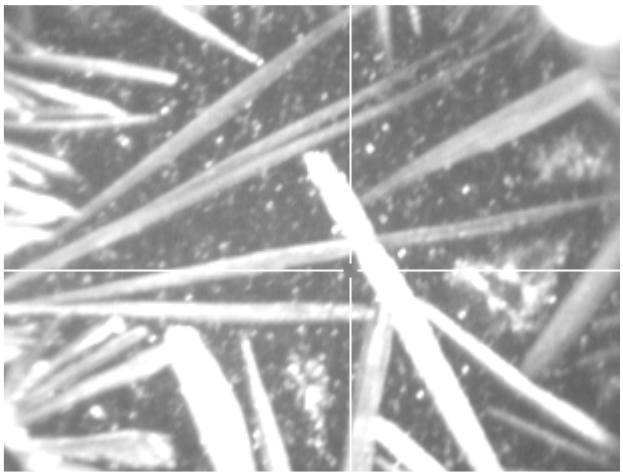

Figure 30: Co-crystalized transferrin and DHB for MALDI analysis (own data)

In a three-dimensional ion trap, ions are captured in a calm and orderly state (see Figure 29 e). Excitation and fragmentation of ions with a certain m/z is similar to the linear ion trap.

In Fourier transform ion cyclotron mass spectrometry (FT-ICR-MS) ions got trapped with strong magnetic fields. Typically, a combination with a linear trap is used (see Figure 29 f). This ensures an efficient isolation, fragmentation and detection of the ionized analytes.

One of the most important new developments in the field of mass spectrometry in recent years is the Orbitrap mass analyzer. In 2000, Alexander Makarov published his work on his functional prototype. Orbital Trapping is a further development of the classic ion trap. Ions get trapped in an electrostatic field by orbiting around an axial electrode in harmonic oscillations with frequency proportional to $(m/z)^{-1/2}$ [115]. The stability of the ions is achieved solely by orbiting around the electrode. The frequency of the oscillations is converted into mass spectra similarly to FT-ICR-MS, but since no magnetic field is required, the costly cooling with liquid helium is eliminated. Due to the high mass resolution, mass accuracy, resolving power, and dynamic range [116,117], mass spectrometry analysis with the Orbitrap mass analyzer is now an important pillar for the research of biopharmaceuticals [18].

1.10.1. Protein Identification by Mascot Database

Protein analysis, carried out with a classical proteolytic sample digestion and peptide separation by liquid chromatography, is not completed by mass spectrometry detection. The final information, namely which proteins are contained in the original sample, has not yet been clarified. This information can be obtained by software support, for example with the Mascot database (http://www.matrixscience.com/, 08.08.2018). Thousands of proteins in complex matrix can be identified with this software [118]. However, how can conclusions be drawn from the results of LC-MS/MS analysis on the proteins? For this, the results must be converted into a corresponding file format (e.g. mzML) to be able to evaluate the peak lists with Mascot scan. A clear identification of all proteins with a high score and good sequence coverage is the goal here. In order to be able to specify the search, different parameters can be defined in advance. Since different proteolytic enzymes digest proteins differently (e.g. trypsin vs. pepsin), a correct selection is essential. In addition, parameters such as the state of charge of the peptides (e.g. +1, +2, +3), precursors and ion fragment mass tolerances (e.g. ±0.2 Da) can be set. Mascot database search uses probability scoring to judge whether a result is significant and not a random event. Scores, greater than 67 are considered significant ($p < 0.05$) [119,120]. Another interesting information that can be deduced from the results of Mascot is a possible autodigestion of the proteolytic enzyme. This phenomenon occurs, for example, during a tryptic digestion and can be eliminated by immobilizing the enzyme on colloidal gold [70].

All this information is ultimately essential to be able to classify the results correctly. Computer-aided protein identification tools have greatly simplified and accelerated the evaluation of LC-MS/MS results and enabled the analysis of complex samples.

1.11. Intact Protein Determination of Genotropin (additional project, not published)

In this chapter, the method described in Höldrich et al. [69] for the characterization of intact proteins, the growth hormone genotropin was analyzed. This study has not been published yet, but it is a vivid example for intact protein determination using on-line SPE LC-MS/MS.

1.11.1. Preliminary

Genotropin or somatropin/ somatotropin is a human growth hormone for growth control by stimulating the liver. It is used as drug for Growth Hormone (GH) treatment, e.g. for treating conditions which can result in short stature and can stimulate an amino acid uptake and protein synthesis in muscles.

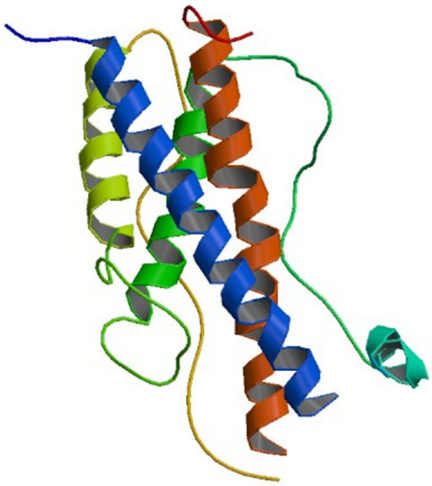

Figure 31: Molecule structure of genotropin (http://www.drugbank.ca)

Somatropin uses zinc as ligand at the positions 44 and 200. It has 191 amino acids (217 amino acids in total with 26 amino acids as signal peptide at the position 1-26), a molecular weight (MW) of approximately 22.129 kDa and a theoretical isoelectric point (pI) of 5.27. The molecular weight and the pI were calculated with the pI/MW

calculator from ExPASy (forwarded from www.uniprot.org). Somatropin has two disulfide bonds at the positions 79↔191 and 208↔215.

1.11.2. Method for Intact Protein Determination by On-line SPE

Genotropin® MiniQuick 0.2 mg powder and resolvent for the preparation of a solution for injection was used for research. Therefore, 1 µL of the ready-to-use drug solution was taken for the mass determination. The detection was carried out with a Triple TOF 5600+ quadrupole time-of-flight mass spectrometer from Sciex (Concord, Ontario, Canada) equipped with a DuoSpray source operated in positive mode using a 50 µm ID microelectrospray ionization (µESI) needle from Sciex. For the on-line SPE (solid phase extraction) installation a Phenomenex® security guard system with a C4/Butyl 300 Å wide pore column as a trapping material for protein enrichment and desalting steps was used (see picture for installation below).

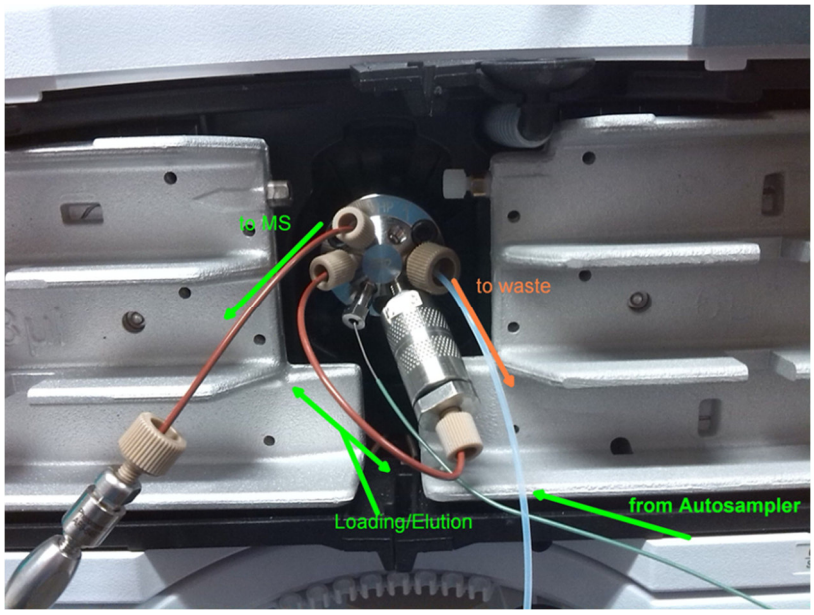

Figure 32: Installation on-line SPE; photographed by A. Sievers-Engler, method published by Höldrich et al., 2016 [69] (Source: Adrian Sievers-Engler, photograph printed with permission)

The analytes were detected in reversed flow direction (back flow mode). As mobile phase, double deionized water with 0.1 % formic acid was used in channel A for

loading the sample on the column and flush out buffers, salts and all other molecules which did not interact with the column into the waste. Acetonitrile with 0.1 % formic acid in channel B was used for flushing the sample into the ion source of the mass spectrometer. For the chromatographic conditions see the table below.

Table 2: Parameters on-line SPE

Time [min]	Flow Rate [µL min^{-1}]	ddH_2O [%]	Acetonitrile [%]
0	250	100	0
2	250	100	0
2.01	500	5	95
3	500	5	95
4	500	0	100
5	500	100	0

The measurement had to be performed in intact protein mode. Therefore, the CEM/MCP voltage was reduced by 100 V. All relevant settings for the mass spectrometer are displayed in the table below.

Table 3: Parameters mass spectrometer

Parameter	Setpoint
Curtain gas [psi]	35
Nebulizing gas [psi]	60
Drying gas [psi]	50
Source Temperature [°C]	550
Ion spray voltage [V]	5500
Start mass [Da]	500
End mass [Da]	4000
Declustering potential [V]	230
Collision energy [eV]	30
Transmission	100 % @ 1250
Time bins to sum	60

1.11.3. Results of Intact Protein Determination for Genotropin

The protein mass was determined by manual calculation and with the Bio Tool Kit for Analyst® from Sciex.

1.11.3.1. Definition of Mass in Mass Spectrometry

In the following, various common scientific terms are used for "mass" and these are briefly described here because of their differences [121].

The molecular mass of a substance (e.g. a protein) represents the mass of a molecule which is equal to the sum of the masses of all atoms contained in that molecule. It is often referred to as molecular weight, which is not entirely correct, as no weight or force is measured in mass spectrometry.

The values of nominal mass, monoisotopic mass and average mass differ by the isotope weights used for the calculation. The consideration of the mass defect also contributes to the determination and definition. Thus, the nominal mass of a molecule is composed of its most common naturally occurring stable isotopes. Here, however, the mass defect is not considered. The difference between the nominal mass and the monoisotopic mass in mass spectrometry is the mass defect. For its determination the exact mass of the most abundant isotopes is used. The average mass of a molecule is determined from the average masses of the constituent elements. Monoisotopic mass and average mass differ more with increasing molecular mass. This is especially true for peptides and proteins, as they have a high content of hydrogen, which in turn has a high mass defect. The mass of carbon serves as a reference of the atomic mass unit and its mass defect of carbon is negligible.

The accurate mass or the analytically determined accurate mass is an experimentally determined value. For the identification of proteins by mass spectrometry the accurate mass is determined on proteolytic fragments (bottom up approach) or in intact protein mode (bottom down).

The exact mass is a calculated value summing up all atomic masses of the most abundant isotopic species of the molecule.

1.11.3.2. Intact Mass Determination by Manual Calculation

The intact genotropin sample was analyzed with a Triple TOF 5600+ quadrupole time-of-flight mass spectrometer from Sciex. Below the TIC (Total Ion Current) chromatogram of the sample is shown.

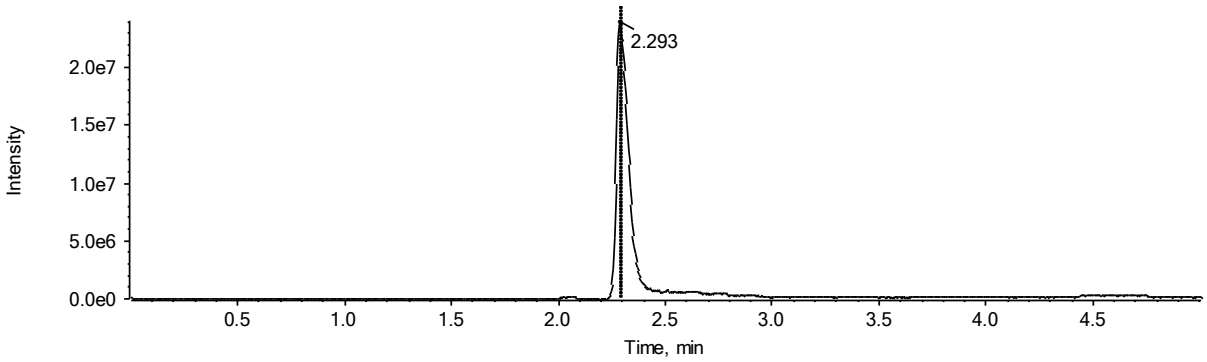

Figure 33: TIC chromatogram of the intact genotropin sample

The TIC represents the whole intensity of the ion current of a determined mass range. In the case of an intact protein determination with ESI-MS a typical charge envelope of the protein will be found (see below). ESI produces distinct multiply charged protein species with varying charge numbers (protein charge envelope).

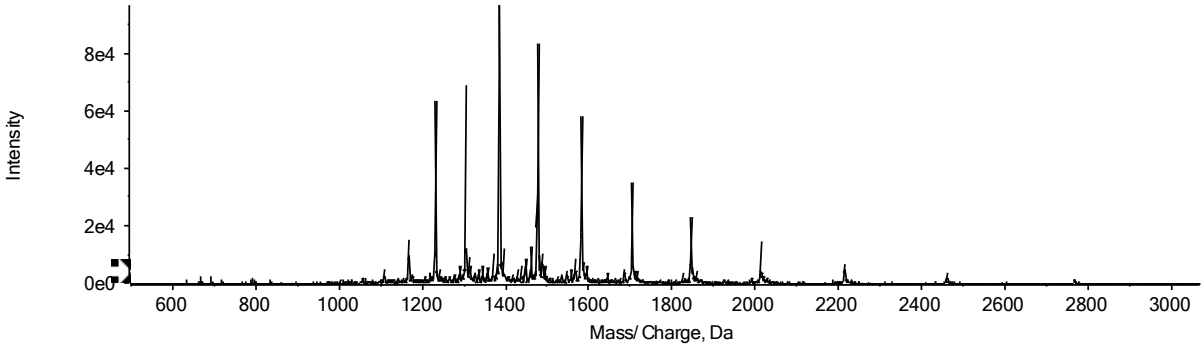

Figure 34:Charge envelope of the intact genotropin sample

By using the different mass-to-charge ratios of the protein charge envelope it is possible to calculate the charge states and the exact mass of the molecule.

The calculation of the molecular mass of the intact protein was performed with the equations 5 - 8 listed below [121]. Here, the accurate mass was determined by the equations 5 and 6. For the exact molecular mass 22129.0497 Da calculated with the pI/MW calculator from ExPASy was taken. The results are displayed in Table 3. The m/z ratios for the manual calculation were taken from the mass list of the analyzed genotropin sample.

$$z = \frac{a - 1.0072}{b - a}$$ Equation (5)

Here, b is the m/z value of the first ion, z is the charge number of the first ion, a is the m/z value of the second (adjacent) ion of lower m/z, and 1.0072 is the mass of one proton.

$$M = z \cdot (b - 1.0072)$$ Equation (6)

By knowing the correct charge (z) the calculation of the exact mass can be performed.

$$Mass\ Error\ [Da] = ExactMass - Accurate\ mass$$ Equation (7)

With the determined exact mass and the accurate mass of the molecule the mass error in Da can be calculated.

$$Mass\ Error\ [ppm] = \frac{Mass\ Error}{Exact\ Mass} \cdot 10^6$$ Equation (8)

With the calculated mass error in Da finally the mass error in ppm for the exact mass can be determined.

Table 4: Mass calculation with equations 1 - 4

	m/z	**z**	**M [Da]**
a	1476.3240	14	22134.0201
b	1581.6820	13	22128.2253
	1703.2796	12	22129.0852
	1845.1388	11	22127.0781
	2012.8078	10	22128.2527
	2214.0034		
	Accurate Mass		**22129.3323**
	Exact Mass **(calculated with ExPASy)**		**22129.0497**
	Mass error [Da]		**0.2826**
	Mass error [ppm]		**12.7694**

For the manual calculations the same mass to charge ratios were taken as the Bio Tool Kit from Sciex used (see Figure 35). As shown in Table 4 the accurate

mass could be determined as 22129.3 Da with a calculated mass error of 0.3 Da (0.2826 Da) and 12.8 ppm.

1.11.3.3. Intact Mass Determination by Bio Tool Kit from Sciex

The intact mass of the same genotropin sample was determined by the Bio Tool Kit from Sciex for comparing the results. In Figure 35 below the MS spectrum of genotropin processed by the Bio Tool kit is shown; the charge state as calculated by the algorithm of eq. 1 within the protein envelope is displayed in red.

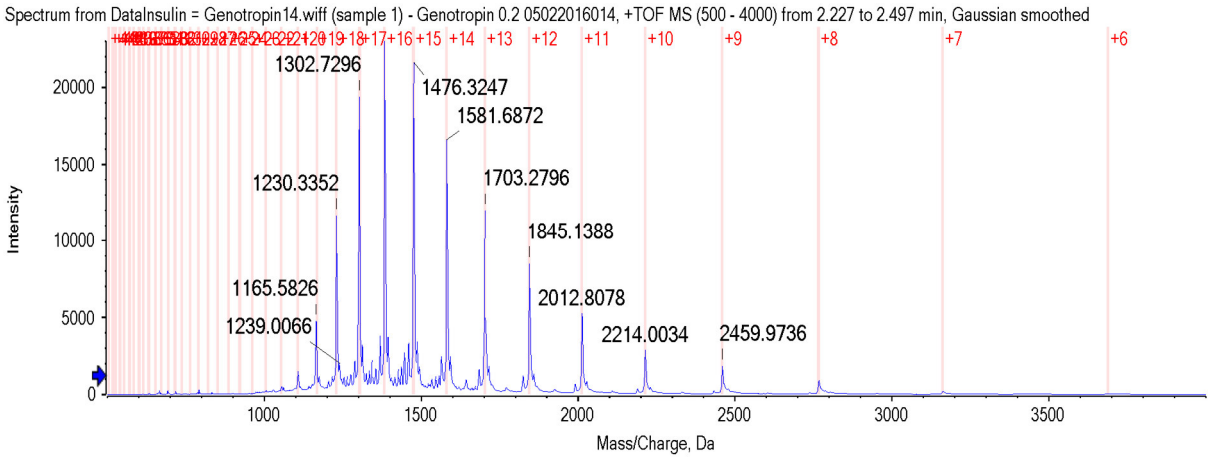

Figure 35: Protein charge envelope of the intact genotropin sample with the Bio Tool Kit from Sciex

A mass range for performing the mass determination has to be chosen (in this case 21000 Da to 23000 Da).

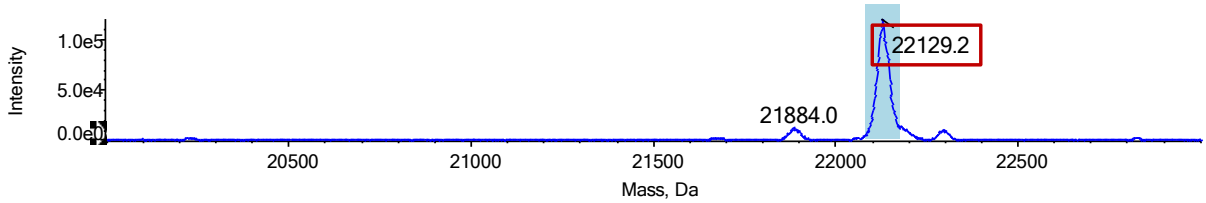

Figure 36: Reconstituted MS spectrum of the intact protein: Calculated intact protein mass of the genotropin sample with the Bio Tool Kit from Sciex marked in red

The intact mass was determined as 22129.2 Da with a mass error of 0.2 Da and 9.0 ppm. An overview of the calculated and determined results of the protein mass for genotropin is displayed in the table below.

Table 5: Overview results of the calculated and determined genotropin protein mass

Protein Mass [Da] from ExPASy

22129.05

Results Manual Integration

Protein Mass [Da]	Mass Error [Da]	Mass Error [ppm]
22129.3	0.3	12.8

Results Bio Tool Kit

Protein Mass [Da]	Mass Error [Da]	Mass Error [ppm]
22129.2	0.2	9.0

1.11.4. Conclusion of Intact Protein Determination of Genotropin

The intact protein mass of the same genotropin sample was determined by manual calculation and with the Bio Tool Kit from Sciex after the analysis with a Triple TOF 5600+ quadrupole time-of-flight mass spectrometer from Sciex. The result for the manual integration was determined as 22129.3 Da with a calculated mass error of 0.3 Da and 12.8 ppm. For this calculation the same mass to charge ratios were taken as the Bio Tool Kit from Sciex used, which determined the protein mass for genotropin as 22129.2 Da with a mass error of 0.2 Da and 9.0 ppm. For both calculations the results are highly comparable. As discussed by K. Strupat [121] a manual determination of a typical protein envelope leads to correct results. However, current kits/ add-ins, such as the Bio Tool Kit from Sciex, lead to correct results and facilitate the calculation and presentation of the results due to their logical and easy handling.

1.12. List of Figures

1.13. List of Tables

1.14. References

1. Biopharmaceuticals: Definition and Regulation. In: Pharmaceutical Sciences Encyclopedia. doi:10.1002/9780470571224.pse160

2. Abramowicz D, Schandene L, Goldman M, Crusiaux A, Vereerstraeten P, Pauw LD, Wybran J, Kinnaert P, Dupont E, Toussaint C (1989) Release of Tumor Necrosis Factor, Interleukin-2, and Gamma-Interferon in Serum After Injection of OKT3 Monoclonal Antibody in Kidney Transplant Recipients. Transplantation 47 (4):606-608

3. Ecker DM, Jones SD, Levine HL (2015) The therapeutic monoclonal antibody market. mAbs 7 (1):9-14. doi:10.4161/19420862.2015.989042

4. McLaughlin P, Grillo-López AJ, Link BK, Levy R, Czuczman MS, Williams ME, Heyman MR, Bence-Bruckler I, White CA, Cabanillas F, Jain V, Ho AD, Lister J, Wey K, Shen D, Dallaire BK (1998) Rituximab chimeric anti-CD20 monoclonal antibody therapy for relapsed indolent lymphoma: half of patients respond to a four-dose treatment program. Journal of Clinical Oncology 16 (8):2825-2833. doi:10.1200/jco.1998.16.8.2825

5. Edwards JCW, Szczepański L, Szechiński J, Filipowicz-Sosnowska A, Emery P, Close DR, Stevens RM, Shaw T (2004) Efficacy of B-Cell–Targeted Therapy with Rituximab in Patients with Rheumatoid Arthritis. New England Journal of Medicine 350 (25):2572-2581. doi:10.1056/NEJMoa032534

6. Busse W, Corren J, Lanier BQ, McAlary M, Fowler-Taylor A, Cioppa GD, van As A, Gupta N (2001) Omalizumab, anti-IgE recombinant humanized monoclonal antibody, for the treatment of severe allergic asthma. Journal of Allergy and Clinical Immunology 108 (2):184-190. doi:10.1067/mai.2001.117880

7. Castro M, Mathur S, Hargreave F, Boulet L-P, Xie F, Young J, Wilkins HJ, Henkel T, Nair P (2011) Reslizumab for Poorly Controlled, Eosinophilic Asthma. American Journal of Respiratory and Critical Care Medicine 184 (10):1125-1132. doi:10.1164/rccm.201103-0396OC

8. Flood-Page P, Swenson C, Faiferman I, Matthews J, Williams M, Brannick L, Robinson D, Wenzel S, Busse W, Hansel TT, Barnes NC, Group obotIMS (2007) A Study to Evaluate Safety and Efficacy of Mepolizumab in Patients with Moderate Persistent Asthma. American Journal of Respiratory and Critical Care Medicine 176 (11):1062-1071. doi:10.1164/rccm.200701-085OC

9. Monoclonal Antibodies (mAbs) Market Analysis By Source (Chimeric, Murine, Humanized, Human), By Type of Production, By Indication (Cancer, Autoimmune, Inflammatory, Infectious, Microbial, Viral Diseases), By End-use (Hospitals, Research, Academic Institutes, Clinics, Diagnostic Laboratories) And Segment Forecasts, 2018 - 2024 (2016).115

10. Beck A, Wagner-Rousset E, Ayoub D, Van Dorsselaer A, Sanglier-Cianferani S (2013) Characterization of Therapeutic Antibodies and Related Products. Anal Chem (Washington, DC, U S) 85 (2):715-736. doi:10.1021/ac3032355

11. Bobaly B, D'Atri V, Goyon A, Colas O, Beck A, Fekete S, Guillarme D (2017) Protocols for the analytical characterization of therapeutic monoclonal antibodies. II – Enzymatic and chemical sample preparation. Journal of Chromatography B 1060:325-335. doi:https://doi.org/10.1016/j.jchromb.2017.06.036

12. Monzo A, Sperling E, Guttman A (2009) Proteolytic enzyme-immobilization techniques for MS-based protein analysis. TrAC Trends in Analytical Chemistry 28 (7):854-864. doi:https://doi.org/10.1016/j.trac.2009.03.002

13. Gates R (2013) New Enzymes for Antibody Characterization from Sigma-Aldrich. Biofiles - Your Biology Resource 8 (2)

14. Florkin M (1957) [Discovery of pepsin by Theodor Schwann]. Rev Med Liege 12 (5):139-144

15. Northrop JH (1929) CRYSTALLINE PEPSIN. Science 69 (1796):580

16. Konigsberg W, Goldstein J, Hill RJ (1963) The structure of human hemoglobin. VII. The digestion of the beta chain of human hemoglobin with pepsin. The Journal of biological chemistry 238:2028-2033

17. Schmelzer CEH, Schöps R, Ulbrich-Hofmann R, Neubert RHH, Raith K (2004) Mass spectrometric characterization of peptides derived by peptic cleavage of bovine β-casein. Journal of Chromatography A 1055 (1):87-92. doi:https://doi.org/10.1016/j.chroma.2004.09.003

18. Fornelli L, Ayoub D, Aizikov K, Beck A, Tsybin YO (2014) Middle-Down Analysis of Monoclonal Antibodies with Electron Transfer Dissociation Orbitrap Fourier Transform Mass Spectrometry. Analytical Chemistry 86 (6):3005-3012. doi:10.1021/ac4036857

19. Reusch D, Haberger M, Falck D, Peter B, Maier B, Gassner J, Hook M, Wagner K, Bonnington L, Bulau P, Wuhrer M (2015) Comparison of methods for the analysis of therapeutic immunoglobulin G Fc-glycosylation profiles—Part 2: Mass spectrometric methods. mAbs 7 (4):732-742. doi:10.1080/19420862.2015.1045173

20. An Y, Zhang Y, Mueller H-M, Shameem M, Chen X (2014) A new tool for monoclonal antibody analysis: Application of IdeS proteolysis in IgG domain-specific characterization. mAbs 6 (4):879-893. doi:10.4161/mabs.28762

21. Wagner-Rousset E, Bednarczyk A, Bussat MC, Colas O, Corvaia N, Schaeffer C, Van Dorsselaer A, Beck A (2008) The way forward, enhanced characterization of therapeutic antibody glycosylation: comparison of three level mass spectrometry-based strategies. Journal of chromatography B, Analytical technologies in the biomedical and life sciences 872 (1-2):23-37. doi:10.1016/j.jchromb.2008.03.032

22. Drenth J, Jansonius JN, Koekoek R, Swen HM, Wolthers BG (1968) Structure of Papain. Nature 218:929. doi:10.1038/218929a0

23. Ezekiel Amri FM (2012) Papain, a Plant Enzyme of Biological Importance: A Review American Journal of Biochemistry and Biotechnology 8 (2):99-104. doi:10.3844/ajbbsp.2012.99.104

24. Sahoo B, Sahu SK, Bhattacharya D, Dhara D, Pramanik P (2013) A novel approach for efficient immobilization and stabilization of papain on magnetic gold nanocomposites. Colloids and Surfaces B: Biointerfaces 101:280-289. doi:https://doi.org/10.1016/j.colsurfb.2012.07.003

25. Cleland WW (1964) Dithiothreitol, a New Protective Reagent for SH Groups*. Biochemistry 3 (4):480-482. doi:10.1021/bi00892a002

26. Getz EB, Xiao M, Chakrabarty T, Cooke R, Selvin PR (1999) A Comparison between the Sulfhydryl Reductants Tris(2-carboxyethyl)phosphine and Dithiothreitol for Use in Protein Biochemistry. Analytical Biochemistry 273 (1):73-80. doi:https://doi.org/10.1006/abio.1999.4203

27. Roco MC, Williams RS, Alivisatos P, Science N, Technology TCCo, Interagency Working Group on Nanoscience E, Technology (2000) Nanotechnology Research Directions: IWGN Workshop Report: Vision for Nanotechnology in the Next Decade. Springer,

28. Society R, Engineering RAo (2004) Nanoscience and Nanotechnologies: Opportunities and Uncertainties. Royal Society,

29. Höldrich M, Liu S, Epe M, Lämmerhofer M (2017) Taylor dispersion analysis, resonant mass measurement and bioactivity of pepsin-coated gold nanoparticles. Talanta 167:67-74. doi:https://doi.org/10.1016/j.talanta.2017.02.010

30. Holleman AF, Wiberg E, Wiberg N (1995) Lehrbuch der anorganischen Chemie. de Gruyter,

31. Miura K-i, Tamamushi B-i (1953) The Relation between Colour and Particle Size of Gold Sols. Journal of Electron Microscopy 1 (1):36-39. doi:10.1093/oxfordjournals.jmicro.a049742

32. Malola S, Lehtovaara L, Enkovaara J, HÃ¤kkinen H (2013) Birth of the Localized Surface Plasmon Resonance in Monolayer-Protected Gold Nanoclusters. ACS Nano 7 (11):10263-10270. doi:10.1021/nn4046634

33. Eustis S, El-Sayed MA (2006) Why gold nanoparticles are more precious than pretty gold: Noble metal surface plasmon resonance and its enhancement of the radiative and nonradiative properties of nanocrystals of different shapes. Chemical Society Reviews 35 (3):209-217. doi:10.1039/B514191E

34. Saha K, Agasti SS, Kim C, Li X, Rotello VM (2012) Gold Nanoparticles in Chemical and Biological Sensing. Chemical Reviews 112 (5):2739-2779. doi:10.1021/cr2001178

35. Wu H-P, Yu C-J, Lin C-Y, Lin Y-H, Tseng W-L (2009) Gold nanoparticles as assisted matrices for the detection of biomolecules in a high-salt solution through laser desorption/ionization mass

spectrometry. Journal of the American Society for Mass Spectrometry 20 (5):875-882. doi:10.1016/j.jasms.2009.01.002

36. Mouradian S, Nelson CM, Smith LM (1996) A Self-Assembled Matrix Monolayer for UV-MALDI Mass Spectrometry. Journal of the American Chemical Society 118 (36):8639-8645. doi:10.1021/ja953585j

37. Cobley CM, Chen J, Cho EC, Wang LV, Xia Y (2011) Gold nanostructures: a class of multifunctional materials for biomedical applications. Chemical Society Reviews 40 (1):44-56. doi:10.1039/B821763G

38. Nagahori N, Nishimura S-I (2006) Direct and Efficient Monitoring of Glycosyltransferase Reactions on Gold Colloidal Nanoparticles by Using Mass Spectrometry. Chemistry – A European Journal 12 (25):6478-6485. doi:doi:10.1002/chem.200501267

39. Schaming D, Remita H (2015) Nanotechnology: from the ancient time to nowadays. Foundations of Chemistry 17 (3):187-205. doi:10.1007/s10698-015-9235-y

40. Hornyak GL, Patrissi CJ, Oberhauser EB, Martin CR, Valmalette JC, Lemaire L, Dutta J, Hofmann H (1997) Effective medium theory characterization of Au/Ag nanoalloy-porous alumina composites. Nanostructured Materials 9 (1):571-574. doi:https://doi.org/10.1016/S0965-9773(97)00127-X

41. Hunt LB (1976) The true story of Purple of Cassius. Gold Bulletin 9 (4):134-139. doi:10.1007/BF03215423

42. Mie G (1908) Contributions to the Optics of Turbid Media, Especially Colloidal Metal Solutions. Ann Phys (Weinheim, Ger) 25:377-445

43. Khlebtsov N, Bogatyrev V, Dykman L, Khlebtsov B, Staroverov S, Shirokov A, Matora L, Khanadeev V, Pylaev T, Tsyganova N, Terentyuk G (2013) Analytical and Theranostic Applications of Gold Nanoparticles and Multifunctional Nanocomposites. Theranostics 3 (3):167-180. doi:10.7150/thno.5716

44. Cabral RM, Baptista PV (2014) Anti-cancer precision theranostics: a focus on multifunctional gold nanoparticles. Expert Review of Molecular Diagnostics 14 (8):1041-1052. doi:10.1586/14737159.2014.965683

45. Tatur S, Maccarini M, Barker R, Nelson A, Fragneto G (2013) Effect of Functionalized Gold Nanoparticles on Floating Lipid Bilayers. Langmuir 29 (22):6606-6614. doi:10.1021/la401074y

46. Turkevich J, Stevenson PC, Hillier J (1951) The nucleation and growth processes in the synthesis of colloidal gold. Discuss Faraday Soc No. 11 (Copyright (C) 2013 American Chemical Society (ACS). All Rights Reserved.):55-75. doi:10.1039/df9511100055

47. Turkevich JS, P. C.; Hillier, J. (1951) Coagulation of colloidal gold. Discuss Faraday Soc 11:55

48. Frens G (1972) Particle size and sol stability in metal colloids. Kolloid-Zeitschrift und Zeitschrift für Polymere 250 (7):736-741. doi:10.1007/BF01498565

49. Frens G (1973) Controlled nucleation for the regulation of the particle size in monodisperse gold suspensions. Nature (London), Phys Sci 241 (Copyright (C) 2013 American Chemical Society (ACS). All Rights Reserved.):20-22

50. Schmid G (1992) Large clusters and colloids. Metals in the embryonic state. Chemical Reviews 92 (8):1709-1727. doi:10.1021/cr00016a002

51. Schmid G (1994) Clusters and colloids: from theory to applications, vol 112. VCH Weinheim,

52. Brust M, Walker M, Bethell D, Schiffrin DJ, Whyman R (1994) Synthesis of thiol-derivatised gold nanoparticles in a two-phase Liquid–Liquid system. Journal of the Chemical Society, Chemical Communications (7):801-802. doi:10.1039/C39940000801

53. Engvall E, Perlmann P (1971) Enzyme-linked immunosorbent assay (ELISA) quantitative assay of immunoglobulin G. Immunochemistry 8 (9):871-874. doi:https://doi.org/10.1016/0019-2791(71)90454-X

54. Van Weemen BK, Schuurs AHWM (1971) Immunoassay using antigen—enzyme conjugates. FEBS Letters 15 (3):232-236. doi:10.1016/0014-5793(71)80319-8

55. Ambrosi A, Airò F, Merkoçi A (2010) Enhanced Gold Nanoparticle Based ELISA for a Breast Cancer Biomarker. Analytical Chemistry 82 (3):1151-1156. doi:10.1021/ac902492c

56. Zhu FF, Peng J, Huang Z, Hu LM, Zhang GG, Liu DF, Xing KY, Zhang KY, Lai WH (2018) Specific colorimetric ELISA method based on DNA hybridization reaction and non–crosslinking gold nanoparticles aggregation for the detection of amantadine. Food Chemistry 257:382-387. doi:https://doi.org/10.1016/j.foodchem.2018.03.033

57. Ching KH (2015) Lateral Flow Immunoassay. In: Hnasko R (ed) ELISA: Methods and Protocols. Springer New York, New York, NY, pp 127-137. doi:10.1007/978-1-4939-2742-5_13

58. Parolo C, de la Escosura-Muñiz A, Merkoçi A (2013) Enhanced lateral flow immunoassay using gold nanoparticles loaded with enzymes. Biosensors and Bioelectronics 40 (1):412-416. doi:https://doi.org/10.1016/j.bios.2012.06.049

59. Rojanathanes R, Sereemaspun A, Pimpha N, Buasorn V, Ekawong P, Wiwanitkit V (2008) Gold Nanoparticle as an Alternative Tool for a Urine Pregnancy Test. Taiwanese Journal of Obstetrics and Gynecology 47 (3):296-299. doi:https://doi.org/10.1016/S1028-4559(08)60127-8

60. Thanh NTK, Rosenzweig Z (2002) Development of an Aggregation-Based Immunoassay for Anti-Protein A Using Gold Nanoparticles. Analytical Chemistry 74 (7):1624-1628. doi:10.1021/ac011127p

61. Rafał W, Jan K, Shane M (2015) A miniaturised image based fluorescence detection system for point-of-care-testing of cocaine abuse. Measurement Science and Technology 26 (8):085401

62. Musshoff F, Hokamp EG, Bott U, Madea B (2014) Performance evaluation of on-site oral fluid drug screening devices in normal police procedure in Germany. Forensic Science International 238:120-124. doi:https://doi.org/10.1016/j.forsciint.2014.02.005

63. Vanstechelman S, Isalberti C, Van der Linden T, Pil K, Legrand S-A, Verstraete AG (2012) Analytical Evaluation of Four On-Site Oral Fluid Drug Testing Devices. Journal of Analytical Toxicology 36 (2):136-140. doi:10.1093/jat/bkr016

64. Pehrsson A, Blencowe T, Vimpari K, Langel K, Engblom C, Lillsunde P (2011) An Evaluation of On-Site Oral Fluid Drug Screening Devices DrugWipe® 5+ and Rapid STAT® Using Oral Fluid for Confirmation Analysis. Journal of Analytical Toxicology 35 (4):211-218. doi:10.1093/anatox/35.4.211

65. Dreaden EC, Alkilany AM, Huang X, Murphy CJ, El-Sayed MA (2012) The golden age: gold nanoparticles for biomedicine. Chemical Society Reviews 41 (7):2740-2779. doi:10.1039/C1CS15237H

66. Chen Y, Gu X, Nie C-G, Jiang Z-Y, Xie Z-X, Lin C-J (2005) Shape controlled growth of gold nanoparticles by a solution synthesis. Chemical Communications (33):4181-4183. doi:10.1039/B504911C

67. Jana NR, Gearheart L, Murphy CJ (2001) Seed-Mediated Growth Approach for Shape-Controlled Synthesis of Spheroidal and Rod-like Gold Nanoparticles Using a Surfactant Template. Advanced Materials 13 (18):1389-1393. doi:10.1002/1521-4095(200109)13:18<1389::AID-ADMA1389>3.0.CO;2-F

68. Westcott SL, Oldenburg SJ, Lee TR, Halas NJ (1998) Formation and Adsorption of Clusters of Gold Nanoparticles onto Functionalized Silica Nanoparticle Surfaces. Langmuir 14 (19):5396-5401. doi:10.1021/la980380q

69. Höldrich M, Sievers-Engler A, Lämmerhofer M (2016) Gold nanoparticle-conjugated pepsin for efficient solution-like heterogeneous biocatalysis in analytical sample preparation protocols. Analytical and Bioanalytical Chemistry 408 (20):5415-5427. doi:10.1007/s00216-016-9657-y

70. Hinterwirth H, Lindner W, Laemmerhofer M (2012) Bioconjugation of trypsin onto gold nanoparticles: Effect of surface chemistry on bioactivity. Anal Chim Acta 733 (Copyright (C) 2012 American Chemical Society (ACS). All Rights Reserved.):90-97. doi:10.1016/j.aca.2012.04.036

71. Kimling J, Maier M, Okenve B, Kotaidis V, Ballot H, Plech A (2006) Turkevich Method for Gold Nanoparticle Synthesis Revisited. J Phys Chem B 110 (Copyright (C) 2013 American Chemical Society (ACS). All Rights Reserved.):15700-15707. doi:10.1021/jp061667w

72. Polte J, Ahner TT, Delissen F, Sokolov S, Emmerling F, Thunemann AF, Kraehnert R (2010) Mechanism of Gold Nanoparticle Formation in the Classical Citrate Synthesis Method Derived from Coupled In Situ XANES and SAXS Evaluation. J Am Chem Soc 132 (4):1296-1301. doi:10.1021/ja906506j

73. Brust M, Walker M, Bethell D, Schiffrin DJ, Whyman R (1994) Synthesis of thiol-derivatised gold nanoparticles in a two-phase Liquid-Liquid system. Journal of the Chemical Society, Chemical Communications (7):801-802. doi:10.1039/C39940000801

74. Kalishwaralal K, Deepak V, Ram Kumar Pandian S, Gurunathan S (2009) Biological synthesis of gold nanocubes from Bacillus licheniformis. Bioresource Technology 100 (21):5356-5358. doi:http://doi.org/10.1016/j.biortech.2009.05.051

75. Gauthier MA, Gibson MI, Klok H-A (2009) Synthese funktioneller Polymere durch polymeranaloge Reaktionen. Angewandte Chemie 121 (1):50-60. doi:10.1002/ange.200801951

76. Piper DW, Fenton BH (1965) pH stability and activity curves of pepsin with special reference to their clinical importance. Gut 6 (5):506-508

77. Hermanson GT (2013) Bioconjugate Techniques (Third edition). In. Academic Press, Boston. doi:https://doi.org/10.1016/B978-0-12-382239-0.00001-7

78. Wang ZL (2000) Transmission Electron Microscopy of Shape-Controlled Nanocrystals and Their Assemblies. The Journal of Physical Chemistry B 104 (6):1153-1175. doi:10.1021/jp993593c

79. Akita T, Okumura M, Tanaka K, Kohyama M, Haruta M (2006) Analytical TEM observation of Au nano-particles on cerium oxide. Catalysis Today 117 (1):62-68. doi:https://doi.org/10.1016/j.cattod.2006.05.010

80. Haiss W, Thanh NTK, Aveyard J, Fernig DG (2007) Determination of Size and Concentration of Gold Nanoparticles from UV-Vis Spectra. Anal Chem (Washington, DC, U S) 79 (Copyright (C) 2013 American Chemical Society (ACS). All Rights Reserved.):4215-4221. doi:10.1021/ac0702084

81. Hendel T, Wuithschick M, Kettemann F, Birnbaum A, Rademann K, Polte J (2014) In Situ Determination of Colloidal Gold Concentrations with UV-Vis Spectroscopy: Limitations and Perspectives. Anal Chem (Washington, DC, U S) 86 (22):11115-11124. doi:10.1021/ac502053s

82. Hinterwirth H, Wiedmer SK, Moilanen M, Lehner A, Allmaier G, Waitz T, Lindner W, Laemmerhofer M (2013) Comparative method evaluation for size and size-distribution analysis of gold nanoparticles. J Sep Sci 36 (17):2952-2961. doi:10.1002/jssc.201300460

83. Leschonski K (1984) Representation and Evaluation of Particle Size Analysis Data. Particle & Particle Systems Characterization 1 (1-4):89-95. doi:10.1002/ppsc.19840010115

84. James AE, Driskell JD (2013) Monitoring gold nanoparticle conjugation and analysis of biomolecular binding with nanoparticle tracking analysis (NTA) and dynamic light scattering (DLS). Analyst 138 (4):1212-1218. doi:10.1039/C2AN36467K

85. Hackley VA, Clogston JD (2011) Measuring the Hydrodynamic Size of Nanoparticles in Aqueous Media Using Batch-Mode Dynamic Light Scattering. In: McNeil SE (ed) Characterization of Nanoparticles Intended for Drug Delivery. Humana Press, Totowa, NJ, pp 35-52. doi:10.1007/978-1-60327-198-1_4

86. Pusey PN (1987) The effect of polydispersity on the crystallization of hard spherical colloids. J Phys France 48 (5):709-712

87. Rogošić M, Mencer HJ, Gomzi Z (1996) Polydispersity index and molecular weight distributions of polymers. European Polymer Journal 32 (11):1337-1344. doi:https://doi.org/10.1016/S0014-3057(96)00091-2

88. Dragovic RA, Gardiner C, Brooks AS, Tannetta DS, Ferguson DJP, Hole P, Carr B, Redman CWG, Harris AL, Dobson PJ, Harrison P, Sargent IL (2011) Sizing and phenotyping of cellular vesicles using Nanoparticle Tracking Analysis. Nanomedicine: Nanotechnology, Biology and Medicine 7 (6):780-788. doi:https://doi.org/10.1016/j.nano.2011.04.003

89. Gambinossi F, Mylon SE, Ferri JK (2015) Aggregation kinetics and colloidal stability of functionalized nanoparticles. Advances in Colloid and Interface Science 222:332-349. doi:https://doi.org/10.1016/j.cis.2014.07.015

90. Nietsche R Malvern Short Course – ZETAPOTENTIAL, Malvern Instruments GmbH, Herrenberg.

91. Sze A, Erickson D, Ren L, Li D (2003) Zeta-potential measurement using the Smoluchowski equation and the slope of the current–time relationship in electroosmotic flow. Journal of Colloid and Interface Science 261 (2):402-410. doi:https://doi.org/10.1016/S0021-9797(03)00142-5

92. Orlando L. Sanchez Munoz B (2002) Affinity Electrophoresis In Cappillary Format, A Physical-Organic Tool For Studying Interactions In Biomolecular Recognition. Polytechnics University of Havana, Cuba, Havana, Cuba

93. Doane TL, Chuang C-H, Hill RJ, Burda C (2012) Nanoparticle ζ -Potentials. Accounts of Chemical Research 45 (3):317-326. doi:10.1021/ar200113c

94. Clogston JD, Patri AK (2011) Zeta Potential Measurement. In: McNeil SE (ed) Characterization of Nanoparticles Intended for Drug Delivery. Humana Press, Totowa, NJ, pp 63-70. doi:10.1007/978-1-60327-198-1_6

95. Reza Nejadnik M, Jiskoot W (2015) Measurement of the Average Mass of Proteins Adsorbed to a Nanoparticle by Using a Suspended Microchannel Resonator. Journal of Pharmaceutical Sciences 104 (2):698-704. doi:https://doi.org/10.1002/jps.24206

96. Hawe A, Hulse WL, Jiskoot W, Forbes RT (2011) Taylor Dispersion Analysis Compared to Dynamic Light Scattering for the Size Analysis of Therapeutic Peptides and Proteins and Their Aggregates. Pharmaceutical Research 28 (9):2302-2310. doi:10.1007/s11095-011-0460-3

97. Taylor Geoffrey I (1953) Dispersion of soluble matter in solvent flowing slowly through a tube. Proceedings of the Royal Society of London Series A Mathematical and Physical Sciences 219 (1137):186-203. doi:10.1098/rspa.1953.0139

98. Aris R, Taylor Geoffrey I (1956) On the dispersion of a solute in a fluid flowing through a tube. Proceedings of the Royal Society of London Series A Mathematical and Physical Sciences 235 (1200):67-77. doi:10.1098/rspa.1956.0065

99. WHITEPAPER - Understanding Taylor Dispersion Analysis (2015).8

100. Lowry OH, Rosebrough NJ, Farr AL, Randall RJ (1951) Protein measurement with the Folin phenol reagent. The Journal of biological chemistry 193 (1):265-275

101. Waterborg JH (2002) The Lowry Method for Protein Quantitation. In: Walker JM (ed) The Protein Protocols Handbook. Humana Press, Totowa, NJ, pp 7-9. doi:10.1385/1-59259-169-8:7

102. Bradford MM (1976) A rapid and sensitive method for the quantitation of microgram quantities of protein utilizing the principle of protein-dye binding. Analytical Biochemistry 72 (1):248-254. doi:https://doi.org/10.1016/0003-2697(76)90527-3

103. Smith PK, Krohn RI, Hermanson GT, Mallia AK, Gartner FH, Provenzano MD, Fujimoto EK, Goeke NM, Olson BJ, Klenk DC (1985) Measurement of protein using bicinchoninic acid. Analytical Biochemistry 150 (1):76-85. doi:https://doi.org/10.1016/0003-2697(85)90442-7

104. Sapan CV, Lundblad RL, Price NC (2010) Colorimetric protein assay techniques. Biotechnology and Applied Biochemistry 29 (2):99-108. doi:10.1111/j.1470-8744.1999.tb00538.x

105. Protein assay technical handbook: Tools and reagents for improved quantitation of total or specific proteins. ThermoFisher Scientific. https://www.thermofisher.com/content/dam/LifeTech/Documents/PDFs/COL04277-Protein-Assay-TechHB-Global-FINAL-Lowres.pdf (2017).

106. Hartree EF (1972) Determination of protein: A modification of the lowry method that gives a linear photometric response. Analytical Biochemistry 48 (2):422-427. doi:https://doi.org/10.1016/0003-2697(72)90094-2

107. Reinhard Matissek GS (2006) Lebensmittelanalytik, vol 03. Springer-Verlag Berlin Heidelberg,

108. Michaelis L, Menten ML, Johnson KA, Goody RS (2011) The original Michaelis constant: translation of the 1913 Michaelis-Menten paper. Biochemistry 50 (39):8264-8269. doi:10.1021/bi201284u

109. Cornish-Bowden A (2015) One hundred years of Michaelis–Menten kinetics. Perspectives in Science 4:3-9. doi:https://doi.org/10.1016/j.pisc.2014.12.002

110. Lineweaver H, Burk D (1934) Determination of enzyme dissociation constants. J Am Chem Soc 56:658-666. doi:10.1021/ja01318a036

111. Briggs GE, Haldane JB (1925) A Note on the Kinetics of Enzyme Action. The Biochemical journal 19 (2):338-339

112. Aebersold R, Mann M (2003) Mass spectrometry-based proteomics. Nature 422:198. doi:10.1038/nature01511

113. Fenn JB, Mann M, Meng CK, Wong SF, Whitehouse CM (1989) Electrospray ionization for mass spectrometry of large biomolecules. Science 246 (4926):64

114. Karas M, Hillenkamp F (1988) Laser desorption ionization of proteins with molecular masses exceeding 10,000 daltons. Analytical Chemistry 60 (20):2299-2301. doi:10.1021/ac00171a028

115. Makarov A (2000) Electrostatic Axially Harmonic Orbital Trapping: A High-Performance Technique of Mass Analysis. Analytical Chemistry 72 (6):1156-1162. doi:10.1021/ac991131p

116. Makarov A, Denisov E, Lange O, Horning S (2006) Dynamic range of mass accuracy in LTQ orbitrap hybrid mass spectrometer. Journal of The American Society for Mass Spectrometry 17 (7):977-982. doi:10.1016/j.jasms.2006.03.006

117. Makarov A, Denisov E, Kholomeev A, Balschun W, Lange O, Strupat K, Horning S (2006) Performance Evaluation of a Hybrid Linear Ion Trap/Orbitrap Mass Spectrometer. Analytical Chemistry 78 (7):2113-2120. doi:10.1021/ac0518811

118. Bouyssié D, de Peredo AG, Mouton E, Albigot R, Roussel L, Ortega N, Cayrol C, Burlet-Schiltz O, Girard J-P, Monsarrat B (2007) Mascot File Parsing and Quantification (MFPaQ), a New Software to Parse, Validate, and Quantify Proteomics Data Generated by ICAT and SILAC Mass Spectrometric Analyses: Application To the Proteomics Study of Membrane Proteins from Primary Human Endothelial Cells. Molecular & Cellular Proteomics 6 (9):1621-1637. doi:10.1074/mcp.T600069-MCP200

119. Koenig T, Menze BH, Kirchner M, Monigatti F, Parker KC, Patterson T, Steen JJ, Hamprecht FA, Steen H (2008) Robust Prediction of the MASCOT Score for an Improved Quality Assessment in Mass Spectrometric Proteomics. J Proteome Res 7 (Copyright (C) 2012 American Chemical Society (ACS). All Rights Reserved.):3708-3717. doi:10.1021/pr700859x

120. Perkins DN, Pappin DJC, Creasy DM, Cottrell JS (1999) Probability-based protein identification by searching sequence databases using mass spectrometry data. Electrophoresis 20 (Copyright (C) 2012 American Chemical Society (ACS). All Rights Reserved.):3551-3567. doi:10.1002/(sici)1522-2683(19991201)20:18<3551::aid-elps3551>3.0.co;2-2

121. Strupat K (2005) Molecular weight determination of peptides and proteins by ESI and MALDI. Methods Enzymol 405:1-36. doi:10.1016/s0076-6879(05)05001-9

2. Aim of the Work

The aim of the present work was to explore new and further possibilities for sample preparation in protein and antibody analysis. There are several published and well established enzymatic and chemical methods for bioprocess and quality control strategies in biopharmaceutical production. So, what had to be developed new and what advantages could be expected here?

First at all gold was used as a basic carrier for the development of new heterogeneous nanobiocatalysts. Advantages, such as the simple transfer of the colloidal suspension by pipetting, but also the possibility of complete separation of the catalysts from the sample solution by standard bench top centrifuges due to the high specific density of gold, led to the choice of this nanomaterial. Other characteristics, such as simple methods for the synthesis of GNPs, various well-established analytical methods for characterization, and the ability to work in small volumes down to 1 µL can be positively mentioned here. Especially in the analysis of biopharmaceuticals such as monoclonal antibodies, working with small sample volumes from a financial point of view, but also due to the amount of sample material available, is essential. In addition, the handling of small sample volumes is sufficient for analysis by liquid chromatography and high-resolution mass spectrometry.
Gold nanoparticles are available for various immobilization strategies for peptides, proteins, carbohydrates, DNA, RNA and many more. Many conjugation strategies can be readily adapted due to the straightforward surface modification of gold e.g. by self-assembled monolayer formation with thiolated ligands.

The full-particle separation of the catalysts is an important point in the analysis of protein samples, for example when working with enzymes. They can show auto digestion and are thus present in the final protein analysis with characteristic peptides in the sample. Whether these enzymes have been added to the sample as a catalyst or whether they were part of

the sample cannot be easily clarified in the final discussion. However, if these enzymes as catalysts are immobilized, they can be completely separated from the sample.

These material-specific advantages make them a useful tool for analyzing various types of biopharmaceutical samples, such as therapeutic peptides and proteins, including monoclonal antibodies. Durability and reusability of catalysts should be important issues in development.

The present work deals with the synthesis of heterogenous nanobiocatalysts and the complete characterization of all synthesis steps with well-established methods such as Vis-spectroscopy, DLS, zeta potential measurements and protein assays. In addition, further characterization methods should be discussed and, if possible, compared with above methods. In addition, methods will be investigated and developed for the determination of functional parameters regarding enzyme activity. Methods for the investigation of biopharmaceuticals are to be examined and newly developed in order to finally ensure a practical applicability of the heterogeneous nanobiocatalysts.

3. Results and Discussions

3.1. Gold nanoparticle-conjugated pepsin for efficient solution-like heterogeneous biocatalysis in analytical sample preparation protocols

Markus Höldrich, Adrian Sievers-Engler, Michael Lämmerhofer

Institute of Pharmaceutical Sciences, Pharmaceutical (Bio-)Analysis, University of Tübingen, Auf der Morgenstelle 8, 72076 Tübingen, Germany

Anal Bioanal Chem (2016) 408:5415–5427

Abstract

Immobilization of enzymes on mesoporous microparticulate carriers has traditionally been accompanied by reduction in enzyme activity. Herein, we document that immobilization of pepsin via amide coupling on gold nanoparticles (GNPs) with carboxy-terminated hydrophilic PEG_7-shell resulted in a heterogeneous nanobiocatalyst with essentially equivalent turnover rates k_{cat} (90 %) and enhanced catalytic efficiencies k_{cat}/K_M (107 %) compared to homogeneous catalysis with pepsin in free solution for cytochrome C as model substrate. This heterogeneous catalyst showed further at least equivalent bioactivity in a digestion reaction of a protein mixture consisting of cytochrome C, bovine serum albumin and myoglobin. UHPLC-ESI-QTOF-MS/MS analysis of the digests with subsequent Mascot database search allowed unequivocal identification of all proteins with high score and good sequence coverage. The functionalized nanoparticles were further characterized by Vis spectroscopy in terms of the surface plasmon resonance (SPR) band, by dynamic light scattering (DLS) with regard to hydrodynamic diameters, and in view of their ζ-potentials at each step of synthesis and surface modification, respectively. These measurements have also revealed that the pepsin-functionalized GNPs are sufficiently stable over at least 1 month providing satisfactory shelf life to the heterogeneous catalyst. Advantageously, the pepsin-GNP bioconjugate can be conveniently removed after reaction by simple centrifugation steps which makes them a useful tool for analysis of therapeutic peptides and proteins, including monoclonal antibodies. The practical utility of the nanobiocatalyst was documented by digestion of a monoclonal antibody which yielded the $F(ab')_2$ fragment with a mass of 97,619.4 Da.

Keywords

Gold nanoparticle, bioconjugate, heterogeneous nanobiocatalyst, quadrupole time-of-flight mass spectrometry, enzyme kinetics, monoclonal antibody fragment $F(ab')_2$

Introduction

Workflows in protein analytics, e.g. in proteomics and analysis of protein therapeutics, commonly involve enzymatic digestion protocols prior to their LC-MS/MS analysis [1]. Thereby, most popular for proteolytic cleavage into peptide fragments is trypsin which is very efficient and yields short peptides with Arg or Lys at the C terminal end. Due to very short peptide fragments MS identification often fails leading to incomplete sequence information. Alternative enzymes are also often utilized, in proteomics primarily Lys-C, Glu-C, chymotrypsin and pepsin [1] and in therapeutic protein (i.e. monocolonal antibody) analysis pepsin, papain, IdeS [2] or ideally a combination of these biocatalysts [1]. These enzymes can also be very helpful for stereochemical configuration-dependent sequence elucidations of therapeutic peptides and peptidic natural products [3]. To avoid detrimental interferences from enzyme and confusing results in such applications, immobilization of these biocatalysts to solid surfaces, e.g. beaded agarose or monolithic supports, has been suggested as viable option to enable straightforward removal of the enzyme after the proteolytic reaction [4]. There are a number of other advantages associated with such heterogeneous catalysts, amongst which ameliorated enzyme stability, reusability are prominent ones [5,6]. Often, however, bonding to solid supports results in reduction of bioactivity of immobilized enzymes mainly because of hindered substrate access to the active site or unfavorably altered conformation of immobilized enzyme [5,6]. In an attempt to overcome such limitations of heterogeneous catalysts, researchers have evaluated nanomaterials as carriers for enzyme immobilization [7,8]. In fact, a number of studies reported increased activities and enhanced reaction rates as well as improved stabilities when enzymes were immobilized on nanocarriers [9,10].

In general, according to IUPAC nanomaterials have a length scale of less than 100 nm in at least one dimension [11]. This gives them peculiar properties of which their large surface-to-volume ratio is perhaps the most significant one in terms of heterogeneous bionanocatalysis for providing a large surface for functionalization with enzyme and a

large interface for enzyme-substrate reactions [12-14]. Frequently utilized nanoscaled supports for nanobiocatalysts comprise magnetic nanoparticles [8], silica nanoparticles, polymeric nanomaterials, metal oxides, nanofibers and metallic nanoparticles onto which enzymes have been immobilized by adsorption, covalent bonding, ionic interactions, via affinity tags, by crosslinking, or physical entrapment (entanglement) in a polymeric network [7,8]. Amongst the latter gold nanoparticles (GNPs) received particular attention and belong to one of the most intensely studied nanomaterials [15]. They can be prepared by a straightforward and low-cost size-controlled synthesis by reduction and stabilization of gold(III) chloride with citrate according to Turkevich-Frens [16,17]. Through a nucleation and growth-controlled mechanism [15,18,19] GNPs can be obtained in the size range between 1 and 50 nm. Furthermore, convenient quality control by Vis-spectroscopy due to the surface plasmon resonance (SPR) band with absorbance maximum around 520 nm makes this material attractive as carrier for biofunctionalized nanomaterials [20,21]. Besides adsorptive bonding of enzymes by ionic and hydrophobic interactions, enzymes can be conveniently immobilized via bifunctional ligands containing a terminal thiol group for direct attachment to the GNP surface and dative Au-S bond through self-assembled monolayer (SAM) formation [22] and subsequent conjugation of enzyme [12,23]. For this reason it is not further surprising that GNPs have become popular enzyme carriers for sample preparation in protein analysis, e.g. with trypsin [12,24,25], for enzyme-based sensor devices [26], for immunoassays [27,28], for theranostic applications e.g. in vivo tumor targeting and detection by surface-enhanced Raman scattering [29].

In this work, we report on the synthesis and characterization of pepsin-modified heterogeneous nanobiocatalysts based on a gold core with a hydrophilic PEG_7 shell onto which pepsin was covalently attached and their proteolytic performance for sample preparation in protein analytics. Pepsin is a digestive protease with a molecular weight around 36 kDa and an isoelectric point (pI) at approximately 3.2 [30][31]. Pepsin cleaves peptide bonds of proteins preferentially at the C-terminal side of phenylalanine and

leucine residues [32,33]. It is sometimes used in proteomics as alternative to trypsin (roughly estimated in about 0.4% of proteomic studies [1]), but also for antibody digestion near the hinge region to produce specifically $F(ab')_2$ and Fc fragments [2]. For this reason, it was also a popular enzyme target for its immobilization to various supports such as microparticles [34,35], magnetic beads [36], monoliths [37,38], nanospray emitter [39], planar surfaces low-density polyethylene (PE) films, or on polycarbonate (PC) plates, on microscope glass slides [40]dextran-modified fused-silica capillaries [41] and on fibers [42]. In a few studies, pepsin was immobilized on nanoparticulate carriers such as alumina nanoparticles ([43]), anisotropic gold nanoclusters [44] and colloidal gold [45]. However, the weak physical binding in these studies with non-covalent immobilization is regarded suboptimal in terms of chemical stability of these nanobiocatalysts as they have a tendency for enzyme leaching from the surface. To alleviate such limitations we propose herein covalently linked pepsin-GNP conjugates with an optimized surface chemistry that provides both chemical as well as colloidal stability and does not compromise bioactivity

Materials and Methods

Materials

Pepsin (from hog stomach, E.C.3.4.23.1, 3651 U mg^{-1}) was received from Fluka (Steinheim, Germany). Albumin, from bovine serum (BSA, EC Number 232-936-2, MW 66 kDa) was obtained from Sigma-Aldrich (Munich, Germany). Cytochrome C (CYC_HORSE, from horse heart, EC Number 232-700-9, MW 12,270 Da) and myoglobin (MYG_HORSE, from horse skeletal muscle, EC Number 309-705-0, MW 16,900 Da) were supplied by Calbiochem (Darmstadt, Germany).

Gold (III) chloride trihydrate ($HAuCl_4 \cdot 3H_2O$), trisodium citrate, tris(hydroxymethyl)-aminomethane (Tris), N-(3-dimethylaminopropyl)-N'-ethylcarbodiimide (EDC), O-(2-

carboxyethyl)-O'-(2-mercaptoethyl)heptaethylene glycol (HS-PEG_7−COOH), Folin & Ciocalteu's phenol reagent glycerol, a silver staining kit and monoclonal anti-HSA antibody for ELISA were obtained from Sigma-Aldrich (Munich, Germany).

Preparation of GNPs and Immobilization of pepsin

The preparation of GNPs was based on the reduction and simultaneous stabilization of gold (III) chloride trihydrate with trisodium citrate in accordance to the Turkevich-Frens method [16,17,12,46]. For the synthesis of 10 mL solution of GNPs, 5.05 mg $HAuCl_4$ (1.28 mmol in 11.25 mL double deionized water corresponding to a final concentration of 1.14 mM) was used and heated up to the boiling point and kept under reflux under constant stirring. Afterwards 1.25 mL of 20.5 mM trisodium citrate solution (6.03 mg mL^{-1}) was added (final concentration of 2.28 mM in a total volume of 11.25 mL) and heated for further 10 minutes, while the color turned red. The GNP solution was allowed to cool down and stirred at room temperature for another 60 minutes. The GNP solution was finally stored at + 4°C until usage [47].

To obtain covalently immobilized pepsin, first 1 µL of HS-PEG_7−COOH solution was added to 1 mL of above prepared GNP solution and the bifunctional linker immobilized overnight under constant stirring at room temperature. Afterwards the solution was centrifuged at 12,000 rpm and resuspended in 20 mM MES buffer pH 4.5. This washing step was repeated twice. 50 µL of EDC (12 mM in MeOH) to activate carboxylic acids and 250 µL pepsin (6 mg mL^{-1} in 20 mM MES buffer pH 4.5) were added and stirred for two hours at room temperature. The nanoparticles were washed in 20 mM Tris-HCl buffer pH 7.5 twice to cap residual activated carboxylic groups. The supernatant of the first washing step was used for protein quantification by Lowry assay (see below) [12].

The resultant nanoparticles were washed twice and resuspended in in double deionized water and characterized after each step of surface functionalization by Vis spectroscopy, DLS and ζ-potential measurements (see Fig. 1 and Electronic Supplementary Material Fig. S1).

In an additional study, in one synthesis batch nanoparticles of each step of surface functionalization were tested for their stability over 35 days. For this purpose, all samples were diluted 1:5 with double deionized water (ddH_2O) and characterized by Vis spectroscopy (see Electronic Supplementary Material Fig. S2).

Vis Spectroscopic Characterization of Nanoparticles as well as Size and Zeta Potential Measurements

The SPR band was measured by Vis-spectroscopy after each step of surface modification acquiring spectra in the wavelength range between 350 and 800 nm. All measurements were performed with a VWR UV-1600PC Spectrophotometer. The differently functionalized nanoparticles were further characterized by DLS and their ζ-potentials, derived from electrophoretic mobility measurements, before and after each step of chemical modification using a Zetasizer Nano ZS instrument (Malvern Instruments, Herrenberg, Germany). The Zetasizer was equipped with a He-Ne laser and the detection was performed at 173° backscatter detection mode. Samples were diluted in double deionized water (1:5; v/v) and measured as triplicates. Each value was the mean of 15 sub-runs.

Chromatographic Characterization of Pepsin Activity

A kinetic study was performed with pepsin in solution and with functionalized heterogeneous nanobiocatalysts with immobilized pepsin to determine the Michaelis-Menten parameters. Thus, several concentrations of CYC were digested in 20 mM sodium acetate pH 4.5 for 10 minutes at 37 °C. The digestion was stopped by adding 0.2 mL of 0.1 M NaOH to 0.8 mL reaction mixture (0.6 mL reaction buffer + 0.1 mL pepsin + 0.1 mL CYC stock solutions with different concentrations) to achieve neutral pH. For the study of pepsin in homogeneous solution as control reaction, 100 µL enzyme solution (2.5 mg mL^{-1} stock solution, 0.25 mg mL^{-1} final concentration) in above buffer was used for the digestion. The approach with the immobilized pepsin was performed in

1 mL total volume of the nanoparticle solution (0.7 mL nanoparticle solution in reaction buffer + 0.1 mL CYC stock solutions with different concentrations). Therefore Pepsin@GNP was centrifuged at 12,000 rpm for 10 minutes and resuspended in 0.7 mL 20 mM sodium acetate pH 4.5. The supernatant after the centrifugation step was discarded. After stopping the digestion by adding 0.2 mL 0.1 M NaOH (total volume reaction mixture 1 mL) the nanoparticles were centrifuged and the supernatant was analyzed by LC-UV for quantification of undigested CYC.

Michaelis-Menten parameters K_M and v_{max} were calculated by linear and bilinear equations according to Lineweaver-Burk diagrams [48]. A calibration function was established and used to quantify undigested CYC in the reaction mixture. All samples were measured as triplicates. For the LC analysis method of undigested CYC, an Agilent 1100 series HPLC instrument with a binary gradient pump, vacuum degasser, autosampler, column oven and a variable wavelength detector was used. The separation was performed with a 10 minutes gradient on a monolithic poly(styrene-co-divinylbenzene) ProswiftTM RP-1S 4.6 x 50 x 4.6 mm ID column from Dionex (ThermoFisher Scientific) with 50 mM ammonium formate pH 3.5 containing 5 % ACN in channel A and ACN + 5 % 50 mM ammonium formate pH 3.5 in channel B (0-2 minutes 20 % B, 2-6 minutes 60 % B, 6.01-10 minutes 20 % B). The flow rate of the mobile phase was 1 mL/min and the column temperature was set to 40 °C. The injection volume was 5 µL and detection was performed at 280 nm.

The method was validated considering the ICH Guidelines. Linearity, precision and accuracy were evaluated. The LOD and LOQ were determined as the concentrations with a signal-to-noise ratio of 3:1 and 9:1, respectively (see Electronic Supplementary Material Fig. S3 and Fig. S4 as well as Table S1).

Protein Determination by Lowry Assay

The amount of immobilized pepsin was determined by Lowry assay [49]. Briefly, the supernatant collected after the enzyme immobilization step was used for the

quantification of non-immobilized pepsin. Applying the mass balance equation, the immobilized amount of enzyme could then be back calculated. A calibration function was set up with free pepsin in 20 mM MES buffer pH 4.5 in the range 0.05 to 1 mg/mL. 25 µL of the sample/standard/blank were mixed with 125 µL of Lowry A solution and reacted for 20 minutes. Afterwards 12.5 µL Folin & Ciocalteu's phenol reagent (Lowry reagent B) was added and reacted for further 30 minutes before measurement. Lowry reagent A was freshly prepared every day (2.45 mL 4% Na_2CO_3 anhydrous in ddH_2O, 2.45 mL 0.1 M NaOH, 0.1 mL 2% Na-K-tartrate in ddH_2O and 0.05 mL $CuSO_4 \cdot 5H_2O$ in ddH_2O). Folin & Ciocalteu's phenol reagent was commercially available from Sigma-Aldrich.

For the photometric determinations a Versa max microplate reader from Molecular Devices was used and the wavelength was set to 650 nm. All measurements were carried out at room temperature. For more details see also Electronic Supplementary Material Fig. S5 and Fig. S6.

Protein digestion with pepsin-conjugated GNPs

BSA, CYC and MYG (0.2 mg mL^{-1} each of each protein) were utilized as model proteins to test the digestion efficiency of conjugated pepsin. For this purpose, 0.2 mL of the protein mixture was transferred to 1 mL of the nanoparticle suspension (Pepsin@GNP in 1 mL 20 mM sodium acetate pH 4.5). The reaction with the nanoparticle approach was stopped by centrifugation (12,000 rpm for 10 minutes) resulting in a clear supernatant for LC-MS/MS analysis. For the digestion protocol with free pepsin 0.3 mg ml^{-1} pepsin was used (0.25 mg mL^{-1} final concentration in 1.2 mL total volume) and, to 0.8 mL pepsin in digestion buffer was given 0.2 mL of the protein mixture. 100 µL aliquots were taken and the reaction was stopped by adding 20 µL of 0.1 M NaOH before injecting the sample for LC-MS7MS analysis.

The digestion of the protein mixture was performed in 20 mM sodium acetate buffer pH 4.5 at 37 °C from 4 to 24 hours digestion time. As control a sample at 0 h digestion time

was also taken and analyzed. Blank samples as 20 mM sodium acetate pH 4.5 were prepared as well.

Recyclability (see Electronic Supplementary Material Fig. S7) and pepsin leaching from Pepsin@GNP bioconjugate (see Electronic Supplementary Material Fig. S8) were also examined.

LC-MS/MS Method

All samples were injected via PAL HTC-xt autosampler (CTC Analytics, Zwingen, Switzerland). The separation was performed with an Agilent 1290 LC-system (Agilent Technologies, Waldbronn, Germany) on an Aeris Peptide C18 (3.6 µm 150 x 2.1 mm ID) column from Phenomenex (Torrance, CA, USA) with a 90 minutes gradient containing ddH_2O with 0.1 % (v/v) formic acid in channel A and acetonitrile with 0.1 % (v/v) formic acid in channel B (0-5 minutes 5 % B, 5-60 minutes from 5 to 60 % B, 60-65 minutes from 60 to 95 % B, 65-70 minutes 95 % B, 70-72 minutes to 5 % B, 72-90 minutes 5 % B). The peptide masses were detected with the quadrupole time-of-flight mass spectrometer Triple TOF 5600+ from Sciex (Concord, Ontario, Canada) equipped with a DuoSpray source operated in ESI positive mode. The source temperature was set to 350 °C and the ion spray voltage floating was 5500 V. The pressure of the ion source gases 1-3 was 50, 40 and 30 psi. Finally, the declustering potential was set to 100 V and the collision energy to 10 V. Ions were measured in information dependent data acquisition (IDA) mode for ions greater than 100 Da with an intensity threshold greater than 10 counts per second. Accumulation time for MS (survey scan) and MS/MS experiments were set to 250 ms. The dynamic background subtraction was activated and the collision energy for all MS/MS experiments was set to 25 V.

A Mascot search was performed to detect the digested protein and to examine the occurrence of autodigestion of the immobilized pepsin. Mascot version 2.0.05 was used with the Swiss-Prot database. Pepsin-A was selected as the enzyme. Precursor and fragment ion mass (monoisotopic) tolerance was set to ±0.2 Da. Peptide charge state

was set to +1, +2, +3 and one missed cleavage was allowed. Taxonomy and Modifications were not specified.

More detailed results on the UHPLC-ESI-QTOF-MS/MS analysis of the digested protein mix can be found in the Electronic Supplementary Material Fig. S9 to Fig. S12 as well as Table S2.

Antibody digestion with Pepsin@GNP

For this experiment the intact mass of monoclonal anti-HSA from an ELISA kit was determined before and after the digestion with immobilized pepsin by UHPLC-μESI-QTof-MS.

For the digestion 100 μL Pepsin@GNP in 20 mM sodium acetate pH 4.5 was mixed with 100 μL anti-HSA (1:100 dilution in 20 mM sodium acetate pH 4.5). The digestion was performed at 37 °C for 4 hours. To obtain a clear supernatant for analysis the nanobiocatalysts were centrifuged (12,000 rpm for 10 minutes).

LC-MS Method for the determination of intact protein masses

A Zorbax column (SPE 300 Å C18 5 μm 35 x 0.3 mm ID) from Agilent (Santa Clara, CA, USA) was used for online SPE. Within the first two minutes the column was used for desalting and enrichment of the sample with a flow of 50 μL/min 100 % ddH2O with 0.1 % (v/v) formic acid in channel A. From 2.01 to 8 minutes the adsorbed, desalted proteins were eluted from the SPE column and flushed into the mass spectrometer with 50 μL/min 100 % acetonitrile containing 0.1 % (v/v) formic acid in channel B. A two minutes pre-equilibration step was performed to reach the starting conditions of the method. The protein masses were detected with the quadrupole time-of-flight mass spectrometer Triple TOF 5600+ from Sciex (Concord, Ontario, Canada) equipped with a DuoSpray source operated in μESI positive mode, using a 50 μm I.D. μESI-needle (Sciex). The source temperature was set to 400 °C and the ion spray floating voltage (ISFV) was 5100 V. Nebulizer gas (GS1) was set to 40 psi, drying gas (GS2) to 40 psi

and curtain gas to 30 psi. Finally, the declustering potential (DP) was set to 230 V and the collision energy (CE) to 30 V. TOF-MS scan ranged from 500 to 4000 Da. For intact protein detection Sciex's Intact-Protein script was activated, Q1 transmission was set to 100 % at 1250 m/z and sensitivity was increased by summing 60 time bins. Data processing and identification of the intact protein mass was performed with the Bio Tool Kit from Sciex.

Results and Discussion

Synthesis and Characterization of Functionalized GNPs

Citrate-capped GNPs were prepared according to the method by Turkevich-Frens [16,17]. This approach is based on the reduction of $HAuCl_4$ by trisodium citrate and allows a straightforward size-controlled synthesis of GNPs in the range of 10 to 30 nm by variation of the molar citrate-to-gold tetrachloride ratio in the range between 6:1 and 2:1 [47]. Citrate ions attached to the GNP surface after synthesis are responsible for the good colloidal stability of the resultant nanoparticle suspensions. A convenient strategy for enzyme immobilization on nanoparticulate carriers represents adsorptive bonding driven by attractive electrostatic interaction forces. This approach towards heterogeneous nanobiocatalysts was examined herein as well, yet found to be suboptimal in terms of stability of resultant nanocolloids. Therefore, immobilized pepsin, having pI between 2 and 3 according to literature, may easily detach under reaction conditions (pH between 1-4), contaminating the resultant reaction solution after removal of the nanoparticles with proteinogenic material which may interfere with final analytical determinations. Hence, a covalent attachment strategy of pepsin was adopted following the reaction scheme presented in Fig. 1. The bifunctional linker HS-PEG_7-COOH was first self-assembled in a dense monolayer on the gold surface via stable dative thiol-gold bond. It was previously shown that this linker provides stable SAMs (self-assembled monolayers) with surface

coverages of 4.29 ± 0.45 ligands per nm^2 [50]. The PEG linker supports colloidal stability and prevents non-specific binding of proteins. It was found that enzyme-GNP conjugates have better colloidal stability when the enzyme was bonded via a PEG linker as compared to corresponding alkyl linkers and compared to adsorptively bonded enzyme-GNP conjugates as well [12]. Longer spacers turned out to be advantageous in terms of bioactivity, and therefore the bifunctional linker HS-PEG_7-COOH was selected in the current work as first choice. The terminal carboxylic groups constitute reactive anchor functionalities for bonding of pepsin by direct amide coupling with EDC under weakly acidic conditions. As a last step in the synthesis, remaining EDC-activated carboxylic groups were capped with Tris moieties yielding the final pepsin-functionalized GNPs with residual carboxylic acid groups. The latter are supportive for the colloidal stability and shelf life of the resultant bionanocatalyst.

All nanoparticles were characterized after each step of synthesis and surface modification, respectively, by Vis spectroscopy for measurement of changes of the SPR band, by DLS analysis for nanoparticle size (i.e. hydrodynamic diameter) characterization and by determination of the ζ-potential. The results are illustrated in Fig. 2.

Citrate-stabilized GNPs obtained by synthesis with a 2:1 molar ratio of citrate/$HAuCl_4$ revealed a mean diameter of 31.4 ± 0.9 nm according to DLS measurements and a ζ–potential of -34.7 ± 1.7 mV. Such nanoparticle sizes were recently found to be favorable over smaller ones for protein immobilization [12]and were therefore used as starting carrier for all batches of modified GNPs in this study. The final concentration of the GNP solution of 1.5 x 10-6 mM was calculated with the results of the DLS measurements and the Lambert-Beer law [47].

Vis spectroscopy represents the most straightforward and useful tool for quality control of surface modification. Alterations in size, size distribution and shape as well as chemical changes at the surface lead to shifts of the characteristic SPR band which is found as an absorption band with a maximum at around 525 nm according to the Mie theory [51,52].

As displayed in Fig. 2a, the SPR band as monitored by Vis spectroscopy is slightly shifted to higher wavelength upon each step of surface modification

(from λ_{max} = 525 ±0.6 nm for citrate-capped GNPs to λ_{max} = 528 ±1 nm after pegylation to λ_{max} = 532 ±1.7 nm after bonding of pepsin) and confirms successful bonding of the respective ligand at each step. It becomes further evident that no significant aggregation occurs upon pegylation which yielded carboxy-terminated GNPs nor after enzyme immobilization which afforded the final pepsin-conjugated GNPs. Aggregation typically leads to broad absorption bands with λ_{max} > 550 nm which are absent in the current Vis spectra (Fig. 2a) [46]. Narrow absorption bands are observed for all three studied particle types due to absence of aggregation. The slightly broader absorption band for the pepsin-modified GNPs may be due to asymmetrically-shaped particles and departure from strictly spherical shape after enzyme immobilization [47].

Sufficient colloidal stability is also confirmed by the ζ–potentials of the modified particles. In any case, ζ–potentials were < -25 mV (Fig. 2b) which is indicative for sufficient electrostatic repulsion overcoming attractive van der Waals interactions that are the prime cause for aggregation of nanoparticles.

Nanoparticle diameters were measured by DLS. As expected, with each layer of surface modification the size of the resultant nanoparticles increased confirming successful ligand attachment. The bifunctional PEG_7 linker with terminal carboxylic group has a length of about 3.5 nm [50]. After its bonding to the GNP surface by SAM formation the diameter of the nanoparticle grew from 31 nm to 52 nm which is in good agreement with expectations. The slight difference between theoretical and experimental values may be due to strong solvation of pegylated GNPs. The sphere equivalent particle diameter further increased to 105 nm after coupling of pepsin to the carboxy-terminated GNPs (Fig. 2b).

The surface coverage of pepsin on the GNPs was determined by protein quantification with Lowry assay measuring free pepsin in the supernatant after the reaction and applying mass balance considerations The pepsin concentration on the GNPs was

determined to 0.25 ± 0.03 mg mL^{-1} (7.24 ± 0.87 x 10-6 mol/L) For sake of comparison, also the data for nanoparticles with pepsin adsorptively bonded directly to citrate-capped GNPs are included in Fig. 2b. It can be seen that the diameter was significantly smaller (66 nm) as expected due to the missing PEG-shell. Most notably, the ζ-potential of this adsorptively bonded bioconjugate was much lower as compared to the covalently bonded pepsin-GNP conjugate. In fact, it turned out that such GNPs are less stable, may easily aggregate and show reduced shelf life making them less suitable for the intended analytical purpose. In contrast, covalent pepsin-modified GNPs with PEG-linker showed excellent stability over extended period (see also Electronic Supplementary Material Fig. S1). Hence, the covalent immobilization strategy proposed herein is favorable in particular also from viewpoint of shelf-life of the functionalized nanoparticles as well as with regards to bleeding of enzyme into the reaction mixture in the course of sample preparation giving rise to interferences in the subsequent analysis.

Characterization of heterogeneous nanobiocatalyst by Michaelis-Menten enzyme kinetics

As a simple test to characterize the functionality of the new nanoparticulate biocatalyst, cytochrome C (CYC) was digested with pepsin-GNP bioconjugate in comparison to homogeneous catalysis with free pepsin and the data were processed in accordance to the formalism of the Michaelis-Menten enzyme kinetics. Three replicate batches of incubations at each substrate concentration level (n = 3) were examined for both free and immobilized enzyme. In order to allow a representative comparison, the enzyme concentration was kept constant in reactions with free and immobilized pepsin (concentrations of pepsin were 7.24 x 10^{-6} for free and 7.24 ±0.87 x 10^{-6} mol/L incubation, respectively, for immobilized pepsin). For this purpose, an LC-UV method for the quantitative determination of non-digested CYC was developed and validated according to ICH guidelines (details about method validation and method performance are given in the Electronic Supplementary Material Fig. S3, Fig. S4 and Table S1). The assay, based

on separation of the intact CYC protein from digested peptides which elute more or less unretained in the established RPLC method with poly(styrene-co-divinylbenzene) monolithic column, allowed accurate and precise quantification of undigested CYC. For the quantitative evaluation of the enzyme kinetics the reaction rate was determined from the time-dependent decrease of educt (CYC). Incubations of variable concentrations of substrate (CYC) with free and immobilized pepsin were analyzed following the formalism of the Michaelis-Menten equation (see Fig. 3). Both, nonlinear and linear curve fitting to derive K_M and v_{max} gave insufficient quality of fit for both, digestion with free and immobilized enzyme. From the linear representation in accordance to the Lineweaver-Burk diagram in Fig. 2b, the nonlinear behavior is evident. Nevertheless, for a rough estimation of the kinetic parameters K_M and v_{max} were calculated from the data plotted according to the Lineweaver-Burk-diagram. The results are summarized in Table 1. K_M values of 29 (±3) µM and 21 (±2) µM for free and immobilized pepsin, respectively, have been calculated indicating that immobilization did not negatively affect affinity of the substrate to the enzyme. Apparently, access of CYC to the catalytic site is not hindered considerably by the linkage of pepsin to GNPs and the chemical bonding does not seem to induce major conformational changes in the enzyme with negative effects on bioactivity. At this point it is, however, also quite clear that due to the intrinsic structural heterogeneity of the heterogeneous nanobiocatalyst originating from polydispersity in size, shape, protein coverage and in particular orientation each individual microscopic state of the enzyme conjugate may possess distinctly unique kinetic properties. As a consequence, this characteristic kinetic parameter K_M of the pepsin-GNP conjugate actually represents macroscopically a weighted average value of individual microscopically distinct nanobiocatalysts. Since the non-directed immobilization by the selected amide coupling leads to random protein orientation and hence presumably to hindered access of the active site in some orientations, the decrease of the macroscopic K_M value by 27% relative to free pepsin is not further surprising. The maximal rates of enzymatic reaction v_{max} achieved by free pepsin and heterogeneous pepsin

nanobiocatalyst at maximum (saturating) substrate concentrations are also very similar (v_{max} = 4.4±0.3 and 3.5±0.2 x 10^{-8} M s^{-1}, respectively). Furthermore, knowledge of the total enzyme concentration in the reaction allows calculation of the turnover number k_{cat} which was 6.1 x 10^{-3} s^{-1} and 4.5 x 10^{-3} s^{-1} for free and immobilized pepsin. This corresponds to a catalytic constant for the heterogeneous nanobiocatalyst of 78 % of free pepsin which may be regarded as equivalent to homogeneous catalysis. Even more so the ratio k_{cat}/K_M, which is a characteristic parameter to describe the catalytic efficiency, is even higher for the immobilized pepsin. Consequently, it can be concluded that immobilization of pepsin to pegylated GNPs affords a nanobiocatalyst which can benefit from properties of heterogeneous catalysis (like easy removal) while still exhibiting kinetic properties like a homogeneous biocatalyst.

As mentioned above, nonlinearity was found in Lineweaver-Burke diagrams for both free and immobilized pepsin. To more adequately characterize enzyme kinetics a biphasic behavior was assumed and bilinear Lineweaver-Burke diagrams exploited for deriving characteristic parameters. A summary of the results is given in Table 1. It can be seen that at higher CYC concentration levels the K_M values ($K_{M,2}$) increase by a factor of around 10 indicating lower affinity of the substrate to both free and immobilized enzyme. At the same time, theoretical v_{max} values increase by a factor of ca. 4 at high substrate concentrations. Overall, catalytic efficiencies are by a factor of ca. 2 lower in the high concentration regime. In any case this nonlinear behavior may indicate feedback inhibition or competitive binding of peptidic products. Such feedback inhibition has been reported previously for other pepsin-catalyzed reactions as well [53].

Protein digestion with free and GNP-conjugated pepsin

To test on a wider scope the performance with a more complex sample, the functionalized heterogeneous nanobiocatalyst with immobilized pepsin was evaluated for its digestion capability of a protein mixture composed of bovine serum albumin (BSA), CYC and myoglobin (MYG) in comparison to its free analog. Again, for comparison the

pepsin content was adjusted to be similar for both incubations with free and immobilized pepsin. The resultant protein digests sampled at 0, 4, 12, and 24 h were analyzed by UHPLC-ESI-QTOF-MS/MS measurements in data-dependent IDA scan mode and the exported peak list subjected to Mascot search in order to elucidate the quality of digestion in a time-dependent manner by monitoring scores of protein identification and corresponding sequence coverages. Fig. 4a-4d show chromatograms of the pepsin digests resulting at different digestion times with pepsin-GNP conjugate and Fig. 4e-4h the corresponding chromatograms obtained with free pepsin.

It can be seen in Fig. 4a that immediately after addition of pepsin-GNP conjugate to the protein mixture peptides appear in the chromatogram, while digested peptides are virtually absent in the free enzyme incubation (Fig. 4e) (see also Fig.5a). This could indicate accelerated reaction with the immobilized pepsin, maybe owing to a higher local pepsin concentration on the enzyme-GNP conjugate as compared to that in free solution despite the approximately equal overall presence of pepsin in the system. Another explanation might be continued digestion during workup while spinning down the pepsin-modified GNPs. After 4 h, BSA and MYG are completely digested both with immobilized and free enzyme (Fig. 4b and 4f). 39 and 42 peptides were detected with immobilized and free pepsin, respectively (Fig. 5b). The number of detected peptides was not significantly altered after 12h (Fig. 4c and 4g as well as fig. 5c), and only slightly increased after 24 h digestion (Fig. 4d and 4h as well as fig. 5d). From the Venn diagrams [54] in Fig. 5 it is clearly evident that the heterogeneous pepsin-bionanocatalyst shows a larger, or at least similar, number of digested peptides as free pepsin.

Mascot database search uses probability-based scoring to judge whether a result is significant and not a random event, and scores greater than 67 are deemed to be significant ($p<0.05$) [55,56]. Scores for the distinct digested samples are depicted in Fig. 6a. It can be seen that the Mascot search enables identification of the proteins with high scores (>100) in all digests after 4 h digestion time or more, not only for pepsin in solution but also the pepsin-GNP conjugate. In fact, the scores of the Mascot search were on

average even higher for the immobilized pepsin. Moreover, sequence coverages > 20% in the digests with 4 and 12 h digestion times for the heterogeneous nanoparticle-based biocatalyst allows to conclude that its bioactivity and catalytic performance is at least of equal quality as compared to pepsin in free solution which cannot be conveniently removed by brief spinning (Fig. 6).

A common problem of digestion using proteolytic enzymes in solution in sample preparation is autodigestion. This problem can be largely eliminated with immobilized enzymes. It was therefore carried out a dedicated search for signature peptides originating from pepsin in the protein digests. However, in the present case neither in solution nor in digests from immobilized pepsin, auto-digestion could be detected. However, this issue might get more important if reaction times need to be extended for proteins which are more resistant to digestion by pepsin.

On the other hand, no pepsin contamination was present in the incubation in case of the immobilized pepsin nanobiocatalyst whereas the soluble enzyme might represent an impurity and interference in the analyzed protein sample in conventional reaction incubations. No pepsin was bleeding from the GNP-pepsin conjugate in the course of digestion of CYC (see Electronic Supplementary Material Fig. S18).

Last but not least, the immobilized pepsin@GNP nanobiocatalyst can be re-used. Recyclability was tested and it was found that up to 3 cycles of re-use the digestion performance (sequence coverage) was largely maintained at the same level while after 3 reuse cycles its digestion performance started to decline (see Electronic Supplementary Material Fig. S7).

Comparative peptide mapping

In order to gain insight into the proteolytic specificity of the conjugated pepsin and to compare its performance with free pepsin, also in terms of missed cleavages and peptide homology, a closer lock into the peptide fragments obtained by digestion of the protein

mix (CYC, MYG, BSA) for 4h with Pepsin@GNP and free pepsin in solution was undertaken. Fig. S9-S11 of the Electronic Supplementary Material show an overview of precursors generated by Pepsin@GNP, overlays of XICs of protein-specific peptides for each CYC, MYG and BSA, and an exemplary MS/MS spectrum of a model peptide. Figure 7 illustrates the protein sequences of CYC (Fig 7a) and MYG (Fig. 7b), and the peptides identified in corresponding digests of free and immobilized pepsin are indicated by arrows covering the respective sequence (corresponding map for BSA can be found in the Electronic Supplementary Material Fig. S10). Solid arrows show the fragments cut by pepsin in solution, dashed arrows the fragments cut by Pepsin@GNP. 100 % homology was found in the generated peptide fragments in case of CYC yielding a sequence coverage of 68 % for CYC both with free and gold-conjugated pepsin (Fig. 7a). Only two missed cleavages are found (F in position 11 and L in position 69). The former missed cleavage may be due to K in P3 while the latter could be a result of the negative effect on cleavage exerted by Pro at P3'. Moreover, the N-terminal tail was not identified by Mascot. To a large extent, good but slightly lower homology between heterogeneous and homogeneous catalysis was also found for MYG (Fig. 7b). While identified peptides were identical over large sequences at the N- and C-terminal tails, in the range between position 50 and 105 peptides and sequence coverage were different for the two approaches of digestion. Both missed to cleave at positions 3 (L), 44 (F), 47 (F), 73 (L) and 152 (F). Sequence coverage was 72 % and 62 % for MYG by free pepsin and Pepsin@GNP, respectively. Overall, good homology in generated peptide fragments between immobilized and free pepsin was found also for BSA (see Electronic Supplementary Material Fig. S12).

Determination of the antibody mass before and after digestion with Pepsin@GNP

In addition to the characterization of the heterogeneous nanobiocatalysts by model proteins (BSA, CYC and MYG) a digestion of a real sample, a monoclonal antibody, in accordance with the intended purpose of use of the developed heterogeneous

nanobiocatalyst should demonstrate its functionality. Pepsin digestion of IgG under non-denaturing conditions yields antibody fragments which are particularly useful for middle-up mass measurement for characterization of therapeutic antibodies by high-resolution MS. Since pepsin cleaves IgG at the C-terminal side of the inter-heavy-chain disulfides in the hinge region, it produces a bivalent antigen binding fragment, $F(ab')_2$, with a molecular mass of about 100 kDa.

HR-MS using a QTOF equipped with a μESI sprayer and a C18 online trap column for desalting of the protein sample was used for characterization of the intact monoclonal antibody and the fragment obtained by digestion with pepsin@GNP. In the established assay, the protein elutes at around 5 min from the trap column, well separated from the salt plug at around 2.5 min (Fig. 8a). The MS spectrum of the intact monoclonal antibody is shown in Fig. 8b. It shows the characteristic charge envelope in the range +50 to +100, as expected. The deconvoluted MS spectrum of the intact anti-HSA antibody revealed a mass of about 149 kDa with a number of isoforms (insert) (Fig. 8c). The same experiment with the antibody fragment obtained by digestion with Pepsin@GNP resulted in a single peak with a mass of 97,619.4 Da for $(Fab')_2$. These results clearly document the functionality of the immobilized pepsin nanobiocatalyst and evidence its practical utility for therapeutic protein characterization.

Conclusions

Pepsin A was successfully immobilized on gold nanoparticles via bifunctional PEG_7-linker resulting in efficient functionalized heterogeneous nanobiocatalysts with good colloidal stability and shelf life over at least a month. Characterization of the enzyme kinetics of the pepsin-GNP bioconjugate in comparison to free pepsin by digestion of the model protein cytochrome C clearly revealed that the enzyme fully retained its catalytic efficiency after immobilization on this nanoparticulate carrier. Digestions of protein mixtures followed by UHPLC-ESI-QTOF-MS/MS analysis with subsequent protein

identification by Mascot database search documented the pertinent bioactivity of the pepsin-GNP bionanocatalyst and its utility for protein analysis and characterization, respectively. By measuring in intact protein mode it was possible to determine the $(Fab')_2$ fragment after digestion of anti-HSA with Pepsin@GNP.

While the heterogeneous pepsin-GNP bionanocatalyst showed equivalent kinetic performance and catalytic efficiency, it offers significant additional benefits, thus combining favorable properties of homogeneous and heterogeneous catalysis. It can be pipetted like a solution due to the stable colloidal suspension which facilitates sample handling, automation, and miniaturization of sample preparation protocols, properties which are characteristic for homogeneous catalysis, Due to the high density of the metallic gold nanoparticle core, the heterogeneous bionanocatalyst can be easily spinned down on a minispin in a few minutes at low rpm, equipment which is available in virtually any lab and does not involve complicated procedures. In the current enzyme-GNP bioconjugate, the enzyme is freely accessible on the surface of the nonporous gold particle and not deeply buried inside a pore channel such as in more common heterogeneous catalysts in which enzymes are immobilized on mesoporous microparticles, such as (crosslinked) agarose. Due to this fact, diffusion limitations are thought to be less serious on enzyme-GNP bionanocatalysts. On contrary more common microparticulate heterogeneous catalysts may seriously suffer from diffusion limitations in intraparticulate pore spaces which may easily lead to substrate depletion as well as product accumulation at intraparticulate active enzyme centers. Overall, however, the removal of the functionalized heterogeneous nanobiocatalysts by centrifugation bevor the analytical determination is the striking advantage, both for single as well as coupled digestion or sample preparation protocols. This is of utmost importance in primarily intended application fields such as for therapeutic peptide and protein characterization as well as (sequence and stereoconfiguration) analysis of (lipo)peptides from natural pools where enzyme contaminations might easily interfere with the analysis and complicate the interpretation of results.

Acknowledgements

We acknowledge support by the “Struktur- und Innovationsfonds Baden-Württemberg (SI-BW)” and the German Science Funds (DFG no. INST 37/821-1 FUGG). We are grateful to Prof. Rolf Daniels for providing access to the Zetasizer Nano instrument for DLS and ζ-potential measurements.

Compliance with ethical standards

Conflict of interest

The authors declare no competing conflict of interest.

Figures and Figure Captions:

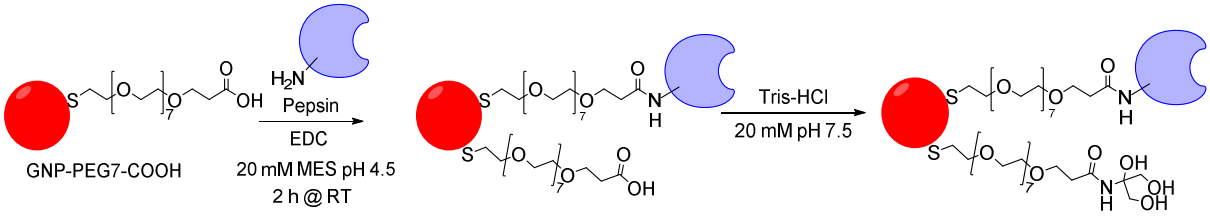

Fig. 1 Reaction scheme for functionalization of GNPs with bifunctional crosslinker and pepsin.

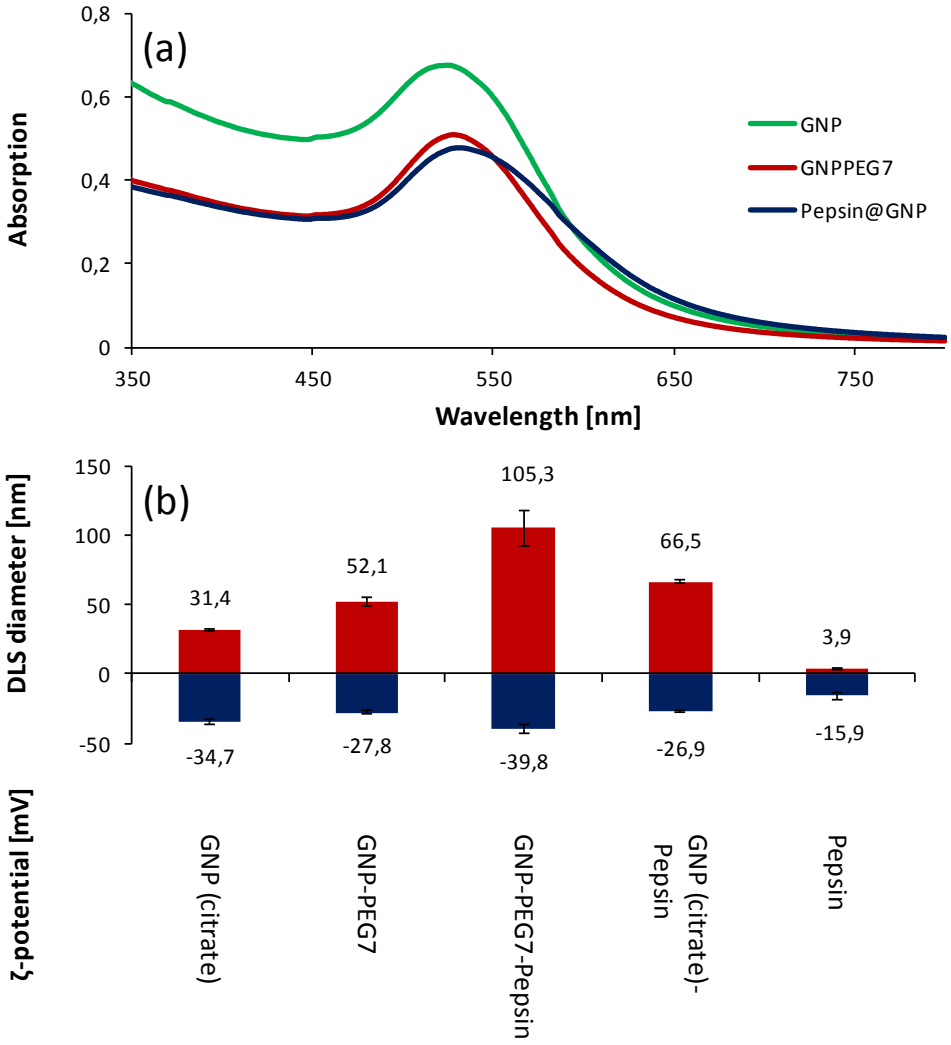

Fig. 2 Characterization of nanoparticles after each step of synthesis and surface functionalization, respectively. (a) Vis spectra showing slight shifts of the SPR band upon surface modification, (b) size (hydrodynamic diameters) as measured by DLS and ζ-potentials of all nanoparticle stages, along with adsorptively immobilized pepsin-modified nanoparticles as well as free pepsin.

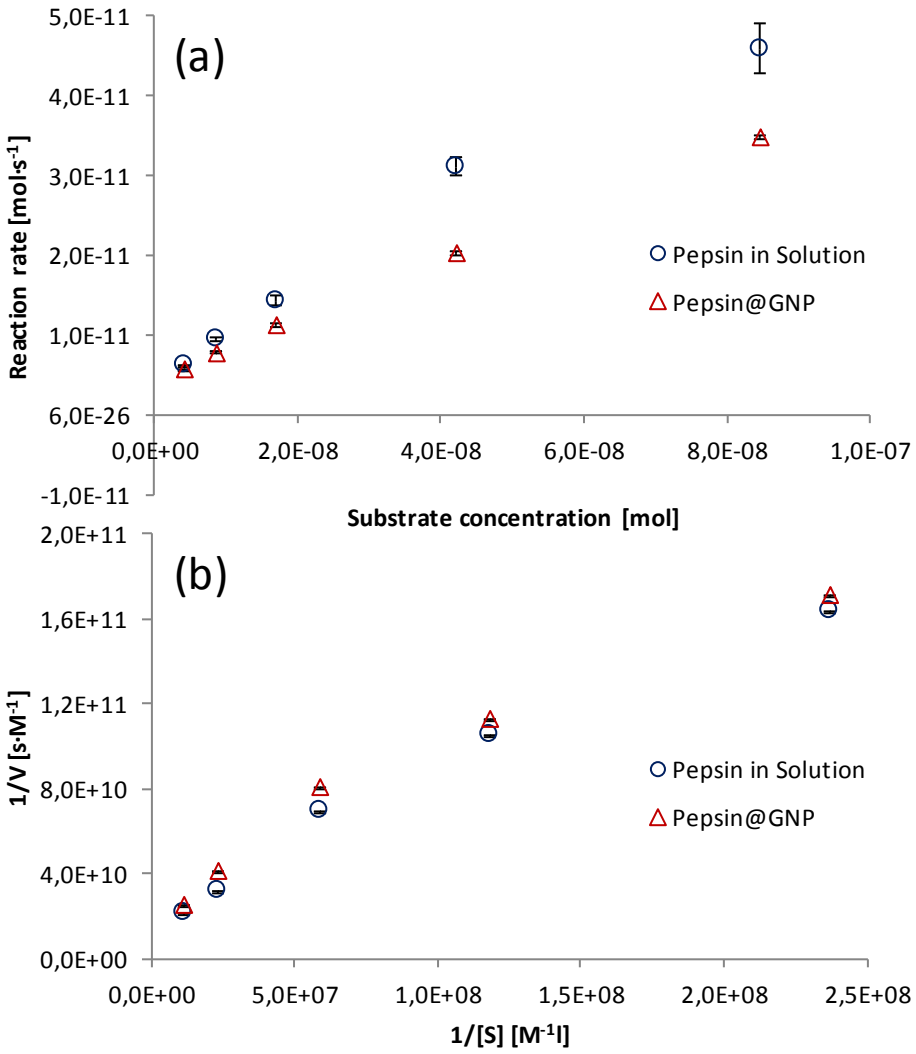

Fig. 3 Characterization of bioactivity of free and GNP-conjugated pepsin by Michaelis Menten enzyme kinetics in nonlinear representation (a) and linearized form according to Lineweaver-Burk diagram.

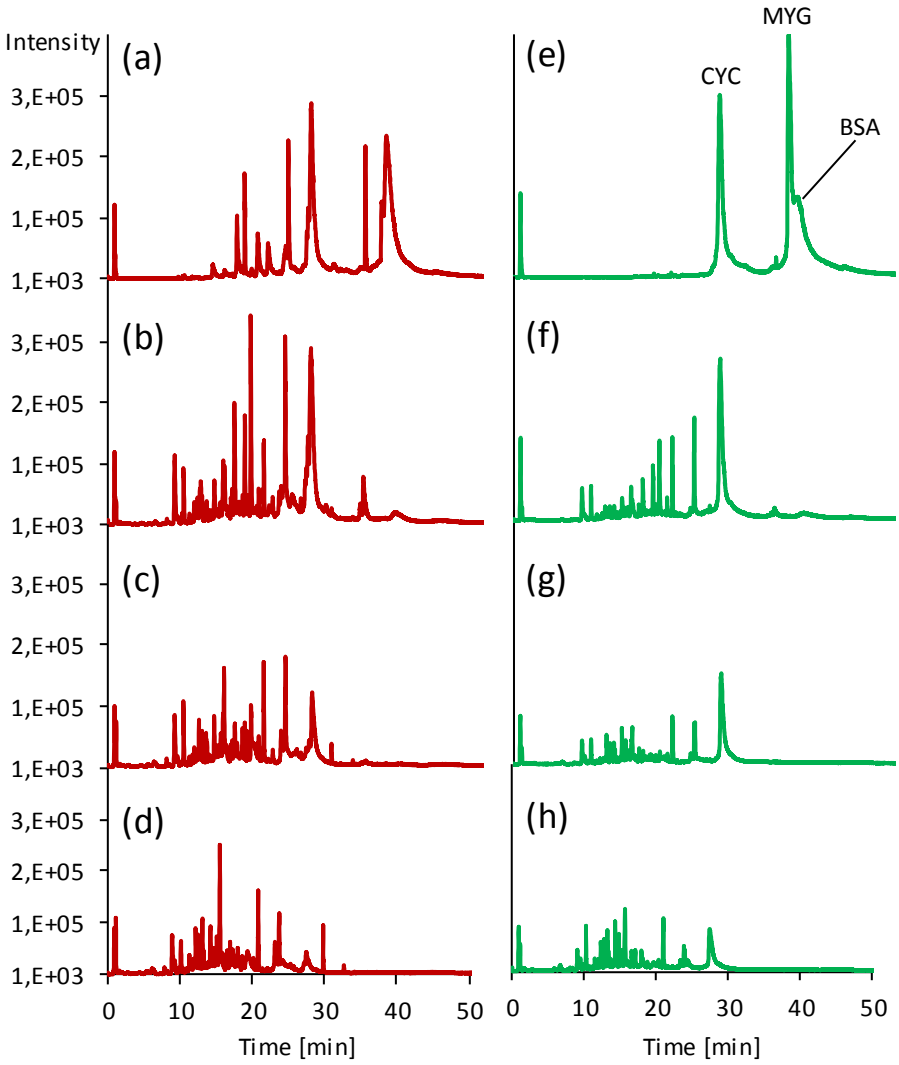

Fig. 4 UHPLC-ESI-QTOF-MS/MS measurements (TIC) of a protein mix digested with GNP-conjugated pepsin (a-d) and free pepsin (e-h) for 0 h (a,e), 4 h (b,f), 12 h (c,g) and 24 h (d,h).

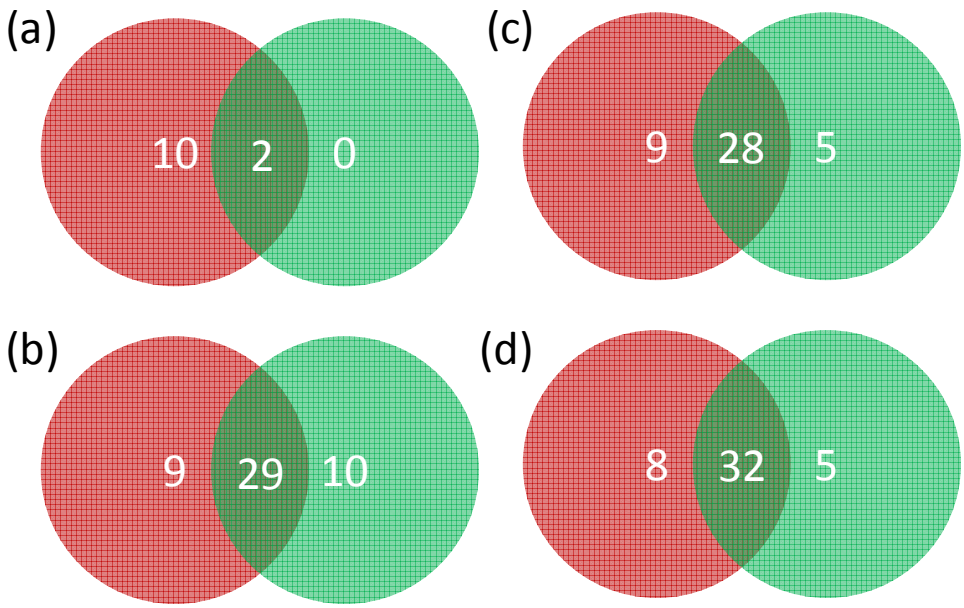

Fig. 5 Venn diagrams comparing numbers of peptides detected in samples digested with GNP-conjugated pepsin (red circle), free pepsin (green circle) and both (intersection) a) immediately after admixing the enzyme to the incubation mixture i.e. 0 h, b) after 4h, c) after 12 h, and d) after 24 h of digestion time.

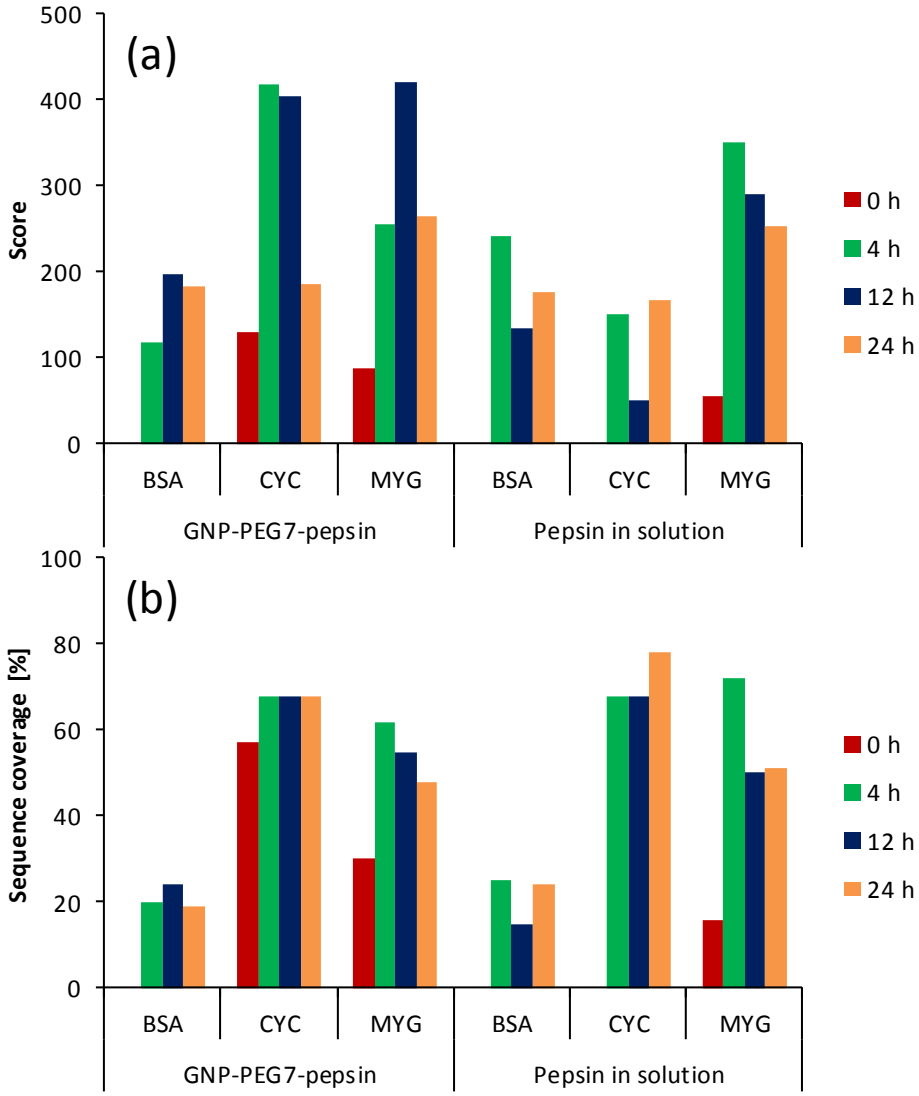

Fig. 6 Mascot search results for protein identification in digests of a protein test mixture composed of BSA, CYC and MYG obtained with GNP-PEG_7-pepsin and pepsin in solution which shows the score (a) and the sequence coverage (b) after 0, 4, 12 and 24 h digestion time (for corresponding chromatograms see Fig. 4). The Mascot search using MS/MS data of the IDA scan mode was performed with the SwissProt database.

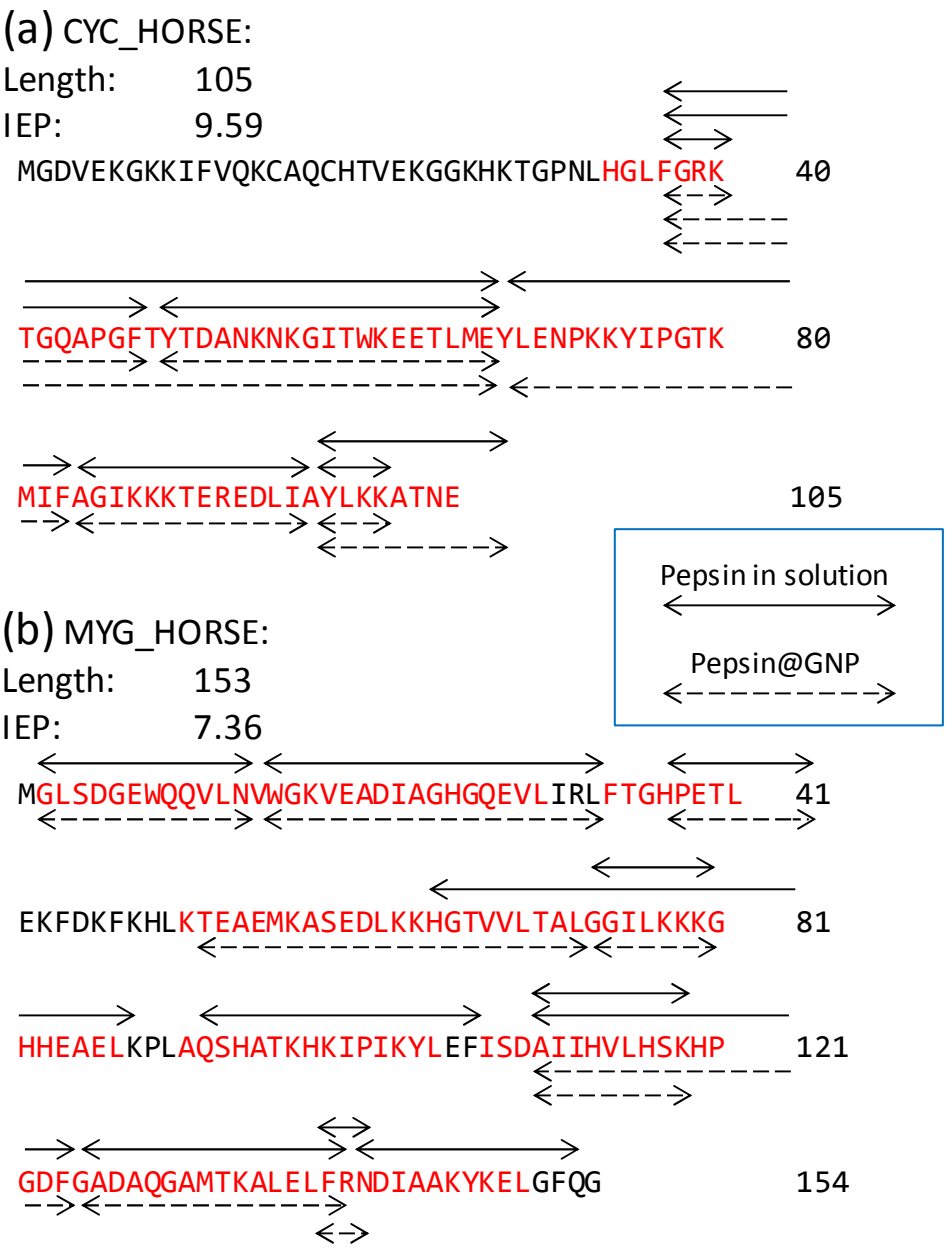

Fig. 7 Sequence of CYC (a) and MYG (b) with identified peptides found in digests with free pepsin in solution (solid arrows) and pepsin-modified GNPs with HS-PEG$_7$−COOH spacer (dashed arrows). Peptides were determined by Mascot search and compared with reference to the protein sequences.

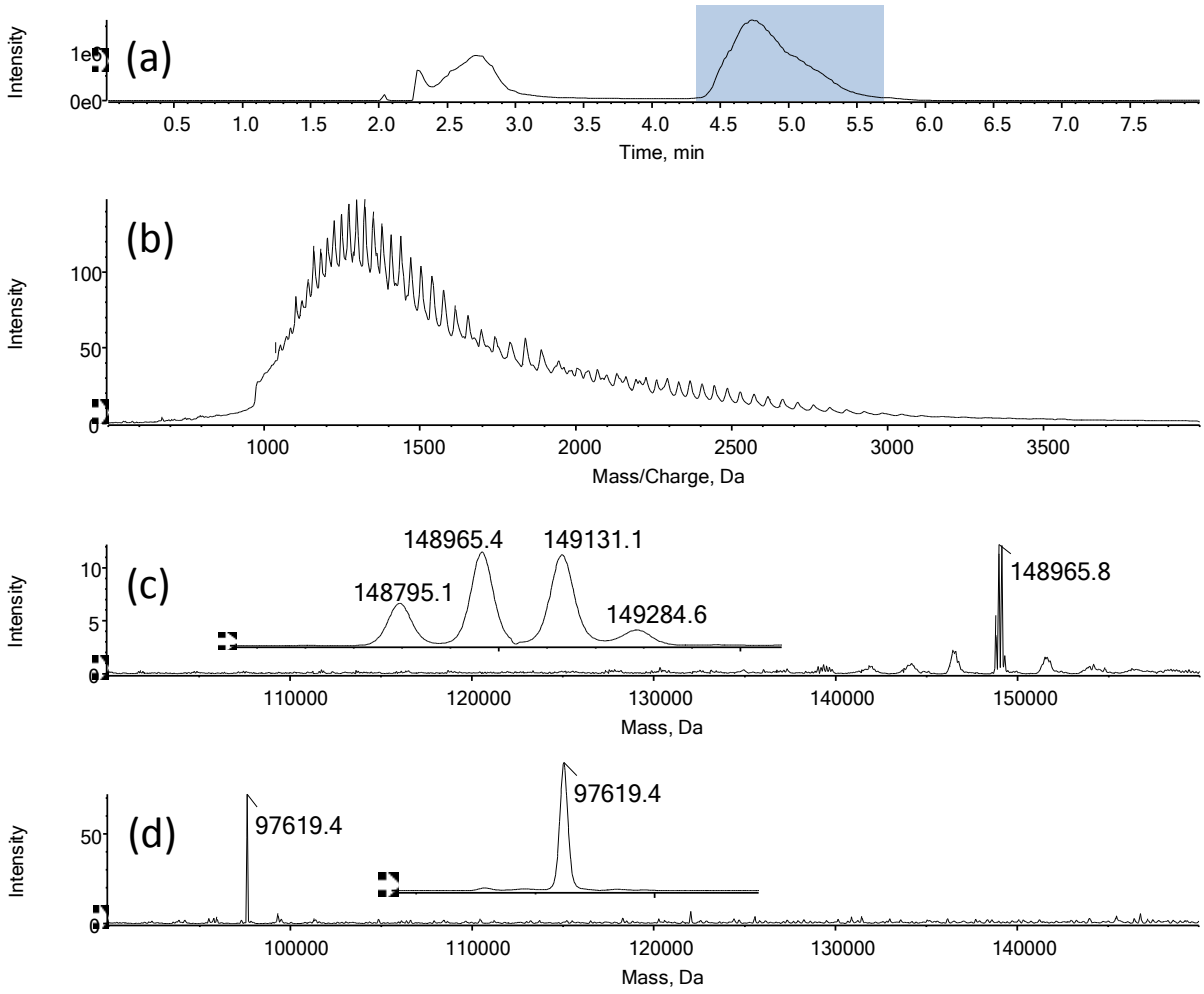

Fig. 8 Digestion of monoclonal antibody with Pepsin@GNP. TIC (a) and TOF-MS spectrum (b) of intact anti-HSA as measured by online-SPE µESI-QTOF-MS. The TOF-MS spectrum was taken at the indicated area between t_R 4.5 and 5.5.min and shows the charge envelope of anti-HSA. The mass spectra (c) and (d) depict the intact protein mass of anti-HSA before (c) and after (d) digestion with Pepsin@GNP.

References

1. Tsiatsiani L, Heck AJR (2015) Proteomics beyond trypsin. FEBS J 282 (14):2612-2626. doi:10.1111/febs.13287

2. Beck A, Wagner-Rousset E, Ayoub D, Van Dorsselaer A, Sanglier-Cianferani S (2013) Characterization of Therapeutic Antibodies and Related Products. Anal Chem (Washington, DC, U S) 85 (2):715-736. doi:10.1021/ac3032355

3. Gerhardt H, Sievers-Engler A, Jahanshah G, Pataj Z, Ianni F, Gross H, Lindner W, Laemmerhofer M (2016) Methods for the comprehensive structural elucidation of constitution and stereochemistry of lipopeptides. J Chromatogr A 1428:280–291. doi:10.1016/j.chroma.2015.05.065

4. Safdar M, Spross J, Janis J (2014) Microscale immobilized enzyme reactors in proteomics: Latest developments. J Chromatogr A 1324:1-10. doi:10.1016/j.chroma.2013.11.045

5. Zhanga Y, Gea J, Zheng L (2015) Enhanced Activity of Immobilized or Chemically Modified Enzymes. ACS Catal 5 (8):4503-4513. doi:10.1021/acscatal.5b00996

6. Liu J, Yang Q, Li C (2015) Towards efficient chemical synthesis via engineering enzyme catalysis in biomimetic nanoreactors. Chem Commun (Cambridge, U K) 51 (72):13731-13739. doi:10.1039/C5CC04590H

7. Misson M, Zhang H, Jin B (2015) Nanobiocatalyst advancements and bioprocessing applications. J R Soc Interface 12 (102):1-20. doi:10.1098/rsif.2014.0891

8. Vaghari H, Jafarizadeh-Malmiri H, Mohammadlou M, Berenjian A, Anarjan N, Jafari N, Nasiri S (2015) Application of magnetic nanoparticles in smart enzyme immobilization. Biotechnol Lett:Ahead of Print. doi:10.1007/s10529-015-1977-z

9. Johnson BJ, Russ Algar W, Malanoski AP, Ancona MG, Medintz IL (2014) Understanding enzymatic acceleration at nanoparticle interfaces: Approaches and challenges. Nano Today 9 (1):102-131. doi:10.1016/j.nantod.2014.02.005

10. Ding S, Cargill AA, Medintz IL, Claussen JC (2015) Increasing the activity of immobilized enzymes with nanoparticle conjugation. Curr Opin Biotechnol 34:242-250. doi:10.1016/j.copbio.2015.04.005

11. Roco MC, Williams RS, Alivisatos P, Editors (2000) Nanotechnology Research Directions: IWGN Workshop Report; Vision for Nanotechnology R&D in the Next Decade. vol Copyright (C) 2015 American Chemical Society (ACS). All Rights Reserved. Kluwer,

12. Hinterwirth H, Lindner W, Laemmerhofer M (2012) Bioconjugation of trypsin onto gold nanoparticles: Effect of surface chemistry on bioactivity. Anal Chim Acta 733 (Copyright (C) 2012 American Chemical Society (ACS). All Rights Reserved.):90-97. doi:10.1016/j.aca.2012.04.036

13. Homaei A, Barkheh H, Sariri R, Stevanato R (2014) Immobilized papain on gold nanorods as heterogeneous biocatalysts. Amino Acids:Ahead of Print. doi:10.1007/s00726-014-1724-0

14. Bolivar JM, Eisl I, Nidetzky B (2015) Advanced characterization of immobilized enzymes as heterogeneous biocatalysts. Catal Today:Ahead of Print. doi:10.1016/j.cattod.2015.05.004

15. Polte J, Ahner TT, Delissen F, Sokolov S, Emmerling F, Thunemann AF, Kraehnert R (2010) Mechanism of Gold Nanoparticle Formation in the Classical Citrate Synthesis Method Derived from Coupled In Situ XANES and SAXS Evaluation. J Am Chem Soc 132 (4):1296-1301. doi:10.1021/ja906506j

16. Turkevich J, Stevenson PC, Hillier J (1951) The nucleation and growth processes in the synthesis of colloidal gold. Discuss Faraday Soc No. 11 (Copyright (C) 2013 American Chemical Society (ACS). All Rights Reserved.):55-75. doi:10.1039/df9511100055

17. Frens G (1973) Controlled nucleation for the regulation of the particle size in monodisperse gold suspensions. Nature (London), Phys Sci 241 (Copyright (C) 2013 American Chemical Society (ACS). All Rights Reserved.):20-22

18. Ojea-Jimenez I, Romero FM, Bastus NG, Puntes V (2010) Small Gold Nanoparticles Synthesized with Sodium Citrate and Heavy Water: Insights into the Reaction Mechanism. J Phys Chem C 114 (4):1800-1804. doi:10.1021/jp9091305

19. Kumar S, Gandhi KS, Kumar R (2007) Modeling of formation of gold nanoparticles by citrate method. Ind Eng Chem Res 46 (10):3128-3136. doi:10.1021/ie060672j

20. Haiss W, Thanh NTK, Aveyard J, Fernig DG (2007) Determination of Size and Concentration of Gold Nanoparticles from UV-Vis Spectra. Anal Chem (Washington, DC, U S) 79 (Copyright (C) 2013 American Chemical Society (ACS). All Rights Reserved.):4215-4221. doi:10.1021/ac0702084

21. Hendel T, Wuithschick M, Kettemann F, Birnbaum A, Rademann K, Polte J (2014) In Situ Determination of Colloidal Gold Concentrations with UV-Vis Spectroscopy: Limitations and Perspectives. Anal Chem (Washington, DC, U S) 86 (22):11115-11124. doi:10.1021/ac502053s

22. Lin S-Y, Tsai Y-T, Chen C-C, Lin C-M, Chen C-h (2004) Two-Step Functionalization of Neutral and Positively Charged Thiols onto Citrate-Stabilized Au Nanoparticles. J Phys Chem B 108 (7):2134-2139. doi:10.1021/jp036310w

23. Hermanson GT, Editor (1995) Bioconjugate Techniques. vol Copyright (C) 2015 American Chemical Society (ACS). All Rights Reserved. Academic,

24. Cao Y, Wen L, Svec F, Tan T, Lv Y (2016) Magnetic AuNP@Fe3O4 nanoparticles as reusable carriers for reversible enzyme immobilization. Chem Eng J (Amsterdam, Neth) 286:272-281. doi:10.1016/j.cej.2015.10.075

25. Nidhin M, Ghosh D, Yadav H, Yadav N, Majumder S (2015) Structural and functional aspects of trypsin-gold nanoparticle interactions: An experimental investigation. Mater Sci Eng, B 202:46-53. doi:10.1016/j.mseb.2015.09.006

26. Willner I, Baron R, Willner B (2007) Integrated nanoparticle-biomolecule systems for biosensing and bioelectronics. Biosens Bioelectron 22 (9-10):1841-1852. doi:10.1016/j.bios.2006.09.018

27. Ang SH, Yu CY, Ang GY, Chan YY, Alias Yb, Khor SM (2015) A colloidal gold-based lateral flow immunoassay for direct determination of haemoglobin A1c in whole blood. Anal Methods 7 (9):3972-3980. doi:10.1039/C5AY00518C

28. Niu K, Zheng X, Huang C, Xu K, Zhi Y, Shen H, Jia N (2014) A colloidal gold nanoparticle-based immunochromatographic test strip for rapid and convenient detection of staphylococcus aureus. J Nanosci Nanotechnol 14 (7):5151-5156. doi:10.1166/jnn.2014.8703

29. Qian X, Peng X-H, Ansari DO, Yin-Goen Q, Chen GZ, Shin DM, Yang L, Young AN, Wang MD, Nie S (2008) In vivo tumor targeting and spectroscopic detection with surface-enhanced Raman nanoparticle tags. Nat Biotechnol 26 (1):83-90. doi:10.1038/nbt1377

30. Florkin M (1957) Discovery of pepsin by Theodor Schwann. Rev Med Liege 12 (5):139-144

31. Northrop JH (1929) CRYSTALLINE PEPSIN. Science 69 (1796):580

32. Schmelzer CEH, Schoeps R, Ulbrich-Hofmann R, Neubert RHH, Raith K (2004) Mass spectrometric characterization of peptides derived by peptic cleavage of bovine β-casein. J Chromatogr A 1055 (1-2):87-92. doi:10.1016/j.chroma.2004.09.003

33. Goldstein J, Konigsberg W, Hill RJ (1963) The structure of human hemoglobin. VII. The digestion of the β chain of human hemoglobin with pepsin. J Biol Chem 238:2028-2033

34. Huckel M, Wirth H-J, Hearn MTW (1996) Porous zirconia: a new support material for enzyme immobilization. J Biochem Biophys Methods 31 (3,4):165-179. doi:10.1016/0165-022X(95)00035-P

35. Ahn J, Jung MC, Wyndham K, Yu YQ, Engen JR (2012) Pepsin Immobilized on High-Strength Hybrid Particles for Continuous Flow Online Digestion at 10 000 psi. Anal Chem (Washington, DC, U S) 84 (16):7256-7262. doi:10.1021/ac301749h

36. Bandhu A, Sutradhar S, Mukherjee S, Greneche JM, Chakrabarti PK (2015) Synthesis, characterization and magnetic property of maghemite (γ-Fe2O3) nanoparticles and their protective coating with pepsin for bio-functionalization. Mater Res Bull 70:145-154. doi:10.1016/j.materresbull.2015.04.035

37. Han W, Yamauchi M, Hasegawa U, Noda M, Fukui K, van der Vlies AJ, Uchiyama S, Uyama H (2015) Pepsin immobilization on an aldehyde-modified polymethacrylate monolith and its application for protein analysis. J Biosci Bioeng 119 (5):505-510. doi:10.1016/j.jbiosc.2014.10.018

38. Geiser L, Eeltink S, Svec F, Frechet JMJ (2008) In-line system containing porous polymer monoliths for protein digestion with immobilized pepsin, peptide preconcentration and nano-liquid chromatography

separation coupled to electrospray ionization mass spectroscopy. J Chromatogr A 1188 (2):88-96. doi:10.1016/j.chroma.2008.02.075

39. Long Y, Wood TD (2015) Immobilized Pepsin Microreactor for Rapid Peptide Mapping with Nanoelectrospray Ionization Mass Spectrometry. J Am Soc Mass Spectrom 26 (1):194-197. doi:10.1007/s13361-014-1015-8

40. Meridor D, Gedanken A (2014) Enhanced activity of immobilized pepsin nanoparticles coated on solid substrates compared to free pepsin. Enzyme Microb Technol 67:67-76. doi:10.1016/j.enzmictec.2014.09.004

41. Stigter ECA, de Jong GJ, van Bennekom WP (2008) Pepsin immobilized in dextran-modified fused-silica capillaries for on-line protein digestion and peptide mapping. Anal Chim Acta 619 (2):231-238. doi:10.1016/j.aca.2008.04.060

42. Innocent C, Bouhaine N, Djerourou A, Gherrou A, Seta P, Xu ZK (2006) Preparation of catalytic materials by covalent immobilisation of pepsin on cotton fibers activated by tosyl chloride. Mater Sci: Indian J 2 (6):161-168

43. Li J, Wang J, Gavalas VG, Atwood DA, Bachas LG (2003) Alumina-pepsin hybrid nanoparticles with orientation-specific enzyme coupling. Nano Lett 3 (1):55-58. doi:10.1021/nl025778s

44. Sharma B, Mandani S, Sarma TK (2015) Catalytic activity of various pepsin reduced Au nanostructures towards reduction of nitroarenes and resazurin. J Nanopart Res 17 (1):1-12. doi:10.1007/s11051-014-2835-y

45. Gole A, Dash C, Ramakrishnan V, Sainkar SR, Mandale AB, Rao M, Sastry M (2001) Pepsin-Gold Colloid Conjugates: Preparation, Characterization, and Enzymatic Activity. Langmuir 17 (5):1674-1679. doi:10.1021/la001164w

46. Haller E, Lindner W, Laemmerhofer M (2015) Gold nanoparticle-antibody conjugates for specific extraction and subsequent analysis by liquid chromatography-tandem mass spectrometry of malondialdehyde-modified low density lipoprotein as biomarker for cardiovascular risk. Anal Chim Acta 857:53-63. doi:10.1016/j.aca.2014.12.024

47. Hinterwirth H, Wiedmer SK, Moilanen M, Lehner A, Allmaier G, Waitz T, Lindner W, Laemmerhofer M (2013) Comparative method evaluation for size and size-distribution analysis of gold nanoparticles. J Sep Sci 36 (17):2952-2961. doi:10.1002/jssc.201300460

48. Lineweaver H, Burk D (1934) Determination of enzyme dissociation constants. J Am Chem Soc 56:658-666. doi:10.1021/ja01318a036

49. Lowry OH, Rosebrough NJ, Farr AL, Randall RJ (1951) Protein measurement with the Folin phenol reagent. J Biol Chem 193 (1):265-275

50. Hinterwirth H, Kappel S, Waitz T, Prohaska T, Lindner W, Laemmerhofer M (2013) Quantifying Thiol Ligand Density of Self-Assembled Monolayers on Gold Nanoparticles by Inductively Coupled Plasma-Mass

Spectrometry. ACS Nano 7 (Copyright (C) 2013 American Chemical Society (ACS). All Rights Reserved.):1129-1136. doi:10.1021/nn306024a

51. Mie G (1908) Contributions to the Optics of Turbid Media, Especially Colloidal Metal Solutions. Ann Phys (Weinheim, Ger) 25:377-445

52. Malola S, Lehtovaara L, Enkovaara J, HÃ¤kkinen H (2013) Birth of the Localized Surface Plasmon Resonance in Monolayer-Protected Gold Nanoclusters. ACS Nano 7 (11):10263-10270. doi:10.1021/nn4046634

53. Greenwell P, Knowles JR, Sharp H (1969) Inhibition of pepsin-catalyzed reactions by products and product analogs. Kinetic evidence for ordered release of products. Biochem J 113 (2):363-368. doi:10.1042/bj1130363

54. Oliveros JC (2007-2015) Venny. An interactive tool for comparing lists with Venn's diagrams.

55. Koenig T, Menze BH, Kirchner M, Monigatti F, Parker KC, Patterson T, Steen JJ, Hamprecht FA, Steen H (2008) Robust Prediction of the MASCOT Score for an Improved Quality Assessment in Mass Spectrometric Proteomics. J Proteome Res 7 (Copyright (C) 2012 American Chemical Society (ACS). All Rights Reserved.):3708-3717. doi:10.1021/pr700859x

56. Perkins DN, Pappin DJC, Creasy DM, Cottrell JS (1999) Probability-based protein identification by searching sequence databases using mass spectrometry data. Electrophoresis 20 (Copyright (C) 2012 American Chemical Society (ACS). All Rights Reserved.):3551-3567. doi:10.1002/(sici)1522-2683(19991201)20:18<3551::aid-elps3551>3.0.co;2-2

Supplementary Material

Aggregation-induced shift of SPR band

Aggregation in colloidal preparations of (functionalized) GNPs is detrimental for their functionality. For instance, aggregation of pepsin-conjugated GNPs may easily lead to loss of enzymatic activity because of precipitation of aggregates and preclusion of access of substrates to the active site of the immobilized enzyme. Thus, during synthesis and functionalization it is of importance to maintain stable colloidal suspension and monitor colloidal stability. A convenient and simple method to detect colloidal stability and aggregation, respectively, is monitoring the surface Plasmon resonance (SPR) band in the range between 400 and 800 nm of Vis spectra of the nanoparticle suspensions resulting after synthesis and surface modification, respectively. Upon aggregation, the intensity of the original SPR absorbance band at around 520 nm is reduced and a new red-shifted second absorbance band appears at higher wavelength (depending on size of aggregates and original particles e.g. 580 nm) indicating onset of aggregation. The conduction electrons near each particle surface become delocalized and are shared amongst neighboring particles in aggregates causing the surface Plasmon resonance shifting to lower energies which becomes evident as red-shifted SPR band. Fig. S1 shows an example of aggregated GNPs versus stable colloidal suspension. Eventually, aggregation can be observed even visually. The red nanoparticle solution turns to purple or dark, and finally a clear uncolored solution can be observed with black precipitate. Once aggregated, in nearly all cases it is difficult or even impossible to redisperse the aggregates into individual particles forming stable colloidal suspensions. During the current synthesis protocol, it was observed that activation of carboxy-terminated pegylated GNPs by OSu (N-hydroxysuccinimide) easily aggregate, but aggregates disappear upon protein binding. Nevertheless, a direct coupling without OSu activation was employed for this reason herein.

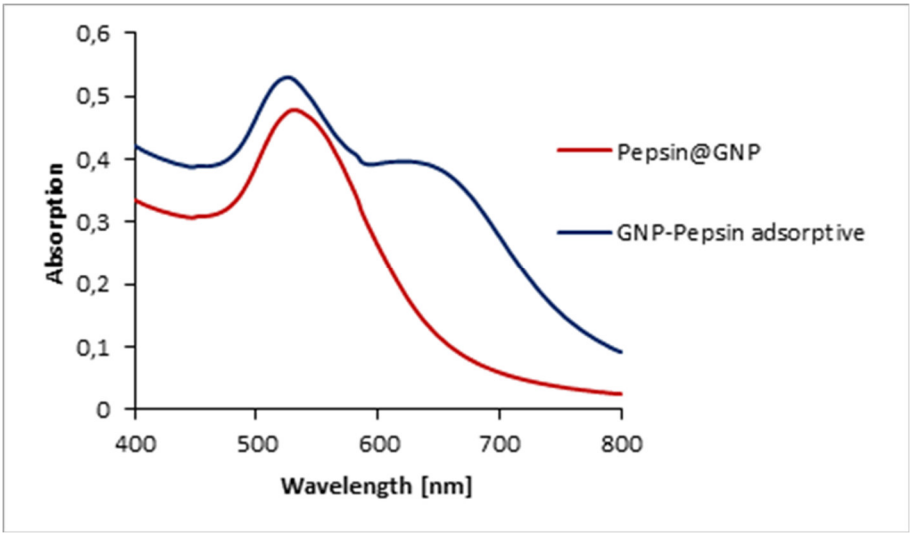

Fig. S1: Vis-spectra of Pepsin@GNP (pepsin-modified GNPs with PEG_7 spacer) and adsorptively bound pepsin on GNPs. Because of a high colloidal stability the peak of Pepsin@GNP shows a good shape. The undefined peak shape of adsorptively bound pepsin is due to particle aggregation.

Stability study of all nanoparticle stages for 35 days

One synthesis batch of pepsin-modified GNPs was used to study the long-term colloidal stability. Thus, an aliquot of each citrate-capped GNPs, pegylated GNPs (GNP-PEG_7-COOH) and pepsin-modified GNPs with PEG_7 spacer were stored in the refrigerator at 4°C in the dark for 35 days. Changes of the nanoparticles, in particular aggregation, were then monitored by Vis spectroscopy measuring Vis spectra between 350 and 800 nm in the first 9 days daily and then once a week and every second week, respectively.

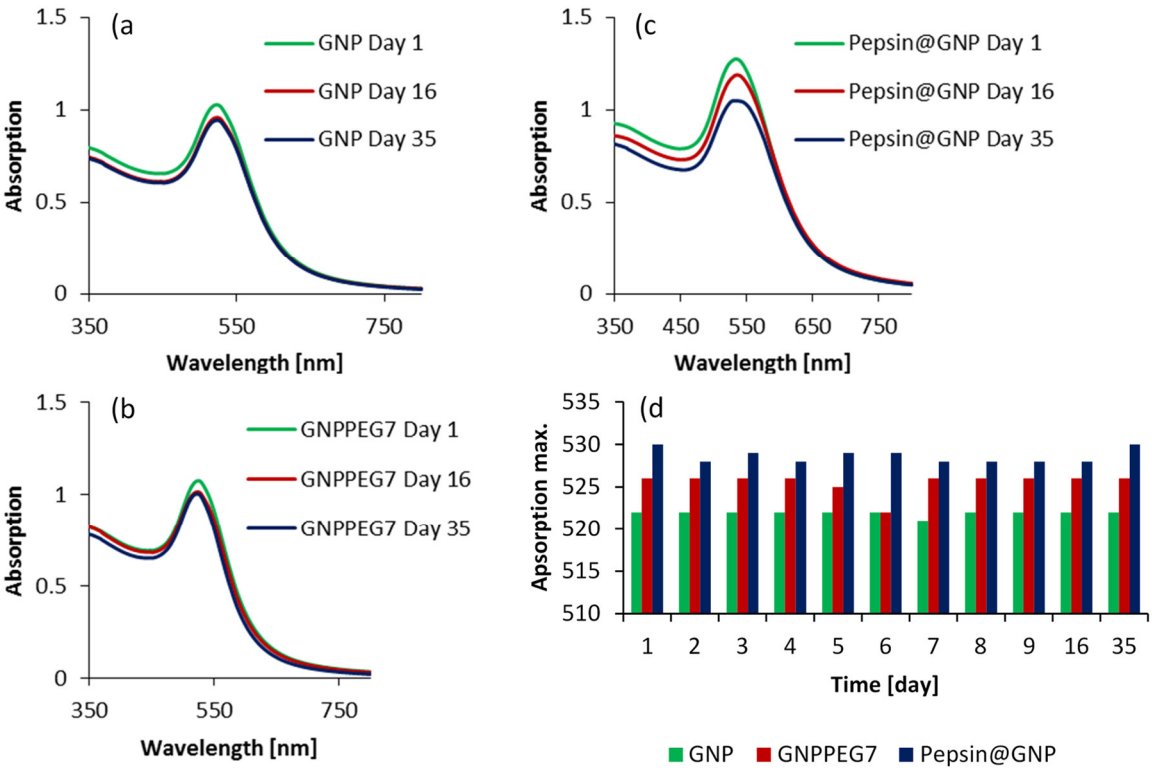

Fig. S2: Colloidal stability and shelf life of functionalized nanoparticles. (a) Citrate-stabilized GNPs, (b) GNPs coated with bifunctional PEG spacer having carboxy-terminated surface and (c) immobilized pepsin-GNP conjugate. (d) Absorption maxima of the SPR band of all nanoparticle stages measured over 35 days. All samples were diluted 1:5 in ddH2O.

The results are illustrated in Fig. S2. As can be seen, essentially no changes in Vis spectra can be found for GNPs (Fig. S1a) and GNPs with PEG-spacer (Fig. S1b) over the entire period. For pepsin-modified GNPs wavelength shifts in absorbance maxima are virtually absent as well and colloidal stability over 35 days is confirmed. However, a slight decline in absorbance of the SPR band between day 16 and 35 may indicate that some nanoparticles have precipitated leading to a slightly reduced concentration in the heterogeneous enzyme suspension. Such slightly lower concentration might, however, be easily and conveniently compensated for by pipetting slightly larger volumes to reaction mixtures in order to keep the total enzyme concentration in reaction incubations

constant. This would guarantee satisfactory batch-to-batch reproducibility of enzymatic reactions when working with one pepsin-GNP conjugate batch over extended period.

Chromatographic assay for the determination of CYC in enzyme kinetics study

An accurate and precise validated HPLC-UV method was set up for the reliable quantitative analysis of undigested CYC in reaction batches of the enzyme kinetics study. For this chromatographic method a polystyrene-co-divinylbenzene monolith column with macropore diameter of 1 µm was selected. This type of columns has been shown to be favorable for fast protein analysis due to convective mass transfer. Due to a small mass transfer resistance term the column can be operated at high flow rates which allow fast analysis with high sample throughput. The mobile phase conditions and gradient profile were adjusted such that the protein was well retained while the digested peptides eluted at the front close to t_0, thereby avoiding interferences with CYC quantification. A representative chromatogram is given in Fig. S3.

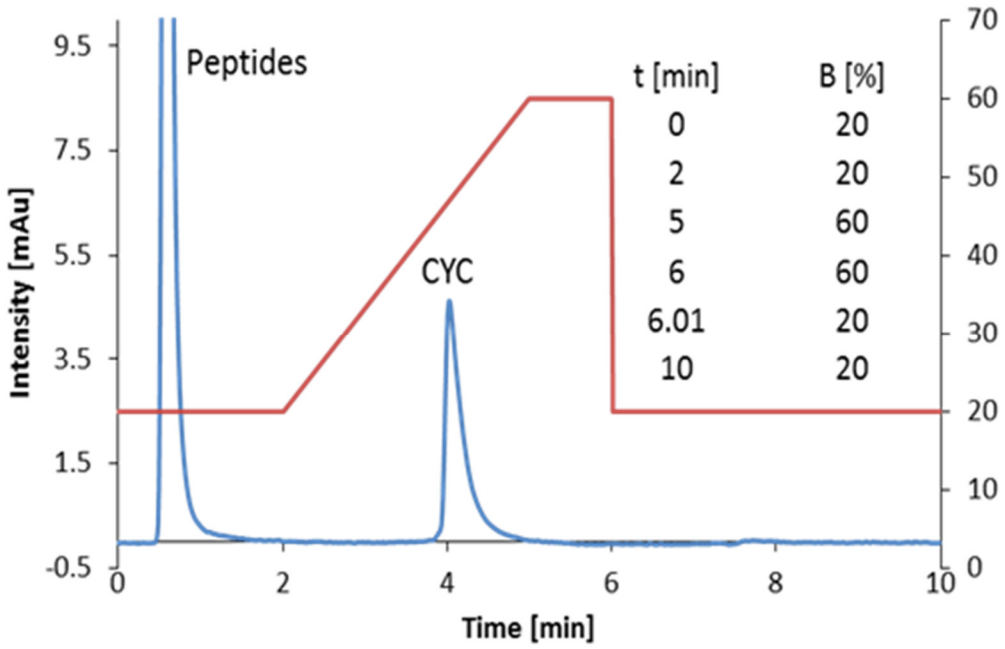

Fig. S3: Representative chromatogram of HPLC determination of undigested CYC in reaction batches from enzyme kinetics study. Experimental conditions: Column, ProswiftTM RP-1S (4.6 x 50 mm, Dionex/ThermoFisher Scientific). Mobile phase, A: 50

mM ammonium formate pH 3.5 + 5 % ACN; B: ACN + 5 % 50 mM ammonium formate pH 3.5; gradient profile see insert; flow rate, 1 mL min^{-1}; column temperature, 40 °C.

The method was validated according to ICH guidelines for method performance characterization in terms of detection limit (DL), quantitation limit (QL), intra-assay and inter-day precision as well as accuracy, and assay specificity.

Thus a calibration function was established by diluting a CYC stock solution of 2 mg/mL in 20 mM sodium acetate buffer pH 4.5 in the range of 0.05, 0.1, 0.2, 0.5, 1 and 2 mg/mL and analyzing the solutions by above HPLC-UV method. The calibration function is shown in Fig. S4. It can be seen that good linearity in the given concentration range was obtained with a determination coefficient R2 of 0.9993. DL (S/N=3:1) and QL (S/N=10:1) were determined as 0.02 mg/mL and 0.08 mg/mL, respectively.

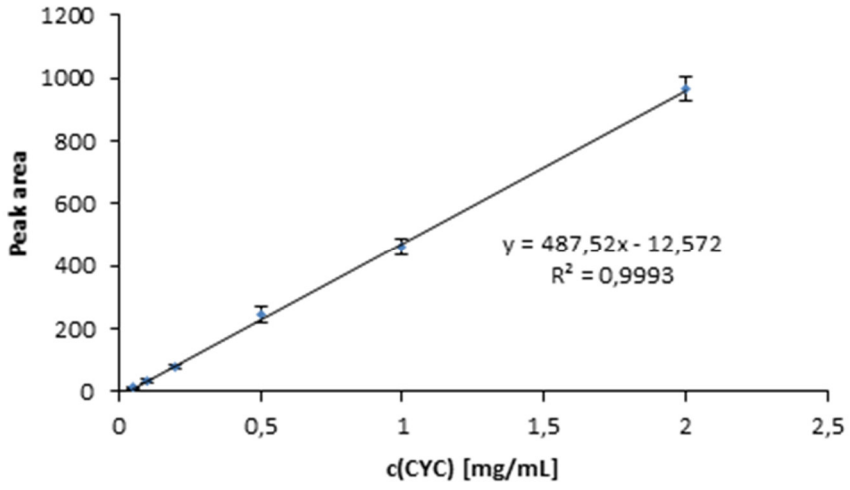

Fig. S4: Calibration function for CYC analyzed in the course of the enzyme kinetics study.

Table S1: Validation parameters for CYC

c(CYC)	0.05 mg/mL	0.1 mg/mL	1 mg/mL	2 mg/mL
accuracy	130.00%	114.67%	102.40%	104.87%
intraday precision	1.15%	0.79%	0.48%	0.31%
interday precision	1.21%	1.08%	0.60%	0.63%

For validating the assay performance intra-assay and inter-day precision and accuracy were validated across the relevant concentration range at three concentration levels (close to LOQ, intermediate and high concentration range) of quality control (QC) samples in three replicates. The results are given as %RSD for precision testing and as %-recovery for accuracy testing. As can be seen from Table S1, RSD values < 1 % in all cases as well as recoveries close to 100 % indicate excellent assay precision and accuracy. The assay was therefore suitable for measuring CYC concentrations in samples from enzyme kinetics study accurately and reliably.

Determination of surface coverage of GNPs with pepsin by Lowry Assay

For determination of surface coverage of GNPs with pepsin, common protein quantification assays were envisaged. Lowry assay was finally selected. In the Lowry assay, peptide bonds of the analyzed protein(s) are first complexed with Cu(II) ions in alkaline solution according to Biuret reaction. In a second step, Cu(II) is reduced to Cu(I) which in turn reduces the yellow Folin-Ciocalteu reagens (phosphomolybdate/phosphotungstic acid). The end product has a blue color. The protein quantity in the sample can be determined by absorbance measurements at 650 or 750 nm against a standard protein curve.

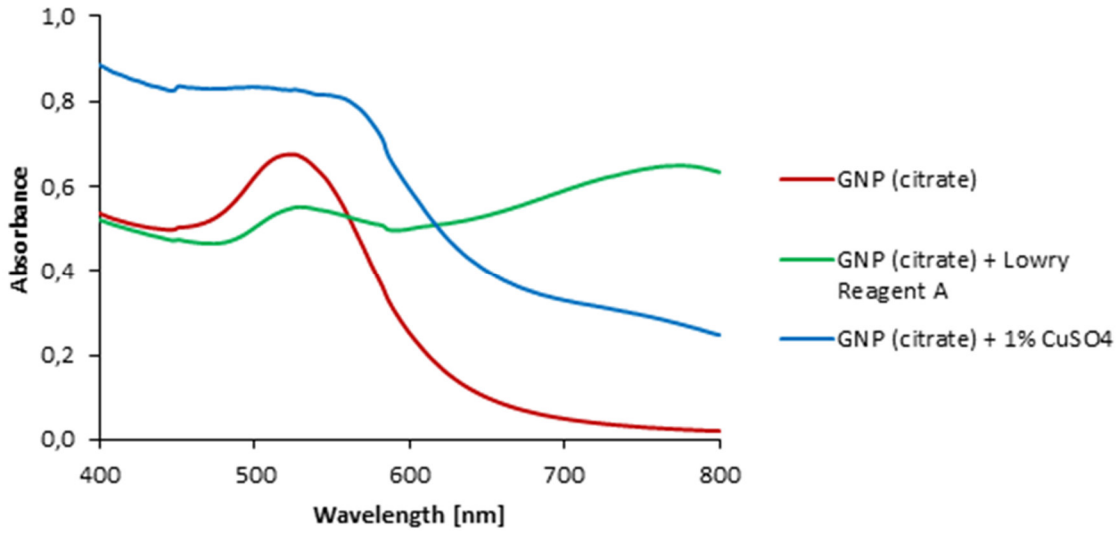

Fig. S5: The behavior of citrate stabilized GNPs in the presence of Lowry reagent A and 1 % CuSO4.

Initially, on-bead protein quantitation using Lowry assay was intended. However, the citrate stabilized GNPs aggregated in the presence of Lowry reagent A (2.45 mL 4% Na2CO3 anhydrous in ddH_2O, 2.45 mL 0.1 M NaOH, 0.1 mL 2% Na-K-tartrate in ddH_2O and 0.05 mL CuSO4·5H2O in ddH2O). In an additional experiment was discovered that the $CuSO_4$ has a considerable negative influence on the colloidal stability of the nanoparticles (Fig. S5). For this reason, the protein concentration of non-immobilized pepsin in the supernatant was finally determined and the immobilized protein calculated by mass balance. The total pepsin concentration in the reaction mixture was 1.2 mg/mL. Thus, a calibration function between 0.05 and 1.0 mg/mL pepsin in 20 mM MES buffer pH 4.5 (the reaction medium) was established (n=3) (Fig. S6). As can be seen, good linearity with a determination coefficient of R^2 = 0.9947 was obtained. Precision of the Lowry assay was good with average RSD values of 7.3 % over the relevant concentration range.

The mean pepsin content of three measured reaction mixtures in the supernatant after the immobilization by Lowry assay was determined to be 0.95 ± 0.11 mg/mL.

Accordingly, the surface coverage of GNPs with pepsin was 0.25 ± 0.03 mg ml^{-1} of pepsin-GNP conjugate solution.

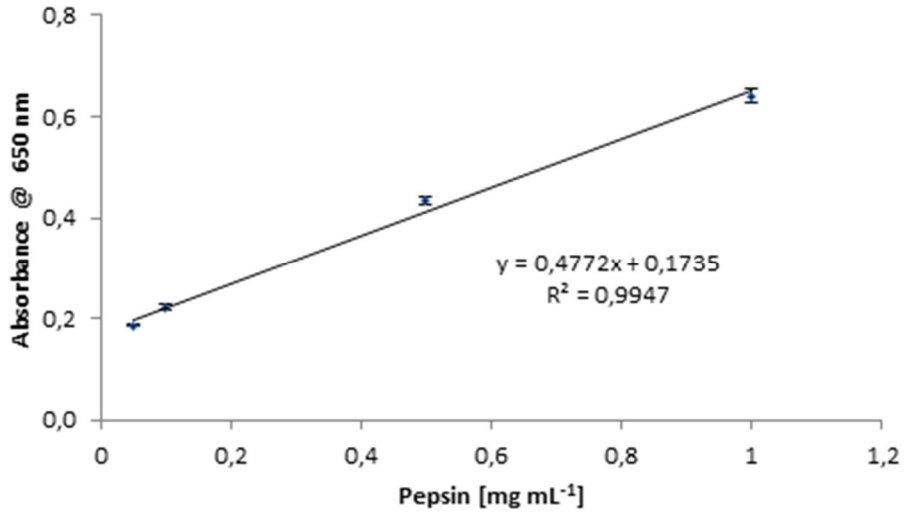

Fig. S6: Calibration function pepsin in 20 mM MES buffer pH 4.5 for Lowry assay.

Recyclability of Pepsin@GNP

CYC (1.2 mg mL^{-1} stock solution) was utilized as model protein to test the digestion efficiency of conjugated pepsin in the course of a re-usability study. For this purpose, 0.2 mL of the protein sample was transferred to 0.8 mL of the nanoparticle suspension (Pepsin@GNP in 1 mL 20 mM sodium acetate pH 4.5). The digestion was performed at 37 °C for 4 hours digestion time.

The reaction with the nanoparticle incubation was stopped by adding 0.2 mL of 0.1 M NaOH to reach neutral pH value. Pepsin@GNP was separated from the sample by centrifugation (12,000 rpm for 10 minutes) resulting in a clear supernatant for UHPLC-ESI-QTof-MS/MS analysis.

Five aliquots of aforementioned CYC sample were digested using iteratively the same Pepsin@GNP bioconjugate which was recovered by spinning and washed before re-use. Two washing steps in between were performed with 20 mM sodium acetate pH 4.5 (centrifugation at 12,000 rpm for 10 minutes).

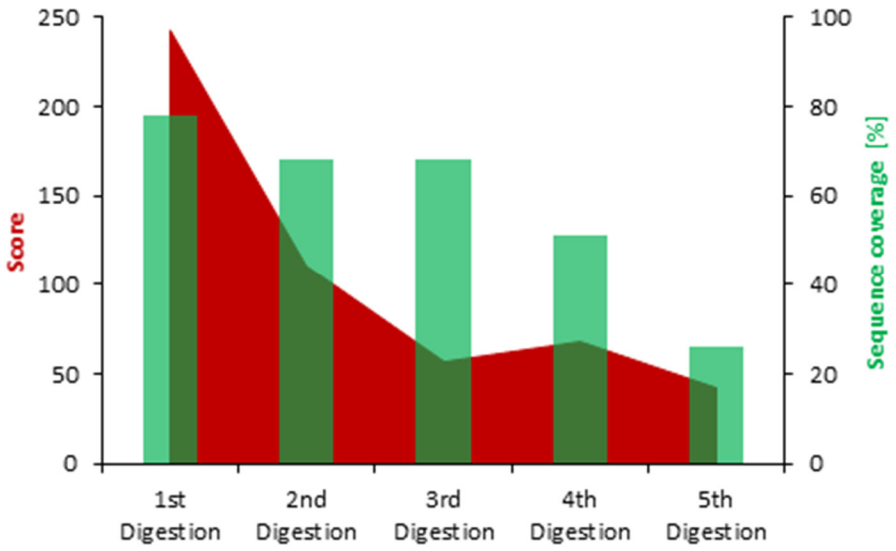

Fig. S7: Recyclability testing. Score and sequence coverage of CYC sample digested by the same Pepsin@GNP material after its re-cycling and washing.

As shown in Fig. S7 it was possible to identify CYC by Mascot search. The score value dropped in the first two cycles (from 242 to 110) but remained more or less constant thereafter (sore of around 50 in the 3rd to 5th re-use). Sequence coverage, on the other hand, remained essentially constant in the first three cycles of re-use (~70 %), dropped to 51 % in the 4th cycle and to 26 in the 5th cycle of re-use. Thus, recyclability of Pepsin@GNP could be demonstrated by this experiment, but the digestion performance was starting to decrease after three cycles of re-use.

Stability of the immobilized pepsin

In this study digestion was performed with immobilized pepsin and pepsin in free solution. For the digestion protocol with free pepsin 0.2 mg ml^{-1} pepsin was used (0.25 mg mL^{-1} final concentration in 1.2 mL total volume) and mixed with 0.8 mL pepsin in digestion buffer. The digestion was performed in 20 mM sodium acetate buffer pH 4.5 at 37 °C for 4 hours digestion time and stopped by adding 0.2 mL of 0.1 M NaOH. The digestion with immobilized pepsin was performed as described in the previous subchapter.

99 µL aliquots of the CYC samples digested by Pepsin@GNP and pepsin in solution were taken and reacted with 1 µL trypsin (1 mg mL^{-1} stock solution in 20 mM Tris-HCl pH 7.5) at 37 °C overnight, stopped by heat shock (95°C for 10 minutes) and analyzed by UHPLC-ESI-QTof-MS/MS.

Protein identification was performed by Mascot search to identify (leached) pepsin.

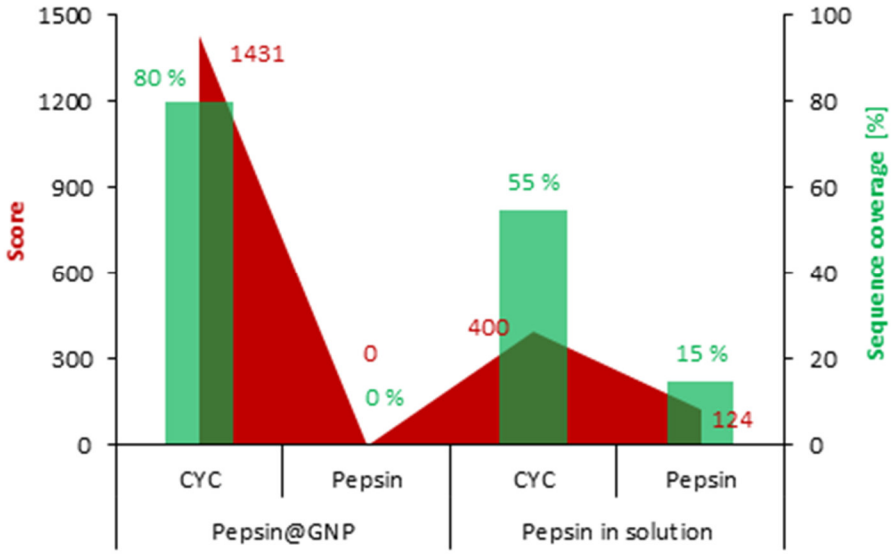

Fig. S8: Score and sequence coverage of the CYC samples digested by trypsin for the determination of (leached) pepsin.

After the coupled digestion protocol of CYC (first digestion by Pepsin@GNP/pepsin in solution, second digestion by trypsin) it was possible to identify CYC by Mascot search for both samples (Fig. S8). After the tryptic digestion pepsin could also be identified for the sample with pepsin in solution but it was not possible to detect pepsin in the Pepsin@GNP sample. That means pepsin is immobilized on the gold nanoparticle and will not bleed off from the particles within the experiments and/or the washing procedure.

Digestion of protein mix with GNP-conjugated pepsin

Fig. S9a shows the TIC of a digest obtained from the protein mix (CYC, MYG, BSA) with pepsin-conjugated GNPs after 4h, and the 2D-plot in Fig. 9b reveals an overview of the

detected peptide precursor ions in dependence of the retention time. The numerous peptide peaks clearly confirm that the immobilized enzyme maintains its bioactivity. Exemplary an XIC of the peptide fragment VVSTQTALA, stemming from BSA, is shown in Fig. 9c and the +TOF MS-spectrum in Fig. 9d. Single and double charged peptide are found in the MS spectrum.

The peak list from IDA scan was loaded into Mascot and database search performed with pepsin as enzyme (other parameters are specified in Experimental part of main document). A number of peptides were identified by Mascot from the peak list. From these signature peptides, the corresponding XICs were extracted for each protein and overlaid (Fig. S10) to document the success of digestion with the new heterogeneous nanobiocatalyst. Fig. S9 illustrates exemplarily the MS/MS spectrum of a characteristic peptide fragment of BSA. As can be seen there is good coverage of the sequence due to b-ions.

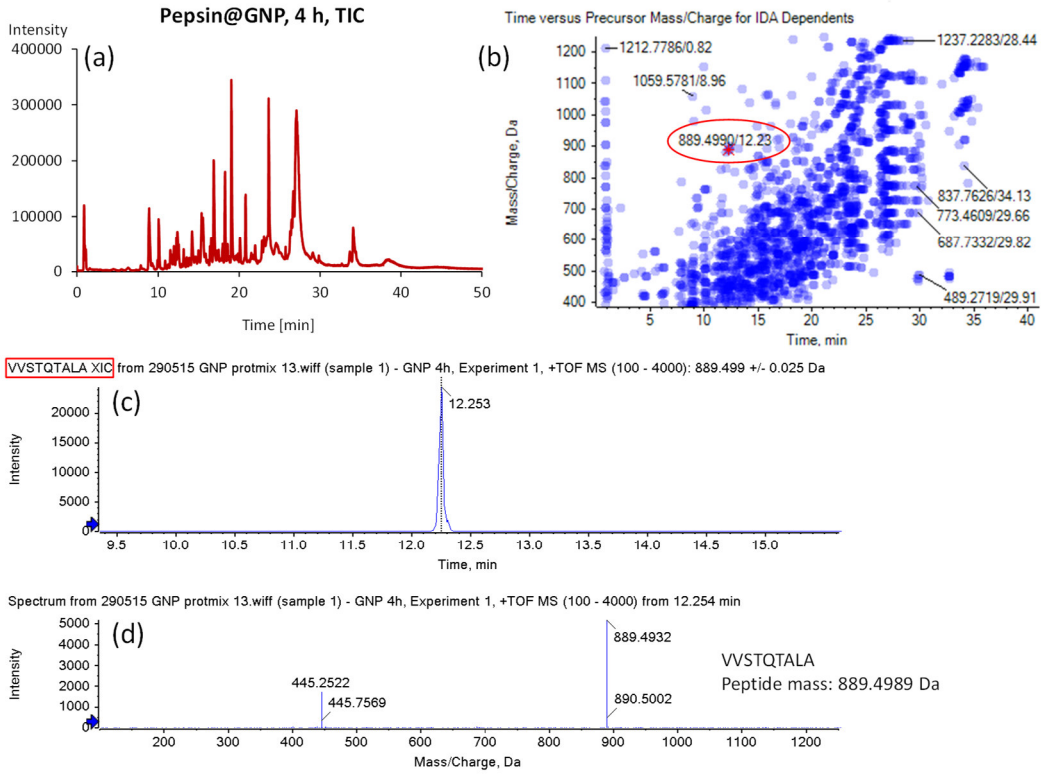

Fig. S9: Exemplary chromatogram of a peptide map obtained by digestion of the protein mix (CYC, MYG, BSA) with Pepsin@GNP conjugate and 4h digestion time (a), detected precursor ions in dependence of retention time (b), exemplary extracted ion chromatogram (XIC) of the peptide VVSTQTALA (c) and corresponding MS spectrum (d).

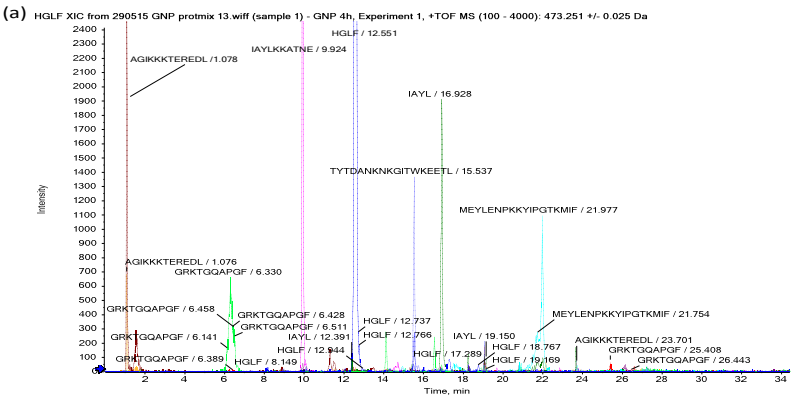

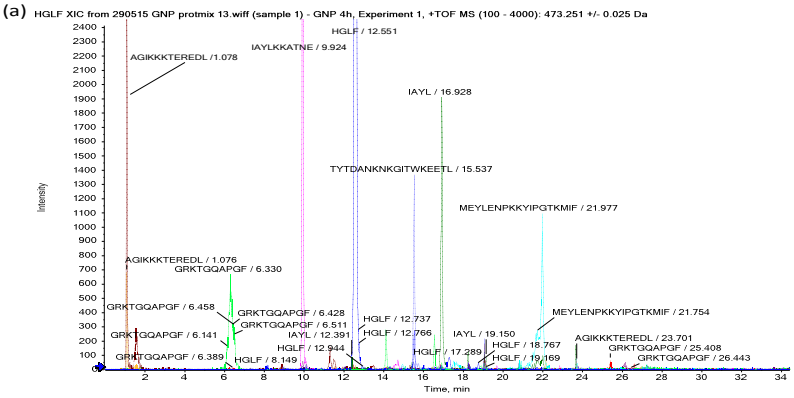

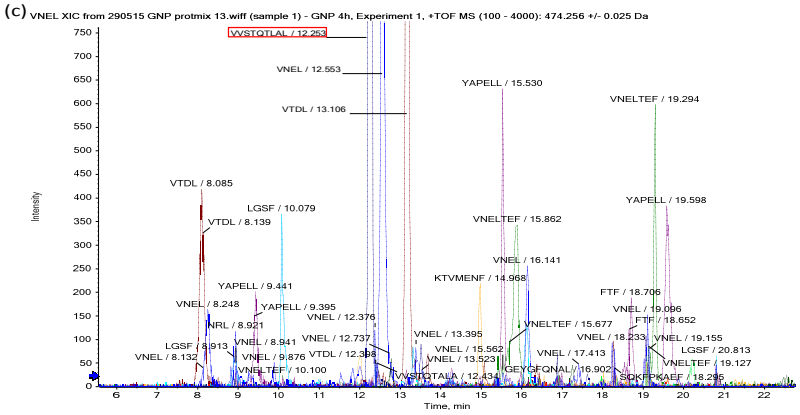

Fig. S10: Overlay of XICs of specific peptides of (a) CYC, (b) MYG, and (c) BSA identified by Mascot search. Digestion with Pepsin@GNP for 4h.

(a)

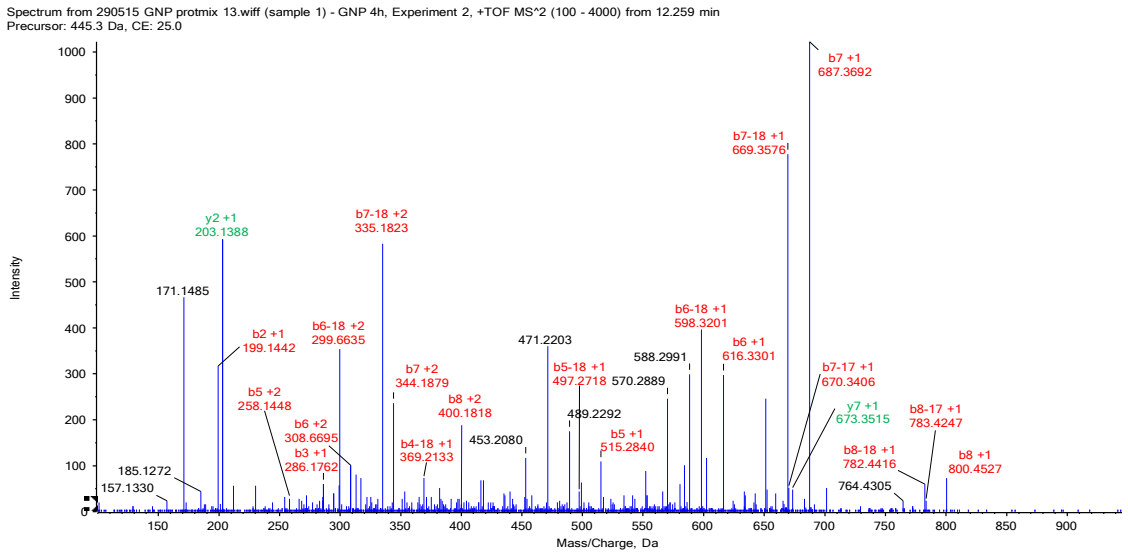

(b)

Symbol	Res. Mass	# (N)	b	b-17	b-18	y	y-17	y-18	# (C)
V	99.06841	1	100.0757	83.04914	82.06513	889.4989	872.4724	*871.4884*	9
V	99.06841	2	199.1441	182.1176	181.1335	790.4305	773.404	772.4199	8
S	87.03203	3	286.1761	269.1496	268.1656	691.3621	674.3355	673.3515	7
T	101.0477	4	387.2238	370.1973	369.2132	604.3301	587.3035	586.3195	6
Q	128.0586	5	515.2824	498.2558	497.2718	503.2824	486.2558	485.2718	5
T	101.0477	6	616.3301	599.3035	598.3195	375.2238	358.1973	357.2132	4
A	71.03711	7	687.3672	670.3406	669.3566	274.1761	257.1496	256.1656	3
L	113.0841	8	800.4512	783.4247	782.4407	203.139	186.1125	185.1285	2
A	71.03711	9	*871.4884*	854.4618	853.4778	90.05496	73.02841	72.04439	1

Fig. S11: Model MS/MS spectrum of peptide VVSTQTALA. Determined b-/y-ions with PeakView of the peptide VVSTQTALA after digestion of the protein mix with Pepsin@GNP for 4 h (mass spectra shown in Fig. 8d of main document). Precursor (+1): 889.4989 Da /(+2): 445.2531 Da.

Peptide mapping for assessment of digestion performance and proteolytic specificity

ExPasy Bioinformatics Resource Portal provides information on the proteolytic specificity of pepsin (http://web.expasy.org/peptide_cutter/peptidecutter_enzymes.html). It is stated that “Pepsin preferentially cleaves at Phe, Tyr, Trp and Leu in position P1 or P1'(Keil, 1992). Negative effects on cleavage are excerted by Arg, Lys and His in position P3 and Arg in position P1. Pro has favourable effects when being located in position P4 and position P3, but unfavourable ones when found in positions P2 to P3'. Cleavage is more specific at pH 1.3. Then pepsin preferentially cleaves at Phe and Leu in position P1 with negligible cleavage for all other amino acids in this position. This specificity is lost at pH ≥ 2“

Table S2: Proteolytic specificities of pepsin according to PeptideCutter tool.

Enzyme name	P4	P3	P2	P1	P1'	P2'
Pepsin (pH1.3)	-	not H,K, or R	not P	not R	F or L	not P
	-	not H,K, or R	not P	F or L	-	not P
Pepsin (pH>2)	-	not H,K or R	not P	not R	F,L,W or Y	not P
	-	not H,K or R	not P	F,L,W or Y	-	not P

Table reprinted from PeptideCutter publicly available under ExPasy Bioinformatics Resource Portal "http://web.expasy.org/peptide_cutter/peptidecutter_enzymes.html"

Fig. 7 of the main document showed already the peptide fragments generated by pepsin in free solution and the Pepsin@GNP conjugate for cytochrome C and myoglobin. Good sequence homology was observed when digestion in free solution and with heterogeneous nanobiocatalyst were compared. Corresponding results for BSA are illustrated in Fig. S10. The majority of peptide fragments generated by pepsin are found in digests of homogeneous and heterogeneous catalysis, while a few were only detected in one of the two approaches. Overall good homology can be found for this larger protein as well.

Fig. S12: Sequence of BSA with identified peptides found in digests with free pepsin in solution (solid arrows) and Pepsin@GNP (dashed arrows). Peptides were determined by Mascot search and compared with reference to the protein sequences.

Venn diagrams (Fig. S12) for identified peptides in protein mix (created with Venny 2.1; http://bioinfogp.cnb.csic.es/tools/venny/index.html)

In the control sample (0 hours) of the protein mixture (BSA, CYC and MYG) no peptides for BSA could be identified, neither for pepsin in solution nor for Pepsin@GNP. The number of identified peptides increase with increasing digestion times and were largely similar for homogeneous and heterogeneous catalysis.

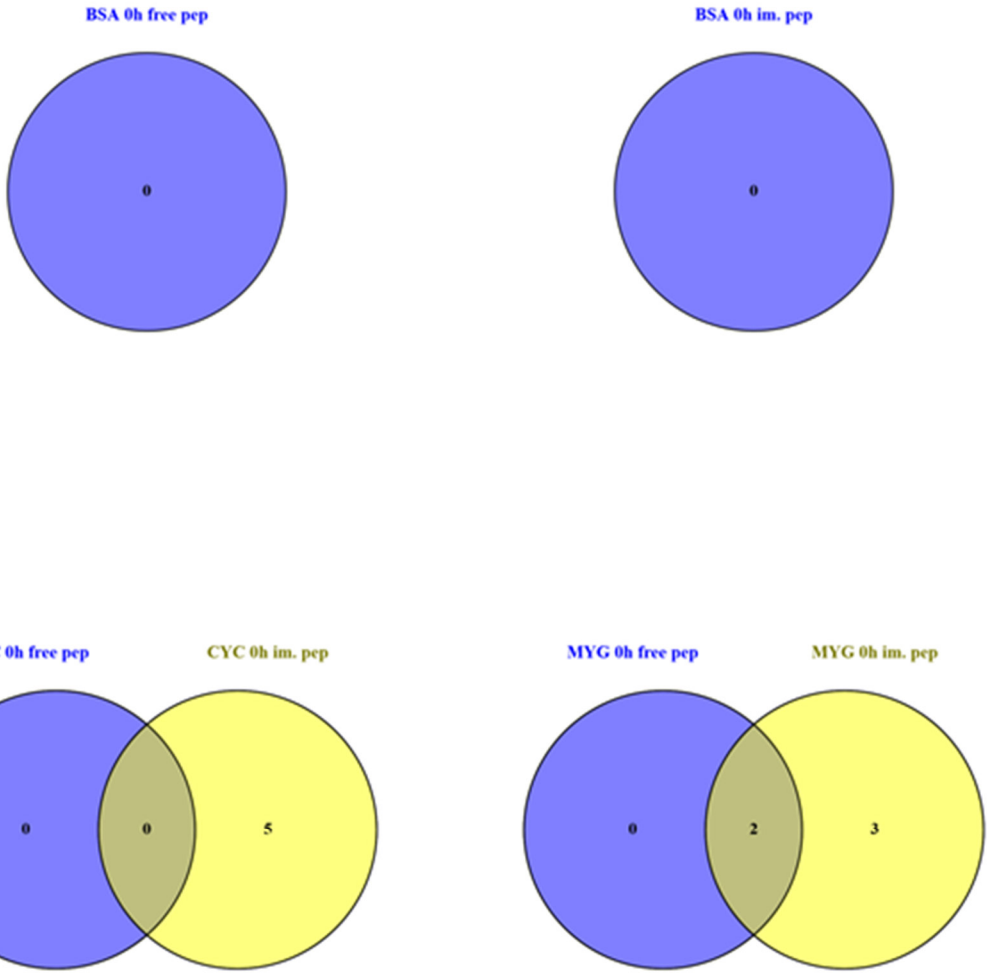

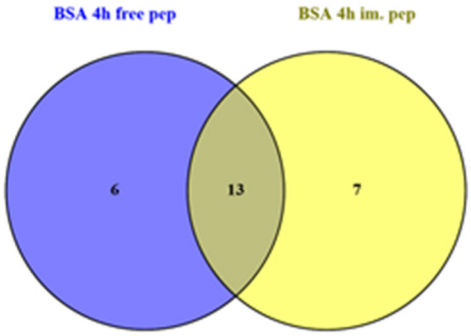
BSA 4h free pep
BSA 4h im. pep
6
13
7

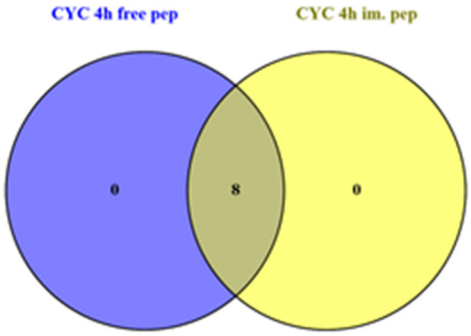
CYC 4h free pep
CYC 4h im. pep
0
8
0

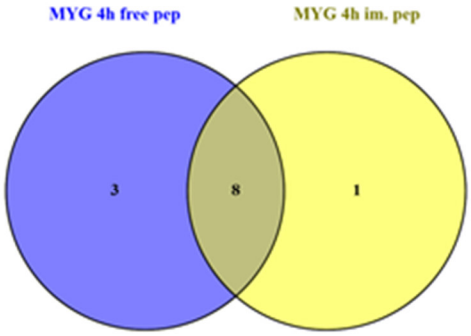
MYG 4h free pep
MYG 4h im. pep
3
8
1

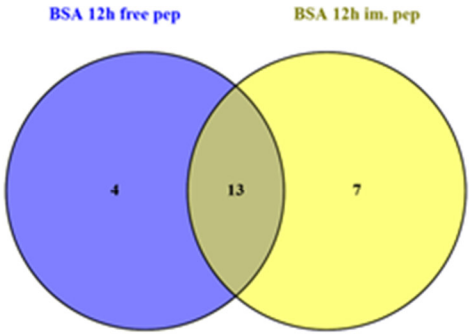
BSA 12h free pep
BSA 12h im. pep
4
13
7

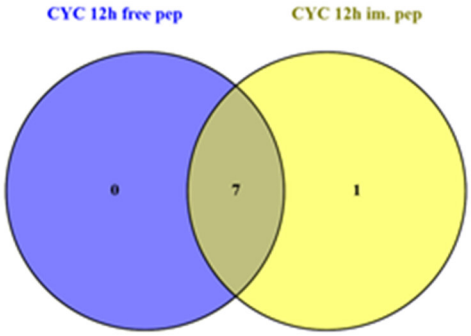
CYC 12h free pep
CYC 12h im. pep
0
7
1

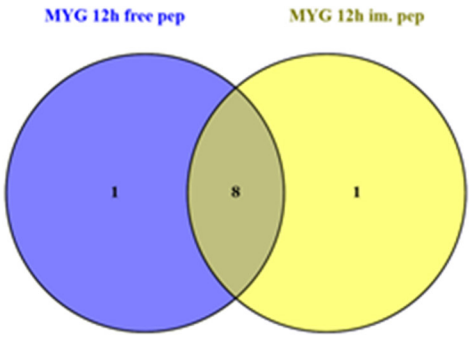
MYG 12h free pep
MYG 12h im. pep
1
8
1

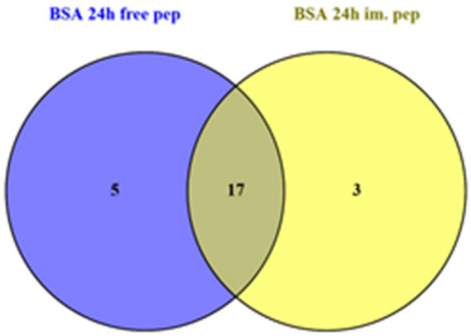
BSA 24h free pep
BSA 24h im. pep
5
17
3

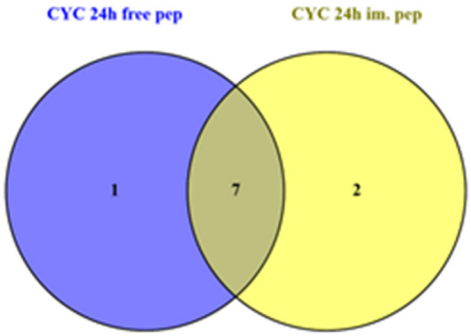
CYC 24h free pep
CYC 24h im. pep
1
7
2

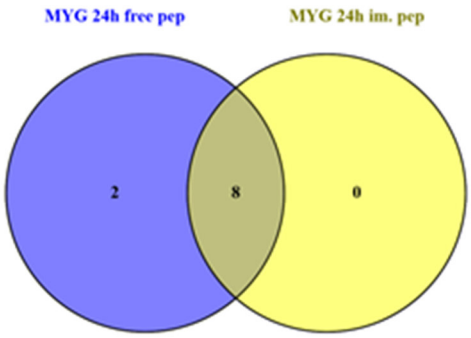
MYG 24h free pep
MYG 24h im. pep
2
8
0

3.2. Taylor dispersion analysis, resonant mass measurement and bioactivity of pepsin-coated gold nanoparticles

Markus Höldrich[1], Siyao Liu[1], Markus Epe[2], Michael Lämmerhofer[1]

[1]Institute of Pharmaceutical Sciences, Pharmaceutical (Bio-)Analysis, University of Tübingen, Auf der Morgenstelle 8, 72076 Tübingen, Germany

[2]Malvern Instruments, Herrenberg, Germany

Talanta 167 (2017) 67–74

Abstract

Immobilized enzyme reactors based on nanoparticulate carriers are becoming increasingly popular. A toolbox of methods is usually utilized for their characterization in order to be capable of assessing their suitability for the intended purpose. In this work, as a model system pepsin was conjugated to gold nanoparticles (GNPs) by a straightforward adsorptive immobilization process. The success of the immobilization procedure was monitored by Vis spectroscopy via shifts of the localized surface plasmon resonance (LSPR) band, size characterization by dynamic light scattering (DLS), and ζ–potential determinations by electrophoretic light scattering. DLS revealed a significantly different hydrodynamic diameter for unmodified GNPs and protein-coated GNPs. However, the hydrodynamic diameters of pepsin-coated GNPs obtained with various concentrations of pepsin in the coating solution were not significantly different. In contrast, Taylor dispersion analysis allowed measuring the slight differences in the hydrodynamic radius. It provided also information on the viscosity of GNP suspensions and diffusion coefficients for the various pepsin@GNP preparations. For the determination of the pepsin surface coverage on the GNPs results from indirect protein quantitation of non-immobilized pepsin by Lowry assay were compared to direct measurement of immobilized pepsin by resonant mass measurements. Reasonable agreement was found. Accurate information on enzyme coverage is of utmost importance for a representative comparison of the turnover numbers and catalytic efficiencies of nanoparticulate immobilized enzyme reactors, which is shown by the adsorptively immobilized pepsin@GNP as model system.

Keywords

Immobilized enzyme reactor, Taylor dispersion analysis, resonant mass measurement, nanoparticle, protein corona, heterogeneous biocatalyst

Introduction

Immobilization of enzymes on nanostructured carriers is an emerging field in various industrial, biomedical and bioanalytical applications [1]. Such nanoparticulate immobilized enzyme reactors (nanoIMERs) promise important advantages as biocatalysts compared to free solution enzyme applications owing to their positive effect on enzyme stability, straightforward removal from the reaction product (e.g. by centrifugation in case of metal nanoparticles or magnetic separation in case of magnetic nanoparticles as carriers), and reusability. Also enhanced reaction rates have been reported for nanoparticle-based biocatalysts [2].

Size is one of the prime structural parameters of such nanobiocatalysts playing a decisive role for the functionality, bioactivity, and toxicity of these functional materials. Although a multitude of methods is available to measure nanoparticle size, it is still not a trivial task to provide accurate, representative values in many instances. Most common methods employed for nanoparticle sizing and size distribution analysis comprises microscopic techniques such as transmission electron microscopy (TEM), scanning electron microscopy (SEM) and atomic force microscopy (AFM) [3], scanning tunneling microscopy (STM) and scanning tunneling spectroscopy (STS) [4], dynamic light scattering (DLS) analysis [5, 6], nanoparticle tracking analysis (NTA) [7, 8], field flow fractionation [9-12], and differential mobility analysis (DMA) [13-18]. Depending on the method more or less deviating results may be obtained [19-21] which makes interpretation sometimes difficult. A particular problem is to have sufficient size resolution, in particular if the materials do not show unimodal distributions. Distinction between minor size variations is also challenging with many of those techniques and DMA appears to become one of the gold standards in this regard, however, has the disadvantage that it is a gas phase technique.

Another challenge in the course of nanobiocatalyst characterization is accurate quantitation of the enzyme immobilized on the surface. Along this line, indirect photometric quantitation of unbound protein in the binding buffer by UV [22, 23] or use of

common protein quantitation assays, e.g. microbicinchonic acid protein assay for this purpose [24], are the most frequently utilized methods. Rarely direct methods have been proposed. Some few examples include the protein surface coverage determination by suspended microchannel resonator with which the amount of IgG coated on polystyrene beads (600 nm) has been measured [24]. Recently, targeted isotope dilution liquid chromatography-tandem mass spectrometry has been proposed for quantification of antibody coupled to magnetic nano- and microparticles involving on-bead tryptic digestion [25]. In another study, the average number of protein molecules bound to the surface of nanoparticles has been estimated by fluorescence correlation spectroscopy inferred from hydrodynamic radii [26, 27].

This report evaluates and compares some alternative techniques for size and surface coverage analysis of nanoparticulate IMERs. Pepsin adsorptively coated onto GNPs from incubation mixture with various pepsin concentrations thus yielding distinct thicknesses of the adsorbed layer has been employed as model system. Characterization of the resultant pepsin@GNP bioconjugates has been performed by Vis spectroscopy, DLS and ζ–potential measurements. Results of size determination by DLS of bioconjugates with different pepsin coating thicknesses are compared with the data from Taylor dispersion analysis. The potential of resonant mass measurement (RMM) as methodology for the direct analysis of the surface concentration of protein on the GNP is elucidated. Resultant data are compared with indirect surface coverage determination using the protein quantitation assay by Lowry of non-immobilized pepsin in the supernatant of the binding solution. The average number of immobilized pepsin was also estimated from the hydrodynamic radii measured by Tylor dispersion analysis using a previously reported model [26]. Finally, the bioactivity of the adsorptively bound pepsin@GNP is compared to free solution and covalently immobilized pepsin@GNP to rule out whether the adsorption process alters the bioactivity of the enzyme.

Materials and Methods

Materials

Pepsin (from hog stomach, E.C.3.4.23.1, 3651 U mg^{-1}), gold (III) chloride trihydrate ($HAuCl_4 \cdot 3H_2O$), cytochrome C, trisodium citrate, tris(hydroxymethyl)-aminomethane (Tris), ammonium acetate, MES, Na_2CO_3 anhydrous, Na-K-tartrate, $CuSO_4 \cdot 5H_2O$, NaOH and Folin & Ciocalteu's phenol reagent glycerol were obtained from Sigma-Aldrich. Ultrapure water was obtained by a PURELAB Ultra water purification system (ELGA LabWater, Ede, The Netherlands).

Preparation of GNPs and adsorption of pepsin

The preparation of GNPs was based on the reduction and simultaneous stabilization of gold (III) chloride trihydrate with trisodium citrate in accordance to the Turkevich-Frens method [28-31]. For the synthesis of 10 mL solution of GNPs, 5.05 mg $HAuCl_4$ (1.28 mmol in 11.25 mL double deionized water corresponding to a final concentration of 1.14 mM) was used and heated up to the boiling point and kept under reflux under constant stirring. Afterwards 1.25 mL of 20.5 mM trisodium citrate solution (6.03 mg mL^{-1}) was added (final concentration of 2.28 mM in a total volume of 11.25 mL) and heated for further 10 minutes, while the color turned red. The GNP solution was allowed to cool down and stirred at room temperature for another 60 minutes. The GNP solution was finally stored at + 4°C until usage.

To obtain adsorptively bound pepsin, first 1 mL GNPs were centrifuged for 10 minutes at 13,400 g. The supernatant was discarded. 1 mL Pepsin in 20 mM MES buffer pH 4.5 in different concentrations (0.0052, 0.052, 0.26, 0.52, 1.04, and 5.2 mg mL^{-1}) was added to the centrifuged GNPs and stirred overnight at 4 °C. Afterwards the solution was centrifuged at 13,400 g and the pellet resuspended in 10 mM Tris buffer pH 7.5. This washing step was repeated twice. The supernatant of the first washing step was used for protein quantification by Lowry assay (see below; the protein concentration of the second

washing solution was below the detection limit) [30]. To disrupt aggregates the nanoparticles were treated in the ultrasonic bath for a few minutes. The resultant nanoparticles were washed twice and resuspended in double deionized water. They were then characterized by Vis spectroscopy, DLS and ζ-potential measurements.

Characterization of nanoparticles

The LSPR band was measured by Vis-spectroscopy before and after surface modification with pepsin acquiring spectra in the wavelength range between 350 and 800 nm. All measurements were performed with a VWR UV-1600PC Spectrophotometer. The differently functionalized nanoparticles were further characterized by DLS and their ζ-potentials, derived from electrophoretic mobility of electrophoretic light scattering (ELS) measurements, before and after pepsin coating using a Zetasizer Nano ZS instrument (Malvern Instruments, Herrenberg, Germany). The Zetasizer was equipped with a He-Ne laser and detection was performed at 173° backscatter detection mode. Samples were diluted in double deionized water (1:5; v/v) and measured as triplicates. Each value was the mean of 15 sub-runs.

A transmission electron microscopy (TEM) image of GNPs is shown in Supplemental Figure S1.

Protein determination by Lowry Assay

The amount of immobilized pepsin was determined by Lowry assay [32]. Briefly, the supernatant collected after the enzyme immobilization step was used for the quantification of non-immobilized pepsin. Applying the mass balance equation, the immobilized amount of enzyme could then be back calculated. A calibration function was set up with free pepsin in 20 mM MES buffer pH 4.5 in the range 0.05 to 1 mg mL^{-1}. 25 µL of the sample/standard/blank were mixed with 125 µL of Lowry A solution and reacted for 20 minutes. Afterwards 12.5 µL Folin & Ciocalteu's phenol reagent (Lowry reagent B) was added and reacted for further 30 minutes before measurement. Lowry

reagent A was freshly prepared every day (2.45 mL 4% Na_2CO_3 anhydrous in ddH_2O, 2.45 mL 0.1 M NaOH, 0.1 mL 2% Na-K-tartrate in ddH_2O and 0.05 mL $CuSO_4 \cdot 5H_2O$ in ddH_2O). Folin & Ciocalteu's phenol reagent was commercially available from Sigma-Aldrich.

For the photometric determinations, a Versa max microplate reader from Molecular Devices was used and the wavelength was set to 650 nm. All measurements were carried out at room temperature.

Resonant mass measurements

Resonant mass measurements (RMM) were performed with the Archimedes instrument (Malvern Instruments, Herrenberg, Germany). A sensor chip with a microchannel of the dimensions 8 x 8 µm2 was used for all experiments. It was initially mass calibrated with a polystyrene standard as specified by the instrument supplier. Afterwards, the sensor was rinsed with ultrapure water employing some sneezing steps to remove all particles from the microchannel. All the samples were diluted with ultrapure water (1:5; v/v) before each measurement. Then, the sample was loaded into the microchannel. The limit of detection was fixed to 0.030 Hz, which was well above the noise level and optimal for detection of the nanoparticles. The measurements were performed at ambient temperature and the number of measured particles was set to 2000 for the sake of adequate statistics. The buoyant mass of the particles was measured before and after coating of pepsin to the GNPs. For the calculation of the dry mass, a density of 19.320 g mL^{-1} was assumed for the GNPs and a density of 1 g mL^{-1} for the fluid.

Taylor dispersion analysis

Taylor dispersion analysis (TDA) was performed with the Viscosizer TD from Malvern Instruments (Herrenberg, Germany). The samples (40 nL) were injected into a looped fused silica capillary with 75 µm ID and 360 µm OD. The sample zone was transported in the capillary by applying a pressure of 140 mBar under a linear flow of ultrapure water

with a linear velocity of 2.4 mm/s. The capillary had a total length of 130 cm, and first and second window were located at a distance of 44 and 85 cm, respectively, from the inlet end. UV absorbance of the analyzed samples was recorded during their passage through the first and second detection window at 214 nm. All measurements were carried out at constant temperature of 20°C.

The nanoparticle samples were concentrated by the factor of 10 for TDA. Thus, 1 mL of the nanoparticle sample was centrifuged at 13,400 g for ten minutes. 0.9 mL of the supernatant was discarded and the remaining 0.1 mL of the concentrated nanoparticle solution was used for analysis after re-suspension.

Bioactivity test of adsorptively immobilized pepsin-conjugated GNPs

Michaelis-Menten kinetics was studied for digestion of cytochrome C (CYC) with free pepsin in solution, adsorptively immobilzed pepsin@GNP and pepsin covalently bonded to GNPs via a bifunctional HS-PEG_7-COOH spacer and amide coupling [33]. A concentration series of CYC was digested in 20 mM sodium acetate pH 4.5 for 10 minutes at 37 °C. The digestion was stopped by adding 0.2 mL of 0.1 M NaOH to 0.8 mL reaction mixture to achieve neutral pH. For the digestion with free pepsin, 100 µL enzyme solution (2.5 mg mL^{-1} stock solution, 0.25 mg mL^{-1} final concentration), 100 µL CYC solution in 600 µL of above buffer were used. For the approach with the immobilized pepsin 1 mL total volume of the nanoparticle solution was used and centrifuged at 12,000 rpm for 10 minutes. The supernatant was removed and the nanoparticle pellet dissolved in reaction buffer as above. 100 µL CYC solution with different concentrations were added and digestion allowed to proceed as describe above. After stopping the digestion by adding 0.2 mL 0.1 M NaOH (total volume of the reaction mixture 1 mL) the nanoparticles were centrifuged and the supernatant was analyzed by LC-UV for quantification of undigested CYC. Michaelis-Menten parameters K_M and V_{max} were calculated according to Lineweaver-Burk diagrams [34].

Undigested CYC in the reaction mixture was quantified by HPLC analysis method using an Agilent 1100 series HPLC instrument with a binary gradient pump, vacuum degasser, autosampler, column oven and a variable wavelength detector. A monolithic poly(styrene-co-divinylbenzene) ProswiftTM RP-1S (50 x 4.6 mm ID) from Dionex (Thermo Fisher Scientific) was employed as column. The mobile phase was composed of 50 mM ammonium formate pH 3.5 containing 5 % ACN in channel A and ACN + 5 % 50 mM ammonium formate pH 3.5 in channel B. The following gradient was programmed: 0-2 minutes 20 % B, from 2 to 6 minutes linear gradient from 20 to 60 % B, 6.01-10 minutes 20 % B (for test chromatogram see also Supplementary Material). The flow rate of the mobile phase was 1 mL/min and the column temperature was set to 40 °C. The injection volume was 5 µL and detection was performed at 280 nm. The method was validated in accordance to ICH guidelines.

Results and Discussion

Synthesis and characterization of pepsin-GNP bioconjugates

The GNP carrier has been synthesized by the widely adopted Frens-Turkevich method [28, 29]. In this procedure, the $HauCl_4$ is reduced by citrate which acts also as capping agent on the surface of the resultant GNPs giving them sufficient colloidal stability due to repulsive electrostatic interactions overcoming the strong van der Waals interactions between nanoparticles which drive aggregation. By adjusting a molar $HauCl_4$-to-citrate ratio of 1:2 a GNP size of 30 nm has been targeted [20, 30, 35] (Supplemental Fig.S1). This larger particle diameter was found to be advantageous as compared to smaller sizes such as 10-20 nm for protein adsorption in a previous study due to higher protein coverage and bioactivity, respectively [30]. According to DLS measurements a hydrodynamic particle diameter of 44.1 ± 0.3 nm has resulted from the GNP synthesis and the ζ-potential of the citrate-capped GNPs was -34.1 ± 0.7 mV documenting that they are sufficiently stable colloids (Table 1).

Aliquots of this GNP batch have then been coated with pepsin using different concentrations in the reaction mixture covering a range between 5 µg/mL and 5 mg/mL. Pepsin is a gastric aspartic proteinase (mol. wt., 34,510 g mol^{-1}) with a pI of about 3.2 (Uniprot, Expasy). It needs acidic conditions for optimal bioactivity (pH between 1 and 2.5 with activity up to 4.5) and is irreversibly denatured at pH > 8.5 [36, 37]. Adsorptive immobilization has been carried out at a pH close to the pI in order to minimize electrostatic repulsion between pepsin and the GNPs during the adsorption process which could compromise the immobilization efficiency. A recent paper has shown that pepsin has a ζ–potential of around 0 mV near pH 5 and therefore MES buffer pH 4.5 was deemed to be a good compromise in terms of mild conditions and attenuation of negative charge on GNPs [38].

The protein-coating success has been monitored by Vis spectroscopy, DLS and ELS (Figs. 1 and 2 as well as Table 1). Vis spectroscopy is a convenient, informative and straightforward method for a quick monitoring of the coating success of GNPs [20]. Such metallic NPs exhibit due to their plasmonic properties a LSPR band which can be excited in the Vis range and is highly sensitive to size, shape, interparticle distance (thus aggregation) as well as to changes in the refractive index of the proximate surrounding media (thus adsorption of e.g. proteins). It can therefore be used to monitor both adsorption of pepsin as well as aggregation of the resultant functionalized GNPs if the surface modification leads to unstable colloids. For the present non-modified citrate-capped GNPs the LSPR band is observed at 525 nm. With increasing pepsin concentration in the incubation mixture, the LSPR band is slightly shifted to higher absorption maxima from 525 to 527 nm. The effect is significant but the shifts are relatively small. On the other hand, it can be seen that the pepsin-GNP bioconjugate prepared from the lowest pepsin concentration (5.2 µg mL^{-1}) in the incubation mixture gets unstable and shows noticeable aggregation as can be derived from the additional absorption band (shoulder) at a wavelength of > 600 nm (Supplemental Fig. S1).

Next, ζ-potentials were determined at neutral pH for all particles. Although not active at pH 7, pepsin is sufficiently stable and does not irreversibly denature in the pH range of 6-7 [36, 37]. At such pH, pepsin is above the pI and thus should generate a negative surface charge, like the citrate-capped GNPs. Indeed, probably due to this reason ζ-potentials are largely constants across all batches of (coated) GNPs (-32.5 ± 2.6 mV) (Fig. 2). This property is consequently not very informative in terms of effectiveness of pepsin immobilization.

Thicker protein coatings are expected when the concentration of pepsin in the incubation mixture was elevated as indicated by the slight shift in LSPR band. DLS should be capable to display this effect as significant size increase. In fact, a significant increase of the hydrodynamic diameter of functionalized GNPs with adsorptively bound pepsin can be found in all pepsin-GNP bioconjugates as compared to non-modified citrate-capped GNPs (Fig. 2). A mean hydrodynamic diameter of 64 ± 2 nm was measured for the pepsin-coated GNPs regardless of the pepsin-concentration in the incubation mixture, except for the batch with 5 µg mL^{-1} pepsin (79.7 ± 5.7 nm) which represents an outlier (probably due to aggregation as indicated by the LSPR band). On the other hand, a diameter of only 44.1 ± 0.3 nm has been measured by DLS for the citrate-capped GNPs indicating pepsin-shell thicknesses of about 10 nm for the bioconjugates (Table 1). DLS was, however, not capable of resolving the size differences for the distinct pepsin-GNP bioconjugates batches prepared from distinct pepsin concentrations. Other methods for precise and accurate NP size classification are therefore required.

Determination of surface coverage by Lowry assay and RMM

The surface coverages of protein-modified solid carriers such as immobilized enzyme reactors are commonly determined indirectly by quantitation of non-immobilized protein in the supernatant of the reaction mixture. This procedure is also frequently adopted for protein immobilization of NPs [22, 24]. Micro-bicinchoninic acid (Micro-BCA) assay or Lowry assay are the most popular protein assays in NP bioconjugation reactions. Herein,

Lowry assay has been used and the protein concentration in the supernatant has been analyzed. Mass balance considerations have resulted in approximated values of immobilized pepsin (Table 1). Results from the Lowry assay suggest that indeed different pepsin coverages are present on the nanoparticles and hence some differences in the hydrodynamic diameters should be measurable.

Besides this indirect method, a direct approach for the determination of adsorptively immobilized protein has been utilized as well. Resonant mass measurement has been recently proposed for such a purpose [24]. RMM uses micro-electromechanical systems (MEMS) technology with a sensor chip having a microfluidic channel (with a dimension of 8×8 μm^2) which harbors a resonant structure embedded inside. The nanoparticles are flushed through the microfluidic channel. When a particle passes the resonator a frequency shift (Δf) occurs which depends on the buoyant mass (MB) of that particle (eq.1)

$$M_B = \Delta f \times S \quad (1)$$

wherein S represents the microchannel resonator's sensitivity (a parameter characteristic for the given chip which can be obtained by calibration). Thus, through initial mass calibration of the chip, RMM is able to detect and count particles as well as measure their mass and size. It has been reported that the resonant frequency of the sensor can be accurately measured [24]. Its mass limit of detection is in the sub-fg range (depending on the sample). From the buoyant mass the dry mass (M) can be calculated by eq. 2 if the particle is composed of a chemically homogenous material as in the case of unmodified GNPs.

$$M = \frac{M_B}{(1-\rho_{fluid}/\rho_{particle})} \quad (2)$$

Wherein ρ_{fluid} and $\rho_{particle}$ are the densities of the transport fluid (here water) and the particle (here gold). Since we are interested in the surface coverage of pepsin on the GNPs, the drymass of protein coated on the GNP is the relevant figure. It has been calculated from the difference of buoyant masses after and before pepsin coating i.e. between the pepsin-coated GNPs and non-coated GNP (ΔMB) in accordance to eq. 3

$$M_{(pepsin\ coating)} = \frac{\Delta M_B}{(1-\rho_{fluid}/\rho_{pepsin})} \quad (3)$$

wherein $M_{(pepsin\ coating)}$ is the average mass of immobilized pepsin on a single GNP. The density of pepsin has been calculated to be ca. 1.42 g mL^{-1} from the exponential function reported by H. Fischer [39] (yielding negatively buoyant particles).

If a sufficiently large number of particles is measured, a representative distribution of the buoyant masses of the citrate-capped and pepsin-coated GNPs can be obtained. Thus, RMM measurements have been performed with citrate-capped GNPs and pepsin-conjugated GNPs obtained with 1 mg mL^{-1} pepsin in the incubation mixture (Fig. 3 and Supplemental Fig. S2). It becomes evident from Fig. 3 that a significant shift in buoyant mass can be observed upon coating of pepsin onto the GNP surface (Fig. 3). The measurements of the particle distributions by RMM were sufficiently repeatable as can be deduced from the overlap of the distribution curves of repetitive experiments (Fig. Supplemental Fig. S2). From Supplemental Fig. S2 it appears that there is a significant fraction of unmodified GNPs or GNPs with very low surface coverage of pepsin in the entire particle population. The determined dry mass of the pepsin coating is given in Table 1. According to eq. 3, 4.2 ± 0.2 fg pepsin per GNP are coated onto the surface according to RMM. This corresponds to 73,513 ± 3,327 pepsin molecules per GNP on average and is in the same order as determined by Lowry assay (Table 1).

Hence, to conclude both Lowry assay and RMM document that pepsin has been successfully immobilized onto the GNPs by this simple adsorptive immobilization approach and Lowry assay indicates that there should be some differences in the hydrodynamic radius of the pepsin-coated GNPs prepared from distinct pepsin concentrations in the reaction mixture.

Taylor dispersion analysis

DLS, Lowry assay and RMM all indicated that pepsin is successfully coated onto GNPs. Unfortunately, DLS did not allow to accurately determine the size differences of the differently coated pepsin-GNP bioconjugates. Furthermore, hydrodynamic diameters

measured by DLS may be easily biased towards larger particles because the intensity of the scattered light is proportional to the sixth power of the radius, which makes the technique highly sensitive for larger particles and distorts particle distributions. Hence, Taylor dispersion analysis (TDA) was tested as alternative method.

TDA became recently popular for the analysis of the hydrodynamic radius and the diffusion coefficient of biopharmaceuticals [40-42]. It has been shown that intra-assay and inter-assay variations were 1.2 % and 3.3 %, respectively, for a mouse IgG2a (100 measurements) indicating its high precision and reliability for protein analysis [42]. In a few reports, TDA has also been used for the characterization of nanoparticles [43-48]. However, it was not considered before for measuring the protein coating thicknesses on GNPs.

Due to the high precision and good accuracy shown in several publications (vide supra), TDA has therefore been applied to measure the hydrodynamic radius in dependence of different pepsin coating thicknesses and has been examined for its capability to resolve the size differences of those functionalized NPs. TDA using Viscosizer TD is suited for particles in the size range with a hydrodynamic radius (R_h) of 0.2 nm - 50 nm. It can also be utilized to determine the diffusion coefficients of molecules and nanoparticles. The method is based on the dispersion of a solute plug in a cylindrical tube under laminar Poiseuille flow driven by slight hydrodynamic pressure [40, 49, 50]). A sample plug is injected into the capillary and moved through the capillary by hydrodynamic pressure. A detector monitors the broadening of the sample zone by measuring the peak width at the two distinct positions of the capillary. The hydrodynamic radius (R_h) can then be derived from eq. 4

$$R_h = \frac{4 \cdot k_B \cdot T \cdot \left(\tau_2^2 - \tau_1^2\right)}{\pi \cdot \eta \cdot r^2 \cdot \left(t_2 - t_1\right)} \qquad (4)$$

wherein t_1 and t_2 are the peak center times at the first and second window, τ_1 and τ_2 are the corresponding standard deviations (band broadening), k_B is the Boltzmann constant, T is the temperature, η is the viscosity, and r is the radius of the capillary.

Initially, the relative viscosity of the NP suspensions has been measured accurately with the Viscosizer TD based on the Poiseuille flow. The viscosity range which can be sufficiently accurately measured by the Viscosizer is between 0.9 cP and 50 cP (or mPa s). For this purpose, a rectangular sample plug (typically 6 µL) of citrate-capped GNPs has been pushed through the capillary and the absorbances have been monitored in the two windows (Supplemental Fig. S3). The edges of the sample plug are sharply detected at the two windows due to refractive index change, and the difference in times when the sample plug edges pass the windows can be readily determined (Δts). The sample measurement is then referenced against the corresponding measurement for a solvent or buffer of known viscosity (e.g. water) (Δtr) enabling the calculation of the viscosity of the sample. This way, relative viscosities of 0.9771 (± 0.0055) cP have been determined for the citrate-capped GNP solutions (n=3).

Next, the hydrodynamic radius and diffusion coefficient of pepsin has been measured, once under conditions as used for immobilization (pH 4.5; 20 mM sodium acetate) and once under optimal bioactivity pH (pH 1; 0.1 M HCl). It is striking that significantly broader peaks have been observed at pH 4.5 than pH 1 (Fig. 4a). Moreover, at pH 4.5 the UV trace reveals many spikes which indicate a tendency for aggregate formation of pepsin at this pH. Consequently, a hydrodynamic diameter as large as 4.4 ± 0.2 nm has been measured at pH 4.5 confirming protein aggregation. The corresponding diffusion coefficient has been calculated to be 48.8 ± 1.8 µm2 s^{-1}. On the other hand, at pH 1 a nice peak shape can be seen without spikes in the UV trace. A hydrodynamic diameter of 0.47 ± 0.03 nm has been determined and the corresponding diffusion coefficient has been calculated to be 459.1 ± 33.4 µm2 s^{-1}.

When the same experiment has been performed with citrate-capped GNPs, peaks corresponding to a bimodal distribution have been detected (Fig. 4b). A very sharp peak is sitting on top of a broad one which has been assigned as the peak corresponding to the GNPs. Since the GNPs have been stabilized by citrate, it has been argued that the superimposed sharp peak originates from citrate in the GNP suspension. Therefore,

citrate has been measured at 10 mg mL^{-1} and a hydrodynamic radius of 0.511 nm and a diffusion coefficient of 419.6 μm^2 s^{-1} resulted. These values have been utilized to deconvolute the GNP peak with a bimodal distribution model [51]. As a result, a hydrodynamic radius of 17.8 ± 0.2 nm has been determined for citrate-capped GNPs and the diffusion coefficient corresponds to 12.1 ± 0.1 μm^2 s^{-1}. Similarly, the hydrodynamic radius of pepsin-coated GNPs has been analyzed and exemplary Taylorgrams are shown in Fig. 4c. The results are summarized in Table 1.

It has been discussed that nanoparticles exposed to protein solutions build up a protein corona by monolayer formation in a stepwise manner [26]. When nanoparticles are exposed to protein solutions of varying concentrations, the protein nanoparticle interactions follows a typical sigmoidal binding behavior and the resultant average hydrodynamic radius R_h increases with the protein concentration in solution until the surface reaches saturation. This dependency of the hydrodynamic radius $R_h(N)$ on the average number of protein molecules bound to the nanoparticle (N) can be described by eq. 5 [26, 27]

$$R_h(N) = R_h(0) \cdot \sqrt[3]{(1 + c \cdot N)} \qquad (5)$$

wherein $R_h(0)$ is the hydrodynamic radius when no protein is bound and c is a scaling factor defining the volume ratio of protein to unmodified nanoparticle ($c = V_P/V_0$). The volumes of protein and nanoparticle can be calculated by $Vi = (4\pi/3)(Rh(i))^3$ taking for $R_h(i)$ the values measured for protein and unmodified nanoparticle by TDA.

Looking at the TDA results it turns out that the NP radius Rh indeed slightly increases with pepsin concentration in the binding solution (Table 1). The outlier for the lowest pepsin concentration (5.2 µg mL^{-1}) could be caused by particle aggregation as already indicated by LSPR (vide supra). Also, with the next two lowest pepsin concentrations (0.052 and 0.26 mg mL^{-1} pepsin in the reaction mixture, respectively) the particle radius did not grow significantly as compared to the citrate-capped GNPs. At higher pepsin concentrations, yet, a clear trend of larger radius can be seen (Fig. 5). In sharp contrast, DLS had problems to resolve these slight changes in hydrodynamic diameters, while the

Viscosizer can depict such small differences in the particle diameter and could be a valuable complementary technique for nanoparticle sizing. A pepsin shell thickness of ca. 6-7 nm can be calculated for the pepsin-coated GNPs prepared from 5 mg mL^{-1} in the binding solution which is in reasonable agreement with DLS measurements (ca. 10 nm; vide supra). The effective dissociation constant derived from the binding isotherm is 30.7 ± 4.1 µM. It shows that pepsin binds to the negatively charged citrate-capped GNPs with micromolar affinity. Using equation 4, the average number of bound pepsin molecules per GNP can be estimated (Table 1). It can be seen that for the pepsin-coated GNPs obtained from 1 mg mL^{-1} pepsin concentration in the binding buffer the determined values agree fairly well, i.e. they are in the same order of magnitude. On the other hand, Lowry assay seems to overestimate the pepsin coverage when close to saturation is achieved (5 mg mL^{-1}) and possibly underestimates the coverage at low pepsin concentrations in binding buffer.

Bioactivity

Reactivity of immobilized enzymes may be compromised by several factors: i) linker and solid supporting particle, respectively, may hinder the access of the substrate to the active site, ii) they may influence the dynamic behavior of the enzyme (dynamic fit upon substrate binding), iii) enzyme adsorption may lead to conformational changes and thus alteration of activities [5, 23]. Hence, as a last question to be addressed the bioactivity of the present adsorptively immobilized pepsin-GNP bioconjugates have been evaluated in comparison to free pepsin and pepsin immobilized covalently on GNPs via a PEG spacer and amide coupling [33]. Cytochrome C has been employed as model substrate and the characteristic kinetic parameters in accordance to Michaelis-Menten formalism have been determined from the decrease in remaining substrate concentration after digestion (Table 2).

It can be seen from Table 2 that K_M is in the same order of magnitude for all three types of biocatalysts, i.e. free, covalently bound and adsorptively immobilized pepsin. In fact,

K_M is slightly lower for the nanoparticulate biocatalysts as compared to pepsin in free solution, yet it is not significantly different between adsorptively bound and covalently linked pepsin@GNPs. It documents that access to the active site is not blocked by the nanoparticulate carrier. The adsorptively immobilized pepsin is also competitive what the maximal velocity is concerned. In fact, it was slightly larger than for the other two varieties of biocatalysts. The turnover number k_{cat} is slightly higher for free pepsin. On the other hand, there is no significant difference between adsorptively bound pepsin and pepsin anchored via a long spacer, which has been deemed to guarantee access of substrate and dynamic flexibility of the biocatalyst. In terms of catalytic efficiency (k_{cat}/K_M), the three biocatalytic systems are largely equivalent.

The data clearly document that the adsorptively bound pepsin is not much compromised in its catalytic activity due to the adsorption process and rules out significant steric hindrance of the active site as well as conformational protein alterations as negative influences on bioactivity. Thus, adsorptive pepsin immobilization appears to be a viable route to nanobiocatalytic materials. One has to assure, though, that the employed reaction conditions do not lead to desorption of the pepsin during reaction; low ionic strength in the incubation solution is therefore a requirement. Otherwise, the advantageous properties of the adsorptively bound nanobiocatalyst over free enzyme would be lost. Consequently, in terms of stability the covalently immobilized pepsin@GNP bioconjugate has certainly considerable advantages.

Conclusions

Immobilized enzyme reactors have become popular in many fields including analytical sample preparation. Enhanced enzyme stability and ease of removal from the reaction product are the most striking arguments to use such materials instead of free enzyme. For certain applications adsorptively bound enzymes on nanoparticles may be a viable route to produce such heterogeneous catalysts and may be attractive due to the simplicity of their preparation. Herein, we presented a set of tools for the characterization

of enzyme-nanoparticle conjugates. Vis spectroscopy, DLS, and ELS are well established methodologies to monitor the synthesis and enzyme coating success as well as colloidal stability. For the accurate size determination, DLS has the shortcoming of a bias in the NP size distributions towards larger particles as they are more sensitively detected. The slight changes due to different surface coverages of enzyme are difficult to detect. Taylor dispersion analysis with Viscosizer TD on the other hand can provide useful information even on the slight differences in hydrodynamic radius as consequence of different pepsin coating thicknesses. Resonant mass measurement with Archimedes is a valuable option to directly measure buoyant and dry masses of single particles in the fg range. Herein, we have determined the number of immobilized pepsin molecules which have been in rough agreement with indirect methods such as Lowry assay for protein quantification of non-immobilized enzyme in the supernatant and back calculation by mass balance considerations. Accurate measurement of the surface-bound enzyme on nanoparticulate IMERs is of importance for the determination of their turnover number and catalytic efficiency, and thus represents a basic requirement for unbiased comparison with free enzyme reactions.

Acknowledgements

We are grateful to Prof. Rolf Daniels for providing access to the Zetasizer Nano instrument for DLS and ζ-potential measurements.

References

[1] M. Misson, H. Zhang, B. Jin, Nanobiocatalyst advancements and bioprocessing applications, Journal of The Royal Society Interface, 12 (2015).

[2] B.J. Johnson, W. Russ Algar, A.P. Malanoski, M.G. Ancona, I.L. Medintz, Understanding enzymatic acceleration at nanoparticle interfaces: Approaches and challenges, Nano Today, 9 (2014) 102-131.

[3] C. Kranz, B. Mizaikoff, Chapter 6 - Microscopic Techniques for the Characterization of Gold Nanoparticles, in: V. Miguel, I.L.-L. Ángela (Eds.) Comprehensive Analytical Chemistry, Elsevier 2014, pp. 257-299.

[4] S. Kano, T. Tada, Y. Majima, Nanoparticle characterization based on STM and STS, Chem. Soc. Rev., 44 (2015) 970-987.

[5] D.-H. Tsai, F.W. DelRio, A.M. Keene, K.M. Tyner, R.I. MacCuspie, T.J. Cho, M.R. Zachariah, V.A. Hackley, Adsorption and Conformation of Serum Albumin Protein on Gold Nanoparticles Investigated Using Dimensional Measurements and in Situ Spectroscopic Methods, Langmuir, 27 (2011) 2464-2477.

[6] V.A. Hackley, J.D. Clogston, Measuring the Hydrodynamic Size of Nanoparticles in Aqueous Media Using Batch-Mode Dynamic Light Scattering, in: S.E. McNeil (Ed.) Characterization of Nanoparticles Intended for Drug Delivery, Humana Press, Totowa, NJ, 2011, pp. 35-52.

[7] M. Wright, Nanoparticle Tracking Analysis for the Multiparameter Characterization and Counting of Nanoparticle Suspensions, in: M. Soloviev (Ed.) Nanoparticles in Biology and Medicine: Methods and Protocols, Humana Press, Totowa, NJ, 2012, pp. 511-524.

[8] N.C. Bell, C. Minelli, A.G. Shard, Quantitation of IgG protein adsorption to gold nanoparticles using particle size measurement, Anal. Meth., 5 (2013) 4591-4601.

[9] A. Zattoni, B. Roda, F. Borghi, V. Marassi, P. Reschiglian, Flow field-flow fractionation for the analysis of nanoparticles used in drug delivery, J. Pharm. Biomed. Anal., 87 (2014) 53-61.

[10] J. Gigault, T.M. Nguyen, J.M. Pettibone, V.A. Hackley, Accurate determination of the size distribution for polydisperse, cationic metallic nanomaterials by asymmetric-flow field flow fractionation, J. Nanopart. Res., 16 (2014) 2735.

[11] S.T. Kim, Y.-J. Lee, Y.-S. Hwang, S. Lee, Study on aggregation behavior of Cytochrome C–conjugated silver nanoparticles using asymmetrical flow field-flow fractionation, Talanta, 132 (2015) 939-944.

[12] A.-R. Jochem, G.N. Ankah, L.-A. Meyer, S. Elsenberg, C. Johann, T. Kraus, Colloidal Mechanisms of Gold Nanoparticle Loss in Asymmetric Flow Field-Flow Fractionation, Anal. Chem., 88 (2016) 10065-10073.

[13] G. Allmaier, C. Laschober, W.W. Szymanski, Nano ES GEMMA and PDMA, new tools for the analysis of nanobioparticles—Protein complexes, lipoparticles, and viruses, J. Am. Soc. Mass Spectrom., 19 (2008) 1062-1068.

[14] S. Guha, M. Li, M.J. Tarlov, M.R. Zachariah, Electrospray–differential mobility analysis of bionanoparticles, Trends Biotechnol., 30 (2012) 291-300.

[15] P.T. Nilsson, A.C. Eriksson, L. Ludvigsson, M.E. Messing, E.Z. Nordin, A. Gudmundsson, B.O. Meuller, K. Deppert, E.C. Fortner, T.B. Onasch, J.H. Pagels, In-situ characterization of metal nanoparticles and their organic coatings using laser-vaporization aerosol mass spectrometry, Nano Res., 8 (2015) 3780-3795.

[16] J. Parshintsev, J. Ruiz-Jimenez, T. Petäjä, K. Hartonen, M. Kulmala, M.-L. Riekkola, Comparison of quartz and Teflon filters for simultaneous collection of size-separated ultrafine aerosol particles and gas-phase zero samples, Anal. Bioanal. Chem., 400 (2011) 3527-3535.

[17] V.U. Weiss, L. Kerul, P. Kallinger, W.W. Szymanski, M. Marchetti-Deschmann, G. Allmaier, Liquid phase separation of proteins based on electrophoretic effects in an electrospray setup during sample introduction into a gas-phase electrophoretic mobility molecular analyzer (CE–GEMMA/CE–ES–DMA), Anal. Chim. Acta, 841 (2014) 91-98.

[18] V.U. Weiss, C. Urey, A. Gondikas, M. Golesne, G. Friedbacher, F. von der Kammer, T. Hofmann, R. Andersson, G. Marko-Varga, M. Marchetti-Deschmann, G. Allmaier, Nano electrospray gas-phase electrophoretic mobility molecular analysis (nES GEMMA) of liposomes: applicability of the technique for nano vesicle batch control, Analyst, 141 (2016) 6042-6050.

[19] N.C. Bell, C. Minelli, J. Tompkins, M.M. Stevens, A.G. Shard, Emerging Techniques for Submicrometer Particle Sizing Applied to Stöber Silica, Langmuir, 28 (2012) 10860-10872.

[20] H. Hinterwirth, S.K. Wiedmer, M. Moilanen, A. Lehner, G. Allmaier, T. Waitz, W. Lindner, M. Lämmerhofer, Comparative method evaluation for size and size-distribution analysis of gold nanoparticles, J. Sep. Sci., 36 (2013) 2952-2961.

[21] A. Dudkiewicz, S. Wagner, A. Lehner, Q. Chaudhry, S. Pietravalle, K. Tiede, A.B.A. Boxall, G. Allmaier, D. Tiede, R. Grombe, F. von der Kammer, T. Hofmann, K. Molhave, A uniform measurement expression for cross method comparison of nanoparticle aggregate size distributions, Analyst, 140 (2015) 5257-5267.

[22] J.E. Gagner, M.D. Lopez, J.S. Dordick, R.W. Siegel, Effect of gold nanoparticle morphology on adsorbed protein structure and function, Biomaterials, 32 (2011) 7241-7252.

[23] P. Satzer, F. Svec, G. Sekot, A. Jungbauer, Protein adsorption onto nanoparticles induces conformational changes: Particle size dependency, kinetics, and mechanisms, Eng. Life Sci., 16 (2016) 238-246.

[24] M. Reza Nejadnik, W. Jiskoot, Measurement of the Average Mass of Proteins Adsorbed to a Nanoparticle by Using a Suspended Microchannel Resonator, J. Pharm. Sci., 104 (2015) 698-704.

[25] N.A. Schneck, K.W. Phinney, S.B. Lee, M.S. Lowenthal, Quantification of antibody coupled to magnetic particles by targeted mass spectrometry, Anal. Bioanal. Chem., 408 (2016) 8325-8332.

[26] C. Röcker, M. Pötzl, F. Zhang, W.J. Parak, G.U. Nienhaus, A quantitative fluorescence study of protein monolayer formation on colloidal nanoparticles, Nat Nano, 4 (2009) 577-580.

[27] M. Mahmoudi, A.M. Abdelmonem, S. Behzadi, J.H. Clement, S. Dutz, M.R. Ejtehadi, R. Hartmann, K. Kantner, U. Linne, P. Maffre, S. Metzler, M.K. Moghadam, C. Pfeiffer, M. Rezaei, P. Ruiz-Lozano, V. Serpooshan, M.A. Shokrgozar, G.U. Nienhaus, W.J. Parak, Temperature: The “Ignored” Factor at the NanoBio Interface, ACS Nano, 7 (2013) 6555-6562.

[28] J. Turkevich, P.C. Stevenson, J. Hillier, The nucleation and growth processes in the synthesis of colloidal gold, Discuss. Faraday Soc., No. 11 (1951) 55-75.

[29] G. Frens, Controlled nucleation for the regulation of the particle size in monodisperse gold suspensions, Nature ., Phys. Sci., 241 (1973) 20-22.

[30] H. Hinterwirth, W. Lindner, M. Laemmerhofer, Bioconjugation of trypsin onto gold nanoparticles: Effect of surface chemistry on bioactivity, Anal. Chim. Acta, 733 (2012) 90-97.

[31] E. Haller, W. Lindner, M. Laemmerhofer, Gold nanoparticle-antibody conjugates for specific extraction and subsequent analysis by liquid chromatography-tandem mass spectrometry of malondialdehyde-modified low density lipoprotein as biomarker for cardiovascular risk, Anal. Chim. Acta, 857 (2015) 53-63.

[32] O.H. Lowry, N.J. Rosebrough, A.L. Farr, R.J. Randall, Protein measurement with the Folin phenol reagent, J. Biol. Chem., 193 (1951) 265-275.

[33] M. Höldrich, A. Sievers-Engler, M. Lämmerhofer, Gold nanoparticle-conjugated pepsin for efficient solution-like heterogeneous biocatalysis in analytical sample preparation protocols, Anal. Bioanal. Chem., 408 (2016) 5415-5427.

[34] H. Lineweaver, D. Burk, Determination of enzyme dissociation constants, J. Am. Chem. Soc., 56 (1934) 658-666.

[35] H. Hinterwirth, S. Kappel, T. Waitz, T. Prohaska, W. Lindner, M. Lämmerhofer, Quantifying Thiol Ligand Density of Self-Assembled Monolayers on Gold Nanoparticles by Inductively Coupled Plasma–Mass Spectrometry, ACS Nano, 7 (2013) 1129-1136.

[36] T.G. Rajagopalan, S. Moore, W.H. Stein, Pepsin from Pepsinogen: PREPARATION AND PROPERTIES, J. Biol. Chem., 241 (1966) 4940-4950.

[37] A.P. Ryle, The Porcine Pepsins and Pepsinogens, Methods Enzymol.1970, pp. 316-336.

[38] I. Dewald, O. Isakin, J. Schubert, T. Kraus, M. Chanana, Protein Identity and Environmental Parameters Determine the Final Physicochemical Properties of Protein-Coated Metal Nanoparticles, J. Phys. Chem. C, 119 25482-25492.

[39] H. Fischer, I. Polikarpov, A.F. Craievich, Average protein density is a molecular-weight-dependent function, Protein Sci., 13 (2004) 2825-2828.

[40] A. Hawe, W.L. Hulse, W. Jiskoot, R.T. Forbes, Taylor Dispersion Analysis Compared to Dynamic Light Scattering for the Size Analysis of Therapeutic Peptides and Proteins and Their Aggregates, Pharmaceut. Res., 28 (2011) 2302-2310.

[41] A. Hawe, S. Zölls, A. Freitag, J.F. Carpenter, S.A. Berkowitz, Chapter 10 - Subvisible and Visible Particle Analysis in Biopharmaceutical Research and Development A2 - Houde, Damian J, Biophysical Characterization of Proteins in Developing Biopharmaceuticals, Elsevier, Amsterdam, 2015, pp. 261-286.

[42] A. Lavoisier, J.-M. Schlaeppi, Early developability screen of therapeutic antibody candidates using Taylor dispersion analysis and UV area imaging detection, mAbs, 7 (2015) 77-83.

[43] F. d'Orlyé, A. Varenne, P. Gareil, Determination of nanoparticle diffusion coefficients by Taylor dispersion analysis using a capillary electrophoresis instrument, J. Chromatogr. A, 1204 (2008) 226-232.

[44] L. Cipelletti, J.-P. Biron, M. Martin, H. Cottet, Polydispersity Analysis of Taylor Dispersion Data: The Cumulant Method, Anal. Chem., 86 (2014) 6471-6478.

[45] U. Pyell, A.H. Jalil, C. Pfeiffer, B. Pelaz, W.J. Parak, Characterization of gold nanoparticles with different hydrophilic coatings via capillary electrophoresis and Taylor dispersion analysis. Part I: Determination of the zeta potential employing a modified analytic approximation, J.Colloid Interf. Sci., 450 (2015) 288-300.

[46] U. Pyell, A.H. Jalil, D.A. Urban, C. Pfeiffer, B. Pelaz, W.J. Parak, Characterization of hydrophilic coated gold nanoparticles via capillary electrophoresis and Taylor dispersion analysis. Part II: Determination of the hydrodynamic radius distribution – Comparison with asymmetric flow field-flow fractionation, J. Colloid Interf. Sci., 457 (2015) 131-140.

[47] L. Cipelletti, J.-P. Biron, M. Martin, H. Cottet, Measuring Arbitrary Diffusion Coefficient Distributions of Nano-Objects by Taylor Dispersion Analysis, Anal. Chem., 87 (2015) 8489-8496.

[48] F. Oukacine, A. Morel, I. Desvignes, H. Cottet, Size-based characterization of nanoparticle mixtures by the inline coupling of capillary electrophoresis to Taylor dispersion analysis, J. Chromatogr. A, 1426 (2015) 220-225.

[49] G. Taylor, Dispersion of Soluble Matter in Solvent Flowing Slowly through a Tube, P. Roy. Soc. Lond.A. Mat., 219 (1953) 186-203.

[50] R. Aris, On the Dispersion of a Solute in a Fluid Flowing through a Tube, P. Roy. Soc. Lond. A Mat., 235 (1956) 67-77.

[51] H. Cottet, J.-P. Biron, M. Martin, Taylor Dispersion Analysis of Mixtures, Anal. Chem., 79 (2007) 9066-9073.

Tables:

Particle	λ_{max} (Vis) [nm]	d_h (DLS) [nm]	ζ (ELS) [mV]	Pepsin molecules per GNP (Lowry)	Buoyant mass (RMM) [fg]	Dry mass M *(pepsin coating)* [fg]	Pepsin molecules per GNP (RMM)	R_h (TDA) [nm]	Diffusion coefficient [$\mu m^2/s$]	$N_{calc.}$ Rh[b]
GNP (citrate capped)	525.0	44.1 ± 0.3	−34.1 ± 0.7	–	2.12 ± 0.08	–	–	17.8 ± 0.2	12.1 ± 0.1	–
Pepsin@GNP 0.0052[a]	525.0	79.7 ± 5.7	−36.9 ± 0.4	n.d.	n.d.	n.d.	n.d.	21.5 ± 0.3	10.0 ± 0.2	–
Pepsin@GNP 0.052[a]	526.0	61.9 ± 2.9	−31.3 ± 0.6	n.d.	n.d.	n.d.	n.d.	17.0 ± 0.5	12.6 ± 0.4	47,321
Pepsin@GNP 0.26[a]	526.0	65.1 ± 1.4	−32.7 ± 0.5	16,002 ± 192	n.d.	n.d.	n.d.	18.3 ± 1.7	11.7 ± 1.3	59,028
Pepsin@GNP 0.52[a]	526.0	66.6 ± 5.2	−30.3 ± 0.7	21,021 ± 1030	n.d.	n.d.	n.d.	19.7 ± 0.1	10.6 ± 0.4	73,639
Pepsin@GNP 1.04[a]	526.5	63.4 ± 1.1	−33.2 ± 1.4	51,745 ± 1638	3.37 ± 0.06	4.23 ± 0.19	73,513 ± 3,327	21.0 ± 0.2	10.2 ± 0.1	89,200
Pepsin@GNP 5.2[a]	527.0	63.8 ± 2.1	−28.9 ± 1.3	314,673 ± 1194	n.d.	n.d.	n.d.	23.7 ± 0.3	9.1 ± 0.1	128,219

n.d., not determined.
[a] [mg mL^{-1}] pepsin in reaction mixture.
[b] Calculated by Eq. (5).

Table 1 Characteristics of functionalized nanoparticles (n=3).

Parameter	Free pepsin[a]	Covalently Bound Pepsin@GNP[a]	Adsorptively Bound Pepsin@ GNP
K_M [M]	$2.93 \pm 0.29 \cdot 10^{-5}$	$2.14 \pm 0.15 \cdot 10^{-5}$	$2.32 \pm 0.15 \cdot 10^{-5}$
V_{max} [M s^{-1}]	$4.44 \pm 0.30 \cdot 10^{-8}$	$3.47 \pm 0.22 \cdot 10^{-8}$	$5.23 \pm 0.36 \cdot 10^{-8}$
k_{cat} [s^{-1}]	$6.13 \pm 0.41 \cdot 10^{-3}$	$4.79 \pm 0.31 \cdot 10^{-3}$	$4.62 \pm 0.32 \cdot 10^{-3}$
k_{cat}/K_M [M^{-1} s^{-1}]	$2.09 \pm 0.12 \cdot 10^{+2}$	$2.24 \pm 0.02 \cdot 10^{+2}$	$2.29 \pm 0.16 \cdot 10^{+2}$

[a] Data taken from: Höldrich et al. (2016), ref [33].

Table 2 Comparison of kinetic data for digestion of cytochrome C as model protein by adsorptively bound pepsin@GNP, covalently-linked pepsin@GNP, and free pepsin.

Figures and Figure Captions:

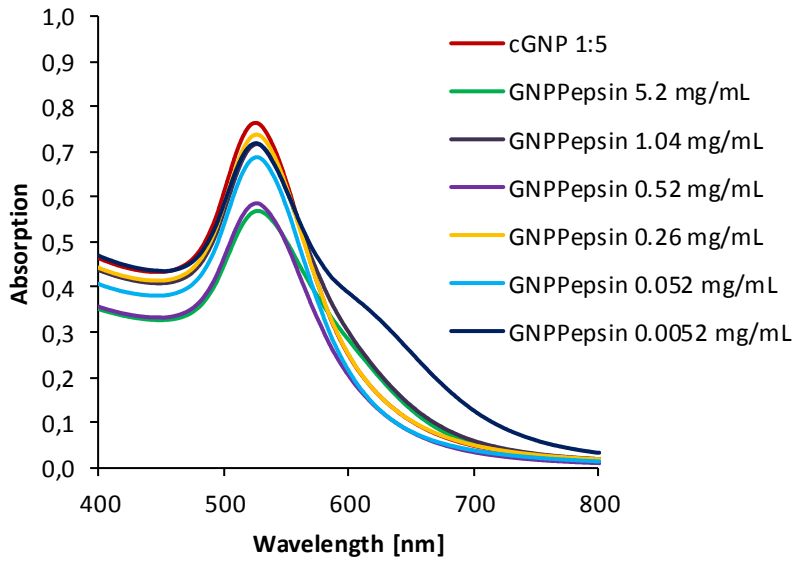

Fig. 1 Vis spectra of citrate capped GNPs and pepsin-conjugated GNPs.

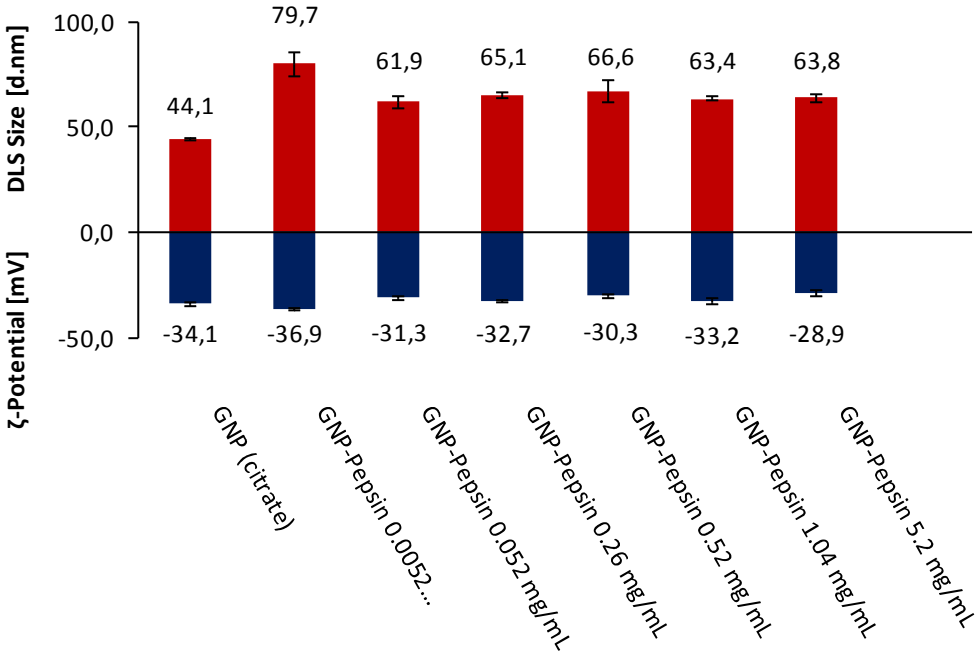

Fig. 2 Hydrodynamic diameters (nm) as determined by DLS and ζ–potentials (mV) as measured by ELS of citrate-capped GNPs as well as pepsin-coated GNPs.

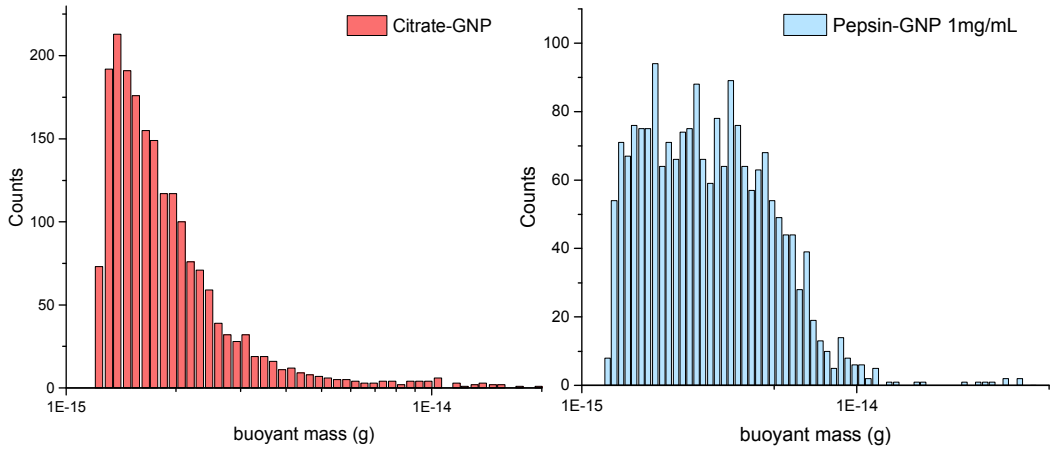

Fig. 3 Histograms of buoyant mass measurement by RMM of citrate-capped GNPs and pepsin-coated GNPs (obtained from 1.04 mg mL^{-1} pepsin in reaction mixture). Samples were diluted 1:5 (v/v) with ultrapure water before measurement.

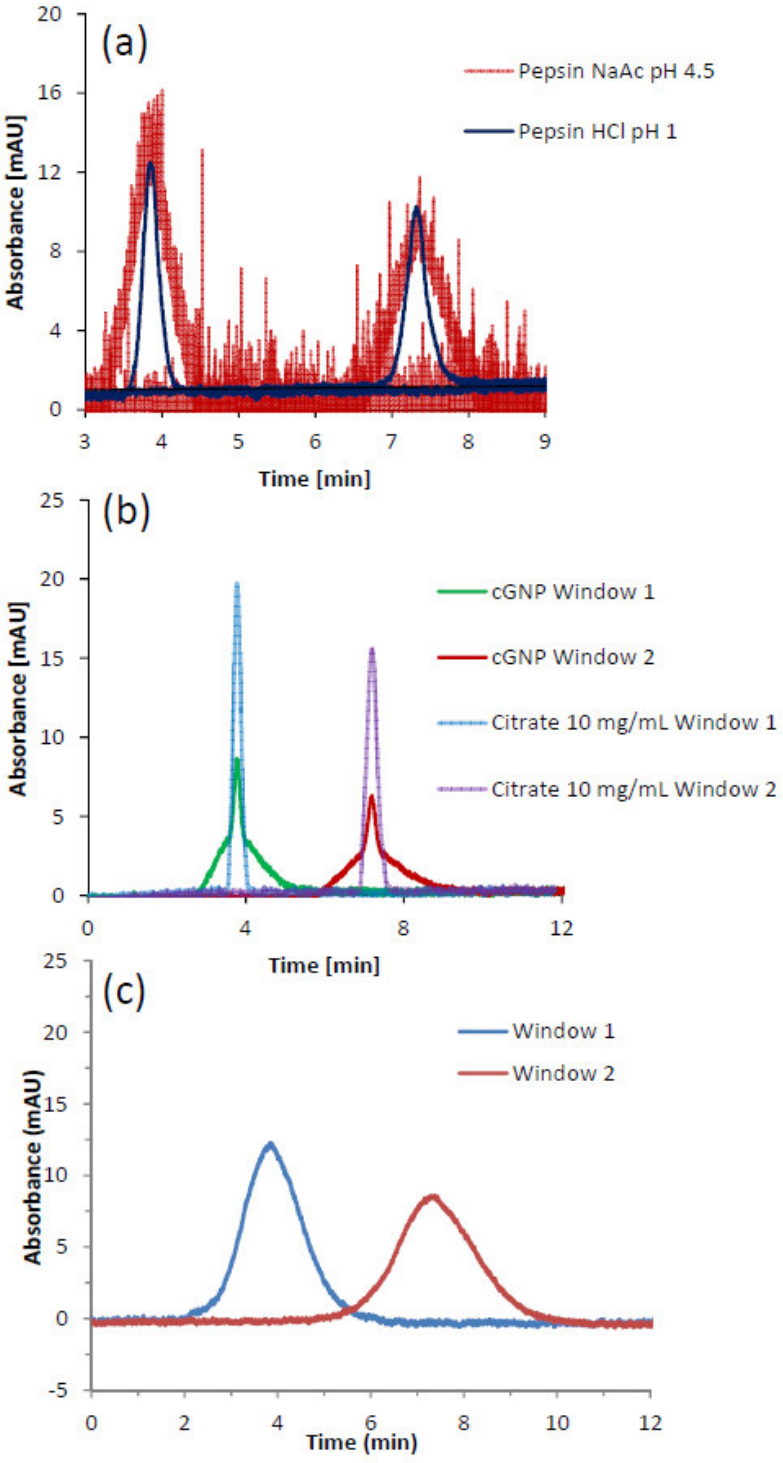

Fig. 4 Taylorgrams as measured for (a) pepsin at two distinct pH values, (b) citrate and citrate-capped GNPs, and (c) pepsin-coated GNPs prepared from 5 µg mL^{-1} in binding buffer (comparison with 5 mg mL^{-1} in binding buffer can be found in supplemental Fig. S4).

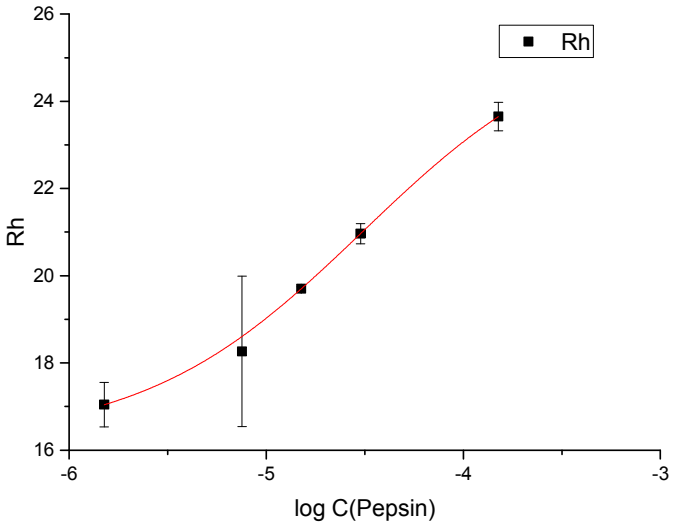

Fig. 5 Hydrodynamic radius in dependence on pepsin-concentration in binding buffer as measured by Taylor dispersion analysis with Viscosizer TD.

Supplementary Material

Characterization of nanoparticles

Transmission electron microscopy (TEM) images were acquired by Philips CM200 (acceleration voltage 200 kV, equipped with a CompuStage goniometer, a CCD Camera System (Gatan Orius SC600) and a carbon free vacuum system. For this purpose, GNPs were deposited on standard support films of amorphous carbon spanning Cu grids. The grids were immersed in the GNP suspension and withdrawn. The solution was evaporated leaving back a high number density of GNPs (typically >100 GNPs per μm^2). The Cu grids were the transferred to the microscope using a single tilt holder.

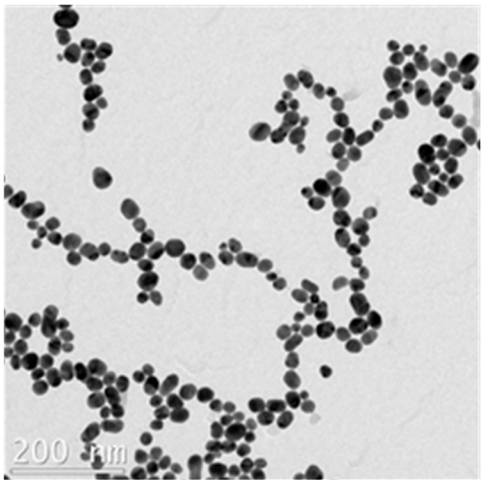

Figure S1: TEM image of citrate-stabilized GNPs (average particle size dTEM ~30 nm, dDLS ~ 40 nm).

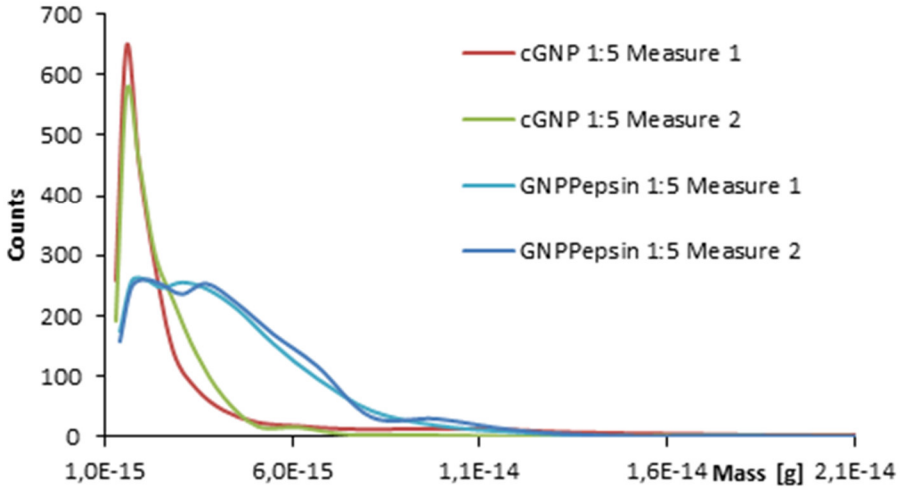

Figure S2 Mass shift of buoyant mass measurement by RMM of citrate-capped GNPs and pepsin-coated GNPs (obtained from 1.04 mg mL^{-1} pepsin in reaction mixture). Samples were diluted 1:5 (v/v) with ultrapure water before measurement.

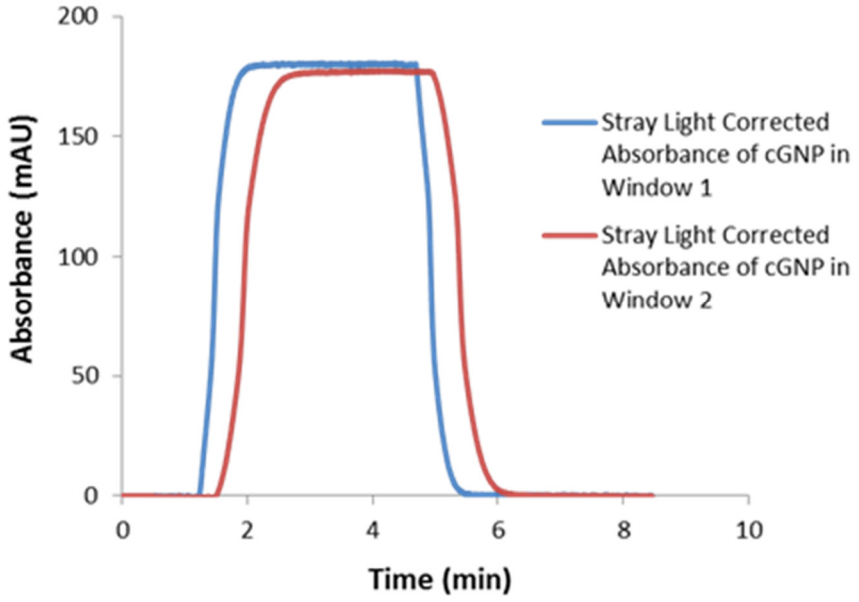

Figure S3 Viscosity measurement of citrate-stabilized GNPs with Viscosizer TD from straylight corrected signal shifts in window 1 and 2 as well as reference to a sample with known viscosity.

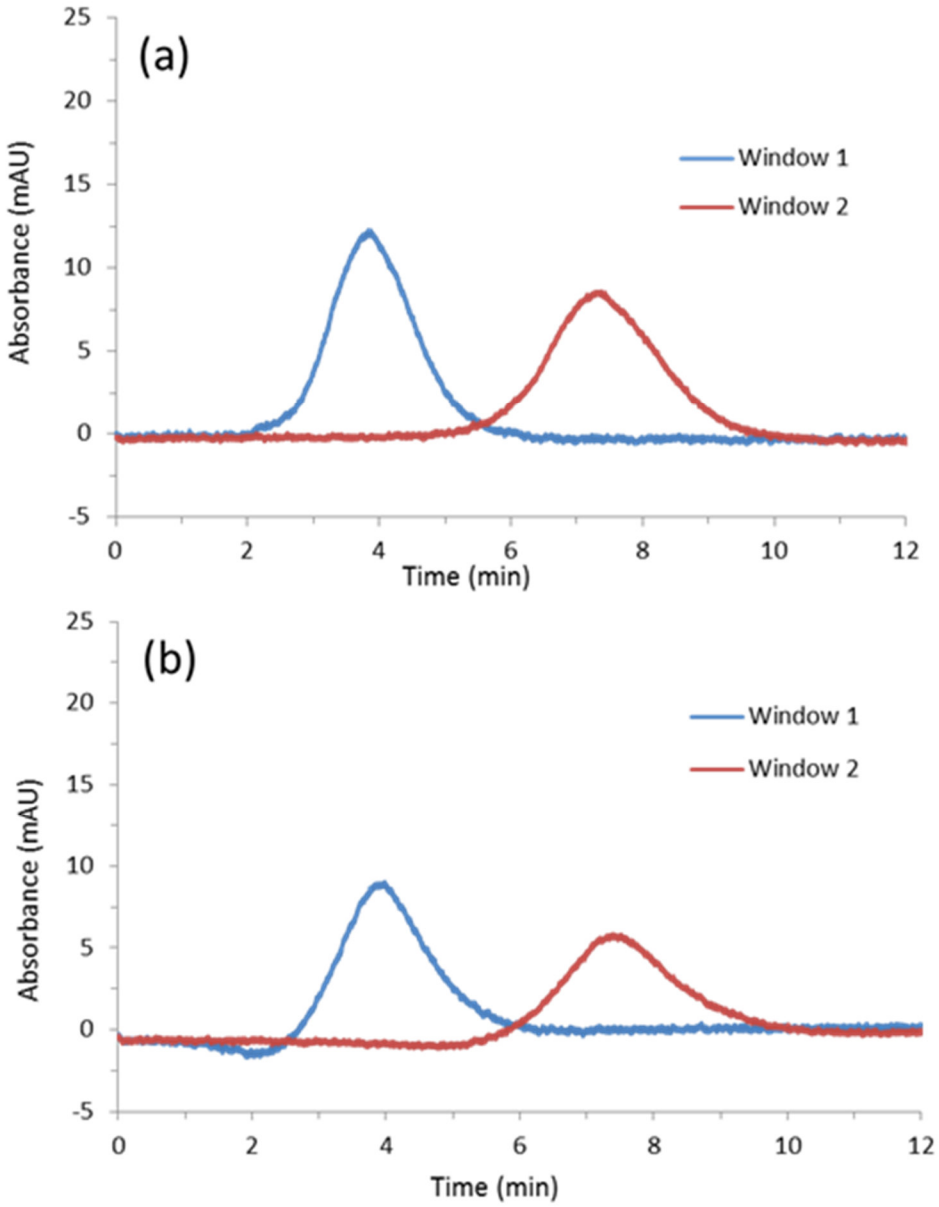

Figure S4 Exemplary Taylorgrams of pepsin-coated GNPs prepared from (a) 5 µg mL^{-1} and (b) 5 mg mL^{-1} in binding buffer).

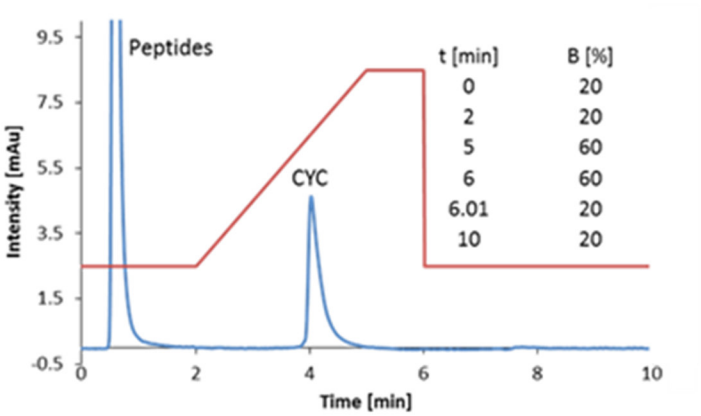

Figure S5 Exemplary test chromatogram of cytochrome C digestion.

3.3. Papain-functionalized gold nanoparticles as heterogeneous biocatalyst for bioanalysis and biopharmaceuticals analysis

Siyao Liu, Markus Höldrich, Adrian Sievers-Engler, Jeannie Horak,

Michael Lämmerhofer

Institute of Pharmaceutical Sciences, Pharmaceutical (Bio-)Analysis, University of Tübingen, Auf der Morgenstelle 8, 72076 Tübingen, Germany

Analytica Chimica Acta 963 (2017) 33-43

Abstract

Surface-modified gold nanoparticles (GNPs) were synthesized via layer-by-layer process with alternating cationic polyallylamine and anionic poly(acrylic acid) polyelectrolyte layers leading to a highly hydrophilic biocompatible shell supporting colloidal stability. Afterwards, papain was covalently immobilized on the modified GNPs via amide coupling between the amino groups on papain and the terminal carboxylic groups of the modified GNPs by using N-(3-dimethylaminopropyl)-N'-ethylcarbodiimide and N-hydroxysulfosuccinimide sodium as coupling agents. The resultant papain-functionalized gold nanoparticles were characterized by surface plasmon resonance, dynamic light scattering and zeta potential measurements. The new technology resonant mass measurement was applied for determining the average number of papain molecules immobilized per GNP by measurement of the single nanoparticle buoyant mass in the range of femtograms. The activity of the immobilized enzyme was estimated by determination of the kinetic parameters (K_m, V_{max} and k_{cat}) with the standard chromogenic substrate Nα-benzoyl-DL-arginine-4-nitroanilide hydrochloride. It was found that K_m of immobilized and free enzyme are in the same order of magnitude. On contrary, turnover numbers k_{cat} were significantly higher for GNP-conjugated papain. Further, the gold nanobiocatalyst was applied for digestion of polyclonal human immunoglobulin G to yield protein fragments. The resultant fragment mixture was further analyzed by high-performance liquid chromatography-microelectrospray ionization-quadrupole-time-of-flight mass spectrometry, which demonstrated the applicability of the bioreactor based on papain functionalized GNPs. The immobilized papain not only has higher catalytic activity and better stability, but also can be easily isolated from the reaction medium by straightforward centrifugation steps for reuse.

Keywords:

Immobilized papain, gold nanoparticle, resonant mass measurement, sample preparation, biopharmaceuticals (biologicals) analytics, immobilized enzyme reactor

Introduction

Enzymes with a number of excellent properties (high activity, selectivity and specificity) are extensively used to catalyze a wide range of commercially important processes [1]. However, some limitations exist for the applications of enzymes, such as low stability and high sensitivity to the employed conditions. Therefore, immobilization techniques of enzymes (leading to immobilized enzyme reactors, IMERs) emerged as a powerful strategy to overcome some of these limitations [2-9, 10]. They received particular interest due to some advanced properties such as high catalytic efficiency, improved stability, elimination of self-digestion, flexible control of the reaction, easy removal after reaction, no contamination of the product with enzyme and repetitive usage [4, 11-14]. Enzymes immobilized on nanomaterials possess considerable prospect in various fields, because the catalytic properties of enzymes can be flexibly combined with the unique features of nanomaterial structures [12, 15-19].

Silica nanoparticles [20], polystyrene [4] and magnetic nanoparticles [21] have been frequently utilized for the enzyme immobilization by covalent binding, entrapment, adsorption, ionic binding, affinity binding and so on [22-24]. A growing number of studies suggested that immobilizing enzyme on nanomaterials can enhance reaction rates while improving enzyme stability [25-28]. Amongst the nanomaterials, gold nanoparticles (GNPs) have received great attention in biology, biochemistry and biomedical research areas due to controlled geometrical, excellent optical and flexible surface chemical properties [29]. GNPs can be synthesized in a straightforward and low-cost method by reduction of gold(III) chloride. Due to the chemical inertness of gold they possess excellent chemical stability and due to charged capping groups on their surface also a high colloidal stability. They can be easily further functionalized with appropriate organic

or biological ligands which form the basis for their extremely broad applications. Like for other metal nanoparticles, a surface plasmon resonance (SPR) band can be observed in the visible spectrum which is the result of the collective oscillation of electrons in the conduction band of gold nanoparticles in resonance with a specific wavelength of incident light [30]. For gold nanoparticles it results in a strong absorbance band in the visible region (around 525 nm). The exact wavelength maximum as well as width of the absorption band depends on the nanoparticle size and shape, size distribution, and morphological uniformity of GNPs [31, 32]. SPR measurement is therefore a straightforward and useful tool to characterize GNPs and monitor the success of surface modification as well as to evaluate the aggregation status of GNP suspensions. If a second peak can be observed in the red-shifted region of the UV-VIS spectrum, it implies that aggregation of GNPs occurred. The large surface-to-volume ratio of GNPs provides considerable promise for the bioconjugation with various receptor molecules (e.g. proteins, DNAs, aptamers, antibodies, or lectins) [33]. The bioconjugation chemistries used for the immobilization are generally derived from the protein labeling chemistries by using various commercial crosslinkers based on maleimides, succinimidyl esters and so on. In addition, carboxylic and amino groups of proteins are widely used as the reactive sites for conjugation through amide bond formation [34].

Papain, a cysteine protease with broad specificity present in the latex of *Carica papaya*, catalyzes the hydrolysis of peptide, ester and amide bonds. Therefore, it is extensively employed in food, pharmaceutical, biology and biomedical researches [35-40]. In recent years, preparing Fab fragments with papain via specific digestion above the hinge region (the site of the disulfide bonds which connect the two heavy chains) of the whole antibody attracted some attention. The Fab fragment is a monovalent antibody structure harboring the CDR (complementarity-determining region) without Fc portion. It can still specifically recognize and bind to antigens. In biopharmaceuticals research and quality control, Fab fragments are prepared to characterize the protein on an intermediate level instead of the whole intact immunoglobulin (middle up and middle down). Middle-up refers to the

analysis of an antibody after its cleavage into large fragments, e.g. by reduction or limited proteolytic cleavage. Proteins of such smaller size are easier to analyze than larger proteins like intact antibody and can be detected with better sensitivity. Middle-down refers to the mass measurement of the gas phase fragmentation of antibody fragments, in analogy to the mass measurement of the gas phase fragmentation of intact protein in top-down analysis [41]. An antibody digested by papain generates two Fab fragments (about 50 kDa) and one Fc fragment (also about 50 kDa). Pure Fab fragment can be obtained after purification of digests by affinity chromatography (with protein A to remove the Fc part), ion exchange, and size exclusion chromatography [39, 40].

The main goal of this study was to prepare stable immobilized papain on GNPs for use in sample preparation protocols of antibody analytics. For this purpose, it is necessary that the obtained immobilized papain nanobiocatalyst has sufficient colloidal stability and satisfactory bioactivity to yield useful Fab fragments for analytical characterization by mass spectrometry via enzyme digestion. In this research, surface-modified GNPs with highly hydrophilic and biocompatible shell were first prepared from oppositely charged polyelectrolytes via their alternating deposition by a layer-by-layer process (LBL) onto citrate stabilized GNPs [42-44]. The immobilization process was carried out by using cross-linker agents to link the carboxylic group on the surface of carboxy-modified GNPs with the amino group on papain [42-44]. The covalent (instead of adsorptive) bonding was selected for irreversible immobilization to avoid enzyme leaching from the support surface [45]. The number of immobilized papain molecules on GNPs is an important figure for the determination of the immobilization efficiency. Resonant mass measurement (RMM) was applied herein to measure the mass increase of the nanoparticles upon immobilization of papain and determine the surface coverage [46]. It is well-known that papain, like other proteases, is prone to auto-digestion. The resultant peptides will cause the contamination of the protein digestion products. Therefore, immobilization of proteases like papain on a solid support is a good solution to eliminate this kind of contamination produced by auto-digestion [47]. In addition, the papain-

functionalized GNPs can be easily removed from the reaction solution by a simple centrifugation process, which also terminates the digestion. Therefore, using immobilized papain makes it easy to control the reaction time without using any stop reagents which normally introduce contamination to the product solution.

Experimental

Materials

Papain (EC 3.4.22.2) was purchased from Acros Organics (Geel, Belgium). Human immunoglobulin G (Gammanorm) (h-IgG) was obtained from Octapharma (Heidelberg, Germany). The lot employed in this study was already expired. Gold(III) chloride trihydrate ($HAuCl_4 \cdot 3H_2O$), trisodium citrate, poly(acrylic acid, sodium salt) solution (PAA, Mw. ~ 15,000, 35% in H_2O), poly(allylamine hydrochloride) (PAH, Mw.~17,500), N-(3-dimethylaminopropyl)-N'-ethylcarbodiimide (EDC), N-hydroxysulfosuccinimide sodium (sulfo-NHS), sodium phosphate monobasic dihydrate, sodium carbonate anhydrous, sodium hydroxide, K-Na-tartrate (potassium sodium tartrate), N-benzoyl-DL-arginine-4-nitroanilide hydrochloride (BNpNA) and p-nitroaniline, copper(II) sulfate, Folin & Ciocalteu's phenol reagent glycerol, 2-amino-2-(hydroxymethyl)-1,3-propanediol (Tris base), acrylamide/bis-acrylamide (30% solution), glycerol, and a ProteoSilver TM silver staining kit were obtained from Sigma-Aldrich (Munich, Germany). Ammonium persulfate was from AppliChem (Darmstadt, Germany). HPLC-grade acetonitrile was purchased from JT Baker Chemical Co. (Deventer, The Netherlands). Double deionized water (produced by Elga Purelab Ultra ELGA, System LabWater, Celle, Germany) was used throughout synthesis of functionalized GNPs and analytical procedures including LC-MS.

Preparation of papain-functionalized GNPs

Gold nanoparticles were prepared according to the Turkevich-Frens method with some modifications [48]. In brief, 25.25 mg $HAuCl_4$ was dissolved in 50 mL water (with a final concentration of 1.14 mM) and then heated at 170˚C under reflux and constant stirring for 10 min. Afterwards 6.25 mL trisodium citrate (2.28 mM) was added and heated for another 10 min under reflux and constant stirring. Then the colloidal solution was kept stirring without heating for an additional 60 min to cool down to room temperature. The obtained citrate-GNP solution was stored at 4 ˚C for further usage.

The surface modification of GNPs was realized via the layer-by-layer process (LDL) reported by Schneider and Decher [49]. In brief, citrate-stabilized GNP suspensions were first centrifuged (12000 rpm, 10 min), the supernatant discarded and the pellet washed with water to remove citrate from the supernatant. Afterwards 10 mL citrate-GNP suspension was added dropwise to the same volume of PAH solution (20 mg mL^{-1}, 10 mL) under continuous vigorous stirring, and then kept gently stirring for 30 min at room temperature in the dark. To remove excess PAH, the reaction mixture was centrifuged (12000 rpm, 15 min), the supernatant discarded and the pellet washed twice with 10 mL water. The second layer coating process was performed according to the first coating step but PAH was replaced by PAA (20 mg mL^{-1}). After removal of the supernatant and two washing steps performed as above, the modified GNPs (GNP/PAH/PAA) were resuspended in 20 mM phosphate buffer (pH 6.8). Subsequently, 20 µL EDC (12 mM) and 20 µL sulfo-NHS (60 mM) solutions in water were added into 760 µL GNP/PAH/PAA suspension to yield activated carboxylic groups in the form of sulfo-NHS esters which were further coupled with amino groups on the surface of papain. For this purpose, 800 mL activated GNP/PAH/PAA suspension was added dropwise into 200 µL papain solution with four different concentrations (1 mg mL^{-1}, 2 mg mL^{-1}, 5 mg mL^{-1}, 10 mg mL^{-1}) under continuous vigorous stirring. The reaction mixture was then stirred gently for 2 h, and allowed to stand for 12 h at room temperature. To remove excess papain, the obtained papain-GNP suspension was centrifuged (12000 rpm,

15 min), the supernatant discarded and the pellet washed with water. The wash procedure was repeated two times and finally the pellet was resuspended in 20 mM phosphate buffer (pH 6.8). The papain-GNP solution was stored at 4 ˚C prior to use.

Characterization

After each step of surface modification, SPR bands of GNPs were measured in the wavelength range between 300 nm and 800 nm with a UV-1600PC spectrophotometer (from VWR, Darmstadt, Germany) to determine the size changes as well as nanoparticle dispersion and aggregation status. Size and size distribution of GNPs were studied by dynamic light scattering (DLS) based on the Brownian motion of the particles using a Zetasizer Nano ZS from Malvern Instruments (Herrenberg, Germany). The stability of the GNP dispersions was determined by zeta potential (ζ-potential) measurements before and after each modification step with the Zetasizer Nano ZS. The Zetasizer Nano ZS was equipped with a He–Ne laser and each measurement was performed at 173 ˚C backscatter detection mode. Each sample was diluted with water (1:5; v/v) before detection and measured in triplicate. Each reported value represents the mean of at least 15 subruns.

Quantitative determination of the immobilized papain

RMM using the Archimedes instrumentation from Malvern Instruments was employed to determine the amount of immobilized papain on nanoparticles. All the samples were diluted with water (1:5; v/v) before each measurement. Before measurements, (mass) calibration of the microchip was performed with 1 μm latex standard and a sample of deuterium. The microchannel was then flushed with purified water before analysis, and the impurities in the system were subsequently removed by sneezing steps. The limit of detection was set to 0.030 Hz, which was well above the noise level and optimal for detection of nanoparticles. Each measurement was carried out at room temperature, and the determination numbers of particles were set to 2000 to ensure satisfactory statistics

of the nanoparticle distributions. The density of gold was 19.320 g mL^{-1}, and the density of fluid was 1g mL^{-1}. With these conditions, the average buoyant masses of particles before and after immobilization of papain were measured. The average real masses (drymass) of papain-GNPs were obtained from the conversion of buoyant mass.

Assays of papain activity

In order to determine the activity of both free papain and immobilized papain, N-benzoyl-DL-arginine-4-nitroanilide hydrochloride (BApNA) was selected as a substrate for the kinetic assays. In principle, BApNA was cleaved by papain to produce p-nitroaniline which was measured with the Versa max microplate reader (from Molecular Devices LLC, Biberach, Germany) at an absorbance of 410 nm. A concentration series of BApNA was digested with papain (free papain and immobilized papain, respectively) in 20 mM phosphate buffer (pH 6.8) at 37 ˚C. For the digestion with papain, different volume of BNpNA stock solutions in phosphate buffer (2 mM) and 50 µL enzyme solution (2 mg mL^{-1}, and 1 mg mL^{-1} in final solution) were added to the 96 wells, and different volumes of phosphate buffer were filled to obtain the final volume of 100 µL. Digestion was performed at 37 ˚C controlled by the microplate reader, and the absorbance of all the samples were recorded every two minutes with kinetics scan mode. For the digestion with papain-GNP, 50 µL papain-GNP solution in 20mM phosphate buffer (pH 6.8) were added and digestion was performed as described above for 10 min. After stopping the digestion by immediate centrifugation, the supernatant was analyzed with microplate reader in endpoint mode. The Michaelis-Menten plot and Lineweaver-Burk plot were built based on the calculated initial velocity. Finally, the kinetic parameters (K_m, V_{max} and k_{cat}) were calculated by using the Lineweaver-Burk equation. All experiments were performed in triplicate.

Antibody digestion with papain-functionalized GNPs

For the antibody digestion, immunoglobulin G solutions were first digested with papain-functionalized GNPs. For digestion, 10 mg mL^{-1} IgG solution was diluted with water to 0.5 mg mL^{-1} and used as stock solution. Subsequently, 100 µL of above solution of immobilized papain on GNPs was mixed with 100 µL IgG solution (0.5 mg mL^{-1}), and incubated at 50 ˚C with gentle shaking at 450 rpm with a Thermoshaker (Peqlab, Erlangen, Germany) for 4h, 8h and 24h, respectively. After digestion, the GNP-based nanobiocatalyst was easily separated from the crude digest by a centrifugation step (12000 rpm, 10 min). Finally, the clear digestion solution (supernatant) was analyzed by sodium dodecyl sulfate polyacrylamide gel electrophoresis (SDS-PAGE) and high-performance liquid chromatography-microelectrospray ionization-quadrupole-time-of-flight mass spectrometry (HPLC-µESI-QTOF-MS) in intact protein mode (vide infra).

SDS-PAGE

A Mini-PROTEAN 3Cell with Mini-PROTEAN 3 PowerPac 300 system (200/240V) obtained from Bio-Rad Laboratories (Munich, Germany) was applied for the SDS-PAGE. The Precision plus protein mix (from Bio-Rad Laboratories) was used as the standard protein marker. A tn percent Tris-HCl gel with a thickness of 0.75 mm and 10 sample wells was prepared according to the product technical information from Bio-Rad Laboratories. All the samples were mixed with non-reducing sample buffer in a ratio of 1:1 (v/v) before application of 7.5 µL into each well. 2 µL of the protein standard were applied. After development of the gel, the protein bands were stained with a Proteosilver Plus Silver Stain Kit from Sigma-Aldrich (Munich, Germany) according to the product technical information.

HPLC-μESI-QTOF-MS method for determination of IgG masses before and after digestion

An Agilent Technologies (Waldbronn, Germany) 1290 Series UHPLC and a PAL-xts (CTC, Zwingen, Switzerland) autosampler were used for chromatographic separation and injection, respectively. A ProSwift RP-4H monolithic capillary column (500 μm ID × 10 cm) from Thermo Scientific (Waltham, Massachusetts, USA) was applied for protein separation. The LC gradient is shown in Table 1. Solvent A consisted of ultrapure water (from Elga Purelab Ultra ELGA) with 0.1 % (v/v) formic acid, and solvent B consisted of acetonitrile with 0.1 % (v/v) formic acid. The flow rate was set to 50 μL/min and injection volume was 3 μl.

Detection was carried out with a Triple TOF 5600+ quadrupole time-of-flight mass spectrometer from AB Sciex (Concord, Ontario, Canada) equipped with a DuoSpray source operated in positive mode using a 50 μm ID microelectrospray ionization (μESI) needle (from Sciex). The source temperature was set to 400 °C and the ionspray voltage floating was 5100 V. Nebulizer gas (GS1) was set to 50 psi, drying gas (GS2) to 40 psi, and curtain gas to 30 psi. Finally, the declustering potential (DP) was set to 230 V, and the collision energy (CE) to 30 V. TOF-MS scan ranged from 500 to 4000 Da. For intact protein detection Sciex's Intact-Protein script was activated, Q1 transmission was set to 100 % at 1250 m/z, and sensitivity was increased by summing 60 time bins. PeakView from Sciex containing the Bio Tool Kit software package was used for data processing and identification of the proteins by a deconvolution procedure.

Result and discussion

Preparation of papain functionalized GNPs

For analytical and bioapplications, the GNPs should support the property of colloidal stabilization in physiological medium as well as provide a large surface for a high

bioconjugation capacity with receptor molecules or, in present case, enzymes [50]. To cope with this goal a LBL activation of the GNP surface was employed before bioconjugation of the enzyme. The schematic presentation for the preparation process of the functionalized GNPs is shown in Figure 1. First, citrate stabilized GNPs were prepared according to the Turkevich-Frens method [48]. In this reaction, citrate played the role as both reducing and stabilizing reagent. Capping citrate anions on the GNP surface provide them with negative charges and give them colloidal stability due to electrostatic repulsion of the particles precluding their van der Waals driven aggregation. Modification with charged polymer reagents (i.e. polyelectrolytes) was supposed to further increase the colloidal stability of GNPs by formation of soft shells on the GNP surface based on electrostatic repulsion and steric hindrance. Moreover, the coated polyelectrolytes provide sufficient anchor groups for covalent bonding of protein. This biocompatible and highly hydrophilic shell was obtained by an alternating deposition of oppositely charged polyelectrolytes on the nanoparticle surface. For the first layer, PAH with multiple positive charges was adsorbed onto the surface of negatively charged GNPs based on electrostatic interactions. Afterwards, addition of the positively charged PAH/GNPs to the negatively charged PAA solutions caused the formation of a second stabilized layer on the surface of GNPs with negative charge. After each modification step, two washing steps were performed to remove unbound polyelectrolyte as well as coexisting particles formed by the nanoaggregation of PAH with PAA [51]. Immobilization of papain on the LBL-modified GNPs was performed by using EDC and sulfo-NHS as activation reagents for amide coupling between carboxylic groups on the surface of the LBL-modified GNPs and amino groups of papain. Immobilization of papain on the first cationic PAH polyelectrolyte layer failed, because the single-layered and positively charged PAH/GNPs were easily aggregated in phosphate buffer (20 mM, pH 6.8) which was commonly used for the immobilization and digestion with papain.

Characterization of functionalized GNPs

In order to monitor the quality of the modified GNPs, various physicochemical characterizations were performed after each surface modification step with analytical techniques such as visible spectroscopy measuring the absorbance maximum (λmax) of the SPR band, DLS for measuring particle size distributions (i.e. hydrodynamic diameters) and electrophoretic light scattering for ζ-potential determinations [52].

The characterization results of the various synthesized nanoparticles with regard to their SPR band are shown in Figure 2. It becomes evident that λmax of the SPR band of citrate-stabilized GNPs (527 nm) and the LBL-modified GNP/PAH/PAAs are essentially identical while it has obviously shifted for the papain-functionalized GNPs (papain-GNPs) towards longer wavelength (543 nm). Furthermore, the broader peak width of papain-GNPs in comparison to GNP/PAH/PAAs and citrate-GNPs reveals that papain has been successfully immobilized. Due to absence of a strong red shifted absorption band at λ > 600 nm, it can be concluded that no significant aggregation of papain-GNPs occurs. During the functionalization process, four different concentrations of papain (0.2, 0.4, 1, and 2 mg mL^{-1}, respectively) in the reaction mixture were used to prepare four batches of papain-GNPs with different sizes and protein-coating thicknesses. Even though a longer wavelength and broader peak shape has been found after immobilization of papain from 0.2 mg mL^{-1} papain reaction solution, it can be interestingly seen from Figure 2b that negligible SPR band shifts result among the four batches of papain-GNP solutions prepared from differently concentrated papain solutions. Therefore, these results imply that SPR is not sensitive enough for detecting these further size and size distribution changes. Therefore, another characterization method, DLS, has been used to reveal the size differences between the four batches of papain-GNPs.

Hydrodynamic diameters (d_h) and ζ-potentials of the different stages of modification are shown separately in Figure 3a and 3b. The citrate-capped GNPs were first prepared with mean diameter of 36.4 ± 0.3 nm and a ζ-potential value of -35.7 ± 0.3 mV. After first layer modification, the size greatly increased to 127.6 ± 5.7 nm with the ζ-potential changing

from the negative value of -35.7 ± 0.3 mV to the positive value of 69.6 ± 3.6 mV. The results confirmed successful modification with PAH. After second layer modification with PAA, the ζ-potential of the nanoparticles changed to a negative value of -44.4 ±1.0 mV with an average size of 126.3 ± 6.3 nm according to DLS measurements. It is striking that the size does not change significantly although effective deposition of the anionic polyelectrolyte PAA is evident from the ζ–potential. The internal repulsive electrostatic interactions between PAH polymer chains which lead to an increase of the shell thickness after first layer deposition appear to be effectively attenuated when the oppositely charged PAA polyelectrolyte is applied on the surface. This might lead to a condensation of the shell thickness so that there is actually not much difference in d_h compared to the stage before. After functionalization with four different concentrations of papain (0.2, 0.4, 1, and 2 mg mL-1, respectively), the hydrodynamic radius d_h grew significantly from 176.2 ± 5.2 nm (for 0.2 mg mL^{-1}) to 1315 ± 136 nm (for 2 mg mL^{-1}). Since severe aggregation was not found in the visible spectra (Fig. 2b), the increase in the hydrodynamic diameters with more papain in the reaction mixture was (largely) attributed to the increased amount of papain on the GNPs.

The ζ-potentials of all these four batches of papain-GNPs still remained highly negatively charged, which indicated that a good colloidal stability persisted. Moreover, it is worth noting that absolute values of the ζ-potential decreased with increasing amounts of immobilized papain. Papain (pI ~ 8.75) which carries a net positive charge in the employed phosphate buffer (pH 6.8) partly compensates negative charges of the 2-step LBL-modified GNPs which might compromise their colloidal stability.

In conclusion, DLS measurements confirm the successful immobilization of papain and that the amount of papain covalently bonded on the GNPs can be readily increased by higher concentrations of papain used during protein coupling reaction. ELS measurements, on the other hand, reveal that ζ-potentials of these nanobioconjugates are large enough to support their colloidal stability.

Loading amount of immobilized papain

RMM was recently introduced as an innovative technology for accurately measuring the mass of nano- and microparticles with detection limits in the range of femtograms to attograms [46, 53-55]. It allows convenient particle classification in the size range of 50 nm to 5 µm if a sufficient number of particles is counted. Therefore, RMM was envisaged as a useful tool in our study for the determination of the average number of papain molecules immobilized on GNPs by using an Archimedes instrument. This instrument accommodates a sensor chip with a microfluidic channel (having a dimension of 8×8 μm^2) in which a resonant structure is embedded inside. When a nanoparticle passes through this microchannel, a shift of the resonant frequency occurs because the resonant structure senses the density difference between the particle ($\rho_{particle}$) and the transport fluid (ρ_{fluid}). Information on the buoyant mass of the nanoparticles can be derived from the resonant frequency shift [46].

The number of particles measured was set to 2000. The average buoyant mass (M_B [fg]) of this nanoparticle population was calculated by conversion from the resonant frequency shift (Δf [s^{-1}]) according to Eq. 1.

$$M_B = \Delta f \times S \quad (1)$$

wherein S [fg s] represents the microchannel resonator's sensitivity. It is a fixed value for each resonator, which reflects a simple linear relationship over the entire range of measurable particles, and has to be determined by a simple calibration procedure. From the buoyant mass the dry mass M [fg] can be calculated for a defined chemically homogeneous particle according to Eq. 2 [46, 56].

$$M = \frac{M_B}{(1-\rho_{fluid}/\rho_{particle})} \quad (2)$$

However, in the present case we are dealing with a composite material i.e. a shell particle in which gold core and protein shell have distinct densities which needs to be considered in the calculations. Hence, a modified version of Eq. 2 has been utilized. By comparing the average buoyant mass changes of GNPs before and after functionalization (ΔM_B), the

average mass of immobilized papain on a single GNP ($M_{(papain\ shell)}$) can be approximated by Eq. 3

$$M_{(papain\ shell)} = \frac{\Delta M_B}{(1-\rho_{fluid}/\rho_{shell})} \quad (3)$$

wherein ρshell is the density of the papain shell. The density of the fluid (water) used was 1g mL^{-1} in all calculations, and the density of the papain shell on the GNP surface was calculated to be 1.43 g cm^{-3} from the exponential function reported by H. Fischer [57]. Hence, the average mass of immobilized papain was obtained. More importantly, with the calculated average mass of a papain molecule from the known molecular weight of papain (23,406 Da), the average number of papain molecules immobilized on each nanoparticle was finally obtained [46]. The particle buoyant mass distributions of LBL-modified GNPs (GNP/PAH/PAA) and papain-GNPs (0.2 mg mL^{-1} and 1 mg mL^{-1}) are shown in Figure 4. The graph in Figure 4a shows a relatively narrow buoyant mass distribution of GNP/PAH/PAA nanoparticles. Surface functionalization with 0.2 mg mL^{-1} papain yielded a slight, but insignificant shift of the average buoyant mass from 3.14 ± 0.06 to 3.42 ± 0.31 fg (Figure 4b and Table 2). On the other hand, for GNPs functionalized with 1 mg mL^{-1} papain solution, a significant shift of the distribution towards a larger average buoyant mass (27.30 ± 2.25 fg) with a broader width indicative for increased polydispersity can be observed (Figure 4c and Table 2).

Therefore, with this technology the average mass of papain per GNP, the concentration of nanoparticles, the concentration of immobilized papain and the number of papain molecules per GNP can be calculated (shown in Table 2). Such knowledge is of importance for the calculation of the turnover numbers (k_{cat}) of the immobilized enzyme nanobioreactors. It can be seen that the average mass increase due to papain immobilization (with 0.2 mg mL^{-1}) on GNP/PAH/PAA corresponds to the mass of $2.39 \pm 2.14 \times 10^4$ papain molecules per single GNP. By using the same calculation for the papain-GNPs (from 1 mg mL-1), the average mass increase corresponds to $2.06 \pm 0.19 \times 10^6$ molecules of papain immobilized per GNP. The factor 100 increase in

surface coverage upon a factor 5 increase of the papain concentration in the reaction mixture is unexpected. However, it is confirmed by the more than proportional size increase as measured by DLS and may have to do with the specific conformational arrangement and morphology, respectively, of the polyelectrolyte coating. Calculations based on the approximately available surface area of GNP/PAH/PAA with a diameter of 126 nm for papain adsorption and the hydrodynamic diameter of papain as estimated by DLS leads to the conclusion that the papain shell is formed by a multilayer bonding on the GNPs. One could imagine bonding of multiple papain molecules on loosely adsorbed loops of the outer PAA polymer chains yielding elevated protein surface coverage.

Furthermore, it can be clearly seen from Table 2 that the nanoparticle concentrations in the suspension continuously decline. The GNP/PAH/PAA solution showed the highest concentration of 1.06×10^{-11} mol L^{-1}, but the concentration decreased after functionalization with papain, which is due to the loss of nanoparticles during reaction. In conclusion, the RMM technology is an effective tool for measuring the average mass of immobilized protein on each nanoparticle.

Determination of kinetic parameters of immobilized and free papain

The enzyme activity of free papain and of the four distinct papain-GNP bioconjugates was evaluated at 37 ˚C and pH 6.8 by investigating the hydrolysis of BApNA as the substrate [48]. In principle, BApNA is cleaved in the presence of papain to produce chromogenic p-nitroaniline (pNA) which exhibits strong absorbance at the wavelength of 410 nm (Suppl. Fig. S1). Thus, the activity of papain can be conveniently measured by the released pNA with a photometric assay. To obtain the Michaelis-Menten parameters (K_m, V_{max}, k_{cat}; see also Suppl. Material), the activities of free and immobilized papain for various concentrations of BApNA were measured and the obtained data were plotted in the form of Lineweaver-Burk plots, as shown in Figure 5a. These plots document a good linear relationship between 1/[S] and $1/v_0$ for both free and immobilized papain. K_m and

V_{max} values of free and immobilized papain were calculated from the intercepts on x- and y-axes, respectively, and the results are summarized in Table 3.

The Michaelis constant K_m is the substrate concentration at which half of the maximal reaction rate ($V_{max}/2$) can be achieved. In free solution, it is independent of the enzyme concentration. Upon immobilization, the enzyme conformation might change, thus negatively (or even positively) influencing enzyme-substrate complex formation. Furthermore, the access of the substrate to the active site might be altered upon immobilization. Both of these properties might change in dependence of the surface coverage. For instance, at low surface concentrations the active site might be better accessible than at high coverage for which sterically hindered and limited access to the enzyme's catalytic site might compromise the rate constant for association and thus affect or alter K_m. The data in Table 3, however, reveal that Michaelis constants K_m remain in the same order of magnitude when different concentrations of papain are immobilized on GNPs, ranging between 1.4 and 2.6 mM (mean = 2.0 ± 0.6 mM; the slight fluctuations represent experimental uncertainties which are in a similar order as for the repetitive experiments with free papain) (see also Suppl. Fig. S2). A comparison of this mean with K_m of free solution reaction reveals that there is no statistically significant difference in K_m. Hence, binding affinity is not compromised upon immobilization of papain [58].

V_{max} of enzyme reactions reflects how fast the biocatalyst can catalyze the biotransformation. V_{max} rises linearly with the enzyme concentration in free solution reactions. This is also observed for the papain-GNP conjugates varying in papain surface concentrations (Fig. 5b). V_{max} values of immobilized papain range from 6.00 ± 0.27 × 10^{-5} mM s^{-1} (0.2 mg mL^{-1} papain in reaction mixture) to 7.12 ± 0.17× 10^{-4} mM s^{-1} (2.0 mg mL^{-1}) (Table 3). The corresponding reaction with free papain reached a V_{max} of 2.03 ± 0.57 × 10^{-4} mM s^{-1}, respectively. A faster reaction with immobilized enzyme is clearly evident. This, in turn, has also the advantage that less enzyme could be used to reach the same maximum reaction rate if it is immobilized to the GNP carrier. This is

highly relevant in biocatalytic industrial applications with precious enzymes and those of limited availability. For instance, the same V_{max} as with 1 mg mL^{-1} papain in free solution can be achieved with papain-GNP conjugated biocatalyst prepared from only 0.54 mg mL^{-1} in the reaction mixture (equivalent concentration Ceq) (Fig. 2b). Thus, a factor of almost 2 less enzyme would be consumed if the supernatant after reaction is discarded and disposed. Actually, since only a small fraction of the enzyme is bonded to the GNPs, the unbound enzyme can be easily recycled from the reaction mixture after centrifugation. For instance, in the reaction with papain-GNP conjugate prepared from 1 mg mL^{-1} the acutally papain concentration in the digestion is only 21.3 µg mL^{-1} (2.9 µg mL^{-1} in the digestion with bioconjugate prepared from 0.2 mg mL^{-1}) Thus, the savings of enzyme are even more pronounced (about factor 100), making this approach with nanoparticulate heterogeneous biocatalysts most attractive for precious enzymes.

A better figure to define and compare the reaction rate of a series of biocatalysts is the turnover number k_{cat}. It is the number of substrate molecules converted to product per enzyme molecule per second. By using the known concentrations of free papain and immobilized papain calculated from RMM, the k_{cat} values were finally calculated to be $4.75 \pm 1.33 \times 10^{-3}$ s^{-1} (free), 0.20 ± 0.02 s^{-1} (conjugated from 1 mg mL^{-1}) and 0.65 ± 0.03 s^{-1} (conjugated from 0.2 mg mL^{-1}), respectively. It becomes striking that the reaction is accelerated by a factor of 137 when free solution enzyme reaction and heterogeneous nanobiocatalysis with papain-GNP conjugate prepared from 1 mg mL^{-1} are compared. Local accumulation of substrate on the surface of the nanobiocatalyst or close to it, thus forming a concentration gradient to the adjacent solution (like in a double layer model) might be invoked as an explanation for this increased reaction rates. Furthermore, the ratio k_{cat}/K_m, a characteristic parameter, was calculated to describe the catalytic efficiency of the immobilized papain in comparison to free papain. It was found that immobilized papain had a much higher ratio k_{cat}/K_m compared to the free papain, which means that the immobilized papain exhibited significantly higher catalytic efficiency. Therefore, from above results it can be concluded that the immobilized enzyme with many additional

advantages provides the higher catalytic efficiency compared to the free papain. Besides acceleration of reaction rates, immobilization on nanoparticulate carriers might be a viable strategy to safe precious enzymes in industrial applications.

SDS-PAGE for monitoring antibody digestion

The primarily intended application of the papain-modified nanoparticles is fragmentation of IgG into smaller fragments which facilitate their MS analysis (middle-down and middle-up) [41]. In the present case, a therapeutic protein, human IgG, was utilized to verify the bioactivity and digestion performance of papain-functionalized GNPs (prepared from 0.2 mg mL^{-1} papain in the reaction mixture) in comparison to in-solution digestion (1 mg mL^{-1} papain). By taking advantage of the heterogeneous biocatalyst, the papain-GNPs can be readily removed after digestion, avoiding the contamination of enzyme into the fragment products. IgG digests obtained from GNP-conjugated and free papain were characterized by SDS-PAGE under non-reducing conditions using silver staining for detection (providing detection limits around 0.25 - 0.5 ng of protein). The resultant gel is shown in Figure 6. It is evident that new bands (at around 50 kDa) appeared in the samples (lanes B,C,D and F,G,H) after digestion. The molecular weight of these protein bands corresponds to the expected IgG fragments. Papain cleaves the intact IgG above the Hinge region to yield three fragments of similar size, two Fab fragments (around 50 kDa each) and one Fc fragment (around 50 kDa as well). In addition, bands around 100 kDa and 25 kDa were also found in the digested samples. It seems that the employed papain does not have enough specificity for the cleavage of IgG just above the Hinge region, but also the $F(ab')_2$ and Fc/2 fragments are obtained. In sharp contrast, in the non-digested IgG solution (lane A), only intact IgG (around 150 kDa) and aggregated forms (ca. 300 kDa) rather than the fragments were found (the large quantities of aggregates can be explained by the fact that the h-IgG used in this study was already expired for a long time). These results clearly indicate that IgG was efficiently digested with papain-functionalized GNPs.

To test for possible bleeding of papain from the nanoparticulate carrier, a suspension of papain-functionalized GNPs was allowed to stand in 10 mM phosphate buffer pH 6.8 overnight. Afterwards the suspension was spinned down and the supernatant was also applied as sample to the gel (lane E). It can be clearly seen that there is no band (E) at the position where papain is expected (ca. 23 kDa region). This implies that, after their removal by centrifugation, papain-GNP conjugates do not cause any background interferences in the gel and that papain is not bleeding from the nanoparticulate carrier due to covalent attachment. From these results it can be derived that the new nanobioreactor is suitable for practical applications.

HPLC-μESI-QTOF-MS method for characterization of IgG fragments after digestion

The generated fragments of human IgG were finally analyzed by HPLC-μESI-QTOF-MS to document the practical applicability of the nanoparticulate enzyme reactor. High resolution-MS using a QTOF equipped with a μESI sprayer and a ProSwift column for separation of proteins were used for the characterization of intact IgG and the fragments digested with papain-GNPs. Detection limits for smaller proteins like IgG fragments are around 500 fg on-column with this μESI setup. Figure 7a shows the total ion chromatogram of the intact IgG before digestion, and Figure 7b shows the deconvoluted mass spectrum of the peak with t_R 14.66 min corresponding to IgG with a mass of around 150 kDa (note, this is not a monoclonal antibody but human IgG isolated from plasma). After digestion, the deconvoluted mass of IgG (150 kDa) disappeared, and meanwhile the fragments (Fab and Fc), eluting at ca. 9.6 min could be detected (Figure 7c). The deconvoluted TOF-MS spectrum in Figure 7d for the peak at 9.6 min shows several peak groups in the range of 50 kDa to 55 kDa corresponding to Fab and Fc, respectively. It can be explained by the fact that human IgG is a collection of immunoglobulin molecules, and therefore a mixture of similar fragments with slightly different masses can be expected for the digested IgG as well.

The TIC chromatogram in Fig. 7c, like the gel, shows some additional peaks. The first two peaks (between t_R 7.7 and 8.5 min) could not be assigned to a reasonable mass. However, the deconvoluted peak (t_R between 8.8 to 9.5 min) showed fragment masses of around 25 kDa, which correspond to the Fc/2 fragments (Fig. 7e). In addition, a peak at t_R of 14.63 min was detected in the digest and it was initially assumed that this peak corresponds to intact human IgG due to incomplete digestion. However, the deconvoluted TOF-MS spectrum of the peak at 14.63 min actually corresponds to a 100 kDa $F(ab')_2$ fragment of human IgG (Fig. 7f) while the intact IgG (150 kDa) was not detected at all. This finding clearly confirms the successful and complete digestion. It seems that the employed papain does not have enough specificity for cleaving the IgG just above the Hinge region, but produces also a $F(ab')_2$ fragment in significant amounts besides Fab. Overall, the LC-MS results clearly document that the new nanoparticulate enzyme reactor has adequate bioactivity and catalytic efficiency for enzymatic IgG fragmentation. The limited specificity of papain both in free and immobilized forms, however, explains why nowadays IdeS (immunoglobulin G-degrading enzyme of Streptococcus pyogenes, a bacterial cysteine protease which specifically cleaves IgGs under their hinge region [41]) is mainly used for middle-down characterization of IgGs by LC-MS. It is obvious that this highly specific enzyme should be immobilized in the same way to afford a highly specific, highly efficient immobilized enzyme reactor which can be easily removed and reused for IgG fragmentation.

Conclusion

In the present study, GNPs were functionalized with papain by a layer-by-layer strategy producing an efficient heterogeneous biocatalyst. Characterization with SPR, DLS and ζ-potential measurements revealed the successful immobilization of papain. The higher amount of papain used in the reaction mixture for immobilization has led to bigger particle sizes than expected. With the RMM technology, the concentration and average buoyant

mass of the GNP biocatalyst was obtained, and the number of papain molecules immobilized on one GNP was calculated. The results implied that GNPs activated with polyelectrolyte layers provided a high loading capacity for papain due to its large surface to volume ratio and the specific surface modification with polyelectrolyte chains. In comparison with free papain, the immobilized papain provides the higher catalytic efficiency with the advantages of easy removal and flexible control of reaction. SDS-PAGE and HPLC-μESI-QTOF-MS characterization proved the successful digestion of IgG with papain-modified GNPs as heterogeneous biocatalyst which indeed shows great potential in bioanalysis. The limited specificity of papain could be overcome by use of IdeS as an enzyme for immobilization.

Acknowledgements

We acknowledge the financial support by the “Struktur- und Innovationsfonds Baden-Württemberg (SI-BW)” and the German Science Funds (DFG no. INST 37/821-1 FUGG). We thank Prof. Rolf Daniels for providing access to the Zetasizer Nano instrument for DLS and ζ-potential measurements. Furthermore, we are grateful to Dr. Markus Epe (Malvern Instruments, Herrenberg, Germany) for resonant mass measurements.

References

[1] P.K. Robinson, Enzymes: principles and biotechnological applications, Essays Biochem., 59 (2015) 1-41.

[2] D. Meridor, A. Gedanken, Enhanced activity of immobilized pepsin nanoparticles coated on solid substrates compared to free pepsin, Enzyme Microb. Technol., 67 (2014) 67-76.

[3] K. Meller, P. Pomastowski, D. Grzywiński, M. Szumski, B. Buszewski, Preparation and evaluation of dual-enzyme microreactor with co-immobilized trypsin and chymotrypsin, J. Chromatogr. A, 1440 (2016) 45-54.

[4] S.A. Ansari, Q. Husain, Potential applications of enzymes immobilized on/in nano materials: A review, Biotechnol. Adv., 30 (2012) 512-523.

[5] Y. Lv, Z. Lin, T. Tan, F. Svec, Preparation of reusable bioreactors using reversible immobilization of enzyme on monolithic porous polymer support with attached gold nanoparticles, Biotechnol. Bioeng., 111 (2014) 50-58.

[6] Y. Liang, C. Wu, Q. Zhao, Q. Wu, B. Jiang, Y. Weng, Z. Liang, L. Zhang, Y. Zhang, Gold nanoparticles immobilized hydrophilic monoliths with variable functional modification for highly selective enrichment and on-line deglycosylation of glycopeptides, Anal. Chim. Acta, 900 (2015) 83-89.

[7] J.R. Freije, P.P.M.F.A. Mulder, W. Werkman, L. Rieux, H.A.G. Niederlander, E. Verpoorte, R. Bischoff, Chemically Modified, Immobilized Trypsin Reactor with Improved Digestion Efficiency, J. Proteome Res., 4 (2005) 1805-1813.

[8] Y. Cao, L. Wen, F. Svec, T. Tan, Y. Lv, Magnetic AuNP@Fe3O4 nanoparticles as reusable carriers for reversible enzyme immobilization, Chem. Eng. J., 286 (2016) 272-281.

[9] E. Calleri, S. Ambrosini, C. Temporini, G. Massolini, New monolithic chromatographic supports for macromolecules immobilization: Challenges and opportunities, J. Pharm. Biomed. Anal., 69 (2012) 64-76.

[10] M. Bonichon, A. Combès, C. Desoubries, A. Bossée, V. Pichon, Development of immobilized-pepsin microreactors coupled to nano liquid chromatography and tandem mass spectrometry for the quantitative analysis of human butyrylcholinesterase, J. Chromatogr. A, 1461 (2016) 84-91.

[11] N. Miletić, A. Nastasović, K. Loos, Immobilization of biocatalysts for enzymatic polymerizations: Possibilities, advantages, applications, Bioresour. Technol., 115 (2012) 126-135.

[12] B.J. Johnson, W. Russ Algar, A.P. Malanoski, M.G. Ancona, I.L. Medintz, Understanding enzymatic acceleration at nanoparticle interfaces: Approaches and challenges, Nano Today, 9 (2014) 102-131.

[13] C. Garcia-Galan, Á. Berenguer-Murcia, R. Fernandez-Lafuente, R.C. Rodrigues, Potential of Different Enzyme Immobilization Strategies to Improve Enzyme Performance, Adv. Synth. Catal., 353 (2011) 2885-2904.

[14] R. DiCosimo, J. McAuliffe, A.J. Poulose, G. Bohlmann, Industrial use of immobilized enzymes, Chem. Soc. Rev., 42 (2013) 6437-6474.

[15] Y. Yu, Z. Chen, S. He, B. Zhang, X. Li, M. Yao, Direct electron transfer of glucose oxidase and biosensing for glucose based on PDDA-capped gold nanoparticle modified graphene/multi-walled carbon nanotubes electrode, Biosens. Bioelectron., 52 (2014) 147-152.

[16] K. Saha, S.S. Agasti, C. Kim, X. Li, V.M. Rotello, Gold nanoparticles in chemical and biological sensing, Chem. Rev., 112 (2012) 2739-2779.

[17] M. Höldrich, A. Sievers-Engler, M. Lämmerhofer, Gold nanoparticle-conjugated pepsin for efficient solution-like heterogeneous biocatalysis in analytical sample preparation protocols, Anal. Bioanal. Chem., 408 (2016) 5415-5427.

[18] W. She, N. Li, K. Luo, C. Guo, G. Wang, Y. Geng, Z. Gu, Dendronized heparin−doxorubicin conjugate based nanoparticle as pH-responsive drug delivery system for cancer therapy, Biomaterials, 34 (2013) 2252-2264.

[19] E. Blanco, H. Shen, M. Ferrari, Principles of nanoparticle design for overcoming biological barriers to drug delivery, Nat. Biotechnol., 33 (2015) 941-951.

[20] L. Sun, H. Liang, Q. Yuan, T. Wang, H. Zhang, Study on a carboxyl-activated carrier and its properties for papain immobilization, J. Chem. Technol. Biotechnol., 87 (2012) 1083-1088.

[21] G.K. Kouassi, J. Irudayaraj, G. McCarty, Activity of glucose oxidase functionalized onto magnetic nanoparticles, Biomagn. Res. Technol., 3 (2005) 1-10.

[22] L.S. Wong, J. Thirlway, J. Micklefield, Direct Site-Selective Covalent Protein Immobilization Catalyzed by a Phosphopantetheinyl Transferase, J. Am. Chem. Soc., 130 (2008) 12456-12464.

[23] T. Tan, J. Lu, K. Nie, L. Deng, F. Wang, Biodiesel production with immobilized lipase: A review, Biotechnol. Adv., 28 (2010) 628-634.

[24] Y. Yücel, Biodiesel production from pomace oil by using lipase immobilized onto olive pomace, Bioresour. Technol., 102 (2011) 3977-3980.

[25] G.A. Petkova, K. Záruba, P. Žvátora, V. Král, Gold and silver nanoparticles for biomolecule immobilization and enzymatic catalysis, Nanoscale Res. Lett., 7 (2012) 287.

[26] S.F. Oliveira, G. Bisker, N.A. Bakh, S.L. Gibbs, M.P. Landry, M.S. Strano, Protein functionalized carbon nanomaterials for biomedical applications, Carbon, 95 (2015) 767-779.

[27] N.R. Mohamad, N.H.C. Marzuki, N.A. Buang, F. Huyop, R.A. Wahab, An overview of technologies for immobilization of enzymes and surface analysis techniques for immobilized enzymes, Biotechnol. Biotec. Eq., 29 (2015) 205-220.

[28] A. Homaei, R. Etemadipour, Improving the activity and stability of actinidin by immobilization on gold nanorods, Int. J. Biol. Macromol., 72 (2015) 1176-1181.

[29] L. Dykman, N. Khlebtsov, Gold nanoparticles in biomedical applications: recent advances and perspectives, Chem. Soc. Rev., 41 (2012) 2256-2282.

[30] N.G. Khlebtsov, Optics and biophotonics of nanoparticles with a plasmon resonance, Quantum Electron+, 38 (2008) 504.

[31] K. Saha, S.S. Agasti, C. Kim, X. Li, V.M. Rotello, Gold Nanoparticles in Chemical and Biological Sensing, Chem. Rev., 112 (2012) 2739-2779.

[32] M.A. Martins, S. Fateixa, A.V. Girão, S.S. Pereira, T. Trindade, Shaping Gold Nanocomposites with Tunable Optical Properties, Langmuir, 26 (2010) 11407-11412.

[33] M.-C. Daniel, D. Astruc, Gold Nanoparticles: Assembly, Supramolecular Chemistry, Quantum-Size-Related Properties, and Applications toward Biology, Catalysis, and Nanotechnology, Chem. Rev., 104 (2004) 293-346.

[34] K.E. Sapsford, W.R. Algar, L. Berti, K.B. Gemmill, B.J. Casey, E. Oh, M.H. Stewart, I.L. Medintz, Functionalizing Nanoparticles with Biological Molecules: Developing Chemistries that Facilitate Nanotechnology, Chem. Rev., 113 (2013) 1904-2074.

[35] B. Sahoo, S.K. Sahu, D. Bhattacharya, D. Dhara, P. Pramanik, A novel approach for efficient immobilization and stabilization of papain on magnetic gold nanocomposites, Colloid. Surface. B, 101 (2013) 280-289.

[36] K. Kinoshita, K. Sato, M. Hori, H. Ozaki, H. Karaki, Decrease in activity of smooth muscle L-type Ca2+ channels and its reversal by NF-κB inhibitors in Crohn's colitis model, Am. J. Physiol., 285 (2003) G483-G493.

[37] K. Shiozaki, M. Yanagida, A functional 125-kDa core polypeptide of fission yeast DNA topoisomerase II, Mol. Cell. Biol., 11 (1991) 6093-6102.

[38] H. Xiang, Y.G. Xiang, M.Z. Lu, L. Guo, H. Eckstein, Total enzymatic synthesis of cholecystokinin CCK-5, Amino Acids, 27 (2004) 101-105.

[39] T.A. Seldon, K.E. Hughes, D.J. Munster, D.Y. Chin, M.L. Jones, Improved Protein-A separation of V(H)3 Fab from Fc after Papain Digestion of Antibodies, J. Biomol. Tech., 22 (2011) 50-52.

[40] Y. Zhao, L. Gutshall, H. Jiang, A. Baker, E. Beil, G. Obmolova, J. Carton, S. Taudte, B. Amegadzie, Two routes for production and purification of Fab fragments in biopharmaceutical discovery research: Papain digestion of mAb and transient expression in mammalian cells, Protein Expr. Purif., 67 (2009) 182-189.

[41] A. Beck, E. Wagner-Rousset, D. Ayoub, A. Van Dorsselaer, S. Sanglier-Cianférani, Characterization of Therapeutic Antibodies and Related Products, Anal. Chem., 85 (2013) 715-736.

[42] S. Mandal, A. Bonifacio, F. Zanuttin, V. Sergo, S. Krol, Synthesis and multidisciplinary characterization of polyelectrolyte multilayer-coated nanogold with improved stability toward aggregation, Colloid Polym. Sci., 289 (2011) 269-280.

[43] C. Boyer, A. Bousquet, J. Rondolo, M.R. Whittaker, M.H. Stenzel, T.P. Davis, Glycopolymer Decoration of Gold Nanoparticles Using a LbL Approach, Macromolecules, 43 (2010) 3775-3784.

[44] S. Pereira, A. Barros-Timmons, T. Trindade, Biofunctionalisation of colloidal gold nanoparticles via polyelectrolytes assemblies, Colloid Polym. Sci., 292 (2014) 33-50.

[45] J. Kim, J.W. Grate, P. Wang, Nanostructures for enzyme stabilization, Chem. Eng. Sci., 61 (2006) 1017-1026.

[46] M.R. Nejadnik, W. Jiskoot, Measurement of the Average Mass of Proteins Adsorbed to a Nanoparticle by Using a Suspended Microchannel Resonator, J. Pharm. Sci., 104 (2015) 698-704.

[47] J. Sproß, A. Sinz, Immobilized monolithic enzyme reactors for application in proteomics and pharmaceutics, Anal. Bioanal. Chem., 395 (2009) 1583-1588.

[48] H. Hinterwirth, W. Lindner, M. Lämmerhofer, Bioconjugation of trypsin onto gold nanoparticles: Effect of surface chemistry on bioactivity, Anal. Chim. Acta, 733 (2012) 90-97.

[49] G. Schneider, G. Decher, From Functional Core/Shell Nanoparticles Prepared via Layer-by-Layer Deposition to Empty Nanospheres, Nano Lett., 4 (2004) 1833-1839.

[50] Y.-C. Yeh, B. Creran, V.M. Rotello, Gold nanoparticles: preparation, properties, and applications in bionanotechnology, Nanoscale, 4 (2012) 1871-1880.

[51] A. Elbakry, A. Zaky, R. Liebl, R. Rachel, A. Goepferich, M. Breunig, Layer-by-Layer Assembled Gold Nanoparticles for siRNA Delivery, Nano Lett., 9 (2009) 2059-2064.

[52] E. Haller, W. Lindner, M. Lämmerhofer, Gold nanoparticle–antibody conjugates for specific extraction and subsequent analysis by liquid chromatography–tandem mass spectrometry of malondialdehyde-modified low density lipoprotein as biomarker for cardiovascular risk, Anal. Chim. Acta, 857 (2015) 53-63.

[53] A.R. Patel, D. Lau, J. Liu, Quantification and Characterization of Micrometer and Submicrometer Subvisible Particles in Protein Therapeutics by Use of a Suspended Microchannel Resonator, Anal. Chem., 84 (2012) 6833-6840.

[54] T.P. Burg, M. Godin, S.M. Knudsen, W. Shen, G. Carlson, J.S. Foster, K. Babcock, S.R. Manalis, Weighing of biomolecules, single cells and single nanoparticles in fluid, Nature, 446 (2007) 1066-1069.

[55] D. Weinbuch, S. Zölls, M. Wiggenhorn, W. Friess, G. Winter, W. Jiskoot, A. Hawe, Micro–flow imaging and resonant mass measurement (archimedes) – complementary methods to quantitatively differentiate protein particles and silicone oil droplets, J. Pharm. Sci., 102 (2013) 2152-2165.

[56] M.G. von Muhlen, N.D. Brault, S.M. Knudsen, S. Jiang, S.R. Manalis, Label-Free Biomarker Sensing in Undiluted Serum with Suspended Microchannel Resonators, Anal. Chem., 82 (2010) 1905-1910.

[57] H. Fischer, I. Polikarpov, A.F. Craievich, Average protein density is a molecular-weight-dependent function, Protein Sci., 13 (2004) 2825-2828.

[58] Y.-Y. Liang, L.-M. Zhang, Bioconjugation of Papain on Superparamagnetic Nanoparticles Decorated with Carboxymethylated Chitosan, Biomacromolecules, 8 (2007) 1480-1486.

Figures and Figure captions:

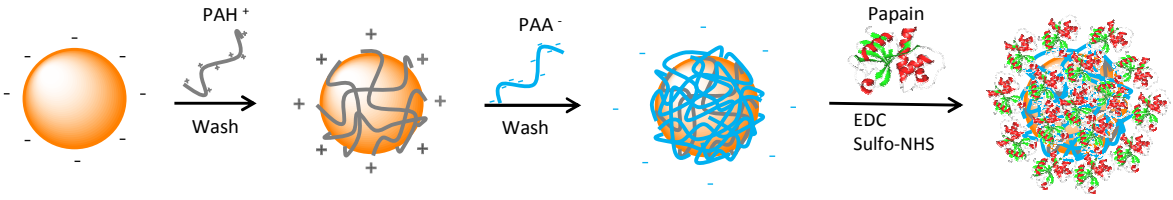

Fig. 1. Schematic presentation of the GNP functionalization process with papain. The surface modification of the GNPs was performed by a layer-by-layer (LBL) polyelectrolyte deposition strategy, and finally carboxylic acid moieties stemming from PAA were functionalized with papain by activation of carboxylic acid groups of the LBL-modified GNPs with EDC and sulfo-NHS as coupling agents and subsequent amide coupling with amino groups of papain. (PAH+, polyallylamine hydrochloride; PAA-, polyacrylic acid sodium)

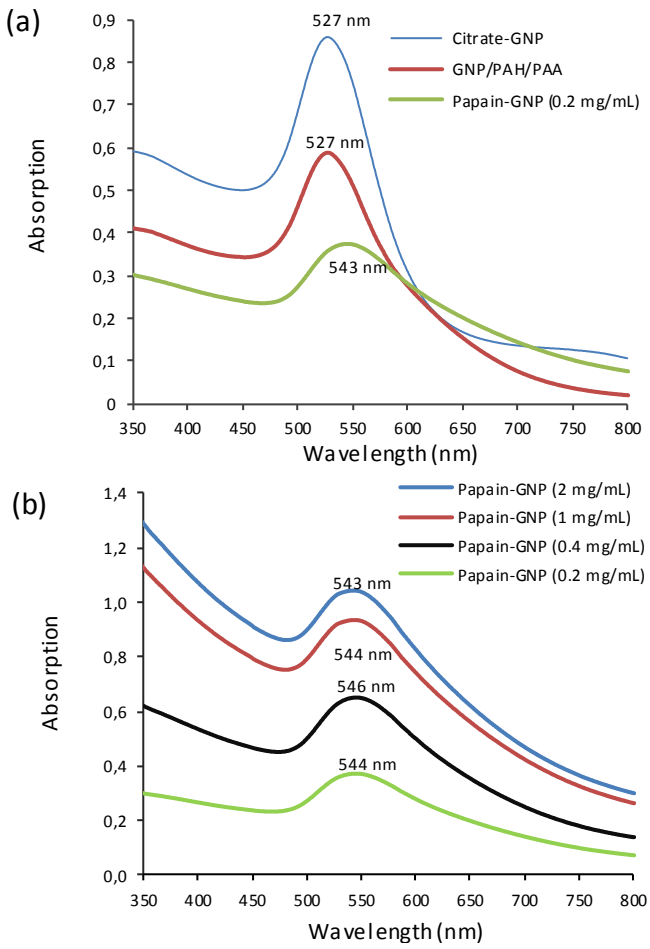

Fig. 2. Characterization of nanoparticles via surface plasmon resonance band. (a) Vis spectra of GNPs after each step of synthesis and surface functionalization. (b) Vis spectra of GNPs after functionalization with four different concentrations of papain in the reaction mixture (0.2, 0.4, 1 and 2 mg mL^{-1}, respectively)

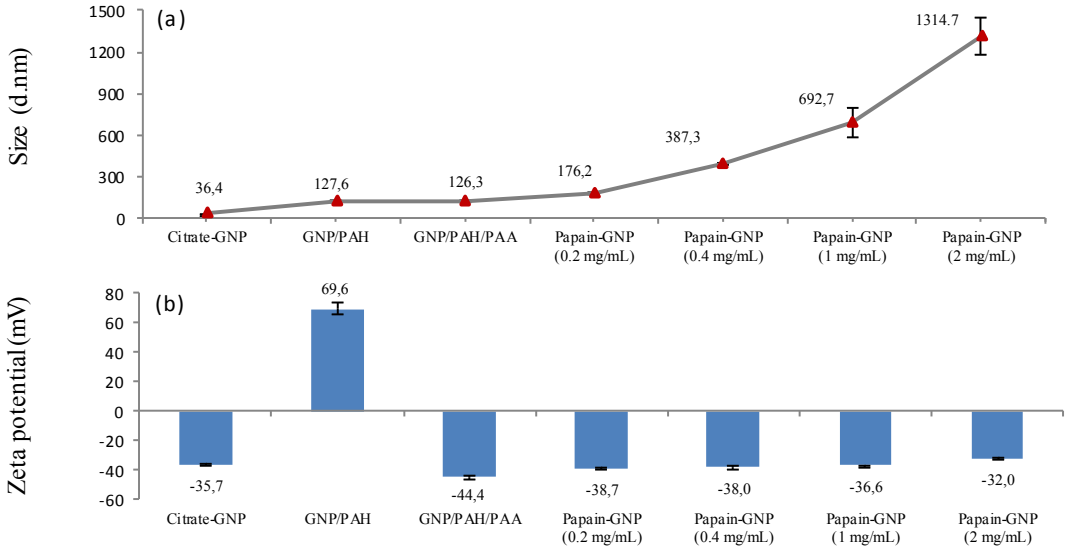

Fig. 3. Characterization of nanoparticles after each step of modification by (a) DLS and (b) ζ-potential measurement (n=3) (note, the indicated concentrations refer to the final papain concentrations in the reaction mixture).

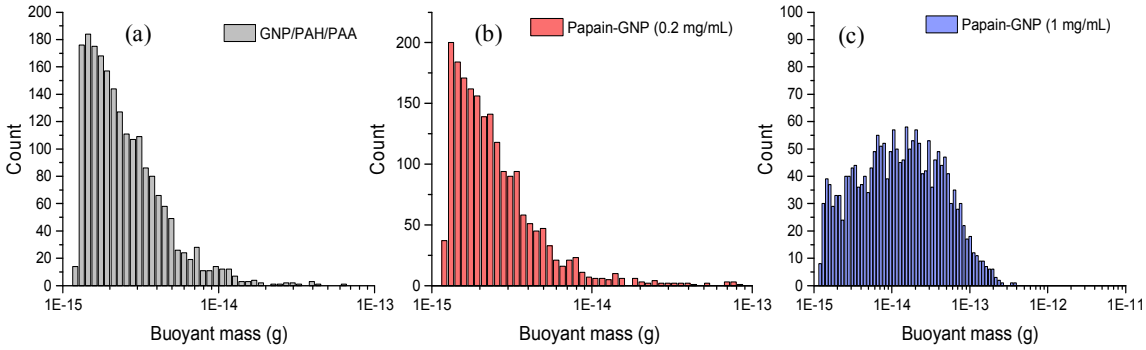

Fig. 4. Distribution of the buoyant mass of particles in 20 mM phosphate buffer (pH 6.8) of LBL-modified GNPs (GNP/PAH/PAA) (a), GNPs functionalized with papain (0.2 mg mL^{-1}) (b) and (1 mg mL^{-1}) (c) (note, the indicated concentrations refer to the final papain concentrations in the reaction mixture).

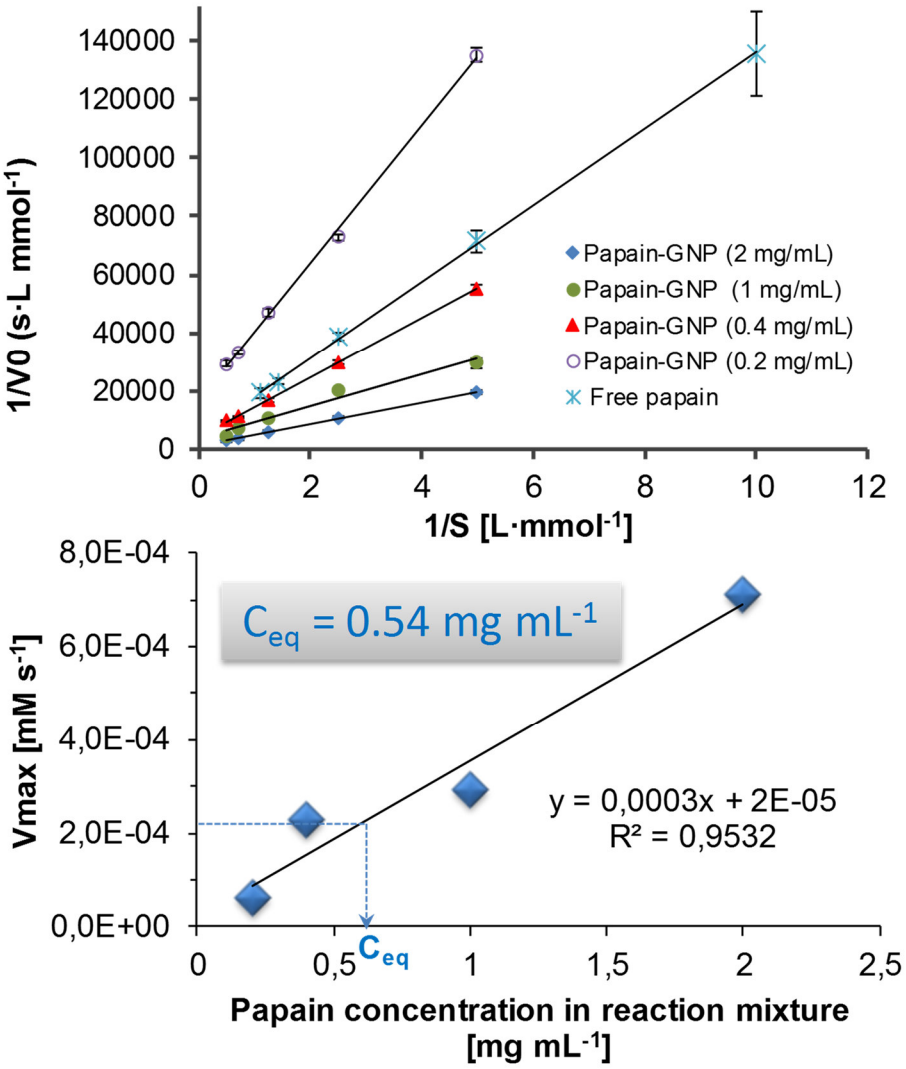

Fig. 5. a) Lineweaver-Burk diagrams for BApNA hydrolysis at pH 6.8 catalyzed by papain-GNP bioconjugates obtained from reaction mixtures with different papain concentrations, and for comparison by free (1 mg mL^{-1}) papain, and (b) effect of different surface coverages (as obtained from different papain concentrations in the reaction buffer) on maximal reaction rates V_{max} (indicated values are mean values of three experiments, n=3, and error bars represent the standard deviations; note, the indicated concentrations refer to the final papain concentrations in the reaction mixture; Ceq represents the equivalent papain concentration needed in the reaction buffer for immobilization to obtain GNP-conjugated papain with the same V_{max} as a 1 mg mL^{-1} free papain solution).

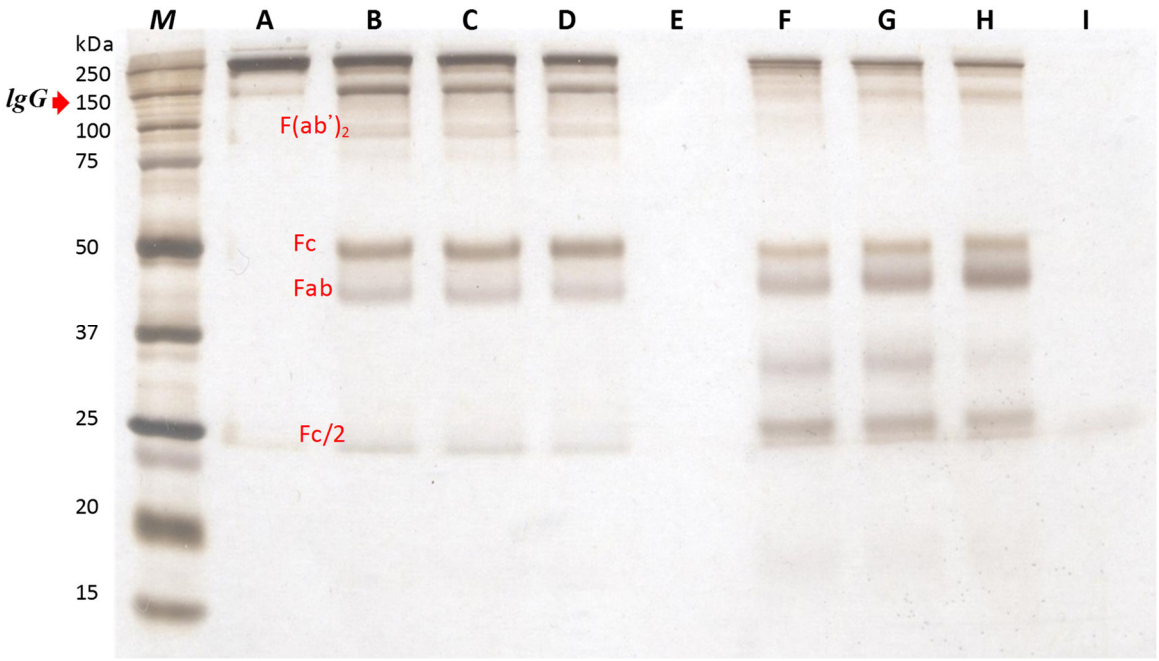

Fig. 6. SDS-PAGE (gel: 10%-Tris-HCl) for non-reduced human IgG digestion samples with silver staining for protein visualization. (M) protein marker; (A) IgG in PB (10 mM, pH 6.8); (B-D) IgG digested with papain-GNPs for 4h (B); for 8h (C); for 24h (D); (E) suspension of papain-GNPs after centrifugation; (F-H) IgG digested with free papain for 4h (F); for 8h (G); for 24h (H); (I) free papain in PB (10 mM, pH 6.8) (note, usually 0.25 - 0.5 ng of protein are considered as limit of detection for silver staining).

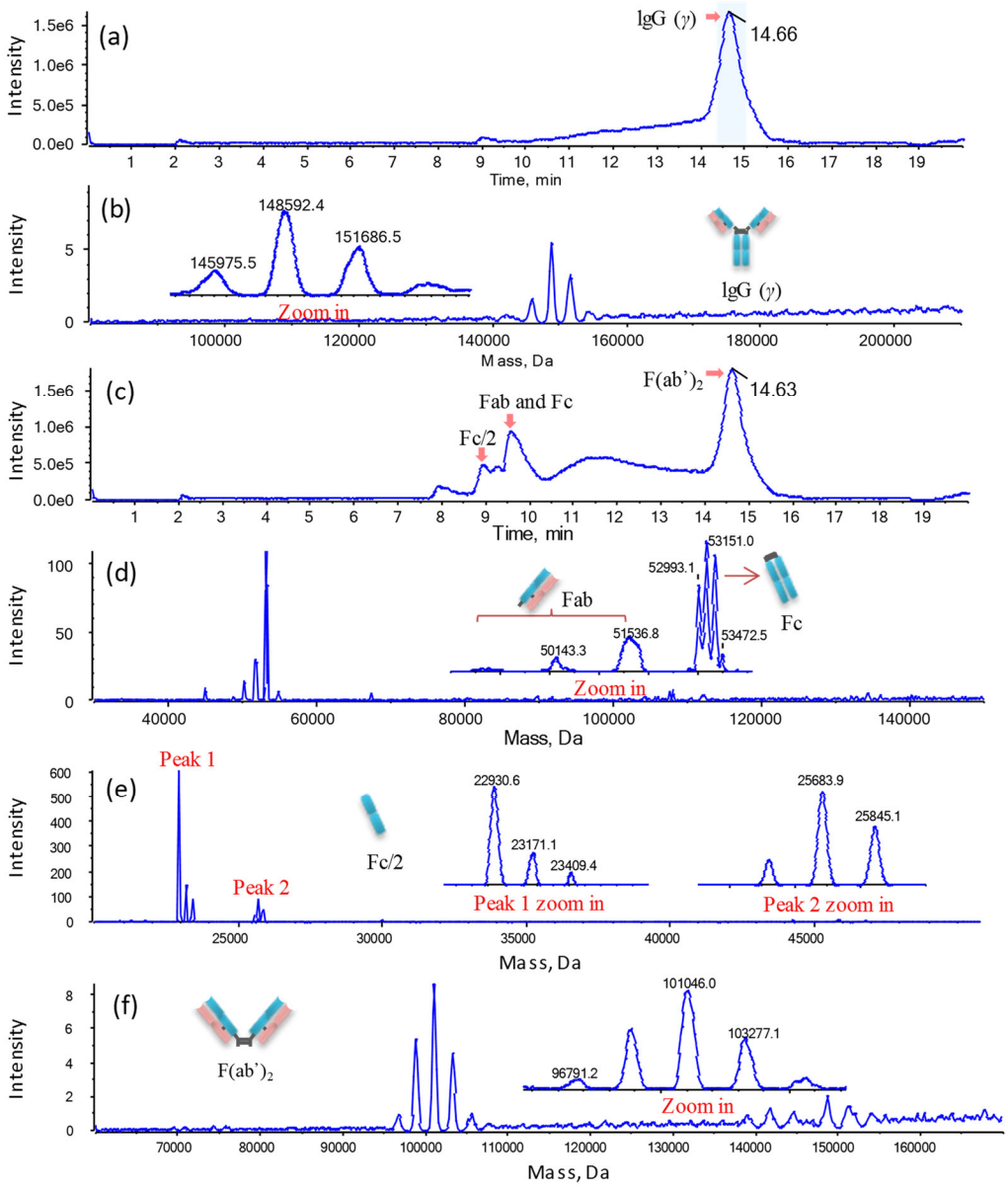

Fig. 7. HPLC-μESI-TOF-MS analysis of human IgG digested with papain-GNP bioconjugate. (a) TIC chromatogram of the IgG before digestion; (b) the deconvoluted TOF-MS spectrum of the peak with t_R 14.66 showing the intact IgG (ca. 150 kDa); (c) TIC chromatogram of human IgG after digestion with papain-GNPs; (d) the deconvoluted TOF-MS spectrum of the peak with t_R 9.62 showing the IgG fragments (Fab and Fc, ca. 50 kDa); (e) the deconvoluted TOF-MS spectrum of Fc/2 fragments (ca. 25 kDa) of the peak at t_R between 8.8 to 9.5 min; (f) the deconvoluted TOF-MS spectrum of the 100 kDa $F(ab')_2$ IgG fragment of the peak at t_R 14.63 min.

Tables:

Step	Total Time (min)	Flow Rate (µL/min)	%A	%B
0	0.0	50	80.0	20.0
1	2.0	50	80.0	20.0
2	12.0	50	65.0	35.0
3	13.0	50	5.0	95.0
4	17.0	50	5.0	95.0
5	17.5	50	80.0	20.0
6	20.0	50	80.0	20.0

Table 1. The LC gradient profile for HPLC-µESI-TOF-MS. Solvent A consisted of ddwater with 0.1 % (v/v) formic acid, and solvent B consisted of acetonitrile with 0.1 % (v/v) formic acid.

Nanobeads	Mean buoyant mass [fg]	Concentration of nanobeads [mol L^{-1}]	Mean mass of papain per GNP [fg]	Concentration of immobilized papain [mol L^{-1}]	Mean number of papain per GNP
GNP/PAH/PAA	3.14±0.06	1.06×10^{-11}	-	-	-
Papain-GNPs [0.2 mg mL^{-1}]	3.42±0.31	7.74×10^{-12}	0.93±0.83	$1.85\pm1.65\times10^{-7}$	$2.39\pm2.14\times10^{4}$
Papain-GNPs [1 mg mL^{-1}]	27.30±2.25	1.43×10^{-12}	80.2±7.3	$2.95\pm0.27\times10^{-6}$	$2.06\pm0.19\times10^{6}$

Table 2. Summary of the experimental results from RMM measurements comprising mean buoyant mass, concentration of nanobeads, mean mass of papain per GNP, concentration of immobilized papain and mean number of papain molecules per GNP (n=3).

Parameter	Papain-GNP (0.2 mg mL^{-1})[a]	Papain-GNP (0.4 mg mL^{-1})[a]	Papain-GNP (1mg mL^{-1})[a]	Papain-GNP (2 mg mL^{-1})[a]	Free papain (1 mg mL^{-1})[b]
K_m [mM]	1.41±0.05	2.32±0.04	1.61±0.03	2.62±0.15	2.71±0.98
V_{max} [mM s^{-1}]	$6.00±0.27\times10^{-5}$	$2.28±0.06\times10^{-4}$	$2.91±0.03\times10^{-4}$	$7.12±0.17\times10^{-4}$	$2.03±0.57\times10^{-4}$
k_{cat} [s^{-1}]	0.65±0.03	n.d.	0.20±0.02	n.d.	$4.75±1.33\times10^{-3}$
k_{cat}/K_m [mM^{-1} s^{-1}]	0.46±0.01	n.d.	0.12±0.03	n.d.	$1.8±0.2\times10^{-3}$
Regression equation	Y=23499X + 16693	Y=10155X + 4382.1	Y=5530.9X + 3432.9	Y=3671.5X + 1404.7	Y=13096X + 5248.1
R^2	0.9988	0.9997	0.9667	0.9980	0.9998

[a] The concentrations refer to the papain concentration used for the immobilization, the final concentration in the digestion solution are 9.25×10^{-8} mol L^{-1} and 1.48×10^{-6} mol L^{-1} for papain-GNP (0.2 mg mL^{-1} and 1 mg mL^{-1}), respectively (see Table 2).

[b] The concentration refers to the final papain concentration in the digestion solution.

Table 3. Summary of the kinetic parameters (K_m, V_{max}, k_{cat}) calculated by Lineweaver-Burk plots for both free papain and immobilized papain (0.2 mg mL^{-1} and 1 mg mL^{-1}, respectively) (Values represent mean ± standard deviation of 3 replicate experiments; n.d., not determined).

Supplementary Material

Determination of kinetic parameters of immobilized and free papain

The enzyme activity of free and immobilized papain was evaluated at 37 ˚C at pH 6.8 by investigating the hydrolysis of BApNA as the substrate (Figure S1). To determine the kinetic parameters (K_m, V_{max}, k_{cat}) the reaction was carried out at variable substrate concentrations with free papain and immobilized papain-GNP conjugates obtained from different concentrations of papain in the reaction mixture. The kinetic parameters were derived from the Lineweaver Burk plots and the results are given in Figure 5 and Table 3 of the main document along with corresponding data of a reaction with 1 mg mL^{-1} free papain.

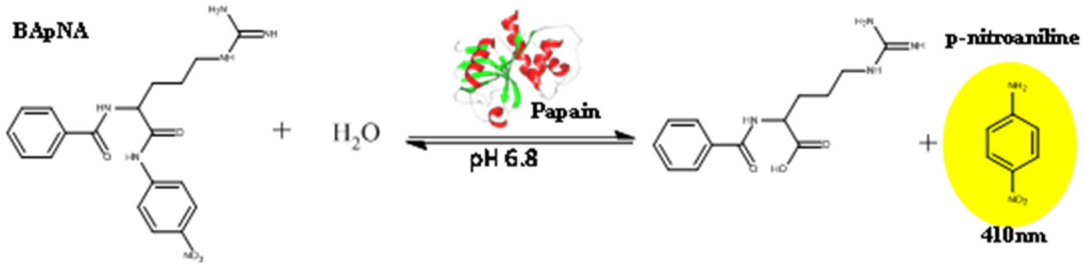

Figure S1: Reaction scheme for the hydrolysis of the substrate BApNA by papain. The activity of papain can be measured by the released p-nitroaniline (pNA) at an absorbance wavelength of 410 nm.

This single-substrate enzyme reaction can be described by the following equation (eq. S1

$$E + S \underset{k_{-1}}{\overset{k_1}{\rightleftharpoons}} ES \xrightarrow{k_{cat}} EP \longrightarrow E + P \qquad \text{(S1)}$$

Wherein E, S, ES, P and EP represent the enzyme, substrate, enzyme-substrate complex, product and enzyme-product complex concentrations, k_1 and k_{-1} are the rate constants for enzyme-substrate association and dissociation, respectively, and k_{cat} is the

rate constant for product formation (also termed turnover number). The kinetics of this reaction is usually investigated by measuring the initial velocities v_0 in dependence of the substrate concentration. The results are then evaluated in terms of the Michaelis-Menten equation (eq. S2)

$$K_m = \frac{k_{-1} + k_{cat}}{k_1} \qquad \text{(S3)}$$

wherein V_{max} is the maximal reaction rate achieved when all enzyme is saturated with substrate ([ES] = [E]t; with [E]t being the total enzyme concentration in the reaction i.e. [E] + [ES]). K_m is the Michaelis constant which is defined by (eq. S3)

$$K_m = \frac{k_{-1} + k_{cat}}{k_1} \qquad \text{(S3)}$$

As mentioned above, the data have been evaluated in the linearized form, i.e. the Lineweaver-Burk plot (eq. S4)

$$\frac{1}{v_0} = \frac{K_m}{V_{\max} \cdot [S]} + \frac{1}{V_{\max}} \qquad \text{(S4)}$$

In a reaction with free enzyme K_m does not change with enzyme concentration in the reaction mixture. Upon immobilization of enzyme, K_m might change with enzyme concentration immobilized on the carrier because the conformation of the enzyme and steric access of the binding site might be altered in dependence of the enzyme's surface concentration. For instance, at low surface concentrations the active site might be better accessible than at high coverage for which limited access to the enzyme's catalytic site might compromise the rate constant for association.

Figure S2 shows a plot of K_m values in dependence of distinct papain concentrations in the reaction mixture during bioconjugation. It becomes evident that K_m is in the same order of magnitude for all 4 bioreactors (Figure S2). Hence, it can be concluded that access to active sites is not compromised at higher papain surface concentrations.

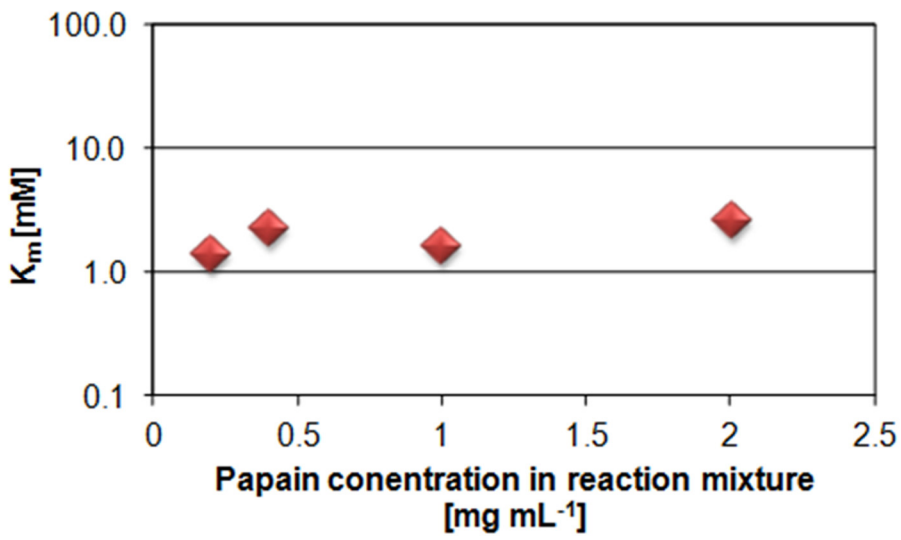

Figure S2: Michaelis-Menten constant versus papain concentration in the reaction mixture in the course of preparation of papain-GNP bioconjugate.

In sharp contrast, V_{max} changes linearly with the enzyme concentration in accordance to eq. S5

$$V_{max} = k_{cat} \cdot [E]_t \quad \text{(S5)}$$

In sharp contrast, V_{max} changes linearly with the enzyme concentration in accordance to eq. S5

$$V_{max} = k_{cat} \cdot [E]_t \quad \text{(S5)}$$

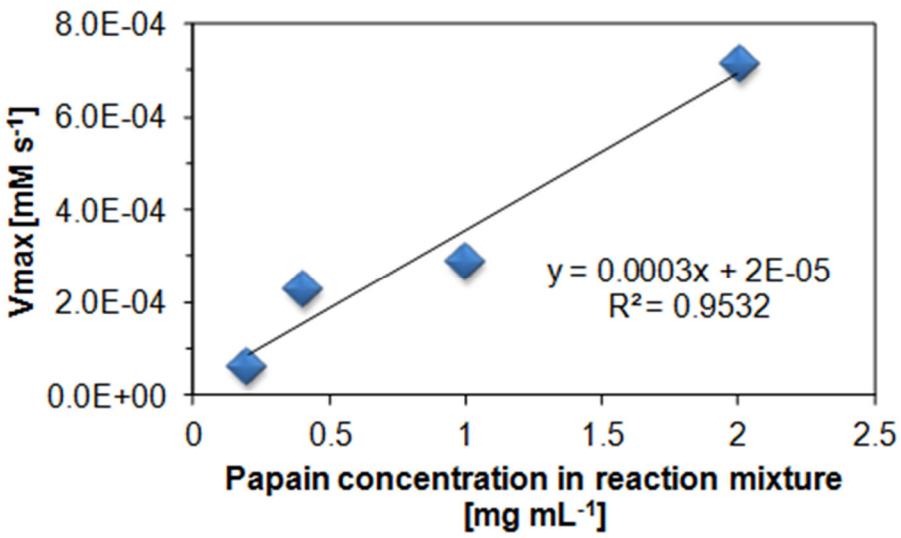

Figure S3: V_{max} in dependence of the papain concentration in the reaction mixture in the course of preparation of papain-GNP bioconjugate (Standard Error of Est. = 0.0000734; P-value intercept = 0.7548; P-value slope = 0.0237).

This is also found for a series of enzyme reactions performed with the bioreactors having distinct papain coverages (Figure S3). Higher enzyme concentrations in the incubation mixture due to use of papain-GNP conjugates with higher surface coverages (which result from higher papain concentrations in the reaction mixtures during protein coupling step) accelerate the conversion.

Eq. S5 can be used to calculate k_{cat}, the turnover number, which is a better figure to define the reaction rate. In this work k_{cat} has been calculated for free papain and two bioconjugates with distinct surface coverage of papain (see Table 3 of main document). Finally, the ratio of k_{cat}/K_m, termed specificity constant or catalytic efficiency, is a measure of how efficiently an enzyme converts substrates into products and is given in Table 3 of the main document as well.

3.4. Accurate and reliable quantification of the protein surface coverage on protein-functionalized nanoparticles

Siyao Liu, Jeannie Horak, Markus Höldrich, Michael Lämmerhofer

Institute of Pharmaceutical Science, Pharmaceutical (Bio-)Analysis, University of Tübingen, Auf der Morgenstelle 8, 72076, Tübingen, Germany

Analytica Chimica Acta 989 (2017) 29-37

Abstract

The ability to accurately quantify the protein coverage on nanoparticles is critical for assessing the quality of the surface chemistry and the success of the functionalization process of protein-nanoparticle conjugates. Surface coverage determination is therefore an integral part in the quality control of protein-modified nanoparticles in industrial nanotechnology. In this work, a novel and conventional method was established for direct quantification of the protein surface coverage on metallic nanoparticles. Different concentrations of pepsin were conjugated to gold nanoparticles (GNPs) by a straightforward adsorptive immobilization process as a model system, and a protein quantitation methodology based on the amino acid analysis of the hydrolysate of the protein-GNP conjugates was established. For this purpose, pepsin functionalized GNPs (pepsin-GNP bioconjugates) were processed via in situ hydrolysis with 6N HCl and subsequent derivatization with 6-aminoquinolyl-N-hydroxysuccinimidyl carbamate (AQC reagent). Direct quantitative amino acid analysis was performed based on measuring the intensity of AQC-glycine derivative by High-performance liquid chromatography with fluorescence detection (HPLC-FLD). The method allows for detection of surface coverages as low as 0.1 µg mL^{-1} pepsin (corresponding to 2.89×10^{-9} mol L^{-1}) in the colloidal solution. Method imprecision for replicated surface coverage determinations was < 5 % RSD and accuracies, as determined by % recoveries, were always in the 98-118 % range. This method allows precise and accurate quantification of protein coverages, even when less than 1 % of the protein in the reaction mixture is immobilized. It was found that the degree of surface coverage of adsorptively bound pepsin on GNPs correlated with the pepsin concentrations in the conjugation reaction mixtures. Washing with phosphate buffer removed weakly bound proteins, i.e. the soft protein corona. The adsorption behavior could be described by a Freundlich isotherm model. This direct and reliable method promises great potential for the accurate quantification of protein coverages of various protein-nanoparticle bioconjugates.

Keywords

gold nanoparticles, protein surface coverage, protein-nanoparticle bioconjugate, amino acid analysis, HPLC-fluorescence detection, protein corona

Introduction

Nowadays, nanoparticles are being extensively used in biomedical and biotechnological research. For instance, nanoparticle-antibody conjugates have been employed as affinity carriers to extract specific biomarkers for mass spectrometric analysis from complex biological samples [1-5]. Due to their controlled geometrical and flexible surface chemical properties, nanomaterials have also acted as excellent solid supports for enzyme immobilization [6]. For all these applications, the assay performance of protein-nanoparticle bioconjugates depends mainly on the interactions between the nanoparticle and protein, including the protein surface coverage and orientation on the nanoparticle surface [7-10]. Therefore, in order to control assay quality and optimize the surface chemistry, it is critical to develop a method for the accurate quantitation of the surface coverage on nanoparticles in order to evaluate the success and reproducibility of nanoparticle-protein conjugation reactions. In addition, accurate quantification of the protein concentration on nanoparticles is a key requirement for the valid assessment of the kinetic performance of enzyme-nanoparticle conjugates, and also for their quality control to make it possible that the enzyme-nanoparticle bioconjugate can be successfully and reproducibly applied as heterogeneous catalyst in industrial processes.

The accurate determination of the protein surface coverage on protein-nanoparticle conjugates is still challenging. To date, only a few studies directed some attention towards the determination of the protein concentration on nanomaterials [11-18]. However, compared to the vast number of scientific articles on nanoparticle synthesis, modification and enzyme immobilization methods, research on protein surface coverages and methods for this purpose are highly underrepresented in nanoscience. Typically, total

protein quantification assays (Lowry assay, Bradford assay and bicinchoninic acid BCA assay) are employed which allow detection of non-immobilized proteins in the supernatant of the binding/reaction mixture with low concentrations [12, 13, 19, 20]. The immobilized protein content can be calculated by mass balance considerations. Thus, these approaches are therefore so-called indirect assays. A validation of these assays is rarely carried out in the context of protein surface coverage determination of such bioconjugates. It is assumed that accuracies may suffer with these indirect protein quantitation assays. For example, the protein content is usually determined in the reaction mixture after removal of the nanoparticles. However, during the following washing steps protein loosely adsorbed to the surface might be desorbed and the protein coverage will hence be altered. Loss of protein, e.g., due to adsorption on other surfaces during the sample preparation might lead to erroneous results as well [7]. Furthermore, these protein quantification assays have limited precision, which may cause problems, if only a small percentage of the protein in the reaction mixture is bound to the nanoparticle surface. For instance, if the imprecision of the assay is 10 % (RSD) and only 1 % of the protein in the reaction mixture gets immobilized, it can rarely be imagined that the protein coverage can be determined with high accuracy by these indirect assays. Besides, these assays are prone to interferences from various chemicals. Therefore, the direct analysis of bound protein is considered highly advantageous in terms of assay accuracy. ELISA assays have been used for the determination of bound proteins (e.g. antibodies) on gold nanoparticles [1, 21]. If such ELISA assays are directly used to detect immobilized proteins, the effect of the matrix (nanoparticle carrier) on the determined protein concentration will remain unclear. Furthermore, ELISA kits are expensive. Fluorescence methods have also been proposed to directly analyze protein concentrations on nanoparticle surfaces [7]. This method involves fluorescence labeling of the protein in order to achieve sufficient sensitivity. Other techniques such as dynamic light scattering (DLS) and nanoparticle tracking analysis (NTA) measure the increase in hydrodynamic diameter after adsorption in order to derive information on surface coverages [14-18, 22,

23]. However, the thickness of the bound protein layer does not directly provide accurate information on bound proteins per nanoparticles. Yet, models have been derived which allow to correlate the average number of protein molecules bound to the nanoparticle to the hydrodynamic radius [24, 25]. Such a model has also been exploited to convert hydrodynamic radii measured by Taylor dispersion analysis (TDA) into protein surface coverages [26]. Recently a technique called resonant mass measurement (RMM) has been proposed to determine the protein mass on single nanoparticles [14, 27-29]. It actually measures the buoyant mass of nanoparticles in a microfluidic channel by frequency shifts of a resonator when a nanoparticle passes by. The buoyant mass can be converted to dry mass, which allows then to calculate the number of proteins per nanoparticle due to knowledge of the numbers of particles, which are counted as well. Another sophisticated method uses an electrospray-differential mobility analyzer (ES-DMA) for the separation of NP and protein-NP conjugates which are coupled to an aerosol particle mass analyzer (APM) that determines mass by a balance of electrical and centrifugal forces. The differential analysis of unmodified carrier and protein-modified NPs allows the quantification of ligand densities [30]. Very recently, a targeted mass spectrometry-based method has been developed to directly measure the amount of antibody covalently bound to magnetic particles [11]. This method involves an on-bead digestion and analysis of a few characteristic tryptic peptides by isotope-dilution liquid chromatography-tandem MS, using selected reaction monitoring acquisition. Unfortunately, all these latter techniques require equipment, which is not widely available in analytical laboratories.

Hence, the aim of this study was to establish a novel and generally applicable strategy for directly quantifying protein coverages on gold nanoparticles based on the reliable method of amino acid analysis following acidic hydrolysis of the protein. In this work, pepsin was employed as the model protein, and different concentrations of protein-GNP bioconjugates coated with different concentrations of pepsin were prepared by a

straightforward adsorptive immobilization process with subsequent washing steps to remove unbound and loosely bound proteins. protein-GNP bioconjugates were chemically digested in situ with 6N HCl to generate free amino acids and GNPs mixtures. After GNP removal and amino acid derivatization, direct quantitative analysis was performed based on measuring the intensity of the AQC-glycine derivative by using HPLC-FLD (Figure 1). An in situ digestion procedure of the bioconjugates was adopted without prior protein elution and isolation steps from nanoparticles, which extended the application ranges to protein-nanoparticle conjugations with different bonding chemistries. This direct, accurate and reliable method with excellent reproducibility shows great potential for quantification of any other proteins on nanoparticles.

Experimental

Materials

Pepsin (from porcine gastric mucosa, E.C.3.4.23.1, 3200-4500 units/mg protein), gold(III)chloride trihydrate ($HAuCl_4 \cdot 3H_2O$), trisodium citrate, 2-(N-morpholino)ethane sulfonic acid (MES) monohydrate, ammonium acetate (NH_4Ac), sodium tetraborate decahydrate, boric acid, 2-amino-2-(hydroxymethyl)-propan-1,3-diol (Tris) base, sodium hydroxide, hydrochloric acid, sodium phosphate monobasic dihydrate and sodium phosphate dibasic dihydrate were purchased from Sigma Aldrich (Germany). 6-Aminoquinolyl-N-hydroxysuccinimidyl carbamate (AQC) was purchased from Synchem (Altenburg, Germany). HPLC-grade acetonitrile was purchased from JT Baker Chemical (Deventer, The Netherlands), and HPLC-grade methanol was bought from Sigma Aldrich. Double deionized water (produced by Elga Purelab Ultra ELGA, System LabWater, Celle, Germany) was used throughout synthesis of GNPs and analytical procedures including HPLC-FLD. Phosphate buffer (PB) (10 mM, pH 7.5) was prepared with sodium phosphate monobasic dihydrate and sodium phosphate dibasic dihydrate.

Preparation of pepsin-GNP bioconjugates

Gold nanoparticles were prepared according to the Turkevich-Frens method with some modifications [1, 20]. In brief, 25.25 mg $HAuCl_4$ were dissolved in 50 mL double deionized water (with a final concentration of 1.14 mM) and then heated at 170°C under reflux and constant stirring for 10 min. Afterwards, 6.25 mL trisodium citrate (2.28 mM) were added and heated for another 10 min under reflux and constant stirring. The colloid solution was then allowed to cool down to room temperature under continuous stirring for an additional 60 min. The obtained citrate-GNP solution was stored at 4 °C for further usage [31]. For the preparation of pepsin-GNP bioconjugates, 1 mL of the above GNP solution was centrifuged and the supernatant removed. To these centrifuged nanoparticles, 1 mL of pepsin solutions with different enzyme concentrations in the range of 0.0052 to 5.2 mg mL^{-1} in 20 mM MES buffer pH 4.5 was added. These reaction mixtures were incubated at 4°C overnight. Afterwards, the pepsin-GNP bioconjugates were washed with 10 mM Tris-HCl (pH 7.5) and 10 mM PB (pH 7.5), respectively. Washing steps with Tris-HCl buffer were performed twice and with PB buffer thrice (centrifugation at 12000 rpm for 15 min, removal of supernatant and resuspension in respective buffer).

Digestion of samples and calibrants

Pepsin solutions with concentrations in the range of 0.001 to 5 mg mL^{-1} were applied as standard calibrants (calibration set 1). To match the same matrix of samples, the same concentration range of pepsin (0.001 to 5 mg mL^{-1}) mixed with GNPs were prepared as a second set of calibrants (calibration set 2, matrix-matched calibration). A third more generic calibration based on amino acid standards was also tested. In this case, the protein concentration was calculated from the determined amino acid concentration, the molecular weight of the protein and the number of the respective amino acid residue in the protein. For this purpose, a calibration series of an amino acid standard mixture (in

the range of 0.0025 to 0.5 mM) was prepared in 0.2 M borate buffer (pH 8.5) (calibration set 3) and was directly used for AQC derivatization (vide infra).

Before protein digestion, 1 mL pepsin-GNP bioconjugates samples were concentrated to 100 µL. For the digestion, one hundred microliter of sample solutions (pepsin, pepsin mixed with GNPs, pepsin-GNP bioconjugates) were first evaporated to dryness in a Thermo Savant ISS110 SpeedVac at 43 ˚C for 2 h. Next, the dried samples were hydrolyzed with 100 µL 6N HCl at 110°C for 24h. Afterwards, the hydrochloric acid in the samples was removed by evaporation in the SpeedVac at 43 °C for 5 h. Finally, 100 µL of 0.2 M borate buffer (pH 8.5) were added to re-dissolve the hydrolysis product by rinsing the inner surface of the vials on a vortex mixer. These protein hydrolysates, redissolved in derivatization buffer, were centrifuged twice (12000 rpm, 15 min) to remove the nanoparticles. The obtained solutions (supernatants) were stored at -20 ˚C for further AQC derivatization.

AQC derivatization

AQC derivatization reagent (3 mg mL^{-1}) was prepared by dissolving purified 3 mg AQC in 1 mL anhydrous acetonitrile. Ten microliter of each obtained hydrolysis product solution (from pepsin, pepsin mixed with GNPs, and pepsin-GNP bioconjugates, respectively) were added to 70 µL of 0.2 M borate buffer (pH 8.5). Afterwards, to each solution 20 µL of AQC solution (3 mg mL^{-1} in acetonitrile) were added. The reaction was allowed to proceed at 55 °C under continuously shaking at 800 rpm for 10 min. The obtained samples containing AQC derivatives of amino acids were directly analysed by HPLC-FLD.

HPLC-FLD analysis

HPLC-FLD analysis was performed on an Agilent 1100 HPLC instrument consisting of a binary pump, autosampler, column compartment and fluorescence detector. Agilent Zorbax Eclipse XDB C18 column (4.6 x 150 mm, 5 µm) was used for the

chromatographic separation. Mobile phase A consisted of 2.5 mM ammonium acetate in water, and mobile phase B consisted of 3.8 mM aqueous NH_4Ac/ACN (30:70; v/v). Amino acid separation was performed at 25°C with gradient elution (0-12 min 1-8 % B, 12-25 min 8-11 % B, 25-27 min 11 % B, 27-29 min 11-20 % B, 29-39 min 20 % B, 39-40 min 20-25 % B, 40-40.1 min 25-100 % B, 40.1-43.1 min 100 % B, 43.4-48 min, 100-1 % B). The flow rate was set to 1 mL min^{-1}, and injection volume was 5 µL. Detection was carried out by fluorescence detection with excitation at 254 nm and emission at 395 nm.

Result and discussion

Development of protein quantification method

The accurate unbiased characterization of protein concentrations on protein-nanoparticle bioconjugates is of prime importance in many fields. Still it represents a major not fully solved challenge. Many of the methods applied for this purpose are biased due to indirect measurements, assumptions in the calculations (e.g. volume dimensions of the immobilized proteins), insufficient precision, bias from complicated sample preparation and other problems. Therefore, we have been looking for a method which circumvents these shortcomings, viz. a method that i) is based on the direct analysis of the purified bioconjugate and not indirectly via free (unbound) proteins, ii) directly measures the protein content without assumptions in calculations, and iii) exhibits high precision. A method that is based on direct hydrolysis of the protein-NP conjugate and classical amino acid analysis of the generated hydrolysate has appeared attractive as it turns out to be the most reliable and precise methodology. In this study, the direct quantification method of protein on nanoparticles was established with adsorptively bound pepsin on GNPs (pepsin-GNP bioconjugates) as a model system. The strategy for directly quantifying adsorbed pepsin on GNPs is depicted in Figure 1a. In general, the samples are first digested with 6 N HCl, evaporated to dryness, redissolved in derivatization buffer, GNPs

removed by centrifugation and the resultant amino acid hydrolysate in derivatization buffer subjected to derivatization with AQC reagent followed by HPLC-FLD analysis.

In the first step, pepsin-GNP bioconjugates have been prepared by straightforward adsorption of pepsin in different concentrations onto GNPs. After conjugation, unbound or loosely bound pepsin has been removed by washing steps (centrifugation and re-dissolution) with 10 mM Tris-HCl (pH 7.5) and 10 mM PB buffer (pH 7.5), respectively. After removal of the supernatants and evaporation to dryness, the pepsin-GNP bioconjugates have been subsequently digested with 6 N HCl. During the digestion process, pepsin bound on GNPs has been completely hydrolyzed to amino acids. This classical method of peptide and protein hydrolysis is well established and has proven to be highly reproducibile. The GNP carrier, on the other side, is chemically stable against HCl, which allows straightforward removal of the GNPs from the hydrolysate by simple centrifugation on a minispin. In order to be able to detect even small quantities of immobilized protein, a concentration step by a factor of 10 has been implemented in the course of the hydrolysis procedure. The obtained hydrolysate solutions containing amino acid and nanoparticles (which aggregated after hydrolysis) have been evaporated to dryness to completely remove HCl and subsequently have been re-dissolved in 0.2 M borate buffer (pH 8.5). Two centrifugation steps have been carried out to remove the GNP pellets from the solutions and the remaining supernatant containing the generated amino acids have been used for derivatization with AQC. The reaction scheme for the derivatization is shown in Figure 1b. AQC is an excellent derivatization reagent for amino acid analysis [32]. It reacts fast with both primary as well as secondary amino acids to form stable AQC-amino acid derivatives, which can be sensitively detected by fluorescence detection with excitation at 250 nm and emission at 395 nm [33, 34]. For the derivatization, 0.2 M borate buffer (pH 8.5) has been selected as the reaction buffer because it provides the highest derivatization yields [33]. Finally, the AQC-amino acid derivatives have been analyzed by HPLC-FLD using a C18 column and gradient elution.

Figure 2a shows a representative chromatogram of a mixture containing the 20 standard amino acids derivatized with AQC. Each peak has been identified by comparing the retention times with single amino acid standard injections. Under optimized conditions, a successful separation of each amino acid has been achieved except for valine and tyrosine (peak 13). Under given conditions they have similar lipophilicity. Arg is accompanied by a second peak, which originates from the derivatizing agent, which is not fully baseline resolved. Since none of these three amino acids was considered to be used for the quantitative analysis herein, no further attempts have been made to separate them because longer gradients would have been necessary at expense of analysis times. For the quantitative analysis of the pepsin concentration the peak of AQC-glycine derivative at retention time 13.67 (± 0.05) min has been selected due to the reason that glycine accounts for 10.7 % related to all amino acids in pepsin (serine for 13.5 %). Consequently, a good sensitivity of the fluorescence signal can be obtained for these two amino acids [35]. However, during the hydrolysis process with 6 N HCl serine can decompose to some degree due to water cleavage (5-15 % destruction) has been reported, which might easily result in inaccurate quantification results. In contrast, a high recovery of over 95 % has been reported for glycine in common protein hydrolysis reactions [32, 36-38]. Whatsoever, also other well resolved amino acids such as Ala, Ile, Leu or Phe can be selected for quantitation e.g. if another protein has to be determined which shows higher contents of these amino acids or for validation purposes.

Calibration and method validation

Calibration can be based either on the protein to be determined, here pepsin, or on the amino acid selected for quantitation, here glycine. The former approach is more straightforward and is preferred if a sufficient amount of the protein is available. The second approach will be selected, if the protein is precious and only limited amounts are amenable. A main requirement in this case is the overall knowledge of the amino acid

sequence and the number of the selected amino acid residue in the protein. Herein, we will compare these two approaches.

First, pepsin has been used for calibration. Two sets of standard solutions, pepsin (calibration set 1) and pepsin mixed with GNPs (matrix-matched) (calibration set 2), have been employed for calibration in order to examine whether the matrix (i.e. the GNPs) represent a problem during digestion and influence hydrolysis yields or decompose amino acids. After acidic hydrolysis and derivatization, the AQC-amino acid derivatives from the hydrolyzed pepsin have been analyzed by HPLC-FLD under optimized conditions. The chromatograms of hydrolyzed pepsin in the concentration range between 0.001 to 2 mg mL^{-1} from calibration set 2 in the presence of GNPs are shown in Figure 2b. It can be seen that the peak intensity of AQC-glycine increases significantly with higher concentration of pepsin used as calibrant, as expected. Calibration curves for these two sets of standards (calibration set 1 and 2) have been obtained by plotting the integrated peak areas of AQC-glycine against pepsin concentrations (see Figure 3a). It is worthwhile noting that these two calibration curves are almost perfectly overlapping with each other. Thus, very similar linear regression equations are obtained for these two calibration curves (shown in Table 1). Both calibration curves show a linear range from 0.001 to 2 mg mL^{-1} with excellent linearity (R2 value of 0.9998 and 0.99994, respectively). Moreover, the limit of detection (LOD; S/N = 3) and the limit of quantification (LOQ; S/N = 10) are identical for the two calibration sets (pepsin, pepsin with GNPs). They have been determined to be 0.0001 and 0.0003 mg mL^{-1}. These results clearly demonstrate the negligible influence of the matrix (gold nanoparticles) on the protein quantification process.

Furthermore, the method using matrix-matched calibration (calibration set 2) has been validated in accordance with the ICH guideline. Thus, intra- and inter-day precision and accuracy have been validated at three concentration levels for quality control (QC) samples (pepsin mixed with GNPs) in three replicates, and all these validation characteristics have been evaluated under the same experimental conditions. The

obtained results are summarized in Table 2 [39]. It can be seen that excellent intra- and inter-day assay precision (< 5 % RSD) and accuracy (98-118 % recovery) can be achieved, which indicates the absence of a significant bias and proves the high reliability of this established method. Overall, all these results demonstrate that the established method can be used for detection and quantification of pepsin on the surface of GNP over a wide concentration range.

Next it has been tested, whether consistent results can be obtained, when amino acid mixtures instead of pepsin are used as calibrants. Thus, a standard amino acid mixture (containing all amino acids in the range of 0.0025 to 0.5 mM) has been prepared as the third set of calibrants (calibration set 3) and injected to the HPLC-FLD. The calibration data are summarized in Table 1. The amino acid sequence of pepsin is well known. It contains 35 glycine residues. With this information in hand, the corresponding protein concentrations can be readily calculated from the determined amino acid (glycine) concentrations. The resultant calibration function is shown in Fig. 3b and compared with the calibration of set 2 (pepsin mixed with GNPs) (Fig. 3b insert).

Similar linearity relationships and calibration functions (slopes and intercepts) of these two curves clearly show the consistency between the amino acid-based calibration and the pepsin-based calibration. The result demonstrates that calibration can be carried out with amino acid calibrants instead of the emanating protein. With the amino acid mixtures for calibration, the novel, yet simple and universal method can be extended to a wide range of proteins showing a great potential for quantification of protein surface coverages on nanoparticles.

Quantification of pepsin on GNPs

To verify the capability of this novel method for the quantification of immobilized proteins, two series of adsorptively bound pepsin-GNP bioconjugates have been synthesized and the protein coverage on the nanoparticles has been quantified by the established method. The bioconjugates have been prepared by adsorption of pepsin onto GNPs

using different concentrations of protein (5.2 µg mL^{-1} to 5.2 mg mL^{-1}) in the reaction mixture. During adsorption, a hard protein corona is gradually formed from the initially loosely bound protein shell through adsorption, desorption and rearrangement processes of the proteins onto the GNPs [40]. After conjugation, purification of pepsin-GNP bioconjugates has to be performed in order to remove the unbound as well as loosely bound proteins. For purification, 10 mM (pH 7.5) Tris buffer (2x washed) has been used for one set of pepsin-GNP bioconjugates, while 10 mM PB buffer (pH 7.5) (3x washed) has been used for the second set. Due to their distinct ionic strengths and different number of washing steps different protein surface coverages might result from their different strength and efficiencies in disruption of electrostatic interactions between protein and gold surface as well as between protein molecules.

For the quantitative analysis of the protein coverage, all pepsin-GNP bioconjugate samples have been analyzed in triplicates using the same hydrolysis and derivatization procedures as described for the pepsin standard solutions. All the measurements of the derivatized amino acid solutions have been performed by HPLC-FLD. The total amount of adsorbed pepsin has been calculated using two distinct calibration curves (matrix-matched pepsin i.e. calibration set 2 as well as amino acid mixtures i.e. calibration set 3). For comparison, the supernatants after protein immobilization were analyzed as well by the same method and used for back-calculation of the adsorbed protein concentration by mass balance considerations (indirect determination) (see Supplementary Material). The results of the indirect method clearly document that this assay format is not reliable (see Supplementary Material). Furthermore, the binding efficiency (%) has been calculated according to Eq. (1)

$$Binding\ efficiency = \frac{Amount\ of\ adsorbed\ pepsin}{Total\ Amount\ of\ pepsin\ in\ reaction\ mixture} \times\ 100\% \qquad (1)$$

To obtain the exact number of immobilized pepsin molecules per GNP, the measured protein concentration has to be divided by the GNP concentration, which has been

determined by resonant mass measurement and has been found to be 1 25 × 10^{-11} mol L^{-1} [26]. All the results are summarized in Table 3 and the corresponding equilibrium isotherms are shown in Fig. 4a. The results in Table 3 show clearly that pepsin adsorption, i.e. the number of pepsin molecules per GNP, increases significantly with the pepsin concentration in the reaction mixture. With the highest pepsin concentration (5.2 mg mL^{-1}) in the reaction mixture, ca. 25,000 pepsin molecules per GNP have remained adsorbed, after washing with Tris buffer. After washing with PB buffer, a surface coverage of only ca. 7,000 pepsin molecules per GNP has been found. On the contrary, the binding efficiency has significantly dropped with increasing pepsin concentration in the reaction mixture. While about 20-30 % of the pepsin in the reaction mixture has been immobilized from the lowest concentration, the percentage of pepsin immobilized has decreased to about 0.2 % at the highest concentration for the bioconjugates washed with Tris buffer. Again, the corresponding numbers have been lower for pepsin-GNP bioconjugates washed with PB. This indicates that the PB washing procedure more efficiently replaces loosely bound protein molecules from the adsorbent surface, either due to the additional washing step (2 times with Tris buffer and 3 times with PB buffer) or due to a more efficient replacement of loosely adsorbed protein molecules on the outer layers.

Various isotherm models have then been fitted to the binding data in Figure 4a. The Langmuir isotherm has shown a poor quality of fit. Thus, a Freundlich model has been tested and has provided a good fit for the adsorption behaviors. The Freundlich sorption isotherm equation is given by Eq. (2),

$$q_e = K_f C_e^{(1/n)} \quad (2)$$

wherein qe is the number of pepsin molecules per GNP and Ce is the equilibrium pepsin concentration (mg mL^{-1}). K_f is the Freundlich constant related to the binding capacity of

GNPs for pepsin, and 1/n is the exponent of non-linearity providing information on the affinity change of GNPs to pepsin with pepsin concentration [41].

The Freundlich parameters K_f and 1/n can be determined by the nonlinear regression and are summarized in Table 4. This sorption behavior can be explained by a gradual decrease of the binding affinity with increasing equilibrium concentration and gives a non-linear isotherm with a negative curvature. The exponent of the Freundlich isotherm is a measure of the deviation from an infinite perfectly homogenous surface. Here it can be assumed that at low concentration the pepsin strongly adsorbs at the gold surface forming a hard protein corona. Once the high affinity sorption sites are mostly occupied, affinity declines for steric reasons. Upon further protein binding, pepsin molecules bind to the protein covered nanoparticles forming a soft protein shell (soft corona). Affinity may be significantly lower for these binding sites explaining the negative curvature. It should be mentioned that a fractal Langmuir isotherm [42, 43] also reasonably well explained the sorption process with the same general interpretation of the sorption process.

Furthermore, the data in Table 3 and 4 provide clear evidence that the surface coverage of pepsin on the GNPs strongly depends on the type of wash buffer. Much higher pepsin concentrations on GNPs can be obtained with Tris buffer (washing twice) compared to PB buffer (washing three times). These results are very similar regardless of which of the two different calibration curves (matrix-matched calibration with pepsin, calibration with amino acid mixtures) have been used for calculation of the surface coverage. At lower coverages, there is a complete overlap as observed for the two adsorption curves in PB buffer.

The same adsorption experiments (pepsin onto GNPs at the same concentrations in the reaction buffer and washing with 10 mM Tris buffer) have been carried out previously in our work and the resultant particles have been characterized by Taylor dispersion analysis (TDA) [26]. It is evident by Figure 4b that the pepsin adsorption curve measured herein follows the same general pattern as the one from the earlier work and is characterized by hydrodynamic diameters (from TDA). This can be regarded as a further

indication of the validity of the novel established method for quantification of protein coverages on GNPs.

It was further of interest to assess whether the determined pepsin concentrations correspond to a protein monolayer on the GNP surface or whether multilayer adsorption results from excessive protein in the reaction mixture. Since the Langmuir model has not been suitable to describe the adsorption process adequately, the latter adsorption characteristic, i.e. multilayer adsorption, has therefore been expected to apply. According to a recent publication, the monolayer adsorption capacity (N_{mono}) at 100 % coverage can be estimated using simple geometric considerations assuming that proteins remain globular on the GNP surface [14, 44]. For its rough theoretical estimation, the surface area of the particles at half a protein diameter above the particle was calculated and divided by the protein cross-sectional area to achieve the theoretical numbers at 100 % coverage [44], as given by eq. 3,

$$N_{mono} = \frac{4 \cdot R^2_{(GNP + protein)}}{R^2_{protein}} \quad (3)$$

wherein RGNP and $R_{protein}$ are the radius of the GNPs and the protein, respectively. For the GNPs used herein a hydrodynamic diameter of 44.1 ± 0.3 nm has been measured by DLS and a dry state diameter of ca. 30 nm by TEM. A hydrodynamic radius of pepsin of 0.47 ± 0.03 nm has been determined recently by TDA [26]. Based on the dry state radius of GNPs by TEM and the hydrodynamic radius of pepsin by TDA, a monolayer capacity of around 4200 pepsin molecules per GNP can be estimated. Using the DLS radius instead, this number would be around 9000 pepsin molecules per GNP. Considering that the radius determined by DLS is typically overestimated to some extent, the former value appears more plausible. Looking at the values in Table 3, it can be noticed that with Tris buffer the monolayer capacity is already reached at the lowest concentration of pepsin in the reaction mixture (0.0052 mg mL^{-1}). At higher pepsin concentrations in the reaction

mixture, the GNPs adsorb further proteins and most probably build up multilayers. A coverage with 9200 pepsin molecules per GNP correspond to a bilayer coating, 15000, 21000, and 27000 molecules per GNP to triple, quadruple, and quintuple layer coatings, respectively (calculations based on TEM radius and hydrodynamic radius of pepsin from TDA). In contrast, with PB buffer protein coverages largely corresponding to monolayer coatings are formed over a wide concentration range of pepsin in the reaction buffer and only at the highest pepsin concentration (5.2 mg mL^{-1}) a second pepsin layer is attached on the surface. It seems that the additional washing step (3x instead of 2x with Tris) or PB more efficiently desorbs loosely bound proteins (soft protein corona) and only the strongly adsorbed protein molecules (hard protein corona) remain adsorbed on the surface after repetitive PB wash. Thus, pepsin-coated GNPs synthesized by this way are supposed to be more stable.

While documented herein with adsorptively bound protein-GNP conjugates, the approach can also be used for covalently linked protein-GNP bioconjugates, as documented in the supplementary material by protein functionalized GNPs obtained by coupling of pepsin to carboxy-PEGylated GNPs (see Supplementary Material).

Conclusion

Protein-nanoparticle conjugates have become very popular in many fields of nanoscience, including immobilized enzyme reactors, nanoparticle-based biosensors and protein-enabled nanomaterials for biomarker enrichment. Therefore, understanding and assessing the surface coverage is of utmost importance for producing protein-nanoparticle conjugates with excellent reproducibility. The determination of the protein coverage on the NP surface constitutes therefore an essential step in quality control. The majority of methods are indirectly analyzing the surface coverage via free protein quantitation in the supernatant of the reaction. Other methods make assumptions during calculation of the protein surface concentration from measured physicochemical

properties. The herein newly established method for protein coverage determination by contrast is directly analyzing the protein concentration on the protein-GNP bioconjugates. It is based on the classical and reliable amino acid analysis of peptides and proteins. The AQC-amino acid derivatives, obtained after in situ digestion of protein-GNP bioconjugates and subsequent derivatization process with AQC reagent, are analyzed by HPLC-FLD, which ensures high sensitivity (0.1 μg mL^{-1} for pepsin, corresponding to 2.89×10^{-9} mol L^{-1}) and allows determination of even the smallest surface concentrations. The calibration curves showed good linearity and high correlation coefficients. Validation experiments demonstrated excellent intra-and inter-day assay precision and accuracy of this method for pepsin quantification. The method is supposed to be valuable for the study of adsorption phenomena of proteins onto nanoparticles in which even minor alterations can be monitored. In order to increase the sample throughput, this method could be transferred to UHPLC with sub-2μm or core-shell particle columns, which provides fast separation with much reduced run times at equal resolutions. This generic approach based on the amino acid analysis strategy turns out to be an accurate method for the determination of protein coverage and shows great potential for quantification of any other protein with easy operation and low cost. It is, however, not applicable to mixtures of proteins. In this case, the analysis based on signature peptides by targeted HPLC-MS/MS analysis seems to be more appropriate.

Acknowledgements

We acknowledge the financial support by the “Struktur- und Innovationsfonds Baden-Württemberg (SI-BW)”. S. L. gratefully acknowledges the support from the China Scholarship Council (CSC).

References

[1] E. Haller, W. Lindner, M. Lämmerhofer, Gold nanoparticle–antibody conjugates for specific extraction and subsequent analysis by liquid chromatography–tandem mass spectrometry of malondialdehyde-modified low density lipoprotein as biomarker for cardiovascular risk, Anal. Chim. Acta, 857 (2015) 53-63.

[2] H. Hinterwirth, G. Stubiger, W. Lindner, M. Lammerhofer, Gold nanoparticle-conjugated anti-oxidized low-density lipoprotein antibodies for targeted lipidomics of oxidative stress biomarkers, Anal. Chem., 85 (2013) 8376-8384.

[3] J.R. Whiteaker, L. Zhao, H.Y. Zhang, L.-C. Feng, B.D. Piening, L. Anderson, A.G. Paulovich, Antibody-based enrichment of peptides on magnetic beads for mass-spectrometry-based quantification of serum biomarkers, Anal. Biochem., 362 (2007) 44-54.

[4] M.S. Lowenthal, H. Gasca-Aragon, J.E. Schiel, N.G. Dodder, D.M. Bunk, A quantitative LC–MS/MS method for comparative analysis of capture-antibody affinity toward protein antigens, J. Chromatogr. B, 879 (2011) 2726-2732.

[5] J. Tang, Y. Liu, D. Qi, G. Yao, C. Deng, X. Zhang, On-plate-selective enrichment of glycopeptides using boronic acid-modified gold nanoparticles for direct MALDI-QIT-TOF MS analysis, Proteomics, 9 (2009) 5046-5055.

[6] L. Dykman, N. Khlebtsov, Gold nanoparticles in biomedical applications: recent advances and perspectives, Chem. Soc. Rev., 41 (2012) 2256-2282.

[7] S.L. Filbrun, J.D. Driskell, A fluorescence-based method to directly quantify antibodies immobilized on gold nanoparticles, Analyst, 141 (2016) 3851-3857.

[8] J. Baniukevic, I. Hakki Boyaci, A. Goktug Bozkurt, U. Tamer, A. Ramanavicius, A. Ramanaviciene, Magnetic gold nanoparticles in SERS-based sandwich immunoassay for antigen detection by well oriented antibodies, Biosensors Bioelectron., 43 (2013) 281-288.

[9] F. Liu, L. Wang, H. Wang, L. Yuan, J. Li, J.L. Brash, H. Chen, Modulating the Activity of Protein Conjugated to Gold Nanoparticles by Site-Directed Orientation and Surface Density of Bound Protein, ACS Appl. Mater. Interfaces, 7 (2015) 3717-3724.

[10] G.J. Worsley, N. Kumarswami, C. Minelli, J.E. Noble, Characterisation of antibody conjugated particles and their influence on diagnostic assay response, Analytical Methods, 7 (2015) 9596-9603.

[11] N.A. Schneck, K.W. Phinney, S.B. Lee, M.S. Lowenthal, Quantification of antibody coupled to magnetic particles by targeted mass spectrometry, Anal. Bioanal. Chem., 408 (2016) 8325-8332.

[12] C.D. Walkey, J.B. Olsen, H. Guo, A. Emili, W.C.W. Chan, Nanoparticle Size and Surface Chemistry Determine Serum Protein Adsorption and Macrophage Uptake, J. Am. Chem. Soc., 134 (2012) 2139-2147.

[13] R.E. Abraham, M.L. Verma, C.J. Barrow, M. Puri, Suitability of magnetic nanoparticle immobilised cellulases in enhancing enzymatic saccharification of pretreated hemp biomass, Biotechnol. Biofuels, 7 (2014) 90.

[14] M.R. Nejadnik, W. Jiskoot, Measurement of the Average Mass of Proteins Adsorbed to a Nanoparticle by Using a Suspended Microchannel Resonator, J. Pharm. Sci., 104 (2015) 698-704.

[15] N.C. Bell, C. Minelli, A.G. Shard, Quantitation of IgG protein adsorption to gold nanoparticles using particle size measurement, Analytical Methods, 5 (2013) 4591-4601.

[16] M. Mahmoudi, I. Lynch, M.R. Ejtehadi, M.P. Monopoli, F.B. Bombelli, S. Laurent, Protein−Nanoparticle Interactions: Opportunities and Challenges, Chem. Rev., 111 (2011) 5610-5637.

[17] A.E. James, J.D. Driskell, Monitoring gold nanoparticle conjugation and analysis of biomolecular binding with nanoparticle tracking analysis (NTA) and dynamic light scattering (DLS), Analyst, 138 (2013) 1212-1218.

[18] C. Minelli, R. Garcia-Diez, A.E. Sikora, C. Gollwitzer, M. Krumrey, A.G. Shard, Characterization of IgG-protein-coated polymeric nanoparticles using complementary particle sizing techniques, Surf. Interface Anal., 46 (2014) 663-667.

[19] A.A. Vertegel, R.W. Siegel, J.S. Dordick, Silica Nanoparticle Size Influences the Structure and Enzymatic Activity of Adsorbed Lysozyme, Langmuir, 20 (2004) 6800-6807.

[20] H. Hinterwirth, W. Lindner, M. Lammerhofer, Bioconjugation of trypsin onto gold nanoparticles: effect of surface chemistry on bioactivity, Anal. Chim. Acta, 733 (2012) 90-97.

[21] H. Hinterwirth, G. Stübiger, W. Lindner, M. Lämmerhofer, Gold Nanoparticle-Conjugated Anti-Oxidized Low-Density Lipoprotein Antibodies for Targeted Lipidomics of Oxidative Stress Biomarkers, Anal. Chem., 85 (2013) 8376-8384.

[22] I. Montes-Burgos, D. Walczyk, P. Hole, J. Smith, I. Lynch, K. Dawson, Characterisation of nanoparticle size and state prior to nanotoxicological studies, J. Nanopart. Res., 12 (2010) 47-53.

[23] M.P. Monopoli, D. Walczyk, A. Campbell, G. Elia, I. Lynch, F. Baldelli Bombelli, K.A. Dawson, Physical−Chemical Aspects of Protein Corona: Relevance to in Vitro and in Vivo Biological Impacts of Nanoparticles, J. Am. Chem. Soc., 133 (2011) 2525-2534.

[24] C. Rocker, M. Potzl, F. Zhang, W.J. Parak, G.U. Nienhaus, A quantitative fluorescence study of protein monolayer formation on colloidal nanoparticles, Nat Nano, 4 (2009) 577-580.

[25] M. Mahmoudi, A.M. Abdelmonem, S. Behzadi, J.H. Clement, S. Dutz, M.R. Ejtehadi, R. Hartmann, K. Kantner, U. Linne, P. Maffre, S. Metzler, M.K. Moghadam, C. Pfeiffer, M. Rezaei, P. Ruiz-Lozano, V. Serpooshan, M.A. Shokrgozar, G.U. Nienhaus, W.J. Parak, Temperature: The “Ignored” Factor at the NanoBio Interface, ACS Nano, 7 (2013) 6555-6562.

[26] M. Höldrich, S. Liu, M. Epe, M. Lämmerhofer, Taylor dispersion analysis, resonant mass measurement and bioactivity of pepsin-coated gold nanoparticles, Talanta, 167 (2017) 67-74.

[27] E. Folzer, T.A. Khan, R. Schmidt, C. Finkler, J. Huwyler, H.-C. Mahler, A.V. Koulov, Determination of the Density of Protein Particles Using a Suspended Microchannel Resonator, J. Pharm. Sci., 104 (2015) 4034-4040.

[28] A.R. Patel, D. Lau, J. Liu, Quantification and Characterization of Micrometer and Submicrometer Subvisible Particles in Protein Therapeutics by Use of a Suspended Microchannel Resonator, Anal. Chem., 84 (2012) 6833-6840.

[29] D. Weinbuch, S. Zölls, M. Wiggenhorn, W. Friess, G. Winter, W. Jiskoot, A. Hawe, Micro–Flow Imaging and Resonant Mass Measurement (Archimedes) – Complementary Methods to Quantitatively Differentiate Protein Particles and Silicone Oil Droplets, J. Pharm. Sci., 102 (2013) 2152-2165.

[30] S. Guha, X. Ma, M.J. Tarlov, M.R. Zachariah, Quantifying Ligand Adsorption to Nanoparticles Using Tandem Differential Mobility Mass Analysis, Anal. Chem., 84 (2012) 6308-6311.

[31] H. Hinterwirth, S. Kappel, T. Waitz, T. Prohaska, W. Lindner, M. Lämmerhofer, Quantifying Thiol Ligand Density of Self-Assembled Monolayers on Gold Nanoparticles by Inductively Coupled Plasma–Mass Spectrometry, ACS Nano, 7 (2013) 1129-1136.

[32] M. Fountoulakis, H.-W. Lahm, Hydrolysis and amino acid composition analysis of proteins, J. Chromatogr., 826 (1998) 109-134.

[33] S.A. Cohen, D.P. Michaud, Synthesis of a Fluorescent Derivatizing Reagent, 6-Aminoquinolyl-N-Hydroxysuccinimidyl Carbamate, and Its Application for the Analysis of Hydrolysate Amino Acids via High-Performance Liquid Chromatography, Anal. Biochem., 211 (1993) 279-287.

[34] J.L. Hong, Determination of amino acids by precolumn derivatization with 6-aminoquinolyl-N-hydroxysuccinimidyl carbamate and high performance liquid chromatography with ultraviolet detection, J. Chromatogr., 670 (1994) 59-66.

[35] J. Tang, P. Sepulveda, J. Marciniszyn, K.C.S. Chen, W.Y. Huang, N. Tao, D. Liu, J.P. Lanier, Amino-Acid Sequence of Porcine Pepsin, Proc. Natl. Acad. Sci. U. S. A., 70 (1973) 3437-3439.

[36] D. Roach, C.W. Gehrke, The hydrolysis of proteins, J. Chromatogr., 52 (1970) 393-404.

[37] A. Tsugita, J.-J. Scheffler, A Rapid Method for Acid Hydrolysis of Protein with a Mixture of Trifluoroacetic Acid and Hydrochloric Acid, Eur. J. Biochem., 124 (1982) 585-588.

[38] M.G. Davies, A.J. Thomas, An investigation of hydrolytic techniques for the amino acid analysis of foodstuffs, J. Sci. Food Agric., 24 (1973) 1525-1540.

[39] M. Höldrich, A. Sievers-Engler, M. Lämmerhofer, Gold nanoparticle-conjugated pepsin for efficient solution-like heterogeneous biocatalysis in analytical sample preparation protocols, Anal. Bioanal. Chem., 408 (2016) 5415-5427.

[40] J. Piella, N.G. Bastús, V. Puntes, Size-Dependent Protein–Nanoparticle Interactions in Citrate-Stabilized Gold Nanoparticles: The Emergence of the Protein Corona, Bioconj. Chem., 28 (2017) 88-97.

[41] W. Hai-Dong, N. Catherine Hui, Y. Qiaoqin, B. Ildiko, Study on protein conformation and adsorption behaviors in nanodiamond particle–protein complexes, Nanotechnology, 22 (2011) 145703.

[42] J. Skopp, Derivation of the Freundlich Adsorption Isotherm from Kinetics, J. Chem. Educ., 86 (2009) 1341.

[43] G. Sposito, Derivation of the Freundlich Equation for Ion Exchange Reactions in Soils1, Soil Sci. Soc. Am. J., 44 (1980) 652-654.

[44] S. Lindman, I. Lynch, E. Thulin, H. Nilsson, K.A. Dawson, S. Linse, Systematic Investigation of the Thermodynamics of HSA Adsorption to N-iso-Propylacrylamide/N-tert-Butylacrylamide Copolymer Nanoparticles. Effects of Particle Size and Hydrophobicity, Nano Lett., 7 (2007) 914-920.

Figure captions:

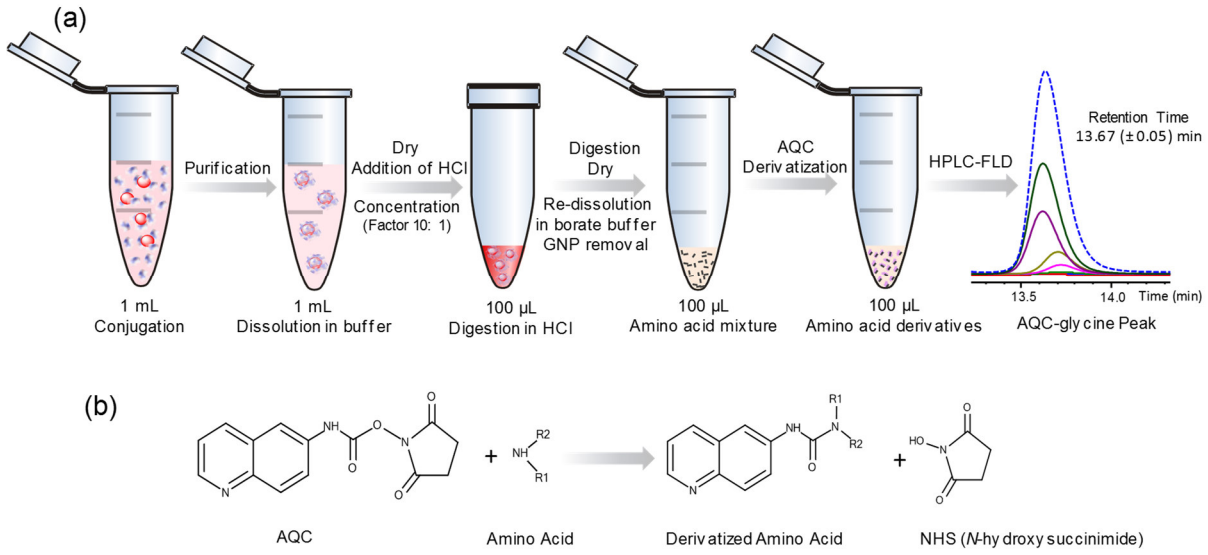

Fig. 1. (a) Schematic illustration of the workflow based on the amino acid analysis performed by HPLC-FLD for the direct quantication of the pepsin amount bound onto gold nanoparticles (GNPs); (b) The reaction scheme of amino acid derivatization with AQC reagent.

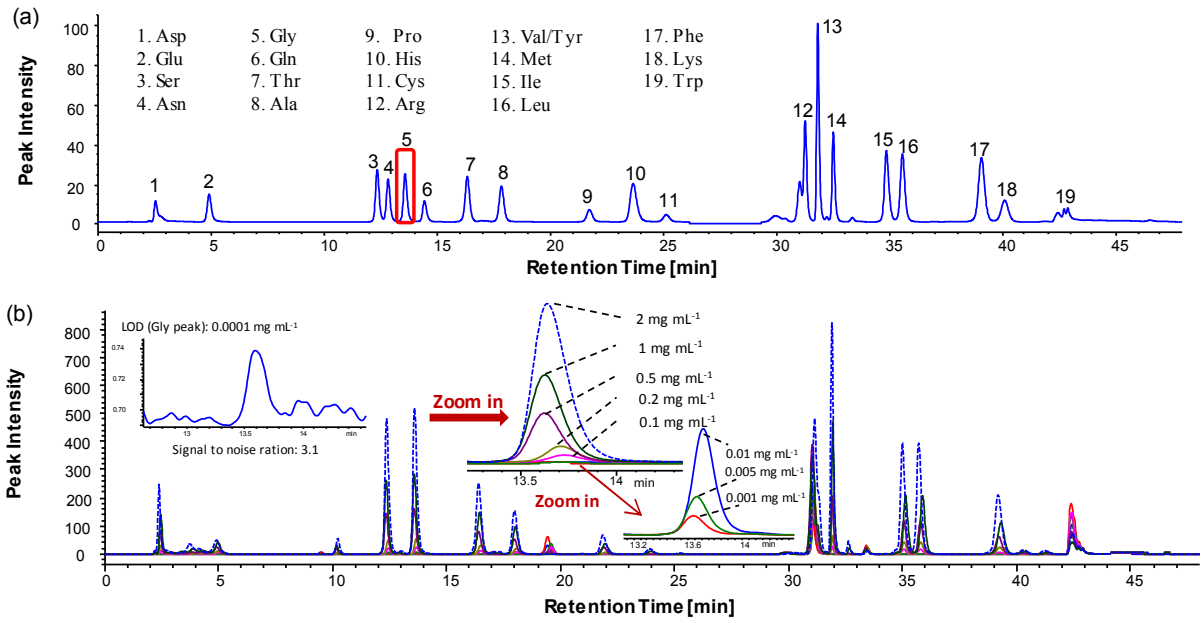

Fig. 2. (a) Optimized chromatographic separation of an amino acid standard mixture (0.1 mg mL^{-1}), which was derivatized with AQC reagent; (b) The chromatograms of calibrants (pepsin mixed with GNP) with different concentrations, after the process of hydrolyzation and derivatization.

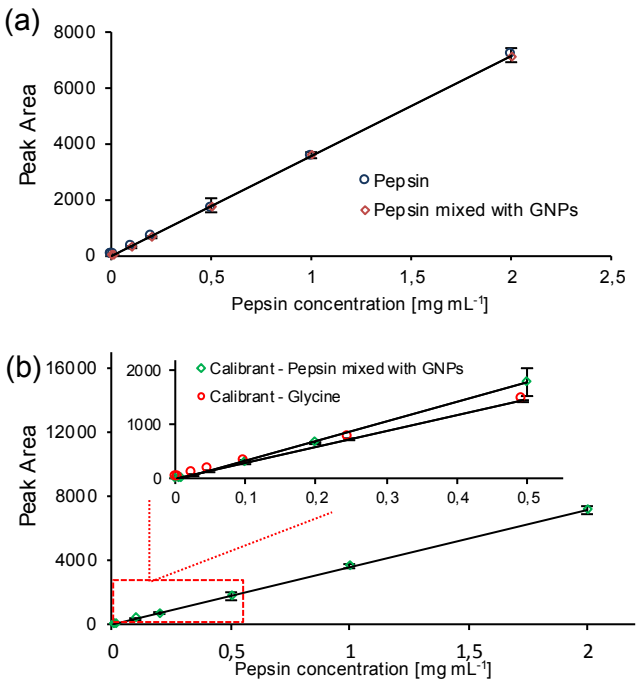

Fig. 3. (a) Calibration curves for the two sets of calibrants, pepsin (calibration set 1) and pepsin mixed with GNPs (calibration set 2), obtained by plotting the integrated peak areas of AQC-glycine against pepsin concentrations (set 1 and 2 are completely overlapped indicating absence of matrix effects); (b) Comparison of the two calibration curves for the set 2 and set 3 (pepsin mixed with GNPs, amino acid mixture as the calibrants), by plotting the integrated peak areas of AQC-glycine against pepsin concentrations. For the amino acid mixture as the calibrant, the pepsin concentrations (x-axis) were obtained from the conversion of the glycine concentrations (35 glycine residues per pepsin molecule).

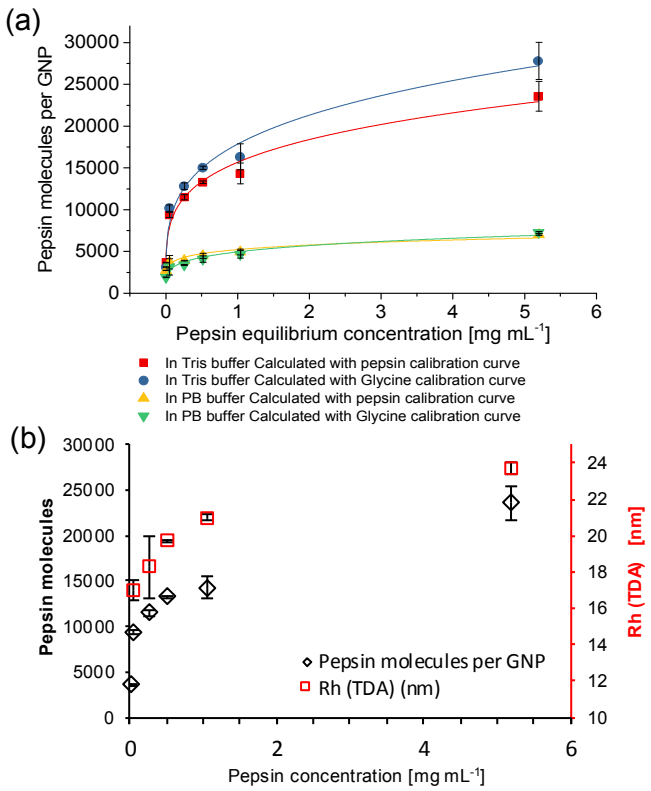

Fig. 4. (a) Adsorption isotherms of pepsin binding onto GNPs. The solid curves are the best fits of the Freundlich adsorption isotherm model to the experimental data. The error bars represent standard deviations; (b) The curves of an increase in hydrodynamic diameter measured by TDA and the increase in pepsin surface coverage measured with the established method (Pepsin concentration on the x-axis refers to the pepsin concentration used for the conjugation reaction).

Tables:

Calibrants	Pepsin (Calibration set 1)	Pepsin and GNP mixture (Calibration set 2)	Amino acid mixtures (glycine)[a] (Calibration set 3)	Amino acid mixtures (pepsin)[b] (Calibration set 3)
Linear range	0.001 to 2 mg mL^{-1}	0.001 to 2 mg mL^{-1}	0.0025 to 0.5 mM	0.00247 to 0.495 mg mL^{-1}
Regression equation	y = 3576.8x - 18.638	y = 3585.0x - 18.182	y = 2886.5x + 0.1502	y = 2918.2x + 0.1502
R^2	0.9998	0.99994	0.99992	0.99992
LOD[c]	0.0001 mg mL^{-1}	0.0001 mg mL^{-1}	0.00008 mM	0.000079 mg mL^{-1}
LOQ[d]	0.0003 mg mL^{-1}	0.0003 mg mL^{-1}	0.00025 mM	0.000247 mg mL^{-1}

[a] The amino acid mixtures were used as the standards, and the calibration curve was obtained with integrated peak areas of AQC-glycine (y-axis) versus glycine concentrations (x-axis).
[b] The amino acid mixtures were used as the standards, and the calibration curve was obtained with integrated peak areas of AQC-glycine (y-axis) versus pepsin concentrations (x-axis) calculated from glycine concentrations (35 glycine residues per pepsin molecule).
[c]LOD, the limit of detection was obtained from the signal to noise ratio 3: 1
[d]LOQ, the limit of quantification was obtained from the signal to noise ratio 10: 1

Table 1. Summary of calibration curves with different standard solutions as the calibrants employing pepsin (calibration set 1), pepsin mixed with GNPs (matrix-matched; calibration set 2), and amino acid mixtures (calibration set 3; results for calibration set 3 are given in two distinct units, once in mM and once in mg mL^{-1} to allow for better comparison).

Concentration of pepsin mixed with GNPs [mg mL^{-1}]	Intra-day (n=3)			Inter-day (n=3)		
	Calculated Concentration [mg mL^{-1}]	Accuracy (%)	Precision R.S.D (%)	Calculated Concentration [mg mL^{-1}]	Accuracy (%)	Precision R.S.D (%)
0.01	0.0118±0.0002	117.76%	2.24%	0.0118±0.0003	118.15%	1.97%
0.75	0.75±0.021	100.46%	2.84%	0.78±0.039	103.92%	4.95%
1.5	1.48±0.043	98.70%	2.89%	1.52±0.063	101.53%	4.11%

Table 2. Accuracy and precision of the amino acid-based HPLC-FLD method for the quantification of pepsin surface coverages on GNPs.

Samples	In Tris-HCl buffer				In PB buffer			
	Results calculated with pepsin (mixed with GNPs) calibration curve		Results calculated with glycine calibration curve		Results calculated with pepsin (mixed with GNPs) calibration curve		Results calculated with glycine calibration curve	
Concentration [mg mL^{-1}]	Binding efficiency (%)	Pepsin molecules per GNP	Binding efficiency (%)	Pepsin molecules per GNP	Binding efficiency (%)	Pepsin molecules per GNP	Binding efficiency (%)	Pepsin molecules per GNP
0.0052	30.60±0.31%	3677 ± 37	25.79±0.28%	3100 ± 46	22.56±0.16%	2710 ±20	15.8±0.20%	1899 ±24
0.052	7.81±0.26%	9382 ± 316	8.48±0.33%	10184 ± 392	3.09±0.67%	3714 ±803	2.62±0.83%	3145 ±997
0.26	1.91±0.05%	11496 ± 317	2.13±0.07%	12810 ±393	0.65±0.01%	3903 ±32	0.56±0.01%	3380 ±40
0.52	1.11±0.01%	13281 ± 159	1.25±0.02%	15028 ±197	0.37±0.03%	4472 ±315	0.34±0.03%	4087 ±391
1.04	0.60±0.05%	14326 ± 1246	0.68±0.06%	16325 ± 1548	0.21±0.01%	4936 ±353	0.19±0.02%	4663 ±438
5.2	0.20±0.01%	23573 ± 1781	0.23±0.02%	27810 ± 2212	0.06±0.00%	7031 ±95	0.06±0.00%	7265 ±118

Table 3. Summarized results of the pepsin binding efficiency and surface coverage (molecules) on GNPs.

Samples		Freundlich parameters		
		R^2	K_f(-)	1/n (-)
Pepsin-GNP resuspended in Tris-HCl buffer	Calculated with the Pepsin calibration curve	0.97	15675 ± 548	0.23 ± 0.022
	Calculated with the Glycine calibration curve	0.97	17849 ± 690	0.26 ± 0.025
Pepsin-GNP resuspended in PB buffer	Calculated with the Pepsin calibration curve	0.92	5220 ± 197	0.14 ± 0.021
	Calculated with the Glycine calibration curve	0.95	4945 ± 192	0.21 ± 0.024

Table 4. Summary of Freundlich isotherm parameters for pepsin adsorption onto GNPs

Supplementary material

Quantification of adsorbed pepsin on GNPs with indirect method

For comparison and to illustrate the problems of indirect determination of the surface coverage, the samples analyzed in Table 3 of the main document were also analyzed by using an indirect assay for pepsin surface coverage quantification.

Experimental

Quantification of pepsin in the supernatant (indirect method)

After the immobilization reaction at 4°C overnight, the reaction mixtures were centrifuged. The supernatant was collected for the indirect quantification of bonded pepsin, and also the Pepsin@GNP pellets were washed for the direct quantification. The washed Pepsin@GNP pellets were further treated as described in the main document. The combined supernatant and washing solutions containing non-immobilized (free) pepsin were evaporated to dryness in a Thermo Savant ISS110 SpeedVac at 43 ˚C for 2 h. Next, the dried samples were hydrolyzed with 100 µL 6N HCl at 110°C for 24h. Afterwards, the hydrochloric acid in the samples was removed by evaporation in the SpeedVac at 43 °C for 5 h. Finally, 100 µL of 0.2 M borate buffer (pH 8.5) were added to redissolve the hydrolysis product by rinsing the inner surface of the vials on a vortex mixer. The obtained solutions were stored at -20 ˚C for further AQC derivatization and RPLC analysis as described in the main document. The bonded pepsin concentration (Cbound) on the GNPs was calculated by mass balance considerations from the total pepsin concentration before immobilization (Ctot) and the free pepsin concentration in the supernatant after immobilization (Cfree) by eq. S1.

$$C_{bound} = C_{tot} - C_{free} \quad \text{(S1)}$$

Fig. S1a shows the quantification results of the supernatant (indirect assay), and in comparison, Fig.S1b presents the quantification results of the Pepsin@GNP pellets (direct assay). Both assay results were calculated with the calibration curve of pepsin mixed with GNPs (calibration set 2). The comparison of these two methods was performed only with the pepsin concentration in reaction solutions from 0.0052 to 1.04 mg mL^{-1} due to the linearity limit (0.001 to 2 mg mL^{-1}) of the calibration curve (5 mg mL^{-1} was outside of the linearity range).

Results and Discussion

The indirect method for pepsin surface coverage determination has been realized based on the quantification of non-immobilized pepsin in the supernatant which has been collected after the pepsin immobilization step. The amount of immobilized enzyme has then been back calculated by applying the mass balance equation (eq. S1). With the indirect method, inaccurate results and even negative values of bonded pepsin concentration have been obtained (Fig. S1a). This can be due to the reason that during the immobilization only a tiny amount of pepsin gets adsorbed onto the GNPs, and therefore caused an insignificant decrease of the pepsin concentration in the supernatant. Negligible changes of the pepsin concentration in the supernatant compared to the initial concentration of pepsin in the reaction mixture (in the order of the experimental error of the method) may therefore translate into large standard deviations, significant bias (i.e. inaccuracy of the method) and even negative results. For example, negative values for surface coverage have resulted at two concentrations (0.0052 and 0.52 mg mL^{-1}) (Fig. S1a). Large standard deviations have been found at two levels (0.26 and 0.52 mg mL^{-1}). Furthermore, besides the negative values also the highest concentration (1.04 mg mL^{-1}) showed a significant bias, e.g. about factor 2 higher concentrations (Fig. S1a).

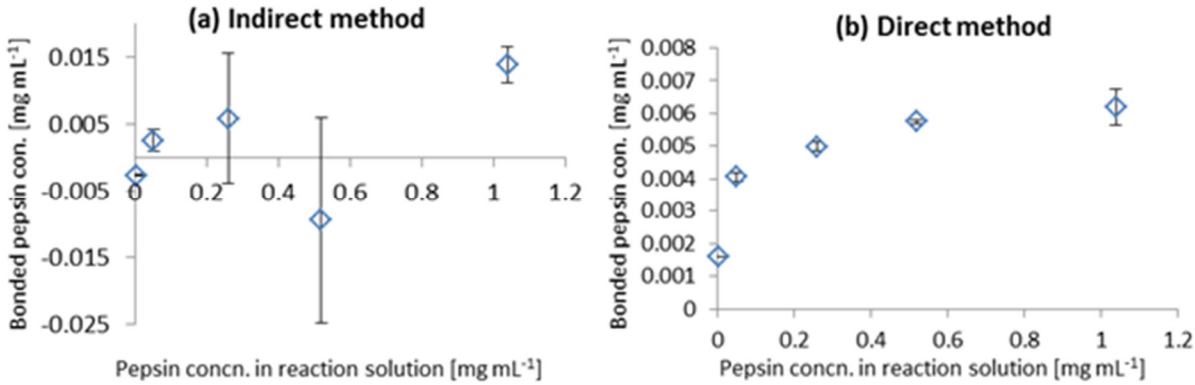

Figure S1. Bonded pepsin concentrations (mg pepsin per mL GNP suspension) quantified with indirect method (a), and the bonded pepsin concentrations obtained with direct method (b).

Quantification of pepsin covalently immobilized on GNPs via a chemical spacer

To document that the method can also be used to covalently immobilized protein-GNP conjugates, pepsin was immobilized on carboxy-pegylated GNPs by amide coupling. The surface coverage was then determined by the direct assay described in the main document for the adsorptively bound pepsin-GNP conjugates.

Experimental

Immobilization of pepsin on GNP via PEG spacer

First, the surface of citrate-capped GNPs was modified with O-(2-carboxyethyl)-O′-(2-mercaptoethyl) heptaethylene glycol (HS-PEG_7-GOOH). One microliter of HS-PEG_7-GOOH solution was added to 1mL citrate-capped GNP solution, and the modification reaction was performed overnight under constant stirring at room temperature. After modification, the obtained solution was washed twice by centrifugation at 12,000 rpm and re-suspension in 20 mM MES buffer pH 4.5. Afterwards, carboxylic acids on the GNP surface were activated with 20 µL N-(3-dimethylaminopropyl)-N'-ethylcarbodiimide (EDC, 12 mM) and 20 µL N-hydroxysulfosuccinimide sodium (sulfo-NHS, 60 mM) for 30 min. After centrifugation, 500 µL pepsin solutions with different concentrations (0.05, 0.25, 0.5,

1, 5 mg mL^{-1}) in 20 mM MES buffer pH 4.5 were added to these centrifuged GNP pellets (from 500 µL HOOC-PEG_7-GNP solutions). The reaction mixture was incubated at 20˚C for 2h. The obtained immobilized pepsin-GNP solutions were washed in triplicate with 10 % isopropanol in 20 mM PB buffer pH 7.5.

Digestion and derivatization

500 µL of obtained immobilized pepsin-GNP solution was centrifuged and the pellets were digested with 100 µL HCl for 24h. After digestion, the digests were dissolved in 100 µL 0.2M borate buffer pH 8.5. Ten microliters of each obtained hydrolysate solution were added into 70 µL 0.2 M borate buffer (pH 8.5), respectively. Afterwards in each solution, 20 µL of AQC solution (3 mg/mL in acetonitrile) was added and reacted at 55 °C under continuously shaking at 800 rpm for 10 min. The obtained amino acid derivative samples have been directly used for the analysis with HPLC-FLD.

Results and Discussion

After the immobilization of pepsin on HOOC-PEG_7-GNPs via amide coupling, the obtained Pepsin-PEG_7-GNPs have been carefully washed with 10% isopropanol in 20 mM PB buffer pH 7.5 to remove the physically adsorbed pepsin from the nanoparticles. After derivatization with AQC, the obtained solutions have been analyzed with HPLC-FLD. Fig.S2 shows the bonded pepsin concentrations on PEG_7-GNPs against the equilibrium pepsin concentrations. It can be clearly seen that the method is applicable to covalently immobilized protein as well. With higher pepsin concentrations in the reaction mixture for amide coupling, the surface coverage increased in accordance to a Langmuir isotherm. At high pepsin concentrations in the reaction buffer (5 mg mL^{-1}), the saturation capacity seems to be reached.

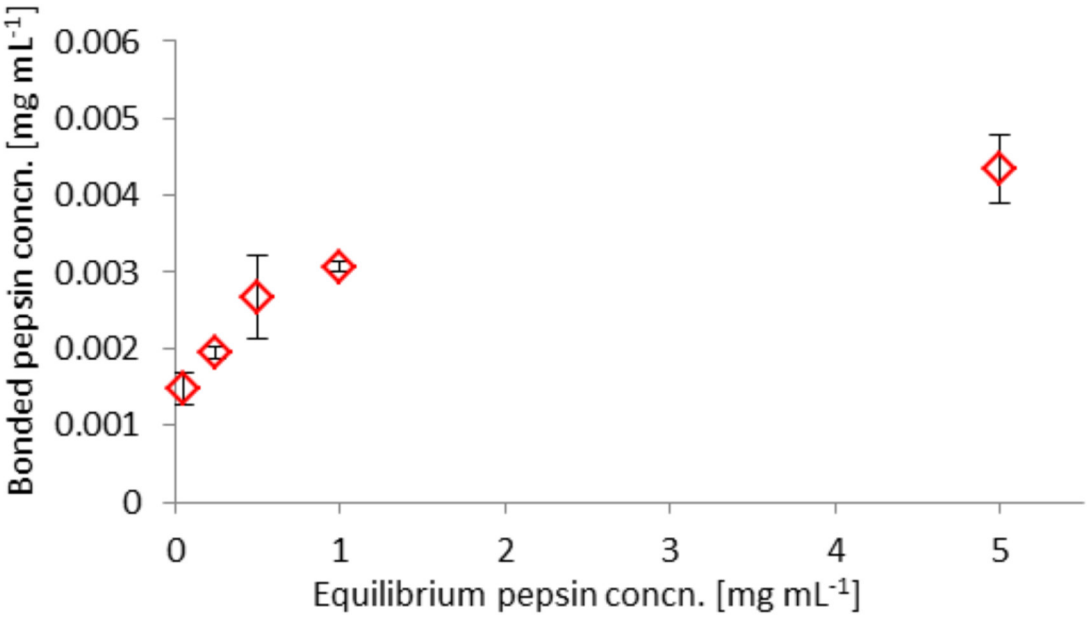

Figure S2. Binding isotherm of covalently immobilized pepsin on HOOC-PEG_7-GNPs (mg pepsin per mL functionalized GNP suspension), and the error bars represent standard deviations.

3.5. Gold nanoparticle-based immobilized enzyme reactors Straightforward and accelerated sample preparation in protein and biopharmaceuticals analysis

Siyao Liu, Markus Höldrich, Helmut Hinterwirth, Michael Lämmerhofer*

Institute of Pharmaceutical Sciences, Pharmaceutical (Bio-)Analysis, University of Tübingen, Auf der Morgenstelle 8, 72076 Tübingen, Germany

chrom+food forum 04 (2017) 34-37

Protein analytics by LC-MS often involves protein digestion to peptides (e.g. tryptic digests) or to smaller protein fragments (e.g. antibodies to antibody fragments). Immobilized enzyme reactors based on nanoparticulate supports are getting popular in this field. Gold nanoparticles turned out to be attractive nanocarriers for enzyme immobilization due to ease of preparation, flexible enzyme conjugation, straightforward sample processing steps, and in particular accelerated digestion kinetics.

Immobilization of enzymes on solid supports (leading to immobilized enzyme reactors, IMERs) emerged as a powerful strategy to overcome some of the limitations of free enzymes in industrial processes and analytical sample preparation procedures, such as low stability, self-digestion, product contamination with enzyme and no repetitive usage of precious enzymes. While immobilization can improve or overcome such shortcomings of homogenous catalysis, concomitant reduction in activity has been frequently reported upon immobilization on microparticulate carriers. Such activity loss can be ascribed to steric hindrance of active sites of enzymes in immobilized state due to unfavorable enzyme orientation, changes in tertiary structure of enzyme upon bonding to a support, and slower diffusion of microparticulate enzyme carriers. Since active enzyme is mostly buried inside the mesoporous channels in microparticulate heterogeneous biocatalysts, fast digestion is limited by mass transfer resistances of substrates which must migrate by diffusion into the mesoporous channels to reach the enzyme on the inner surface. Through optimization of enzyme immobilization, it is however generally possible to maintain enzyme activity and immobilization of enzymes on nanoparticulate carriers turned out to be a successful strategy to enhance enzyme performances. Large surface areas that allow a higher enzyme loading and reduced mass transfer resistance for substrates (enzymes are readily accessible by substrates on the surface of nonporous materials eliminating intraparticulate mass transfer resistances which exist in microparticulate enzyme carriers) promote acceleration of enzyme activity at nanoparticle

interfaces [1]. A wide variety of nanocarriers have been propagated for enzyme immobilization [2]. Magnetic nanoparticles are probably the most popular ones. We use gold nanoparticles (GNPs) as carriers for enzyme conjugation due to its inertness, straightforward size-controlled synthesis, convenient and flexible surface modification by self-assembled monolayer formation, good colloidal stability which allows their handling (pipetting) like solutions similar to homogenous catalysis, and their high density which enables straightforward separation of the nanoparticles from reaction mixtures by simple centrifugation on a minispin.

Synthesis and characterization of protein-conjugated gold nanoparticles

GNPs can be synthesized by the Turkevich-Frens method from $HAuCl_4$ and trisodium citrate [3]. In this reaction, citrate plays the double role as a Au(III) reducing agent and colloidal GNP stabilizing reagent due to capping citrate anions which are attached on the GNP surface and avoid aggregation by electrostatic repulsion. The synthesis follows a nucleation and growth mechanism and thus the size of the GNPs can be conveniently controlled by the $HAuCl_4$ to trisodium citrate ratio. GNPs synthesized by this method range between 10 and 40 nm depending on the HAuCl4 to citrate ratio [4].

Size and size-distribution analysis is an important parameter for the characterization of GNPs and functionalized GNPs. Different methods exist and are utilized for this purpose. However, accurately measuring the size and size distribution is still a challenging task because distinct methods may provide slightly different results [4]. Transmission electron microscopy (TEM) provides information on the average size, size distribution, and shape of nanoparticles, however, lacks information about solution properties such as aggregation which is relevant for assessing the suitability of GNPs in many applications (Fig. 1a). On the contrary, dynamic light scattering (DLS) measures the nanoparticles with their solvation shell. If aggregation occurs in colloidal solutions, size distributions are significantly shifted. If particle distributions are multimodal, the size distributions measured by DLS unfortunately are biased because light scattering intensity increases

with the sixth power of the particle diameter which leads to distortions in favor of large particles. If asymmetric flow field flow fractionation (AsFlFFF, AF4) is employed for sizing, one has to make sure that particle adsorption on the membrane of the channel, which serves as an accumulation wall for larger particles does not distort the size distributions. Last but not least, differential mobility analyzers (DMA), such as nanoelectrospray gas-phase electrophoretic mobility molecular analyzer (nES-GEMMA), have become popular recently for nanoparticle size analysis. nES-GEMMA allows the electrophoretic separation of singly charged particles in an orthogonal applied electric field at high laminar gas flow at atmospheric pressure and from such experiments, the particle diameter can be calculated. Multiply charged ions are generated using an electrospray process and then singly charged particles and neutrals are produced from the multiply charged particles by charge reduction with a Polonium-210 source which are then electrophoretically separated in the gas phase. nES-GEMMA has shown good size resolution, but represents dry state particle diameters. Fig. 1b-1e shows a comparison of size distributions of two distinct batches of GNPs with different average diameters as measured with different techniques. Many other techniques also exist [5].

Enzymes can be immobilized by a variety of methods such as covalent binding, entrapment in adsorbed polyelectrolyte layers, adsorption, ionic binding, affinity binding. However, covalent attachment is preferred in order to avoid bleeding of enzyme from the surface into the reaction mixture. For GNPs this requires the attachment of linkers and a number of bifunctional linkers with reactive group, e.g. carboxylic acid group, for protein coupling on one end as well as thiol group on the other end which enables their immobilization by self-assembled monolayer (SAM) formation have been used (Fig. 1f). It has been found that the surface coverage of those linkers depends on their length ranging from about 6 ligands per nm2 for a C2 spaced linker to about 4 ligands per nm2 for a PEG_7 spaced bifunctional linker (Fig. 1g) [6]. Shorter ligands obviously pack more densely on the surface of GNPs, however, the longer PEG_7 spacer has turned out to be favorable. It greatly supported the colloidal stability, eliminated to large extent non-

specific binding to the nanoparticle surface and assured a sufficient enzyme immobilization density and improved bioactivity [3]. Larger GNPs e.g. 33 nm were favorable as nanocarriers over smaller ones e.g. 18 nm [3].

An alternative concept for GNP functionalization with enzymes represents a layer-by-layer adsorption of polyelectrolytes and subsequent protein bonding by amide coupling reaction [7]. For instance, coating of poly(allylamine) and subsequently with poly(acrylic acid) yields biocompatible and highly hydrophilic carboxy-terminated nanoparticles for enzyme coupling by EDC/sulfoNHS chemistry.

The success of such surface functionalization can be controlled after each step by simple methods such as visible (VIS) spectroscopy, DLS and electrophoretic light scattering (ELS) (Fig. 2). VIS spectroscopy allows to measure the absorbance maximum (λ_{max}) of the surface plasmon resonance (SPR) band (at around 525 nm for GNPs). It depends on the nanoparticle size and shape, size distribution, and morphological uniformity of GNPs, and consequently allows to monitor whether shifts of the SPR band occurred due to immobilization of ligands on the GNP surface, and most importantly whether aggregation occurred, as indicated by a band observed in the red-shifted region of the VIS spectrum. DLS documents the size increase due to immobilization of ligand and enzyme, respectively, and ELS indicates whether ζ-potentials are large enough to support colloidal stability by electrostatic repulsion between modified GNPs. Examples for enzyme conjugated GNPs described hereafter are given in Fig. 2.

Trypsin-conjugated gold nanoparticles

Trypsin is probably the most important enzyme in protein analytics and frequently used in bottom up protein analysis, e.g. in proteomics. Drawbacks are long digestion times (up to 24 h), auto-digestion sub-products and poor enzyme-to-substrate ratio limiting high-throughput protein identification. It was immobilized on GNPs using a bonding chemistry as outlined in Fig. 3a with variable spacers comprising 3-mercaptopropionic acid (MPA), 11-mercaptoundecanoic acid (MUA), 16-mercaptohexadecanoic acid (MHA), HS-PEG_4-

COOH (PEG_4) and HS-PEG_7-COOH (PEG_7) [3]. The effect of the spacer length on trypsin activity was investigated with the standard chromogenic substrate N-benzoyl-DL-arginine-4-nitroanilide hydrochloride (BApNA). With longer spacer length the amount of trypsin bound onto GNPs could be increased significantly and PEG_7 spacer turned out to be advantageous for this and other reasons, namely stabilization of the colloids as well as biocompatibility. Digestions with a protein test mixture revealed that the sequence coverage can be improved with trypsin-GNP bioconjugate having i) a PEG_7 spacer instead of a MHA spacer and ii) when the GNP carrier was 33 nm instead of 18 nm in diameter [3]. BSA digestions further showed higher sequence coverage with GNP-PEG_7-Trypsin compared to Trypsin in free solution digestion. Good sequence coverages could be observed after 1-2 h digestion with GNP-PEG_7-Trypsin. While digestion efficiencies were better with the GNP-PEG_7-Trypsin conjugate as compared to free solution digestion, self-digestion was only observed in the reaction batches with free trypsin.

Pepsin-conjugated gold nanoparticles

Pepsin is another enzyme of significant utility in protein analytics. It is commonly employed in monoclonal antibody digestion near the hinge region to produce specifically $F(ab')_2$ (with a molecular mass of about 100 kDa) and Fc fragment (ca. 50 kDa). Such antibody fragments are particularly useful for middle-up mass measurement for characterization of therapeutic antibodies by high-resolution MS.

Pepsin was conjugated to GNPs by essential the same surface chemistry described above for GNP-PEG_7-Trypsin [8]. However, pepsin is irreversible denatured under the conditions used for trypsin coupling and therefore the reaction buffer had to be adjusted (20 mM MES pH 4.5 instead of 50 mM bicarbonate buffer, pH 8.5 as for trypsin immobilization). With such conditions, the coupling efficiency of pepsin on GNP-PEG_7-COOH was good and about 0.25±0.03 mg mL^{-1} could be conjugated onto GNPs [8]. Due to bonding of bifunctional linker the nanoparticle diameter increased from ca. 30 nm for citrate-capped GNPs to ca. 50 nm, and further to ca. 100 nm after pepsin conjugation

(Fig. 2b). A ζ-potential of around -30 mV ensured a sufficient colloidal stability which is important because aggregated GNPs precipitate and lose their digestion efficiency.

A monoclonal anti-HSA antibody was digested with such GNP-PEG_7-Pepsin conjugate to document the biofunctionality of this bionanocatalyst [8]. The reaction product was characterized by HR-MS using a QTOF equipped with a μESI sprayer and a C18 online trap column for desalting of the protein sample. Non-digested anti-HSA antibody was analyzed as well. The deconvoluted TOF-MS spectrum of the intact monoclonal antibody is illustrated in Fig. 4c [8]. It shows the characteristic mass of about 149 kDa with a number of isoforms. After digestion with pepsin-GNP conjugate a single peak with a deconvoluted mass of 97,619.4 Da for $F(ab')_2$ was detected. These results clearly document the functionality of the immobilized pepsin nanobiocatalyst and evidence its practical utility for therapeutic protein characterization.

Papain-conjugated gold nanoparticles

Papain is another enzyme that can be used for antibody digestion. It is a cysteine protease which cleaves the antibody above the hinge region (the site of the disulfide bonds which connect the two heavy chains) yielding two Fab fragments and one Fc fragment (each ca. 50 kDa). Fab fragments are prepared to characterize the protein on an intermediate level instead of the whole intact immunoglobulin (middle up and middle down).

Papain-GNP conjugates were synthesized by a layer-by-layer (LBL) polyelectrolyte coating approach with alternative deposition of first polyallylamine followed by polyacrylic acid and subsequent enzyme coupling to terminal carboxylates (Fig. 5a) [7]. ζ-Potentials of the modified GNPs indicated the successful coating as they changed from negative to positive upon polyallylamine coating, back to negative after polyacrylic acid deposition (Fig. 2d). DLS meaurement also indicated the successful coating by a significant size increase. It seems that a highly hydrated shell resulted from this LBL activation approach which supported colloidal stability and biocompatibility. It can be further seen in Fig. 2c

that the sizes of the papain-GNP conjugates significantly increased with more papain in the reaction mixtures during amide coupling. Resonant mass measurement (RMM), which measures the buoyant masses of single particles in a microfluidic channel that senses the density differences of the particle and the transport fluid via frequency shifts when the particle passes the sensor, was used to determine the amount of papain per GNP [5, 7]. It was found that the papain-GNP conjugate prepared from 1 mg/mL papain in the reaction mixture had an enzyme coverage of 2.06±0.19 × 106 papain molecules per GNP. Measurements of the enzyme kinetics with the model substrate BApNA showed that the Michaelis constant K_m is not compromised by immobilization and that reaction rate is by a factor of 100 faster with the immobilized papain compared to papain in free solution [7]. This makes it possible to achieve the same reaction rates with much less enzyme which could be of interest for precious enzymes.

The papain-GNP conjugate was then used to digest human IgG (Fig. 5b) and the resultant fragments were analyzed by HPLC-μESI-QTOF-MS (Fig. 5c) [7]. The deconvoluted mass spectrum of the hIgG before digestion showed a group of peaks around 150 kDa (note, this sample is not a monoclonal antibody but human IgG isolated from plasma). After digestion, the deconvoluted mass of hIgG (ca. 150 kDa) disappeared and deconvoluted masses corresponding to fragments (Fab and Fc) in the range of 50–55 kDa emerged. It clearly documents the functionality of the papain-GNP conjugate which may have great utility for antibody analysis.

Conclusions

Enzyme-GNP conjugates can be useful heterogeneous catalysts in protein analytics combining favorable properties of homogeneous and heterogeneous catalysis. Enzyme activity can be maintained by appropriate immobilization schemes. Reaction rates can be significantly enhanced. Enzyme stability is improved and self-digestion eliminated. Such colloidal bionanocatalysts can be conveniently pipetted and enzyme-GNP conjugates can be easily removed after reaction by simple short centrifugation on a tabletop minispin. As

a consequence, they turn out to be useful tools in bioanalysis and biopharmaceuticals analysis.

References

[1] B.J. Johnson, W. Russ Algar, A.P. Malanoski, M.G. Ancona, I.L. Medintz, Understanding enzymatic acceleration at nanoparticle interfaces: Approaches and challenges, Nano Today, 9 (2014) 102-131.

[2] M. Misson, H. Zhang, B. Jin, Nanobiocatalyst advancements and bioprocessing applications, Journal of The Royal Society Interface, 12 (2015).

[3] H. Hinterwirth, W. Lindner, M. Lammerhofer, Bioconjugation of trypsin onto gold nanoparticles: effect of surface chemistry on bioactivity, Anal Chim Acta, 733 (2012) 90-97.

[4] H. Hinterwirth, S.K. Wiedmer, M. Moilanen, A. Lehner, G. Allmaier, T. Waitz, W. Lindner, M. Laemmerhofer, Comparative method evaluation for size and size-distribution analysis of gold nanoparticles, J. Sep. Sci., 36 (2013) 2952-2961.

[5] M. Hoeldrich, S. Liu, M. Epe, M. Laemmerhofer, Taylor dispersion analysis, resonant mass measurement and bioactivity of pepsin-coated gold nanoparticles, Talanta, 167 (2017) 67-74.

[6] H. Hinterwirth, S. Kappel, T. Waitz, T. Prohaska, W. Lindner, M. Lämmerhofer, Quantifying Thiol Ligand Density of Self-Assembled Monolayers on Gold Nanoparticles by Inductively Coupled Plasma–Mass Spectrometry, ACS Nano, 7 (2013) 1129-1136.

[7] S. Liu, M. Hoeldrich, A. Sievers-Engler, J. Horak, M. Laemmerhofer, Papain-functionalized gold nanoparticles as heterogeneous biocatalyst for bioanalysis and biopharmaceuticals analysis, Anal. Chim. Acta, (2017) Ahead of Print.

[8] M. Hoeldrich, A. Sievers-Engler, M. Laemmerhofer, Gold nanoparticle-conjugated pepsin for efficient solution-like heterogeneous biocatalysis in analytical sample preparation protocols, Anal. Bioanal. Chem., 408 (2016) 5415-5427.

Figures and Figure captions

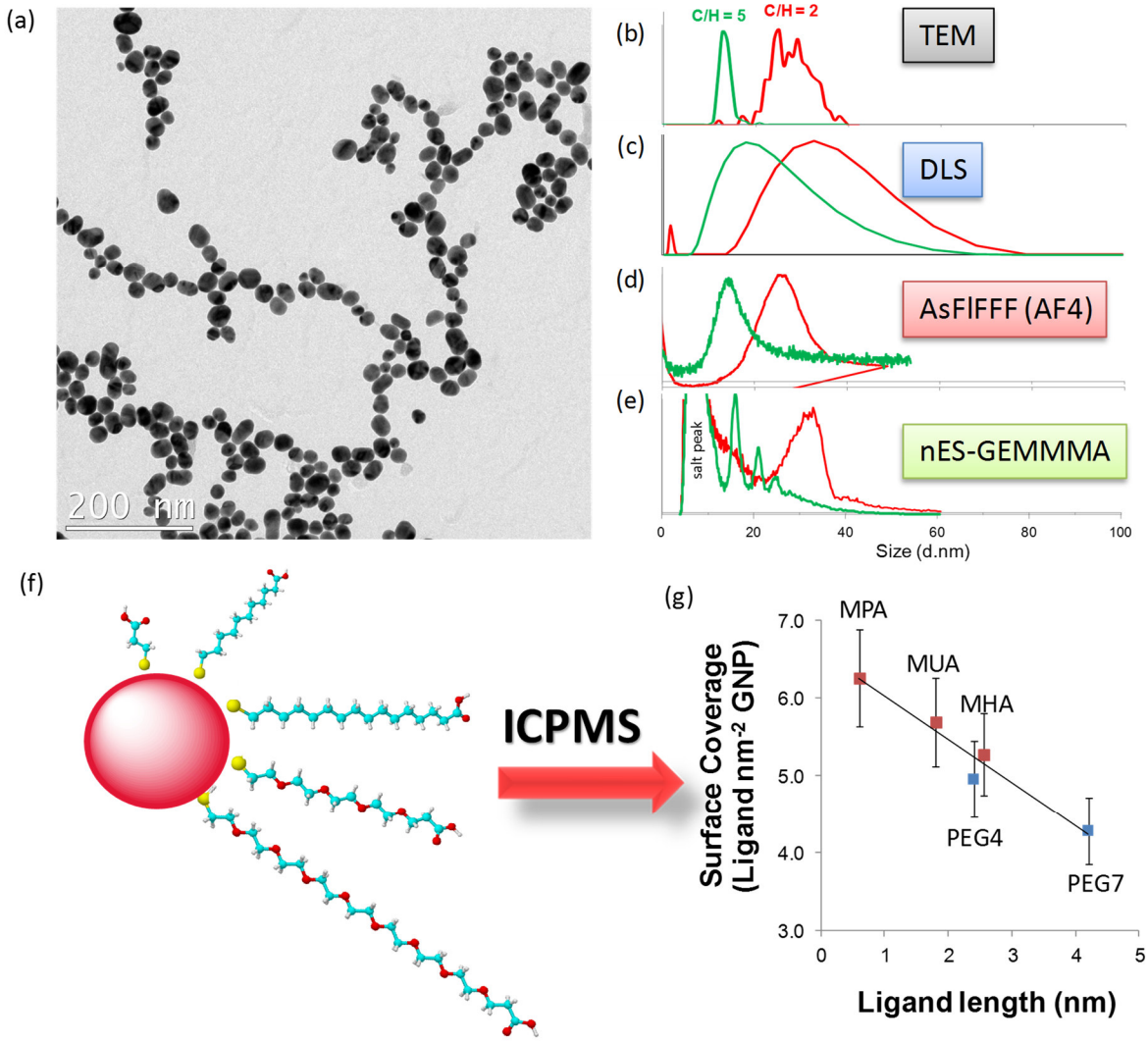

Figure 1. Size determination of GNPs and surface coverage of different bifunctional ligands bonded by self-assembled monolayer (SAM) formation. TEM image of citrate-stabilized GNPs (average particle size dTEM ~30 nm, dDLS ~ 40 nm) (a) [6]. Size distribution of GNPs prepared from two distinct HAuCl4 (H) to trisodium citrate (C) ratios by TEM (b), DLS (c), AsFlFFF (AF4) (d), nES-GEMMA (e) [4]. Scheme for GNPs with different bifunctional ligands assembled on the gold surface via dative thiol-gold bond (f), and their surface coverages as determined by ICP-MS (g) [6] (Abbreviations: MPA,3-mercaptopropionic acid; MUA, 11-mercaptoundecanoic acid; MHA, 16-mercaptohexadecanoic acid; PEG_4, HS-PEG_4-COOH; PEG_7, HS-PEG_7-COOH).

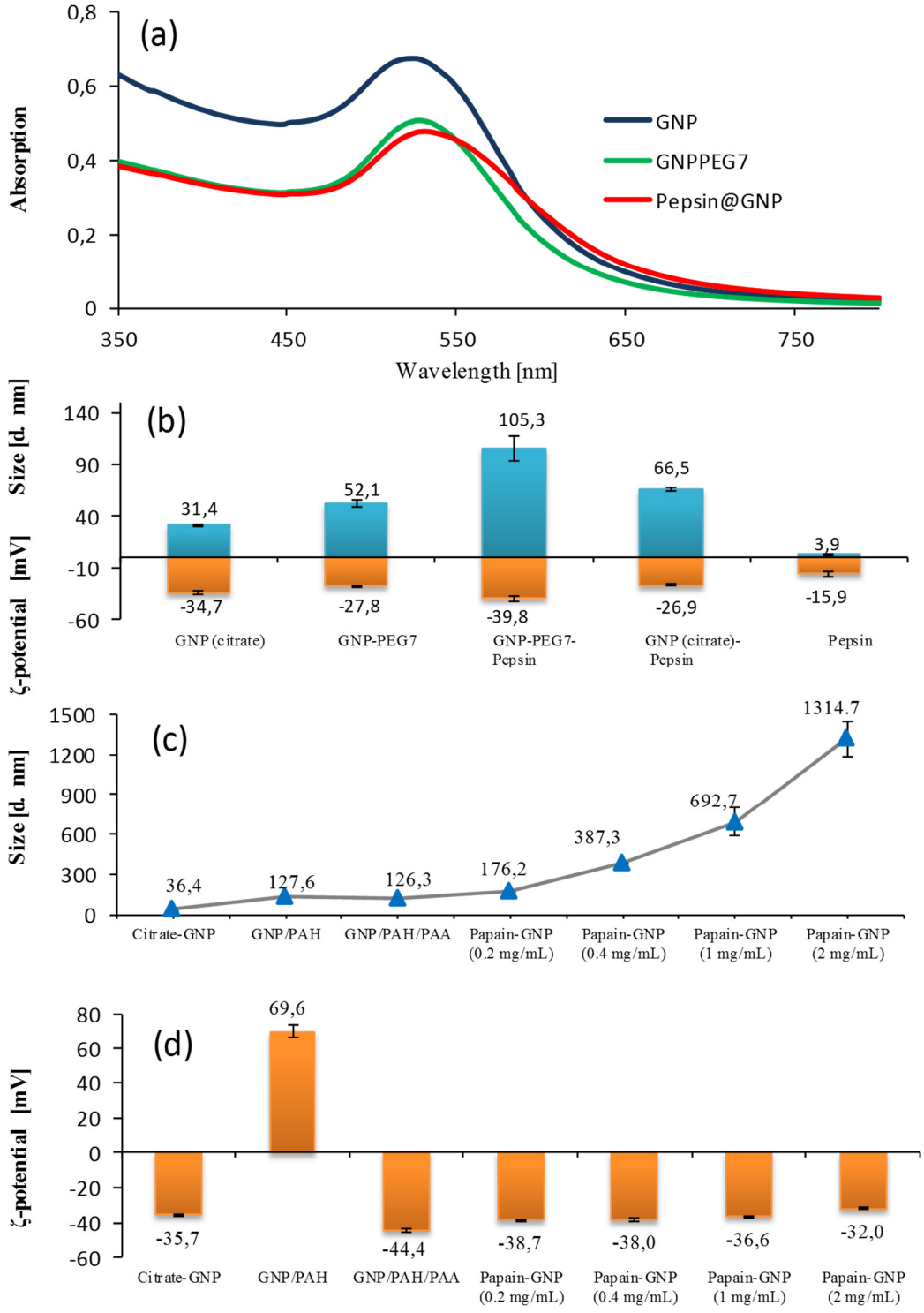

Figure 2. Characterization of enzyme-GNP conjugates. VIS spectroscopy measuring shifts in the surface plasmon resonance band, exemplified by pepsin-PEG_7-GNP conjugate [8] (a). DLS (hydrodynamic particle diameters) and ELS (ζ-potentials) at distinct stages of surface modification as measured for pepsin-PEG_7-GNP conjugate [8]

(b) and papain-GNP conjugate [7] (c and d) (abbreviations: PAH, polyallylamine hydrochloride; PAA, polyacrylic acid).

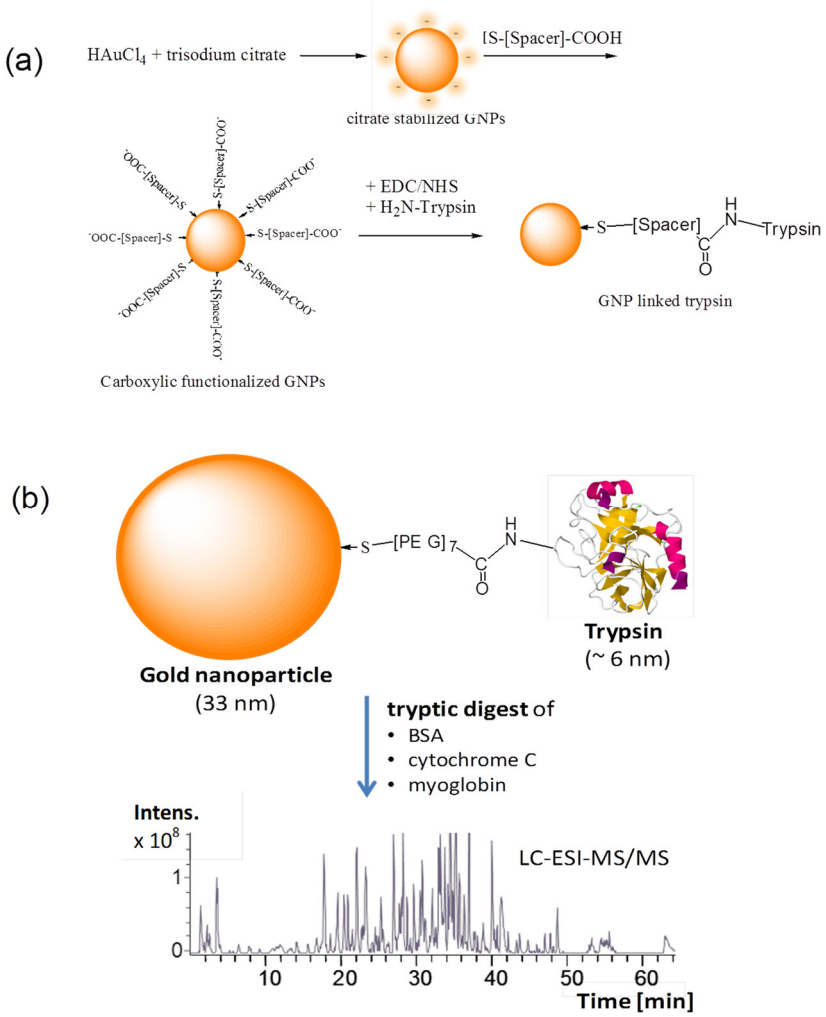

Figure 3. Trypsin-conjugated GNPs. Synthesis of GNPs by Turkevich-Frens method, subsequent modification by SAM formation and immobilization of trypsin by amide coupling (a). Tryptic digestion of a model protein mix followed by HPLC-ESI-MS/MS analysis of the digest (b) [3].

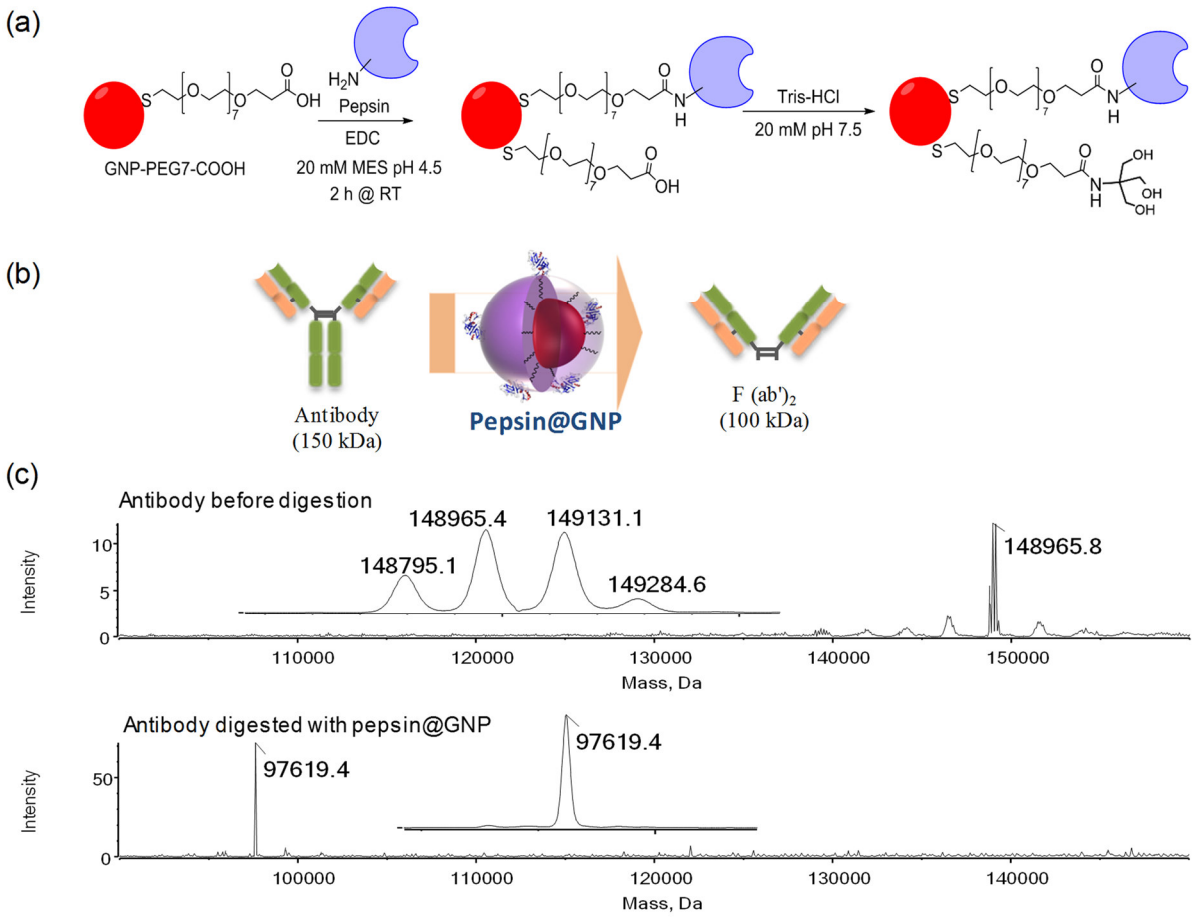

Figure 4. Pepsin-conjugated GNPs. Synthesis scheme (a), monoclonal antibody digestion scheme (b) and deconvoluted ESI-TOF-MS spectra before and after digestion of monoclonal anti-HSA antibody by Pepsin-conjugated GNPs [8].

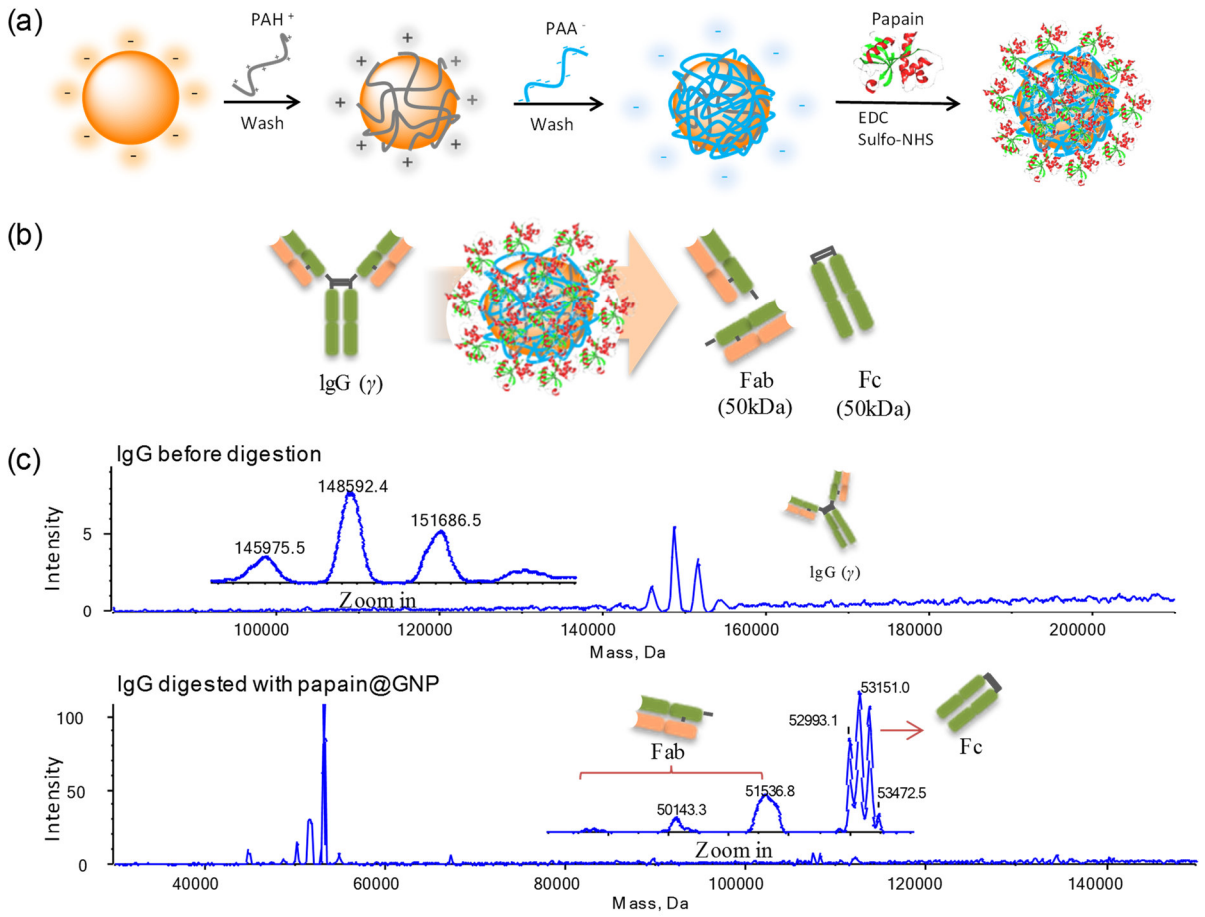

Figure 5. Papain-conjugated GNPs. Synthesis scheme by layer-by-layer approach and subsequent protein coupling (a), human IgG digestion scheme (b) and deconvoluted ESI-TOF-MS spectra before and after digestion of human IgG by Papain-conjugated GNPs [7].

4. Final Conclusions

This dissertation deals with the complete synthesis and characterization of heterogeneous nano biocatalysts based on gold nanoparticles for sample preparation of biopharmaceuticals, such as proteins and antibodies before analysis using high-resolution mass spectroscopy. The aim was to check basic parameters such as functionality and stability of the platform also with regard to the development of a corresponding sample processing tool. Various characterization methods for the different GNP synthesis steps, such as Vis-spectroscopy, DLS, zeta potential, Taylor dispersion analysis, resonant mass measurement and protein assays have been used and compared. The determination of protein functionality was studied by Michaelis-Menten kinetics. For this purpose, a HPLC method was developed and validated according to ICH guideline. Model proteins such as BSA, cytochrome C and myoglobin were analyzed by liquid chromatography coupled with a high-resolution mass spectrometer. With an in-silico protein tool the sample proteins could be deduced due to the peptide pattern.

Basically, the new and advanced method is aimed at quality control of bioprocesses in the biopharmaceutical industry. Due to the complete investigation of the developed nanobiocatalysts, this requirement seems to be fundamentally possible.

The results of the synthesis of the heterogeneous nano biocatalysts show comparable results with the corresponding literature. In a one-month stability study unvaried results could be determined by Vis-spectroscopy, DLS and zeta potential analysis. The results of these characterization techniques could be compared and completed with those of TDA and RMM in order to generate a more versatile toolbox for nanoparticle determination.

In addition, it was possible to conclude that the immobilized pepsin does not bleed from the nanoparticle or undergo auto digestion. This could be determined by using a coupled digestion protocol, on the one hand to confirm the functionality of the immobilized pepsin and

on the other hand to investigate the possible presence of pepsin related peptides in the analytical sample. Therefore, a defined protein mixture was digested with the nano biocatalysts. Afterwards the sample was separated from the nano particles and re-digested with trypsin in order to determine possible characteristic peptides from pepsin by UHPLC-ESI-QTof-MS/MS analysis.

Another functional parameter was the investigation of enzyme activity by Michaelis-Menten kinetics. For this purpose, an analytical HPLC method was developed and validated for the determination of the enzymatic degradation of cytochrome C. The comparison of the enzyme activity of non-immobilized (free) pepsin and immobilized pepsin showed comparable results. The enzyme activity is therefore not adversely affected by the immobilization.

A final comparison of defined protein mix samples was performed by LC-MS/MS for confirming the presence of characteristic peptides related to pepsin digestion. As a biopharmaceutical sample a monoclonal antibody was specifically digested with the newly synthesized heterogeneous nanobiocatalysts and analyzed using the proprietary on-line SPE high-resolution mass spectrometry method. The method was also used for the intact mass determination of the human growth hormone genotropin. This confirmed the practical application of the new nano catalysts and ensured the versatility of the on-line SPE method.

Advantages, such as the handling of the colloidal suspension as a classic liquid (transfer by means of pipettes, etc.), the possibility of a complete separation of the sample solution by bench top centrifuge and the reusability of the catalysts, greatly facilitated the daily research work and made it accessible for the reverse analysis and characterization strategies.

The goal of the present work, namely the development and characterization of new heterogeneous nano biocatalysts for the sample preparation of protein samples and biopharmaceuticals such as monoclonal antibodies, has been fully achieved. The particles

were fully analyzed in terms of size, functionality, stability and practical application. They represent a new and well-established quality control tool of bioprocesses in biopharmaceutical production.

5. Curriculum Vitae

Persönliche Daten:

Name	Markus Höldrich
Geburtsdatum	24.09.1980
Geburtsort	Albstadt, Deutschland

Schulische Ausbildung:

1987 – 1991	Grundschule Langenwand
1991 – 1992	Lutherschule Tailfingen (Hauptschule)
1992 – 1998	Mittlere Reife an der Lammerberg Realschule
2001 – 2003	Abitur an der Technischen Oberschule Stuttgart

Akademische Ausbildung:

2004 – 2011	Studium Diplom-Lebensmittelchemie mit Abschluss (Grundstudium an der Universität Stuttgart, Hauptstudium an der Universität Hohenheim)
04/2011 – 09/2011	Diplomarbeit am Institut für Technische Biochemie Stuttgart unter der Leitung von Prof. Dr. Bernhard Hauer und Dr. Bettina Nestl mit dem Titel „Entwicklung und Optimierung einer Hochdurchsatzanalysemethode zur Charakterisierung von Halohydrin Dehalogenasen und de novo Epoxid Hydrolasen“
02/2012 – 07/2012	Wissenschaftliche Hilfskraft, Institut für Technische Biochemie Stuttgart
2012 – 2016	Dissertation am Institut für Pharmazeutische Analytik und Bioanalytik der Eberhard-Karls-Universität Tübingen unter der Betreuung von Prof. Dr. Michael Lämmerhofer

Beruflicher Werdegang:

1998 – 2001	Berufsausbildung zum Ver- und Entsorger, Stadtverwaltung Albstadt
2003 – 2004	Zivildienst an der Teil-offenen-Tür Haus Tannenhof in Düsseldorf (Wehr-/Ersatzdienst)
2016 –2018	Quality Control Scientist, Catalent Germany Schorndorf GmbH
2018 – dato	QC Laboratory NPI & Compliance Supervisor, Catalent Germany Schorndorf GmbH